ILMATIETEEN LAITOS
METEOROLOGISKA INSTITUTET
FINNISH METEOROLOGICAL INSTITUTE

139
CONTRIBUTIONS

# REMOTE SENSING OF SNOW: FACTORS INFLUENCING SEASONAL SNOW MAPPING IN BOREAL FOREST REGION

**MIIA SALMINEN**

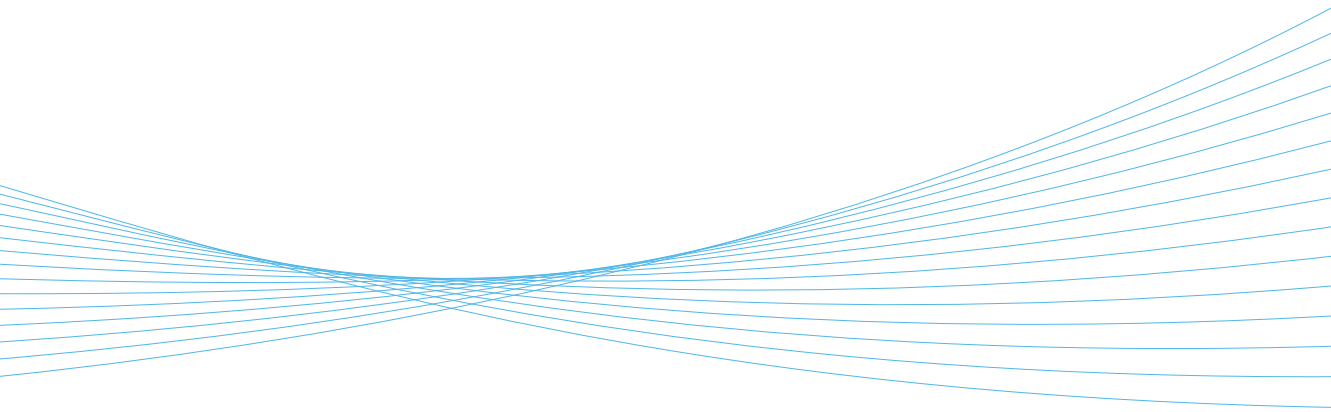

Finnish Meteorological Institute Contributions No. 139

# REMOTE SENSING OF SNOW: FACTORS INFLUENCING SEASONAL SNOW MAPPING IN BOREAL FOREST REGION

Miia Salminen

Department of Geosciences and Geography
Faculty of Science
University of Helsinki
Helsinki, Finland

Academic dissertation

*To be presented, with the permission of the Faculty of Science of the University of Helsinki, for public criticism in Auditorium XV of the Main Building (Fabianinkatu 33) on November 10th 2017, at 12 o'clock noon.*

**Helsinki 2017**

**Author's Contact Details**
Miia Salminen
Finnish Meteorological Institute
P.O. Box 503 (Erik Palménin aukio 1)
FI-00101 Helsinki, Finland
Miia.Salminen@fmi.fi

**Supervisors**
Professor Petri Pellikka, Ph.D.
Department of Geosciences and Geography
University of Helsinki, Finland

Research professor Jouni Pulliainen, Ph.D.
Arctic Research
Finnish Meteorological Institute, Finland

**Pre-examiners**
Dr. Gareth Rees, Ph.D.
Department of Geography and Scott Polar Research Institute
University of Cambridge, U.K.

Professor Cheng Xiao, Ph.D.
College of Global Change and Earth System Science
Beijing Normal University, China

**Opponent**
Professor Julienne Stroeve, Ph.D.
Department of Earth Sciences
University College London, U.K.

ISSN: 0782-6117
ISBN: 978-952-336-036-5
ISBN: 978-952-336-037-2 (pdf)
http://ethesis.helsinki.fi
Helsinki 2017

FINNISH METEOROLOGICAL INSTITUTE

| | | |
|---|---|---|
| Published by | Finnish Meteorological Institute<br>(Erik Palménin aukio 1) P.O. Box 503<br>FIN-00101 Helsinki, Finland | Series title, number and report code of publication<br>Contributions 139, FMI-CONT-139<br><br>Date<br>October 2017 |
| Author(s)<br>Miia Salminen | | Name of project<br><br>Commissioned by |

Title
Remote sensing of snow: Factors influencing seasonal snow mapping in boreal forest region

Abstract

Monitoring of snow cover in northern hemisphere is highly important for climate research and for operational activities, such as those related to hydrology and weather forecasting. The appearance and melting of seasonal snow cover dominate the hydrological and climatic patterns in the boreal and arctic regions. Spatial variability (in particular during the spring and autumn transition months) and long-term trends in global snow cover distribution are strongly interconnected to changes in Earth System (ES). Satellite data based estimates on snow cover extent are utilized e.g. in near-real-time hydrological forecasting, water resource management and to construct long-term Climate Data Records (CDRs) essential for climate research. Information on the quantitative reliability of snow cover monitoring is urgently needed by these different applications as the usefulness of satellite data based results is strongly dependent on the quality of the interpretation.

This doctoral dissertation investigates the factors affecting the reliability of snow cover monitoring using optical satellite data and focuses on boreal regions (zone characterized by seasonal snow cover). Based on the analysis of different factors relevant to snow mapping performance, the work introduces a methodology to assess the uncertainty of snow cover extent estimates, focusing on the retrieval of fractional snow cover (within a pixel) during the spring melt period. The results demonstrate that optical remote sensing is well suited for determining snow extent in the melting season and that the characterizing the uncertainty in snow estimates facilitates the improvement of the snow mapping algorithms. The overall message is that using a versatile accuracy analysis it is possible to develop uncertainty estimates for the optical remote sensing of snow cover, which is a considerable advance in remote sensing. The results of this work can also be utilized in the development of other interpretation algorithms.

This thesis consists of five articles predominantly dealing with quantitative data analysis, while the summary chapter synthesizes the results mainly in the algorithm accuracy point of view. The first four articles determine the reflectance characteristics essential for the forward and inverse modeling of boreal landscapes (forward model describes the observations as a function of the investigated variable). The effects of snow, snow-free ground and boreal forest canopy on the observed satellite scene reflectance are specified. The effects of all the error components are clarified in the fifth article and a novel experimental method to analyze and quantify the amount of uncertainty is presented. The five articles employ different remote sensing and ground truth data sets measured and/or analyzed for this research, covering the region of Finland and also applied to boreal forest region in northern Europe.

Publishing unit: Arctic research

| | | |
|---|---|---|
| Classification (UDC)<br>551.321.7 -032.24 502.6 | Keywords: remote sensing, snow cover, optical methods | |
| ISSN and series title<br>0782-6117 Finnish Meteorological Institute Contributions | | |
| ISBN<br>978-952-336-036-5<br>978-952-336-037-2 (pdf) | Language<br><br>English | Pages<br><br>126 |

ILMATIETEEN LAITOS

| | | |
|---|---|---|
| | | Julkaisun sarja, numero ja raporttikoodi<br>Contributions 139, FMI-CONT-139 |
| Julkaisija | Ilmatieteen laitos (Erik Palménin aukio 1)<br>PL 503, 00101 Helsinki | Julkaisuaika<br>Lokakuu 2017 |
| Tekijä(t)<br>Miia Salminen | | Projektin nimi<br><br>Toimeksiantaja |

Nimeke
Lumen kaukokartoitus: Kausittaisen lumipeitteen kartoitukseen vaikuttavat tekijät boreaalisella metsävyöhykkeellä

Tiivistelmä

Lumipeitteen monitorointi pohjoisella pallonpuoliskolla on tärkeää sekä ilmastotutkimuksen että hydrologiaan ja sääennusteisiin liittyvien operatiivisten sovellutusten kannalta. Kausittaisen lumipeitteen tulo ja sulaminen dominoivat hydrologisia ja ilmastollisia malleja boreaalisilla ja arktisilla alueilla. Alueellinen vaihtelu (erityisesti lumenpeittoalan muutokset keväällä ja syksyllä) sekä pitkän aikavälin trendit globaalin lumipeitteen esiintyvyydessä ovat vahvasti kytköksissä koko maapallon luonnonjärjestelmän kattaviin muutoksiin. Satelliittiaineistoihin perustuvia estimaatteja lumipeitteen laajuudesta hyödynnetään mm. hydrologisissa ennusteissa, vesivarojen hallinnoinnissa ja rakennettaessa pitkän aikavälin aikasarjoja ilmastomuuttujista (Climate Data Record, CDR) ilmastotutkimuksen tarpeisiin. Kvantitatiivisia arvioita lumikartoituksen luotettavuudesta tarvitaan näihin eri käyttötarkoitusiin, sillä satelliittiaineistoihin perustuvien (lumenpeittoala)estimaattien käyttökelpoisuus on paljolti riippuvainen satelliittikuvatulkinnan laadusta.

Väitöskirjatyössä selvitetään optisiin satelliittiaineistoihin perustuvan lumikartoituksen luotettavuuteen vaikuttavia tekijöitä erityisesti boreaalisilla alueilla (joissa on tyypillisesti kausittainen lumipeite). Työssä esitellään metodologia saatujen lumiestimaattien epätarkkuuden arviointia varten. Menetelmä on kehitetty analysoimalla lumenpeittoalan havainnointiin vaikuttavia tekijöitä keskittyen erityisesti kevään sulamiskaudella satelliittipikselin sisältämän lumenpeittoalaosuuden (Fractional Snow Cover, FSC) arviointiin.

Työn tulokset osoittavat, että optinen kaukokartoitus soveltuu hyvin lumenpeittoalan arviointiin sulamiskaudella ja lumiestimaattien epätarkkuuden ja luotettavuuden kuvaaminen helpottaa lumialgoritmien kehittämistä. Työn keskeinen sanoma on, että käyttämällä monipuolista tarkkuusanalyysiä, on mahdollista kehittää luotettavuusarvioita optisen alueen lumipeitteen kaukokartoituksessa, mikä on huomattava edistysaskel tällä tieteenalalla. Tuloksia voidaan hyödyntää myös muun tyyppisten lumentulkinta-algoritmien kehittämisessä.

Tämä väitöskirjatyö koostuu viidestä lähinnä kvantitatiivista data analyysiä käsittelevästä artikkelista kun taas yhteenvetokappale syntetisoi tuloksia pääosin lumialgoritmin tarkkuusnäkökulmasta. Ensimmäiset neljä artikkelia määrittelevät boreaalisen maaston heijastuskertoimen eli reflektanssin tunnusmerkit, jotka ovat olennaisia suoran ja käänteismallinnuksen kannalta (suora malli kuvaa havainnot tutkittavan suureen funktiona). Näissä artikkeleissa määritellään lumen, lumettoman maan ja boreaalisen metsän latvuston vaikutukset satelliitista havaittuun heijastuskertoimeen. Viidennessä artikkelissa selvitetään eri virhelähteiden vaikutukset ja esitetään uusi kokeelliseen aineistoon perustuva analyysimenetelmä saatujen lumiestimaaattien virheen suuruuden määrittämiseksi. Viidessä artikkelissa hyödynnetään eri kaukokartoitus- ja maastomittausaineistoja, jotka on mitattu ja/tai analysoitu tätä tutkimusta varten kattaen Suomen, mutta osin myös boreaalisen metsäalueen pohjoisessa Euroopassa.

Julkaisijayksikkö: Arktinen tutkimus

| | | |
|---|---|---|
| Luokitus (UDK)<br>551.321.7 -032.24 502.6 | Asiasanat: kaukokartoitus, lumipeite, optiset menetelmät | |
| ISSN ja avainnimike<br>0782-6117 Finnish Meteorological Institute Contributions | | |
| ISBN<br>978-952-336-036-5<br>978-952-336-037-2 (pdf) | Kieli<br><br>Englanti | Sivumäärä<br><br>126 |

## Preface

The research summarized in this thesis was carried out both at the Arctic Research unit of the Finnish Meteorological Institute (FMI) and at the Geoinformatics and Land Use Division of the Finnish Environment Institute (SYKE) during the years 2007-2017. After publishing the first article, for the years 2009-2011, work was interrupted by maternity leave and serious illness. The work was concluded and remaining articles were published starting from year 2013.

This work could not have been possible without the support of my present and previous colleagues at Helsinki University of Technology (presently Aalto University), SYKE and FMI. Especially I wish to thank Dr. Sari Metsämäki and Prof. Jouni Pulliainen for developing the *SCAmod* methodology and related research, which forms the basis of my thesis.

I also thank the Department of Geosciences and Geography, University of Helsinki, in particular my supervisor Prof. Petri Pellikka, for making the thesis possible. The work is related to ”Centre of Excellence in Atmospheric Science – From Molecular and Biological processes to the Global Climate (ATM)” and it was supported by several projects funded by the European Union, Academy of Finland and European Space Agency.

I am sincerely grateful to the pre-examiners, Dr. Gareth Rees from the University of Cambridge and Prof. Cheng Xiao from Beijing Normal University, and to my opponent Prof. Julienne Stroeve from the University College London for their time and careful review of my thesis.

On a personal note, I wish to express my gratitude to my Mum Airi and twin boys Jimi and Henri in particular.

Helsinki, October 2017

Miia Salminen

Table of Contents

## List of original publications

**PI.** Salminen, M., Pulliainen, J., Metsämäki, S., Kontu, A., & Suokanerva, H. (2009). The behaviour of snow and snow-free surface reflectance in boreal forests: Implications to the performance of snow covered area monitoring. *Remote Sensing of Environment, 113*, 907-918.

**PII.** Salminen, M., Pulliainen, J., Metsämäki, S., Böttcher, K., & Heinilä, K. (2013). MODIS-derived snow-free ground reflectance statistics of selected Eurasian non-forested land cover types for the application of estimating fractional snow cover. *Remote Sensing of Environment, 138*, 51-64.

**PIII.** Heinilä, K., Salminen, M., Pulliainen, J., Cohen, J., Metsämäki, S., & Pellikka, P. (2014). The effect of boreal forest canopy to reflectance of snow covered terrain based on airborne imaging spectrometer observations. *International Journal of Applied Earth Observation and Geoinformation, 27*, Part A (Special Issue on Polar Remote Sensing), 31-41.

**PIV.** Pulliainen, J., Salminen, M., Heinilä, K., Cohen, J., & Hannula, H.-R. (2014). Semi-empirical modeling of the scene reflectance of snow-covered boreal forest: Validation with airborne spectrometer and LIDAR observations. *Remote Sensing of Environment, 155*, 303-311.

**PV.** Salminen, M., Pulliainen, J., Metsämäki, S., Ikonen, J., Heinilä, K., & Luojus, K. (xxxx). Determination of uncertainty characteristics for the optical satellite data-based estimation of fractional snow cover. *Remote Sensing of Environment*, submitted.



## Author's contribution

| **Publication** | **PI** | **PII** | **PIII** | **PIV** | **PV** |
|---|---|---|---|---|---|
| Original idea | MS,JP | MS,JP,SM | KH,JP,MS | JP | MS, JP |
| Study design | MS,JP,SM | MS,JP,SM | KH,JP,MS,SM | JP,KH,MS | MS,JP,SM |
| Mathematical theory | JP | JP,SM | JP | JP | JP |
| Field/mast/airborne data measurements | MS,AK,HS | - | KH,PP | KH,JP,HRH | KH |
| Field/mast/airborne data analysis | MS | - | KH,JC | KH,JC,JP,HRH | KH |
| Satellite/geospatial data gathering | MS | MS,KB,KH | - | - | MS,JI,KL |
| Satellite/geospatial data analysis | - | MS,KB,SM | - | - | MS,JI |
| Manuscript preparation | MS,SM | MS,SM | KH,MS,PP | MS | MS,JP |
| Overall responsibililty | MS | MS | KH | JP | MS |
| J. Cohen (JC), K. Böttcher (KB), H.-R. Hannula (HRH), K. Heinilä (KH), J. Ikonen (JI), A. Kontu (AK), K. Luojus (KL), S. Metsämäki (SM), P. Pellikka (PP), J. Pulliainen (JP), M. Salminen (MS), H. Suokanerva (HS) | | | | | |

## List of acronyms and symbols

**Acronyms**

| | |
|---|---|
| AATSR | Advanced Along-Track Scanning Radiometer |
| AISA | Airborne Imaging Spectrometer for Applications |
| ASD | Analytical Spectral Devices |
| AVHRR | Advanced Very High Resolution Radiometer |
| BRDF | Bidirectional Reflectance Distribution Function |
| CDR | Climate Data Record |
| DUE | Data User Element |
| Envisat | Environmental satellite |
| EO | Earth Observation |
| ES | Earth System |
| ESA | European Space Agency |
| FMI | Finnish Meteorological Institute |
| FSC | Fractional Snow Cover |
| GlobSnow | European Space Agency (ESA) Data User Element (DUE) funded GlobSnow project |
| IPCC | Intergovernmental Panel on Climate Change |
| LIDAR | Light Detection and Ranging |
| MERIS | Medium Resolution Imaging Spectrometer |
| MODIS | Moderate Resolution Imaging Spectroradiometer |
| NASA | National Aeronautics and Space Administration |
| NDSI | Normalized Difference Snow Index |
| NDVI | Normalized Difference Vegetation Index |
| NWP | Numerical Weather Prediction |
| RF | Radiative Forcing |
| RMSE | Root Mean Squared Error |
| SCAmod | Snow Covered Area model *i.e.* fractional snow cover retrieval method |
| SAR | Synthetic Aperture Radar |
| SE | Snow Extent |
| SYKE | Finnish Environment Institute |
| Terra | NASA's Flagship Earth Observing Satellite |
| TOA | Top-of-Atmosphere |

**Symbols**

| | |
|---|---|
| $\rho$ | Surface reflectance (field & mast-based spectroradiometer, airborne imaging spectrometer) |
| $t^2$ | Two-way apparent forest canopy transmissivity (the tree-top level-observed value) |
| $t^2_{apparent}$ | Two-way apparent forest canopy transmissivity (TOA-observed value) |
| $S^2_{t^2}$ | Variance of forest canopy transmissivity |
| $\rho_{forest}$ | Forest canopy reflectance (surface observed value) |
| $R_{forest}$ | Forest canopy reflectance (TOA-observed value) |
| $S^2_{forest}$ | Variance of forest canopy reflectance |
| $\rho_{ground}$ | Snow-free ground reflectance (surface observed value) |
| $R_{ground}$ | Snow-free ground reflectance (TOA-observed value) |
| $S^2_{ground}$ | Variance of snow-free ground reflectance |
| $\rho_{snow}$ | Wet snow reflectance (surface observed value) |
| $R_{snow}$ | Wet snow reflectance (TOA-observed value) |
| $S^2_{snow}$ | Variance of wet snow reflectance |
| $E_{stat}$ | Statistical error (Random error based on error propagation analysis) |
| $\Delta$ | Systematic error (Error component not described by statistical error) |
| *PE* | Product error (Effective sum of statistical and systematic errors) |
| *BIAS* | Mean of observed residuals (Positive or negative) |
| *RMSE* | Root mean squared sum of residuals (Effective mean, positive) |
| Sr | steradian, unit of solid angle |
| E | Irradiance |
| L | Radiance |

# 1. Introduction

## 1.1 Background

Earth is an integrated system, where physical, chemical, biological and human interactions affect the state of the planet (Steffen et al., 2015). Changes in Earth System (ES), either natural or driven by humans, include changes in climate. Although naturally fluctuating solar radiation determines the global energy balance on our planet, and is the driver for atmospheric and oceanic circulations, recent scientific evidence links human activities to climate change. According to the Intergovernmental Panel on Climate Change (IPCC) the energy balance between incoming shortwave and outgoing longwave solar radiation is influenced by global climate 'drivers', *i.e.* changes in solar radiation, greenhouse gases, aerosols and surface albedo that is highly affected by the Earth's seasonal snow cover (IPCC, 2013). The changes caused by the drivers perturb global radiation budget producing radiative forcing (RF = measure of the net change in the energy budget) that affects the climate. There are complex global feedback mechanisms that determine the eventual response of the climate system to the forcing. The forcing effect can *e.g.* be balanced by storage of energy in the oceans and carbon uptake by forests. Characterization of the dynamics of the climate system is a complex and challenging task considering the system responses to a variety of external forcing and internal natural (periodic or chaotic) variability over a wide range of timescales.

Northern Hemisphere terrestrial snow cover is an important component of the cryosphere, where the Earth's surface is seasonally or perennially frozen (AMAP, 2011). Permanent snow cover exists mostly in Antarctica and Greenland, and seasonal snow in the Northern Hemisphere. The spatial extent of seasonal snow varies according to latitude, occurring north of latitude 40° in North America, 50° in western Europe, 60° in eastern Europe and 30° in Asia, and also in mountainous areas (Rees, 2006). Ephemeral snow can occur southwards from the regions of seasonal snow more randomly. The vast boreal forest zone south of the tundra across Eurasia and North America, characterized by seasonal snow, is the largest continuous land ecosystem in the world (ACIA, 2005). Boreal forest carbon uptake and storage capacity is influenced by snow cover and seasonal snow is one of the most important features in boreal ecology (Pan et al., 2011).

Considerable decline in the extent and duration of snow cover and sea ice, and related changes in permafrost, hydrology, ecology and temperature, have been measured across the high latitudes (AMAP, 2011; Brown and Mote, 2009; Brown and Robinson, 2011; Choi et al., 2010; Flanner et al., 2011; Derksen and Brown, 2012; Hori et al., 2017). Compared to the global increase in annual average temperature the arctic warming has been roughly twice as high, i.e. arctic amplification. Although snow cover is affected by climate change, it also has an influence on the interacting system. In fact, snow cover is a dynamic variable of the Earth System due to its large spatial and temporal variability and several notable physical properties. Snow has high reflectivity and dry snow, in particular, reflects the majority of the incoming sunlight (Warren, 1982; Pellikka and Rees, 2009). Changes in surface albedo due to declining snow cover can cause increases in the absorbed solar radiation, amplifying the initial

global warming, see Fig. 1. Secondly, due to its low thermal conductivity, snow has an insulating effect over the underlying surface that prevents permafrost and the seasonally frozen/thawed layer from energy losses and helps to sustain ice sheets and glaciers (ACIA, 2004; Flanner et al., 2011; Vaughan et al., 2013).

The topic of this thesis concerns snow mapping using remote sensing methods. Albedo is the fraction of incident radiation that is reflected by a surface, while reflectance is defined as this same fraction for a single incidence angle. Therefore, using single satellite images the albedo cannot be directly measured. Instead, it has to be estimated assuming a known pattern of surface (bidirectional) reflectance to cover all the other viewing angles (Painter and Dozier, 2004; Wiscombe and Warren, 1980). In this thesis, satellite observed reflectance is not employed to study the albedo, but the mapping of the snow extent. On the other hand, snow extent on landscape can be used as input to albedo determination in climate models and weather prediction models.

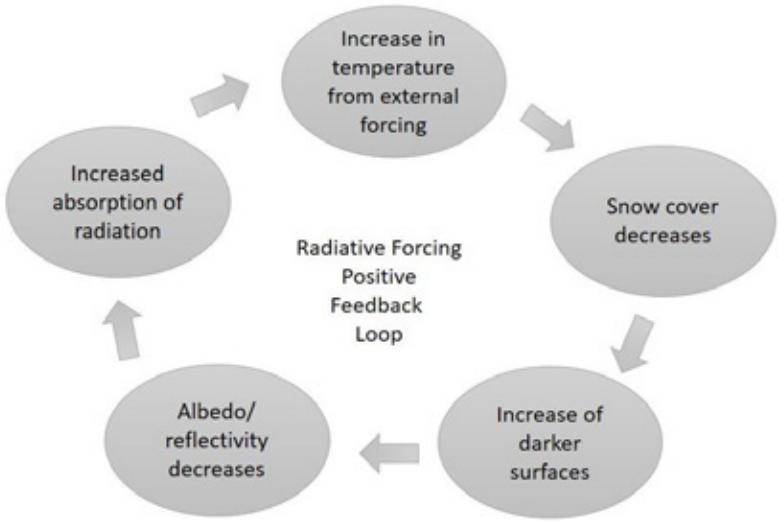


Figure 1. Snow albedo feedback loop. Changes in surface albedo from warming can cause increases in absorbed solar radiation, amplifying the initial warming.

Snow cover has also a direct impact on the hydrological cycle and water balance. Seasonal snow is an enormous fresh water storage during the cold season. After the winter, water is rapidly released from the snowpack during the melting season. Run-off from melting snow favours hydropower production and this economical, clean and renewable energy source has been widely utilized to meet the rising energy needs, although there are environmental concerns. Water resources management and hydropower production need to adapt to the ongoing changes in snow cover duration and winter

precipitation. In regions where the winter precipitation is expected to increase, an increase in run-off is also expected (Callaghan et al., 2011). Moreover, changes in spring snowmelt patterns may have severe consequences, e.g. river flooding. Heavy snowfall may also disrupt air, road and rail transport. In fact, several socio-economic fields are interconnected to the changes in snow cover, such as transport, logistics, forestry, agriculture, irrigation, municipal water supply and recreational activities. Consequently, accurate information on spatial and temporal distribution of snow is essential for reliable run-off and river discharge forecasting, but also for numerical weather prediction (NWP).

Scientists use diverse observation techniques and theoretical models to study the Earth System. Long-term, quality controlled and homogenous datasets are vital for more accurately understanding the ongoing global and regional processes and their effect on climate system and global water cycle. There exists much uncertainty on how fast the Arctic cryosphere will change, will the changes intensify (e.g. the Arctic amplification), what the exact impacts will be (either beneficial or damaging) and how the various feedback mechanisms affect the whole system. Unified monitoring and research is needed to reduce this uncertainty (AMAP, 2011; Bokhorst et al., 2016).

For the above mentioned reasons it is crucial to develop methods for snow cover monitoring and also to find a way to evaluate the accuracy of the obtained snow estimates. Winter maximum extent of snow in the Northern Hemisphere is about 46 million square kilometres (40% of the land areas), so the *in situ* snow measurement network is not sufficient to monitor the annual snow distribution (Rees, 2006). Therefore, remote sensing of snow has been well used for decades to acquire frequent and spatially extensive data coverage for global monitoring purposes. Then again, using both direct ground truth (*i.e. in situ*) and satellite-based snow observations facilitates snow mapping method development and result validation.

Remote sensing techniques mainly use electromagnetic radiation as the source of information. Passive satellite instruments measure either reflected or emitted radiation from the surface and atmosphere, whereas active instruments emit themselves the electromagnetic radiation and measure the (back)scattered fraction. In order to retrieve useful information on the satellite observed radiation intensity, a mathematical relation has to be developed between the observation and the geophysical variable. A commonly used approach is the application of inverse methods. First, a theoretical, empirical or semi-empirical forward model is needed to describe the satellite observation as a function of different variables affecting the observation. For example, the satellite observed Top-of-Atmosphere (TOA) reflectance can be described as a function of e.g. snow covered area percentage (and other affecting factors) for each satellite pixel. Thereafter, remote sensing solves an inverse problem to retrieve the value of a geophysical variable, such as snow covered area, from a satellite observation. In its simplest, a forward model can be analytically inverted. Metaphorically, solving the inverse problem is like trying to determine the type of animal from its footprints. Alternatively, direct linear regression can be developed between the observation and the geophysical variable, if adequate ground truth data on geophysical variable is available for training the empirical algorithm.

In the optical (visible to near infrared) wavelength region remote sensing of snow is based on the very high albedo of snow compared to other natural surfaces (Warren, 1982). Passive optical satellite

instruments can have sufficiently high spectral, spatial and temporal resolution even for small-scale snow mapping purposes, but snow detection is still dependent on daylight and cloud-free conditions (Dietz et al., 2012; Frei et al., 2012; Nolin, 2010). Passive microwave techniques can also detect snow well, operate at night and through cloud cover, but their spatial resolution is coarse and mostly suitable for global applications. High resolution and insensitivity to clouds and daylight can be obtained using active microwave SAR data but the image interpretation is complicated and has limitations, such as that only wet snow cover can be distinguished from the snow-free terrain (Rees, 2006). Thus, finding a suitable instrument and method for snow detection is dependent on the purpose – e.g. regional instantaneous flood monitoring or global decadal climate data record (CDR) time series collection.

The potential of remote sensing in cryospheric and boreal applications is limited by uncertainty, especially concerning the data sets and interpretation methods (Rittger et al., 2013). For instance, applying only a single value for albedo over a broad region can lead to large errors in global energy estimates, and likewise, uncertainty in a snow extent estimate can penetrate into hydrological models (Rittger et al., 2013). A major issue common to most optical (and microwave) approaches in snow remote sensing is the problem of how to accurately detect snow in complex landscapes, under conditions of seasonal, patchy and melting snow, and especially in forested regions (Dietz et al., 2012; Dozier et al., 2009; Frei et al., 2012; Hall and Riggs 2007; Klein et al., 1998; Nolin, 2010). Regional airborne campaigns and high (spatial) resolution satellite data have been successfully used for algorithm development, validation and drainage basin scale research but they are not feasible for large scale operational monitoring purposes. There are spatially and temporally effective optical binary (snow/no snow) snow mapping methods (Hall et al., 2002; Helfrich et al., 2007; Ramsay, 1998), but over the extensive areas of seasonal snow their relatively large satellite footprint contains fractional snow and forest cover. Therefore, various linear unmixing (Painter et al., 2003; 2009; Vikhamar and Solberg, 2002; 2003), empirical and thresholding based (Hall et al., 2002; Salomonson and Appel, 2004; 2006) and inverse model based (Metsämäki et al., 2005; 2012; 2015) methods for mapping the fractional snow cover (FSC) within a satellite pixel have been developed (**PIV**). Compared to stand-alone satellite data-based methods, some combined methods require additional information (such as land cover data) or utilize *in situ* observations and/or modelling results together with remote sensing data as input (Frei et al., 2012). Whatever snow mapping method is applied, it is beneficial to include the consideration of uncertainty in order to facilitate correct data interpretation and a valid meaning for the obtained results.

When model-based inversion algorithm is used for the snow characteristics retrieval, the uncertainty of the retrieval results is dependent on the accuracy of the applied forward model. Therefore, it is essential to determine the uncertainty characteristics of the modelling approach e.g. through error propagation analysis. In contrast to that, in the case of linear regression algorithms, the uncertainty estimate can be obtained from the applied training data (*in situ* observations of the investigated geophysical variable). We focus here on fractional snow cover mapping using a forward model based inverse model. Thereby, we consider the modelling error of satellite observations next.

Even in highly controlled conditions the measurements of physical quantities, such as snow reflectance, are subject to uncertainties. Additionally, all models describing satellite observations include inaccuracies. Thus, when modelling a satellite observation, the uncertainty of the model representation of observation includes both the uncertainty of the actual measurement and that of the applied model[1]. Total (modelling) error of a satellite observation is a sum of these two elements, and it can be considered as a combination of a systematic error component and random (i.e. statistical) error component.

The error in forward modelling of satellite observations directly affects the quality of geophysical variable estimates (obtained by the applied inverse method). Using an error propagation analysis (Taylor, 1982), a random statistical uncertainty estimate of retrieval results can be calculated e.g. for snow covered area percentage using statistical accuracies of each constituent of the applied model as input information. In that case, only random error is included in the uncertainty estimation and the results only describe the precision, which does not necessarily describe the total error. Systematic uncertainty causes the results to be consistently either too small or too large, *i.e.* biased. Thus, estimates of geophysical variables also include both random and systematic components. Total error characteristics can be estimated using *in situ* observations on the geophysical variable under investigation (Fig. 2). However, the availability of the *in situ* data can be a limiting factor (Frei et al., 2012). This thesis defines how to estimate the systematic error of snow characteristics retrieval provided that both the total and statistical errors of the retrieval results (FSC estimates) are known. Further on, the assessed systematic error is used to derive an enhanced consideration of FSC product error.

Independent reference *in situ*, airborne, high resolution satellite and field spectroscopy data have been typically used to qualitatively validate and quantitatively assess the optical snow mapping accuracy, but actual quantitative uncertainty layers in snow products are rare (Dozier et al., 2009; Hall and Riggs, 2007; Metsämäki et al., 2015; Stroeve et al., 2005).

[1] Uncertainty characterizes how well the model represents the actual observation (range of ±values around the accepted truth/*in situ* reference) and should account for both components of the total error. Systematic uncertainty causes the model predictions to be consistently either too small or too large, *i.e.* biased. Random uncertainty is unpredictable and it cannot be deterministically determined. Accuracy is an expression of lack of error.

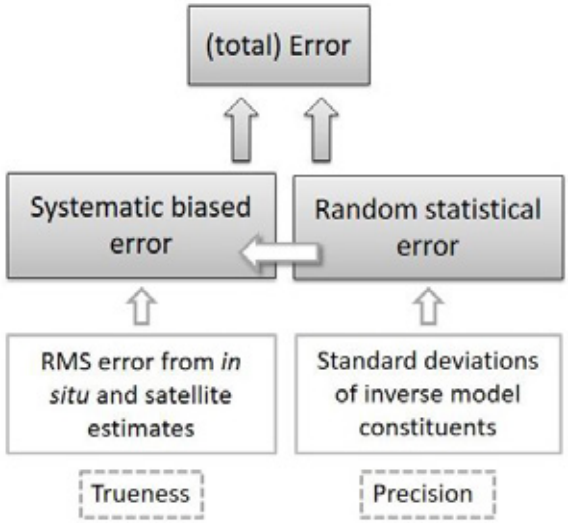


Figure 2. Uncertainty is a quantitative expression of estimation accuracy (e.g. in case of model inversion depending on how well the applied forward model represents the actual remote sensing observation) and it can be depicted by calculating a total error for the observed snow variable estimate. BIAS and RMSE are quantitative expressions of trueness. They are obtained by comparing multiple snow variable observations with reference *in situ* data. The inverse model constituent variability can be described quantitatively by assessing their standard deviation from the average value. Precision defines the closeness of individual estimates representing the same situation *i.e.* ground truth value of the investigated geophysical variable.

## 1.2 Objective of the thesis

The main objective of this thesis is to investigate how to improve snow monitoring methods in order to meet the needs of both operative hydrology and climate research applications. The work is conducted by (a) by experimentally determining reflectance characteristics essential for the forward and inverse modelling of boreal landscapes and (b) by analyzing satellite data retrievals of FSC (fractional snow cover) in order to derive statistical and systematic error characteristics of FSC estimates for the boreal zone. The focus is on optical remote sensing, which is well suited for determining snow extent in the melting season. Thus, the work aims at improving FSC retrieval algorithms and at characterizing the uncertainty in snow estimates and facilitating the improvement of the uncertainty considerations of the existing snow mapping algorithms. This is achieved by first employing an optical, semi-empirical, reflectance model-based *SCAmod* method to demonstrate the various factors affecting snow detection, and then, establishing a novel experimental method to analyze and quantify the amount of uncertainty. Specific objectives of the thesis are:

- Specification of the behaviour of wet snow, dry snow and snow-free ground reflectance in boreal forest utilizing field spectroradiometer measurements in northern Finland (**PI**).
- Determination and analyses of the behaviour of snow-free ground reflectance for the predominant non-forested land cover classes in central, eastern and northern Europe using satellite (MODIS) data (**PII**).
- Investigating the effect of boreal forest canopy to the observed scene reflectance using airborne and mast-borne spectrometer data together with high resolution information on forest (canopy) characteristics (obtained by airborne LIDAR data) in northern Finland (**PIII** and **PIV**).
- Investigating the effect of all error components on the satellite estimated GlobSnow Snow Extent (*i.e.* FSC-product) accuracy using a novel experimental analysis approach and a unique multi-temporal *in situ* FSC reference data set covering the region of Finland (**PV**).

## 2. Earths' surface reflectivity measurements and interpretation

The focus of this thesis is on determining the different factors affecting fractional snow cover (FSC) estimation accuracy using a semi-empirical reflectance model (Metsämäki et al., 2005). The scope is outlined in the following paragraphs, as only those concepts relevant to model-based approach, related data analysis and measurement set-ups handled in **PI-PV** are discussed. Note, that in **PI-PV** the used symbols to denote surface and Top-of-Atmosphere (TOA) reflectance are not consistent. In this summary for the thesis we use R to describe the TOA reflectance and symbol $\rho$ to describe surface reflectance observed by field and mast-based spectroradiometer, and also by airborne imaging spectrometer.

Earth-observing satellites provide unprecedented amounts of global reflectivity information also for remote and inaccessible regions. First, the obtained raw digital raster images need to be pre-processed; calibrated and geo-referenced, as they contain e.g. geometric and radiometric distortions (Rees, 2006). Raw data row and column numbers are geo-referenced with a known spatial location (e.g. latitude-longitude grid) using geolocation data typically provided within the satellite data. The satellite observed radiation intensity reflected from the land surface target is calibrated into a physical quantity such as Top-of-Atmosphere (TOA) radiance (unit of measure: W m-2 sr-1 nm-1) or TOA reflectance (unit of measure: dimensionless). Satellites typically use several discrete wavelength bands located in the visible and infrared region of the electromagnetic spectrum (e.g. MODIS instrument: 0.4 µm to 14.4 µm). The spatial resolution of different wavelength channels also usually varies, being e.g. either 250m, 500m or 1 km for a certain channel. Polar orbiting satellites used in snow remote sensing are typically on a sun synchronous orbit, where the illumination conditions remain similar for different images and their interpretation is more consistent. The spatial coverage, depending on swath width of the instrument, defines the frequency of the observations over a certain location. At high latitudes the instruments typically provide daily observations.

TOA reflectance can be converted to surface reflectance using atmospheric correction methods. However, in this work, atmospheric effects are not corrected (instead standard atmospheric values adjusted to regional conditions are used to shift ground-based reflectances to TOA reflectances, when relevant). TOA reflectances are applied since the employed inversion approach, the *SCAmod* method, is based on the use of TOA reflectances as a static atmospheric correction does not improve the quality of FSC estimates (Metsämäki et al., 2015). In the optical wavelengths, discriminating snow from clouds is difficult due to their similar spectral signatures. This work does not try to tackle the cloud discrimination problem, but instead cloud-free observations are selected.

Although satellite data pre-processing (geo-referencing and radiometric correction) and cloud screening are not emphasized in this thesis, the main pre-processing features for the thesis are summarized next concerning TOA or surface reflectance data. The processing of the satellite data in **PII** was conducted using the Finnish Environment Institute (SYKE) operational snow mapping system. Accordingly, Terra/MODIS Level-1B calibrated radiance products were obtained from NASA archives and converted to cloud screened TOA reflectances at SYKE, to be used in **PII**. The atmospheric and imaging geometry effects were taken into account in the analysis by using a large number of MODIS observations with varying viewing angles and atmospheric conditions. However, the largest (>50°) instrument viewing angles and highest (>75°) sun zenith angles were excluded, since the highest angles are excluded in typical satellite snow mapping algorithms.

In **PV**, ESA GlobSnow Snow Extent (SE) products on FSC (based on Envisat/AATSR TOA reflectances) were downloaded from the FMI Sodankylä satellite data center: www.globsnow.info (Metsämäki et al., 2015). These readily available FSC products were used in the analysis for **PV** instead of processing TOA reflectances. The GlobSnow processing system uses ESA provided Level 1B calibrated and geolocated reflectance data as input for radiometric solar illumination and topography correction and cloud screening at FMI. Then, the pre-processed reflectances are used to calculate the FSC products, yet only for observations at sun zenith angle < 73° due to otherwise occurring decrease in algorithm performance (Metsämäki et al., 2015).

In addition to the above mentioned satellite observations, airborne, mast-based and field spectral observations were utilized in the thesis. In **PI**, the key material is the field spectroradiometer-based reflectances, whereas mast-based reflectances are only used to show the effect of forest canopy to scene reflectance. In **PIII and PIV**, the principal data is the airborne imaging spectrometer-derived reflectance, whereas the airborne LIDAR data was utilized to obtain information on forest (canopy) characteristics. Additionally, in **PIII and PIV**, mast-based spectroradiometer measurements were used to analyse the bidirectional reflectance characteristics (*i.e.* sun and measurement angle bidirectional effects) of the snow covered forested terrain.

Both field and mast-based spectroradiometer observations were analyzed and calibrated to surface reflectances using a white Spectralon reference panel with known reflectance spectrum. Also, airborne observed radiances were cross-calibrated to reflectances using mast-based (Spectralon reference panel-calibrated) reflectance observations. A specific software was used to geometrically correct the airborne imaging spectrometer observations (**PIII** and **PIV**). Major part of the ground-based

observations were obtained at sun zenith angle range of 50°-75°(**PI**), when with mast-based observations, the range was 67°-73° (**PIII**) and 58°-75° (**PIV**). In **PIII** and **PIV**, the airborne imaging spectrometer data with sun zenith angle of about 68° was used.

The surface reflectances can be shifted to TOA reflectances using regional standard atmosphere characteristics when appropriate, e.g. in **PV** (Table 1) to facilitate their comparison with TOA reflectance based model constituents (Metsämäki et al., 2015). In **PI, PIII** and **PIV**, the correspondence of field observations with large scale scene reflectance was performed by using the field and mast-based surface reflectance observations.

## 2.1 Basic concepts of modelling, model inversion and statistical uncertainty analysis

In this thesis, uncertainties in fractional snow cover mapping by a semi-empirical reflectance model based *SCAmod* inversion method are investigated. The method was originally developed for fractional snow mapping in Finland representing boreal forested landscape (Metsämäki et al., 2005; 2012; 2015). After, the method was found to be feasible for hemispheric FSC detection, provided that the forest transmissivity information is available. Forest transmissivity describes how forest cover attenuates the incoming radiation and prevents the visibility to the underlying snow covered or snow-free forest floor. Accordingly, *SCAmod* algorithm considers this as a two-way forest transmissivity, obtained by reflectance observations under full dry snow cover, when the forest clearly stands out (Metsämäki et al., 2005). Also, the forest canopy and shadows contribute to the satellite observations. The European Space Agency's (ESA) Data User Element (DUE) project GlobSnow implemented *SCAmod* inversion method to provide and maintain a global database of Snow Extent (SE) products on Fractional Snow Cover (FSC). The *SCAmod* inversion model originates from a radiative transfer theory based forward model, which describes the satellite scene reflectance as a mixture of partially transparent forest canopy, snow and snow-free ground that are interrelated through forest transmissivity and snow fraction (Metsämäki et al., 2005; 2015). FSC can then be derived by inverting the forward model. Fig. 3 depicts the forward and inverse model concepts in snow remote sensing. The *SCAmod* method is sensitive to the representativeness of the applied parameters, which are generally applicable predetermined reflectances of thick opaque forest canopy, (wet) snow and snow-free ground reflectance, and two-way transmissivity. Therefore, this thesis focuses first on determining the reflectance characteristics essential for the forward and inverse model and then investigating the effect of all the error components on the satellite estimated GlobSnow Snow Extent (*i.e.* FSC-product).

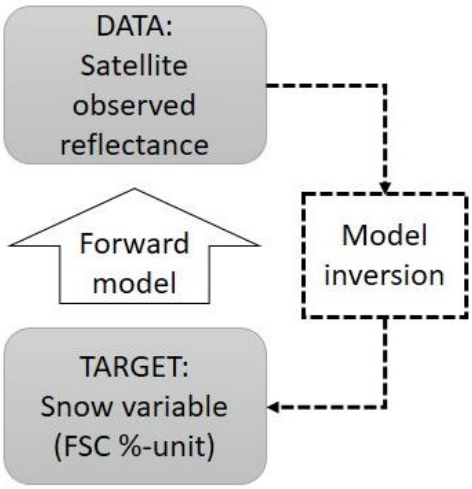


Figure 3. Description of forward and inverse problem (dashed lines) in satellite data-based snow remote sensing. First, a forward model is developed, e.g. a radiative transfer model, where all the factors affecting the observed satellite reflectance of a snow covered landscape are included. Secondly, using an inverse retrieval model, the geophysical snow variable, such as Fractional Snow Cover (FSC), is obtained for each satellite pixel.

In general, a forward model of space-borne observations for a single channel (wavelength band) of observation can be given by

$$y = f(x_1, x_2, \dots, x_n, p_1, p_2, \dots, p_n) + \epsilon \qquad (1)$$

where

$y$ is the (calibrated) space-borne observation (e.g. Top-of-Atmosphere (TOA) reflectance),

$x_1, x_2, \dots, x_n$ denote the geophysical variables (e.g. FSC),

$p_1, p_2, \dots, p_n$ are the parameters affecting the observations (e.g. wavelength of observation, observation geometry, forest coverage on pixel under investigation etc.),

$\varepsilon$ is the uncertainty of space-borne observation $y$ (including all error contributors).

In its simplest, the estimation of one geophysical variable can be obtained by inverting Equation (1):

$$x = f^{-1}(y, p_1, p_2, \dots, p_n) \qquad (2)$$

where parameters $p_1, p_2, \dots, p_n$ are known. The *SCAmod* method is essentially a single channel algorithm according to Equation (2).

On the other hand, if extensive training data (e.g. concurrent *in situ* observations of FSC covering the satellite image) are available, a simple regression model can be used. The linear case corresponding to Equation (2) yields:

$$x = a \cdot y + b \qquad (3)$$

where *a* and *b* are the regression parameters obtained by fitting a regression line between the observed geophysical variable values and corresponding space-borne observations.

The benefit of linear regression is that uncertainty of estimates can be obtained. However, the algorithm cannot be (reliably) extrapolated outside the validity range (e.g. spatial or temporal) of training data.

In case of Equation (2) the statistical accuracy of estimates can be evaluated through error propagation analysis (for any model), if variabilities (standard deviations from the averages) of parameters $p_1, p_2, \dots, p_n$ are known (Taylor, 1982). That leads to:

$$\Delta x = \frac{\partial f^{-1}(y, p_1)}{\partial p_1} \cdot \Delta p_1 + \frac{\partial f^{-1}(y, p_2)}{\partial p_2} \cdot \Delta p_2 + \dots + \frac{\partial f^{-1}(y, p_n)}{\partial p_n} \cdot \Delta p_n \qquad (4)$$

where

$\Delta x$ is the statistical accuracy of the estimated value of geophysical variable (e.g. $\Delta x$ = ΔFSC),

$\Delta p_n$ is the standard deviation of parameter *n* (e.g. snow-free ground reflectance),

$\frac{\partial f^{-1}(y, p_n)}{\partial p_n}$ denotes the sensitivity of inverse model to change in parameter $p_n$ when the satellite observation (TOA reflectance) shows the value *y*.

Equation (4) is the basis of uncertainty considerations in this thesis. Fig. 4 clarifies why Equation (4) can be used to calculate the statistical error *i.e.* how the error in the estimated geophysical variable is dependent on the likely change/variability in the utilized model parameter value.

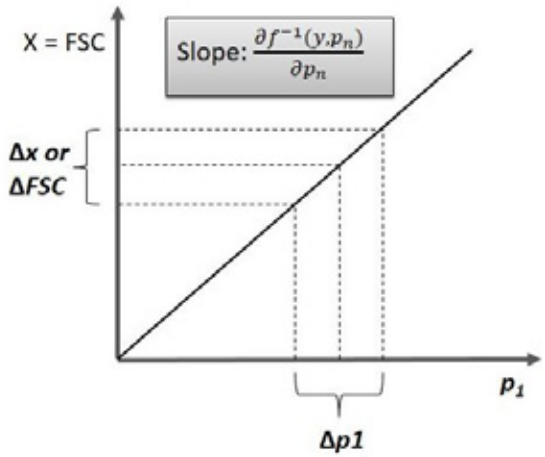


Figure 4. The derivative in Equation (4) corresponds to the sensitivity of the inverse model (with satellite observation *y*) to the change in the utilized parameter value (e.g. snow-free surface reflectance). The uncertainty in parameter value $p_1$ leads to uncertainty in FSC estimate depending on the sensitivity of inverse model to change in $p_1$ (slope of the solid line in graph). The *SCAmod* inverse model applied in this work for the FSC retrieval is non-linear with respect to model parameters. Hence its sensitivity to parameters varies with the level of the parameter value, *i.e.* the shown solid line is actually a curve for high ranges of $p_1$, refer to Chapters 2.3 and 3.1.

## 2.2. Landscape reflectance and its modelling

### 2.2.1 Surface reflectance and satellite observed TOA reflectance

A single satellite instrument observes the landscape target at one viewing angle. Typically, satellite observations are given as reflectance, which corresponds to the isotropic reflectance of Lambertian surface, *i.e.* being a completely diffuse reflector. In this case, the direction of the satellite observation makes no difference. Yet, nearly all natural surfaces are anisotropic reflectors. Thus, for example, determining the spectral and angular structure of snow's Bidirectional Reflectance Distribution Function (BRDF) is important (Painter and Dozier, 2004; Warren, 1982). The BRDF signifies how much of the incident radiation (irradiance *E*) from a specific direction is reflected (radiance *L*) to another specific direction. Therefore, BRDF describes the reflectivity of a landscape target as a function of illumination geometry and viewing geometry, and requires the knowledge of azimuth and zenith angles for directional information (Pellikka, 1998). BRDF is the baseline quantity, from which all the other reflectance values (quantities) can be calculated. So, if the BRDF of snow covered landscape is known, albedo can be calculated by integrating BRDF over all the other directional angles. BRDF and consequently reflectance depends on the wavelength, surface structure (e.g. snow surface roughness,

texture, impurity concentration, grain morphology and liquid water content) and optical properties (e.g. shadowing, scattering, reflection, absorption and emission).

Nicodemus et al. (1977) defined the reflectance terminology based on the incoming and reflected radiance geometry, whereas Shaepman-Strub et al. (2006) continued the work by demonstrating the proper usage of the different surface reflectance quantity terminology common in remote sensing. For instance, Hudson et al. (2006) and Painter and Dozier (2004) measured and defined reflectance quantities for snow targets. In this work, the measured diffuse (cloudy conditions) surface reflectance quantity approximates the hemispherical-conical reflectance factor, whereas the direct (clear sky conditions) surface reflectance approximates the biconical reflectance factor (**PI**, Fig. 3). These definitions are approximations to describe the illumination geometries of the measurable reflectance quantities as in natural conditions the irradiance is not completely hemispherical or directional but a mixture of the both (and depending on the wavelength). The surface reflectance values in **PI** are given as reflectances equivalent to Equation (5), which is a typically used definition of satellite-observed TOA-reflectance. That is, the reported values in **PI** are converted to directional-hemispherical surface level reflectances, assuming that the target is a Lambertian surface, which it is not, in reality. The conversion of the measured quantity to a conceptual quantity is relevant in order to facilitate the comparison between the surface reflectance (reverse atmospheric correction to TOA values also necessary) and space-borne reflectance.

As mentioned above, albedo calculations are not included in the scope of this thesis. Fig. 5 depicts the sun-satellite measurement geometry and related illumination characteristics. In remote sensing, BRDF is often necessary for pre-processing, corrections and image interpretation. In this thesis BRDF is not analysed. The relation between BRDF and reflectance characteristics are described in **PI.**

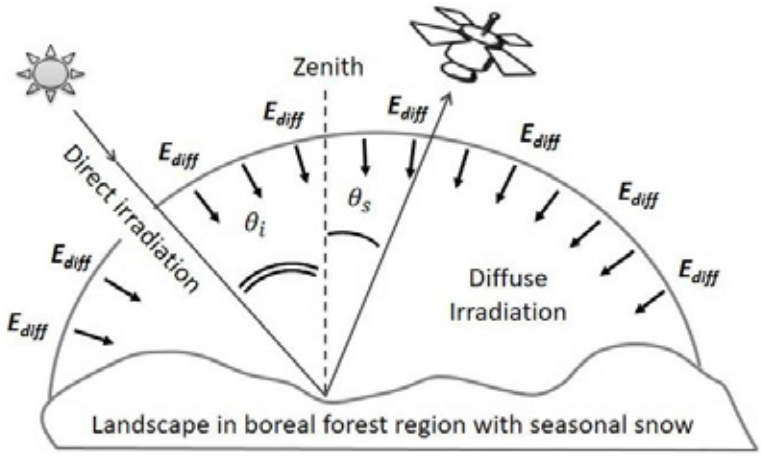


Figure 5. Representation of the sun-satellite measurement geometry of a planar (non-mountainous) landscape. $\theta_i$ is the incidence angle of incoming irradiance (solar zenith angle) and $\theta_s$ is the angle of observation. To simplify,

azimuth angles are not depicted. The landscape surface reflectance can be considered to consist of measurements under direct illumination from the Sun (bidirectional case) and under diffuse $E_{diff}$ illumination (hemispherical-directional case), *i.e.* incoming light from other parts of the sky and/or under cloudy conditions. Note that to be exact both Sun and the satellite instrument occupy a certain spherical angle, but are close to the directional case.

A satellite observation is close to the measurement of BRDF for a certain bidirectional angular composition (if diffuse illumination is small compared with the direct illumination). Note that a satellite measures above the atmosphere and thus the incoming irradiance can be regarded as a direct beam from the Sun and the planet (atmosphere-Earth system) as a surface. Typically, a satellite observation is considered as reflectance with a Lambertian surface assumption (surface is as bright to any direction independent of the angle of incoming radiation). In that case the TOA-observed reflectance is simply:

$$R_{TOA} = \pi \frac{L_{obs}}{E_0 \cos(\theta_i)} \quad (5)$$

where

$R_{TOA}$ is the Top-of-Atmosphere reflectance

$\pi$ is a factor related to Lambertian surface

$L_{obs}$ is the satellite-observed (TOA) radiance

$E_0 \cos(\theta_i)$ is the incoming radiance projected to the surface, the Sun zenith angle of incident radiation is $\theta_i$ (TOA-value).

In case of surface (or at the tree-top level) values we can write Equation (5) using symbol $\rho$ instead of $R$. Fig. 6 clarifies the typical observation geometry and resulting reflectance definition when using an optical satellite instrument.

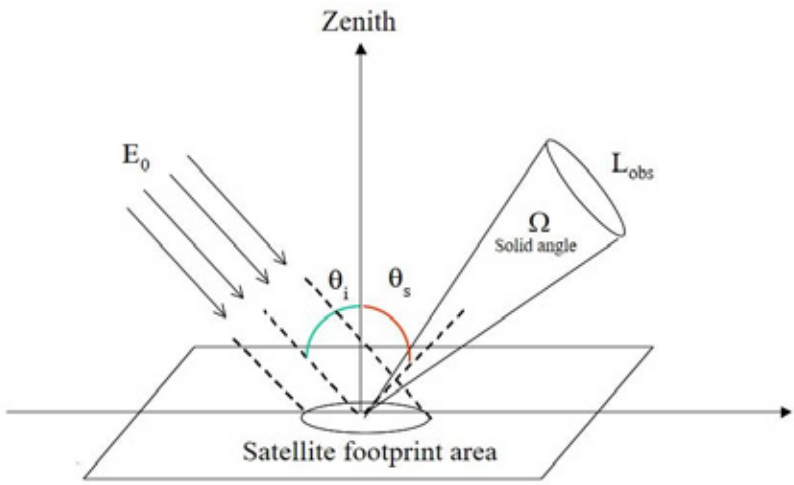


Figure 6. Schematic representation of a satellite measurement. $\theta_i$ is the incidence angle of incoming irradiance and $\theta_s$ is the angle of observation. The incoming irradiance $E_0$ is projected to the Earth's surface (satellite footprint area) with the magnitude of $E_0\cos(\theta_i)$. The reflected radiance $L_{obs}$ is measured by the satellite instrument viewing angle (*i.e.* the radiant flux per unit solid angle $\Omega_{solid\ angle}$). The ratio between the reflected and incoming radiation is given by reflectance according to Equation (5). The azimuth angle is omitted for simplicity.

### 2.2.2 Forested landscape reflectance under snow-covered and snow-free conditions

In the following sub-chapters, the main elements affecting the seasonally snow covered and forested landscape reflectance observations using optical satellite instruments are specified. The reflectance of a forested terrain is contributed by (a) snow reflectance, b) snow-free ground reflectance, (c) forest canopy reflectance and (d) transparency of the forest cover. The effect of snow on canopy (on the reflectance) is considered in **PIII** but it is not further discussed here as the Thesis focuses on snow monitoring on the melting season, when canopy is typically snow-free. The reflectance of snow is primarily studied here using field spectrometer observations in northern Finland, whose measurement set up corresponds to the typical measurement geometry employed by optical satellite instruments (**PI**). Snow-free ground reflectance is investigated by developing a time series analysis method to detect the valid reflectance observation to represent snow-free conditions right after the last traces of snow have disappeared. The results were obtained by using a pixel-wise multi-temporal satellite data set from a large European study area during the snow melt season (**PII**). Forest canopy reflectance and forest canopy transparency (transmissivity) characteristics were obtained by analyzing airborne imaging spectrometer data together with high resolution airborne lidar observations under full dry

snow cover conditions (**PIII** and **PIV**). In Fig. 7 the dominant scattering properties of boreal forest landscape elements are illustrated. The Earth's surface can be thought as a surface when observed from a large distance, such as from a satellite instrument using optical wavelengths.

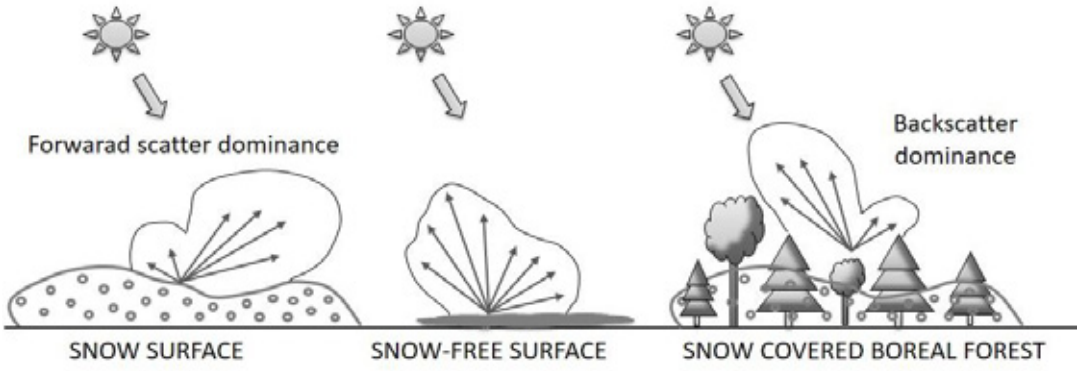


Figure 7. Schematic illustration on the different scattering properties of typical landscape elements in the boreal forest region. For snow, forward scattering is dominant. Depending on the snow-free ground surface type, its scattering properties can vary between forward, complex and backward scattering. Snowy forest is considered as a target, where backscatter dominates the overall scattering (**PIV**; Pellikka, 1998; Peltoniemi et al., 2005).

#### *2.2.2.1 Effect of snow: reflectance characteristics by field and laboratory spectroscopy*

**PI** investigates the behavior of dry and wet snow reflectance based on field spectroscopy campaigns carried out in Sodankylä, northern Finland during the spring winter periods of years 2007 and 2008 (Figs. 8 and 9). Additionally, reflectance of snow-free terrain directly after the snow melt was measured concerning typical landscape features of the boreal forest zone including mineral soil sites, open bogs and other peat lands. These experimentally observed reflectance characteristics are further exploited in **PIV** and **PV**, and in Metsämäki et al. (2015), in order to assess the accuracy of FSC retrieval from satellite data.

The measurement principle was to record the radiance reflected to nadir direction under conditions of total cloud cover representing diffuse lighting conditions and clear sky with dominating direct Sun irradiance that had a moderately varying solar zenith angle range from 50° to 75° (Fig. 9). The spectral radiance measurements at wavelengths from 350 to 2500 nm were calibarated to reflectances by applying reference measurements of a white Spectralon panel, resulting to surface level-observed reflectances, similar to those values given by Formula (5) in the case of TOA reflectances.

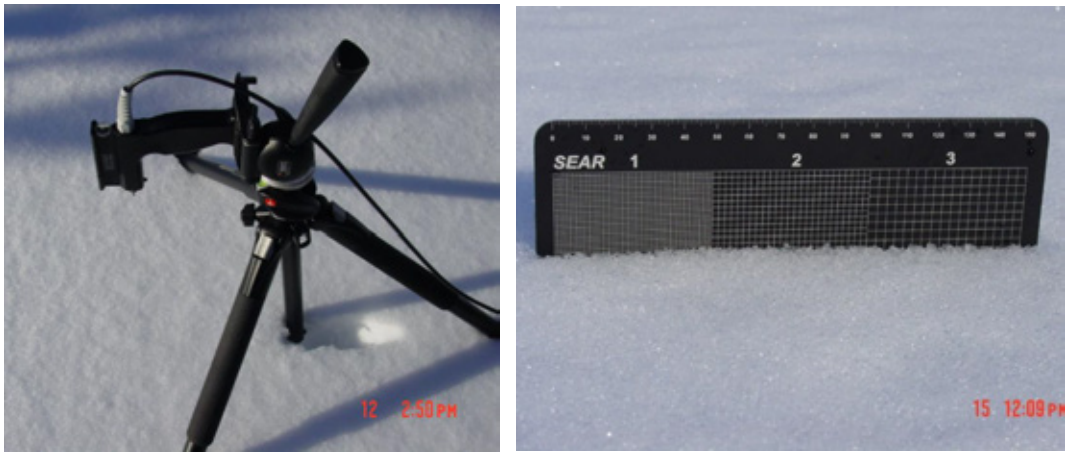


Figure 8. (Left) An example of a field measurement set up of a portable Analytical Spectral Devices (ASD) Field Spec Pro JF spectrometer. The measurement head was mounted on a tripod and the instrument optic cable inside was set to look at nadir (0°) direction with 25° field of view (FOV). The resulting footprint area of the measured snow target is around 20 cm in diameter. Calibrated white optical panel with known reflectance spectrum was used as a reference. (Right) Snow grain size was visually estimated by comparing a snow sample to a snow crystal screen with 1, 2 and 3-mm-grids.

Figure 9. Field spectroradiometer measurement campaign sites in Sodankylä, northern Finland (Left) open sparsely forested bog on 18 April 2007 under direct illumination and (Right) pine dominated forest stand on 27 April 2007 under diffuse illumination. Both the sites were measured under melting snow conditions.

The snow reflectances were investigated in particular for the blue (436-449 nm and 459-479 nm), green (545-565 nm), (yellow-)red (580-680 nm) and infra-red (1628-1652 nm) bands, as these wavelengths are relevant for satellite snow cover monitoring applications using such instruments as MODIS, MERIS

and AVHRR demonstrated in **PI** (as well as for more recent instruments). The obtained snow reflectances indicate that the wet snow reflectance at visible bands is lower than that of the dry snow (close to 1.0 or 100% for dry snow). The visually observed top-layer snow grain sizes for these two categories varied from 0.2 to 2 mm for dry snow and from 0.5 to 3.5 mm for the wet snow, respectively. An important finding was that for wet snow layers thinner than 20 cm the ground below the snow particularly decreases the reflectance, which is highly relevant for FSC estimation from satellite data (Fig. 10). Based on the results of **PI,** the snow reflectance level currently used in *SCAmod* algorithm (used in FSC retrieval for different sensors), was selected to correspond to the observed level of wet snow reflectance. Note that in *SCAmod* investigations the surface level snow reflectance from **PI** is shifted to TOA reflectance using a standard atmospheric propagation approach adjusted to Finnish springtime conditions (Metsämäki et al., 2015). **PV** contains a table of all the currently used *SCAmod* parameter values (**PV**, Table 1). Concerning the use of snow field spectrometry results for FSC retrieval algorithm a relevant aspect is that patchy snow cover (FSC<100%) occurs with wet melting snow conditions. Therefore, wet snow reflectance is selected instead of dry snow as model parameter. On the other hand, for full dry snow cover the used smaller wet snow reference reflectance in *SCAmod* only yields an FSC estimate higher than 100%, which is cut to the 100% top ceiling value. That is, dry patchy snow occurs only seldom or at night with colder temperatures compared to daytime, so there will be no problem in snow detection using the wet snow reference value as model parameter instead of dry snow.

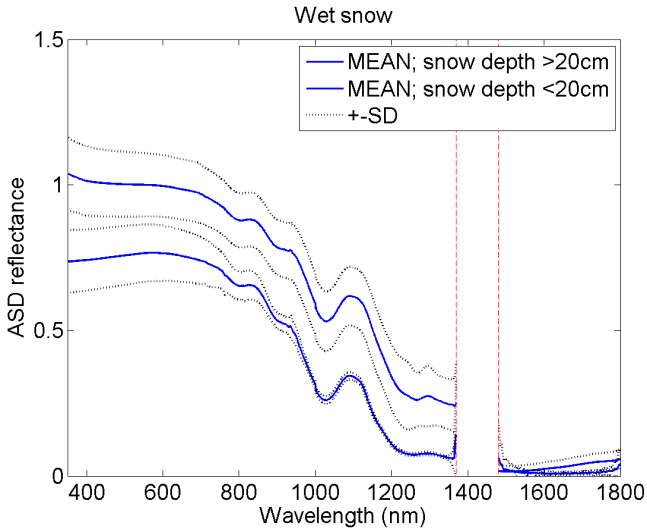


Figure 10. Field spectroradiometer ASD observations of mean reflectance ±standard deviation for wet snow in cases where snow depth is either above or below 20 cm. Results include both direct and diffuse illumination conditions. The wavelength area around 1400 nm is affected by an insufficient signal-to-noise ratio. This figure is adapted from **PI**, ©2009 Elsevier.

**PI** does not analyze the BRDF characteristics of the snow surface. Based on literature, the forward scattering dominates over the backscatter (Hudson et al., 2006; Painter and Dozier, 2004). As the measured surface is thought to be Lambertian in Equation (5), but the snow BRDF is actually anisotropic, the snow surface reflectance calculated according to Equation (5) can yield values higher than 1.0 also for nadir measurement angles (as in **PI** and Painter and Dozier (2004)).

#### *2.2.2.2 Effect of snow-free terrain: reflectance characteristics after snow melt*

The developed method to determine the snow-free ground reflectance after snow melt is based on the analysis of multi-temporal MODIS images during the ablation period (**PII**). The principle of the analysis was the investigation of pixel-wise time-series of MODIS TOA-reflectance for different non-forested or sparsely forested land cover categories. An example of the pixel-wise time-series of TOA reflectance for different MODIS bands is presented in Fig. 11. The example shows a typical behaviour observed for a pixel representing sparse vegetation and tundra (GlobCover Class 150). In total there were 728 pixels representing class 150, for which the analysis was carried out (the criteria in pixel selection was that the area surrounding the pixel should represent the investigated land cover category within a region of 1.5 km x 1.5 km, and that a sufficiently long time-series of satellite observations was available). The analysis was performed in the region depicted in Fig. 12 for different GlobCover classes (Bontemps et al., 2009) including: Agricultural areas/steppe (20), Tundra/Sparse vegetation (150), Wetlands (180), Rainfed croplands (14), Mosaic vegetation/cropland (30), Mosaic forest or shrubland/grassland (110) and Grassland (141). Fig. 12 shows the obtained reference map of snow-free ground reflectance (TOA) directly after the snow melt indicating the mean values of reflectance of each land cover category. A similar map was obtained for the standard deviation of reflectance.

The developed algorithm estimates the snow-free ground reflectance directly after the snow melt. That moment is the point in time when the TOA reflectance observed at the MODIS channel 4 (545-565 nm) drops to its minimum value (in a window of 15 days after the moment when the operational *SCAmod* FSC retrieval algorithm has indicted that FSC has reached the zero value for the pixel under investigation). The snow-free ground reflectances at MODIS channel 4 were also provided by applying a forest canopy transmissivity correction as the apparent forest canopy transmissivity was available for this specific channel.

The motivation in the analysis of snow-free ground reflectance was to improve the performance of *SCAmod* algorithm. The results indicated that some improvement can be achieved by using the spatially varying snow-free ground reflectance according to land cover type. However, the results indicated that the constant value of 0.10 operationally applied with the *SCAmod* (Metsämäki et al., 2015) is a good

overall characteristics in the investigated European domain. Concerning the analysis of statistical error characteristics of FSC estimation the results of **PII** gave a fundamental insight.

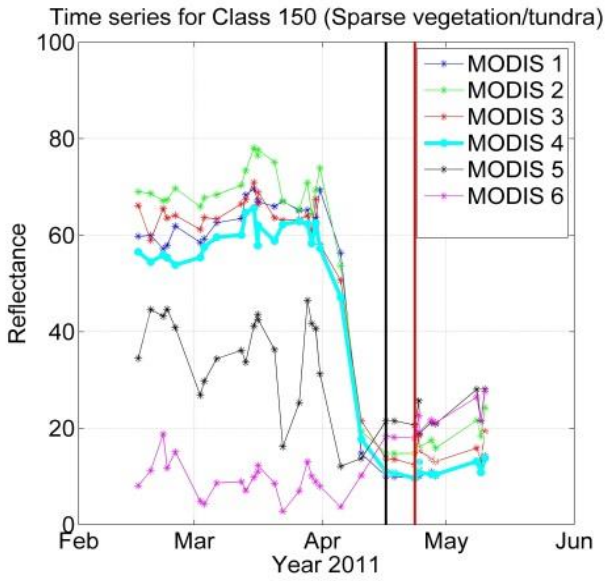


Figure 11. An example of a typical pixel-wise MODIS reflectance time-series used for the determination of snow-free ground reflectance directly after the snow clearance. Black vertical line depicts the moment of estimated snow melt according to operational *SCAmod* algorithm (first observation with FSC=0%). Red vertical line indicates the moment of the extracted snow-free ground reflectance estimates, *i.e.* detected by the minimum value of MODIS band 4 reflectance within the window of 15 days (note that MODIS band 4 time series is highlighted). Also note, that *SCAmod* algorithm, when operationally applied to MODIS data, employs the band 4 (545-565 nm). This figure is adapted from **PII**, ©2013 Elsevier.

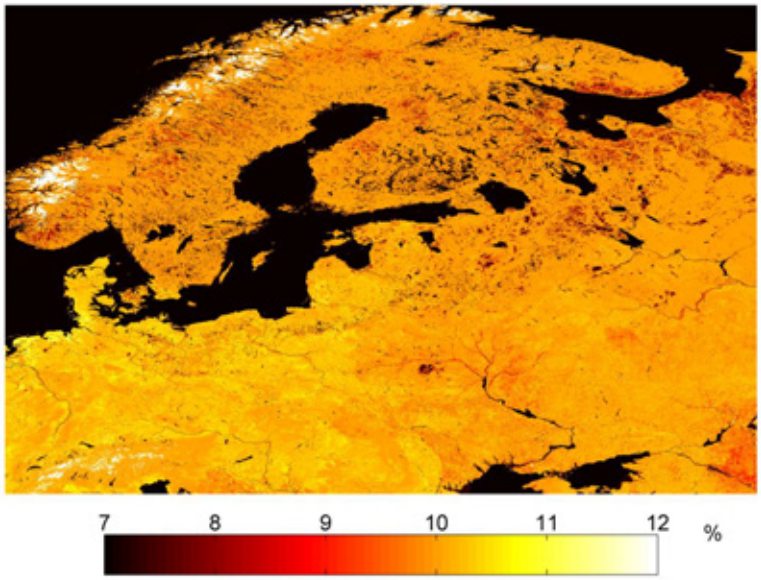


Figure 12. Retrieved map of TOA reflectance of (non-forested or sparsely forested) snow-free ground at the MODIS band 4 (545-565 nm) covering the European study region (**PII**). Snow/ice covered regions are shown by white colour. Note that their reflectance is much higher than the image threshold value of 12%. Forests cover 46.38 % of the total land area. The forest floor reflectance of these areas is considered with a constant value of 10 % (0.10), which is based on the investigations of boreal forests in Sodankylä (**PI**, **PIII** and **PIV**). This figure is adapted from **PII**, ©2013 Elsevier.

#### *2.2.2.3 Effect of forest canopy: reflectance characteristics based on radiative transfer approach*

Results of **PIII** and **PIV** indicate that in case of boreal forests the effect of forest canopy can be described by a simple non-linear radiative transfer approach with a partially transparent scattering (reflecting) canopy (Fig. 13). The results of the two papers show that this concept is valid even without considering the effects of forest openings (**PIV,** Table 3). Forest canopy effects (such as extinction and reflectance) on the scene reflectance were determined by analyzing airborne imaging spectrometer data under full dry snow cover conditions. This analysis was enabled by the detailed tree coverage information derived from lidar observations. The results indicate, that forest canopy constituents can be considered to be distributed equally over the image footprint area for visible band observations (without considering gaps between the trees), see Fig. 13. On the other hand, **PIV** shows that an often applied linear mixing model does not perform as well as the simple radiative transfer model (note that a linear mixing model to treat forest canopy was also investigated in **PI**). A liner mixing model considers a forested landscape as combination of gaps (canopy openings) and non-transparent (opaque) tree foliage. One important

finding was that backscattering dominates the overall observed reflectance of a forested landscape (**PIV**, Fig.8).

A zeroth-order solution of a radiative transfer formula provides the following Equation (6) for the reflectance of forested terrain (**PIV)**:

$$\rho(\lambda) = \rho_{surface}(\lambda)t(\lambda)^2 + (1 - t(\lambda)^2)\rho_{forest} \qquad (6)$$

where

$\rho(\lambda)$ is the reflectance of the forested terrain at wavelength $\lambda$ (note that angles are omitted here for simplicity)

$\rho_{surface}(\lambda)$ is the reflectance of forest floor surface (snow covered, snow free or patchy snow cover)

$t(\lambda)^2$ is the two-way forest canopy transmissivity (transparency) in the angles of incoming irradiance and sensor viewing angle

$\rho_{forest}(\lambda)$ is the reflectance of a thick non-transparent (opaque) forest.

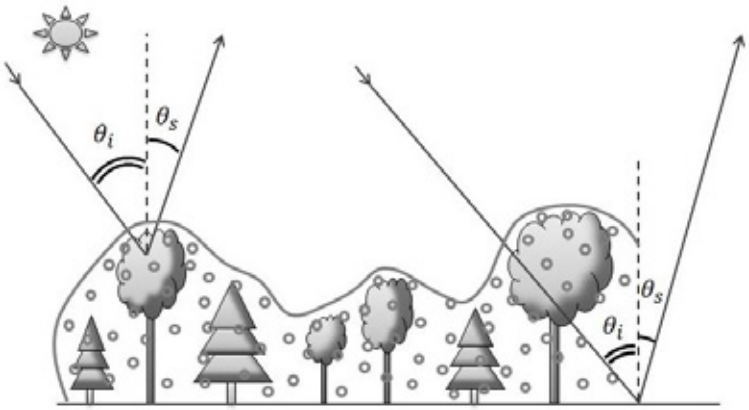


Figure 13. Geometrical consideration of the reflectance of a forested landscape. The forest canopy is partially transparent, which can be described by canopy transmissivity (**PIII** and **PIV**). $\theta_i$ is the incidence angle of incoming irradiance and $\theta_s$ is the angle of observation. The forested scene observed by satellite instrument can be considered as a single turbid layer, where forest gaps are not directly considered – but instead, the forest opening information is taken into account by using the forest transmissivity. The figure is modified after **PIV.**

To summarize, the Earth's surface is not, in fact, a surface even in the optical wavelengths, but specifically vegetation such as boreal forest forms a partially transparent layer. This complex structure can be described in a simplified manner by using radiative transfer approach. In the simplified approach the incoming radiation is thought to reflect to observation direction from forest floor and different canopy constituents within the foliage, branches and trunks (including multiple scattering within the forest layer). This simplification to consider forests in a pixel as a uniform turbid layer enables the development of a simple semi-empirical forward modeling of scene reflectance and the model inversion, see Chapters 2.2.3 and 2.3 below.

### 2.2.3. Semi-empirical modelling of landscape TOA reflectance

Based on empirical observations of (a) reflectance snow free terrain, (b) reflectance of snow and (c) radiative transfer approach for forest canopy effects we can construct a simple semi-empirical model (Metsämäki et al., 2005; 2012) corresponding to Equation (1):

$$y = R_{TOA}(\lambda) = R_{TOAground}(\lambda)t_{apparent}(\lambda)^2(1 - FSC) + R_{TOAsnow}(\lambda)t_{apparent}(\lambda)^2 FSC + \left(1 - t_{apparent}(\lambda)^2\right)R_{TOAforest} \quad (7)$$

where symbol *R* is used instead of $\rho$ as the model describes *TOA* reflectance instead of ground based reflectances ($\rho$ in Equation (6)). Thus, all reflectance contributions as well as the apparent forest canopy transmissivity ($t_{apparent}$) are Top-of-Atmosphere observed values. If FSC = 0 or FSC = 1, Equation (7) reverses back to Equation (6).

The parameters of the semi-empirical scene/landscape TOA reflectance model can be derived from different data sets as described in Chapters 2.2.2.1 – 2.2.2.3 above. Additionally, satellite data itself can be used to derive model parameters. The parameter $R_{TOAforest}$ (reflectance of the opaque, non-transparent, forest canopy) can be approximated by investigating TOA-reflectances from pixels having the highest forest density (full coverage). Similarly, the two-way forest canopy transmissivity ($t^2_{apparent}$) can be estimated from the observed TOA-reflectances obtained at full snow cover conditions (FSC = 1) by fitting the model of Equation (7) to the observed refelectance at the channel under investigation when all other parameters than $t^2_{apparent}$ are known (Metsämäki et al., 2005; 2012).

As a summary, the semi-empirical modelling provides a feasible method to describe satellite observations with as few parameters as possible, which enables a robust model inversion to map FSC reliably in a global scale (Metsämäki et al., 2015), see Chapter 2.3. below.

## 2.3. Retrieval of geophysical parameters by model inversion

The Globsnow product for estimating FSC from ENVISAT AATSR data in **PV** is based on the employment of the *SCAmod* method (Metsämäki et al., 2005; 2012). *SCAmod* is based on Equation (2) above. That is, the forward model of TOA-reflectance according to Equation (7) is inverted and we obtain:

$$x = FSC = f^{-1}(R_{TOA}) = \frac{\frac{1}{t_{apparent}^2} R_{TOA} + \left(1 - \frac{1}{t_{apparent}^2}\right) R_{TOAforest} - R_{TOAground}}{R_{TOAsnow} - R_{TOAground}} \quad (8)$$

The Globsnow product applies only one Envisat/AATSR channel of observation (at the center wavelength $\lambda = 545 - 565$ nm) for the actual FSC estimation according to Equation (8), other channels are only used for cloud screening and for eliminating certain low/mid-latitude non-snowy surfaces.

**PIV** shows that the overall concept of the *SCAmod* is valid. That is, the simple semi-empirical model and its inverse solution to estimate FSC describe realistically the scene and landscape-level reflectance and, in particular, the effect of forest on the reflectance. The limitations of the robust approach include that it cannot be used for observation angles highly tilted from the nadir. The Globsnow SE product on FSC is limited to satellite observation angles close to nadir, and as the swath width of AATSR is only 500 km, the maximum accepted Sun zenith angle is 73° (Metsämäki et al., 2015).

# 3. Accuracy of snow cover retrieval

The error of FSC estimation can be considered to include both a systematic and statistical (random) component. The systematic component arises from the fact that any forward and inverse model, such as in Equations (7) and (8) investigated here, is not an exact representation of the true situation, but merely an approximation. If knowledge of the average value of some model parameter is not exactly correct, the error in it causes a systematic error in the FSC estimates obtained by using the inverse model according to Equation (8). On the other hand, an approximate model includes parameters the values of which vary spatially or temporally (i.e. are not constant), such as ground reflectance after the snow melt. The spatial and temporal variability of parameters can be described by their standard deviation from the average value. This variability causes the statistical (random) error component of FSC estimates. Fig. 14. depicts the behavior of different error components of FSC estimation.

Statistical error can be treated with error propagation analysis (Taylor, 1982), see Equation (4), if standard deviations and average values of model parameters are known (*i.e.* there are proper measurements on their values). Systematic error can be analysed through *in situ* reference data on the geophysical variable under investigation (e.g. FSC), if such data sets are available (as in this thesis). Note that the difference between the observed *in situ* value and the estimated value of, for example, satellite data based fractional snow cover percentage, is denoted as residual. Root-mean-square error (RMSE) is a quantitative measure of the differences between the observed and estimated values.The combined consideration of statistical and random errors allow the determination of total (product) error according to the concept of Fig. 2 above. These aspects are discussed next in Chapters 3.1. and 3.2.

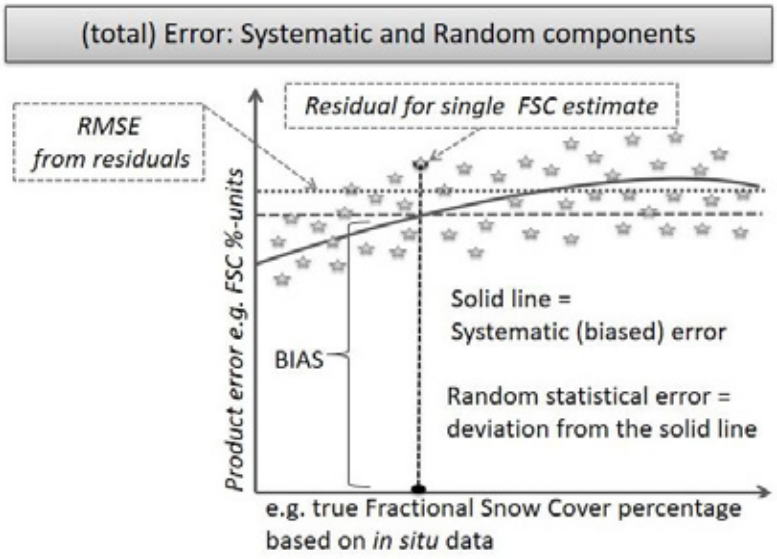


Figure 14. Schematic diagram on the behavior of different error components of FSC estimation. Statistical error describes the random variability resulting from the spatial variability of inverse model parameters, such as the spatial variability of snow-free ground reflectance (from the typical average) for a certain land cover category. Systematic error component and BIAS result from the (unknown) systematic inaccuracy of the applied model. Note that the systematic error from RMS sum of residuals may vary as a function of some variable, whereas BIAS is only one average value of residuals over a set of observations.

## 3.1. Statistical accuracy based on landscape reflectance contributors' characteristics

The theory of error propagation analysis according Equation (4) provides a technique to assess the statistical error of FSC estimates (Taylor, 1982). The GlobSnow FSC product is based on the employment of *SCAmod* approach (Metsämäki et al., 2005). In that case Equation (4) is directly applied to Equation (8). The challenge is, however, how to estimate the average values and fluctuations (standard deviations) of inverse model (according to Equation (8)) parameters, which are:

- Reflectance of the thick (opaque) forest canopy, $R_{TOAforest}$ in (8)
- Apparent forest canopy transmissivity $t_{apparent}$ in (8)
- Reflectance of the snow covered ground before melt-off, $R_{TOAsnow}$ in (8)
- Reflectance of the snow-free ground after melt-off, $R_{TOAground}$ in (8).

Chapters 2.2.2.1 – 2.2.2.3 above describe how the values of these model parameters are investigated and derived in this work.

In practice, the statistical error varies both spatially and temporally depending on landscape physical characteristics of the pixel under investigation (about 1 km x 1 km in case of ENVISAT AATSR-based Globsnow FSC product). Additionally, the level of FSC influences on the statistical accuracy. This is illustrated in Fig. 15. The analysis of statistical error can be performed to any pixel of GlobSnow FSC product, and separately for any individual product. An example of that is shown in Fig. 16: The spatial maps of estimated statistical error and the corresponding estimated FSC. The maps are composites for a period of 14 days (each pixel value is obtained from the first non-cloudy observation during the period).

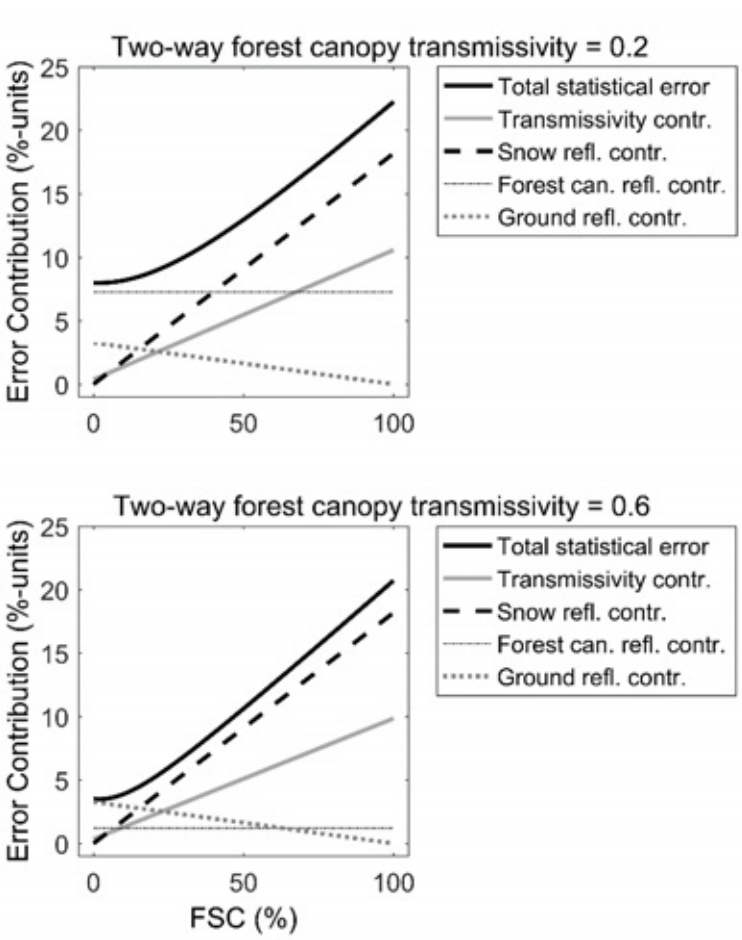


Figure 15. Statistical error component of FSC estimation and its contributors for two typical cases of boreal forest (y-axis: error standard deviation in FSC percentage units) as a function of FSC. Forest canopy transmissivity corresponds to dense (Upper panel) and sparse (Lower panel) boreal forests. The statistical error component and its contributors are determined according Equation (2). This figure is adapted from **PV**, ©2017 Elsevier.

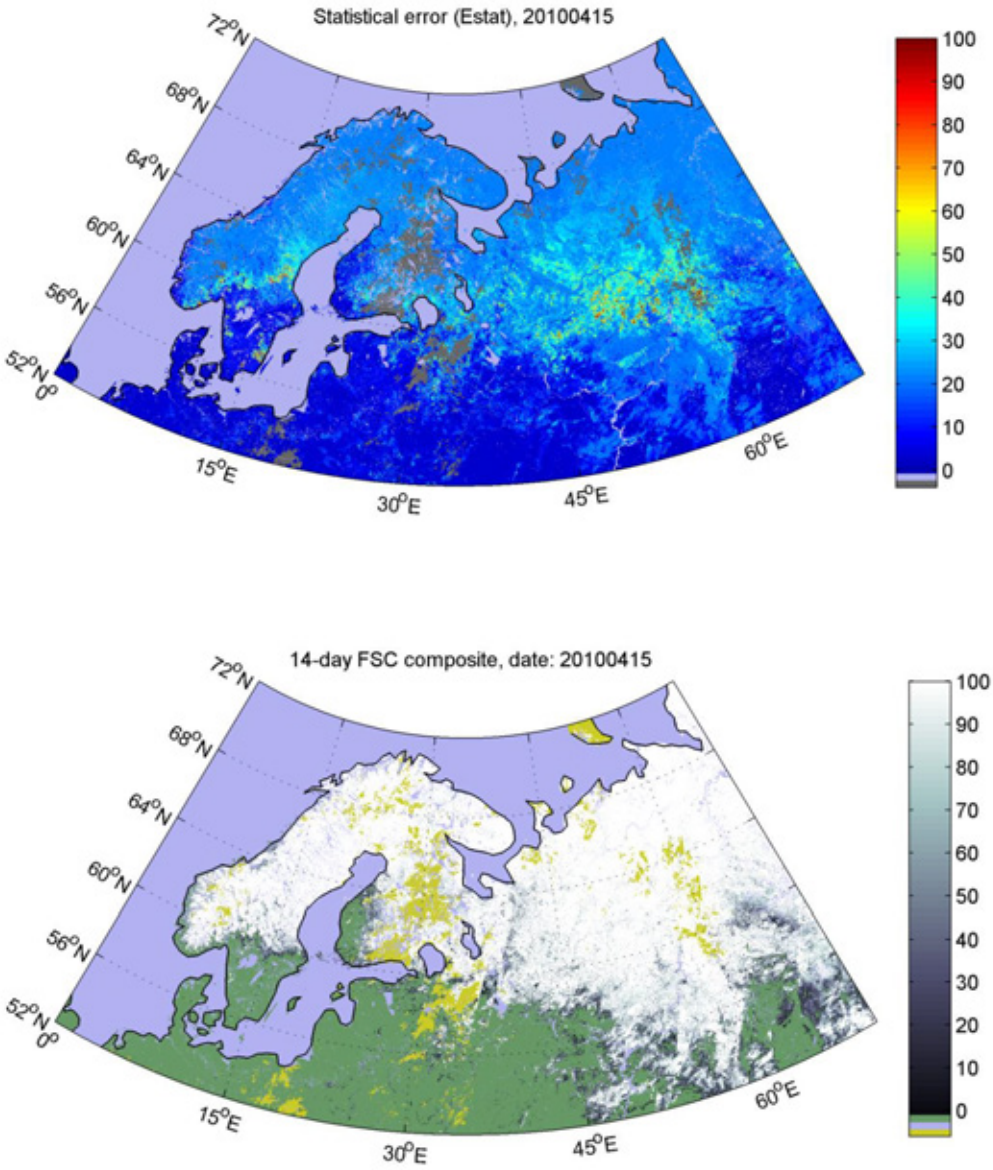


Figure 16. Statistical error (FSC %-units) of GlobSnow FSC estimate for a composite of daily products between April 02 and April 15, 2010 (Upper panel), and the corresponding FSC (%-units) estimation map (Lower panel). Clouds are depicted in brown-grey color (Upper panel), and yellow (Lower panel), respectively. This figure is adapted from **PV**, ©2017 Elsevier.

## 3.2. Consideration of systematic error using independent reference data

The total error in FSC estimation does not include only the statistical error, but may include systematic error contributions arising from unidealities or inaccuracies of the applied forward and inverse model (*SCAmod* here). A reliable way to assess the systematic error is the employment of independent *in situ* reference data on FSC. Thereby, we can assess the residuals of FSC estimates by the satellite product (GlobSnow FSC), and further on, evaluate the systematic error and construct the estimate of FSC product error. Fig. 17 outlines the procedure of conducting this. The *in situ* validation data allows the determination of residuals (true estimation errors) for the region and conditions that the reference data and concurrent satellite product sets cover. When this information is combined with the statistical error estimates of the satellite product, upper panel of Fig. 16, we can assess the error contribution not considered or described by the statistical error. This remaining error contribution is referred to as systematic error (**PV)**. After the systematic error is determined using the validation data set (*in situ* data and corresponding statistical errors from validation satellite products), the product error can be provided by summing the statistical error estimates and assessed systematic error. This can be carried out for any satellite product and any pixel, on a condition that *in situ* validation data ranges over the spatial and observational characteristics of the satellite product. In practice, the additive systematic error can be analyzed for certain intervals of FSC, and a curve giving the systematic error as a function of FSC can be obtained, see Fig. 18. The resulting product error as is simply the root mean squared (RMS) sum of the statistical and systematic errors, **PV**:

$$PE(x,y,t) = \sqrt{(E_{stat}(x,y,t))^2 + (\Delta(\mathrm{FSC}))^2} \qquad (9)$$

This product error varies both spatially (x,y) and temporally (t), since the statistical error $E_{stat}$ is dynamic. Additionally, as stressed by Fig. 18, the systematic error Δ is given as a function of estimated FSC, being larger for the lower levels of FSC. An example of the resulting FSC product error is depicted in Fig. 19 corresponding to Fig. 16. The product error map of Fig. 19 demonstrates that the systematic error increases the overall level of error estimate for the regions of patchy snow (low levels of FSC), but does not influence much on regions with a high FSC.

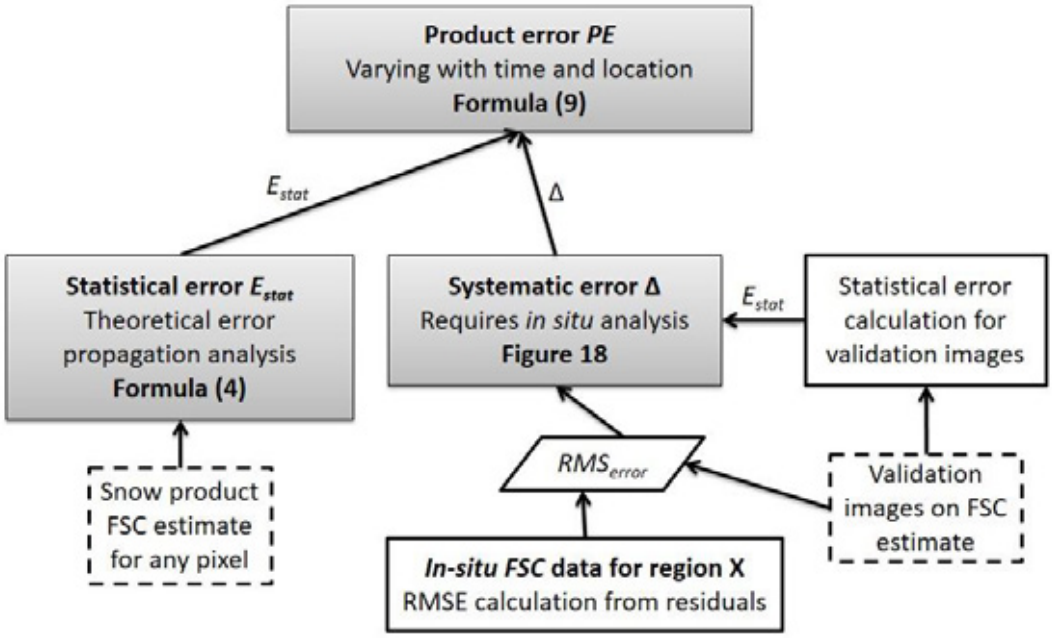


Figure 17. Procedure for the determination of the total product error *PE*. The calculation of systematic error is performed by using *in situ* data set. Here the procedure according to Fig.2 is described in more detail. This figure is modified after **PV.**

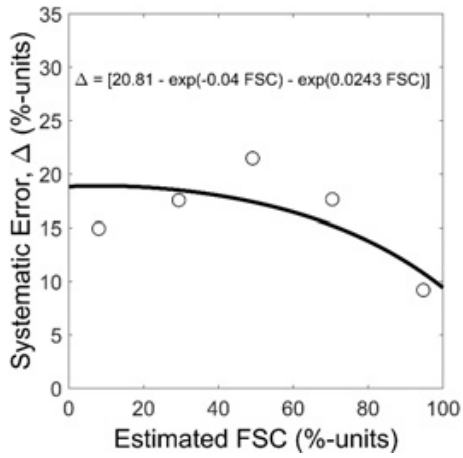


Figure 18. Regression curve to describe the systematic error Δ as a function of FSC. The systematic error here is obtained for FSC interval stratified values (open circles) from the analysis of observed residuals (FSC estimates –

*in situ* reference data) and Globsnow FSC product provided statistical errors, see Fig. 17. The regression curve is fitted to interval stratified values (open circles). This figure is adapted from **PV**, ©2017 Elsevier.

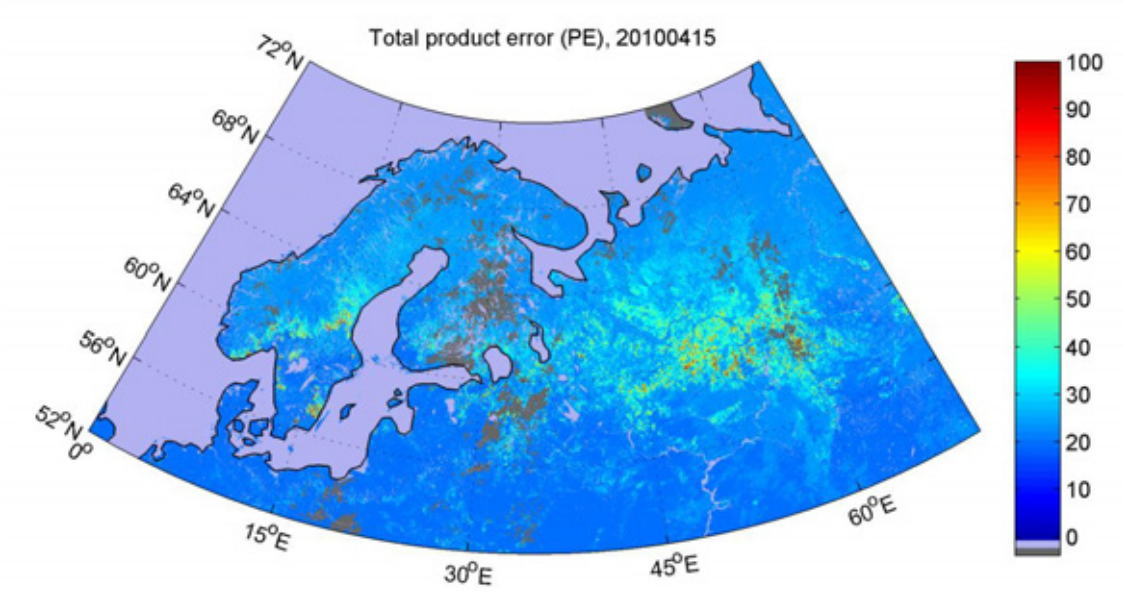


Figure 19. Total FSC product error *PE* (FSC %-units) between April 02 and April 15, 2010 according to Equation (9). The corresponding maps of the statistical error and FSC product are presented in Fig. 16. Clouds are depicted in brown-grey color. This figure is adapted from **PV**, ©2017 Elsevier.

## 4. Conclusions

In this thesis the applicability of various remote sensing data for the assessment and improvement of snow mapping algorithms was described. The thesis focuses on the investigation of scene or landscape level aspects that affect the space-borne observed reflectance of the Earth's surface during the snow melt period. In particular the emphasis is laid on the boreal forest zone. It was shown, that besides satellite data, airborne, field and mast-based spectrometer data can be utilised to investigate the effects of different landscape elements on the overall reflectance. A method to determine the snow-free ground reflectance right after snow melt was developed using satellite data. Further, field and mast-based spectral observations on snow covered, forested and snow-free ground were collected to determine their reflectance characteristics. The spectral information (e.g. mean and standard deviation

of the reflectance contributors) was shown to be beneficial in selecting the optimal wavelength channels and investigating the behaviour of the spectral indices, such as NDSI or NDVI, for the snow detection algorithm.

By assessing the behaviour of different reflectance contributors to the satellite scene reflectance, the work proceeds into the analysis of accuracy characteristics of the retrieval of Fractional Snow Cover (FSC). The variability in the contributing reflectances affects the statistical accuracy of the investigated *SCAmod* snow detection algorithm. Accordingly, the representativeness of the applied values of the reflectance contributors is essential for the algorithm performance. The statistical error based on variability of the applied reflectances was determined first through the theory of error propagation. Yet, an important issue in this work is the consideration of the total FSC product error that includes both the statistical (random) component and error contributions that are systematic in nature. For determining the systematic error a new experimental analysis approach was developed using a unique regional data set covering Finland. The results are applicable for a larger region of European boreal forest with similar non-mountainous landscapes and seasonal snow.

## 5. Summary of the appended papers

The main contents of the original papers are briefly overviewed here.

**Paper I** The behaviour of snow and snow-free ground reflectance was determined by analyzing their statistical features in the optical and infrared (350-2500 nm) wavelengths. The results were used to assess the statistical accuracy and optimal wavelength band selection when applying the *SCAmod* method to different sensors typically used in snow remote sensing. It was concluded that the variability in wet snow and snow-free ground reflectance is a significant (statistical) error contributor in fractional snow cover estimation. It was shown that the standard deviations of the observed reflectances under direct and diffuse illumination conditions do not differ significantly. Thus, the variance in the observations is most likely to be caused by the variability in the measured target characteristics (and not e.g. due to sun zenith angle or viewing geometry). The field spectrometer data was found feasible for the development of the snow mapping algorithm. However, the snow-free ground reflectance was analyzed as one unit including several forest floor samples, without considering different land cover types separately. It was found that concerning the layers of wet snow thinner than 20 cm, the underlying ground below the snow particularly decreases the reflectance. Yet, besides the underlying ground, it is likely that the forest litter also affects the observation.

**Paper II** The behaviour of snow-free ground reflectance after snowmelt was determined for the predominant non-forested land cover classes in Europe using MODIS time-series observations. A new algorithm was developed to capture the moment directly after snow has disappeared. The results are

relevant for the (operational) monitoring of the Fractional Snow Cover (FSC) and can be utilized to assess the error caused by the snow-free ground reflectance (parameter) value and its standard deviation in the snow mapping algorithm. The results show that the performance of the snow mapping algorithm improves if land cover specific values are applied compared to using a fixed average value to all land cover categories, at least for e.g. wetlands. In addition to the obtained statistics of wavelength band reflectances (mean and standard deviation for different land cover classes) and related indices (NDVI, NDSI), one result is a snow-free ground reference map for central, eastern and northern Europe.

**Paper III** The influence of boreal forest stand characteristics on the observed scene reflectance under full dry snow cover was defined. The advantageous experimental measurement setup combining airborne hyperspectral imaging and LIDAR data sets from Finland facilitated the analysis of the effects of the forest canopy to the reflectance. The relation between the forest characteristics and reflectance was nearly exponential, whereas with reflectance indices it was linear.

**Paper IV** further analyses the data set introduced in **Paper III**. In particular, the analysis shows that a simple non-linear model obtained from the zeroth order solution of the radiative transfer equation is a proper approximation for describing the influence of boreal forests to scene reflectance (as suggested by the *SCAmod* approach). Additionally, the results show that backscattering dominates over forward scattering in snow covered boreal forest even though snow itself is a medium dominated by forward scatter.

**Paper V** has the main goal of developing a methodology to assess the total product error in optical, satellite data-based, Fractional Snow Cover (FSC) estimation. First we define a statistical error component through the theory of error propagation, and then utilize a new experimental analysis approach and a unique regional data set covering Finland to calculate the remaining systematic error component. This is demonstrated for northern Europe by applying the Globsnow SE product on FSC.

## References


ACIA, 2004. Impacts of a Warming Arctic: Arctic Climate Impact Assessment. ACIA Overview report. Cambridge University Press. 1020 pp.http://www.amap.no/documents/doc/impacts-of-a-warming-arctic-2004/786

ACIA, 2005. Chapter 14: Forests, Land Management, and Agriculture, in: Arctic Climate Impact Assessment. ACIA Overview report. Cambridge University Press, pp. 781-862. https://www.amap.no/documents/doc/arctic-arctic-climate-impact-assessment/796

AMAP, 2011. Snow, Water, Ice and Permafrost in the Arctic (SWIPA): Climate Change and the Cryosphere. Arctic Monitoring and Assessment Programme (AMAP), Oslo, Norway. xii + 538 pp. https://www.amap.no/documents/doc/snow-water-ice-and-permafrost-in-the-arctic-swipa-climate-change-and-the-cryosphere/743

Bokhorst, S., Pedersen, S.H., Brucker, L., Anisimov, O., Bjerke, J.W., Brown, R.D., Ehrich, D., Essery, R.L., Heilig, A., Ingvander, S., Johansson, C., Johansson, M., Jónsdóttir, I.S., Inga, N., Luojus, K., Macelloni, G., Mariash, H., McLennan, D., Rosqvist, G.N., Sato, A., Savela, H., Schneebeli, M., Sokolov, A., Sokratov, S.A., Terzago, S., Vikhamar-Schuler, D., Williamson, S., Qiu, Y., Callaghan, T.V., 2016. Changing Arctic snow cover: A review of recent developments and assessment of future needs for observations, modelling, and impacts. Ambio. 45, 516–537.

Bontemps, S., Defourny, P., Van Bogaert, E., Arino, O., Kalogirou, V., Perez, J.R., 2011. GlobCover 2009: Product description and validation report. ESA GlobCover 2009 project. http://due.esrin.esa.int/files/GLOBCOVER2009_Validation_Report_2.2.pdf (accessed 23.03.2017)

Brown, R.D., Mote, P.W., 2009. The response of Northern Hemisphere snow cover to a changing climate. J. Clim. 22, 2124-2144.

Brown, R.D., Robinson, D.A., 2011. Northern Hemisphere spring snow cover variability and change over 1922–2010 including an assessment of uncertainty. Cryosphere. 5, 219-229.

Callaghan, T.V., Johansson, M., Brown, R.D., Groisman, P.Y., Labba, N., Radionov, V., Bradley, R.S., Blangy, S., Bulygina, O.N., Christensen, T.R., Colman, J.E., Essery, R.L.H., Forbes, B.C., Forchhammer, M.C., Golubev, V.N., Honrath, R.E., Juday, G.P., Meshcherskaya, A.V., Phoenix, G.K., Pomeroy, J., Rautio, A., Robinson, D.A., Schmidt, N.M., Serreze, M.C., Shevchenko, V.P., Shiklomanov, A.I., Shmakin, A.B., Sköld, P., Sturm, M., Woo, M.-ko, Wood, E.F., 2011. Multiple Effects of Changes in Arctic Snow Cover. Ambio. 40, 32–45.

Choi, G., Robinson, D.A., Kang, S., 2010. Changing Northern Hemisphere snow seasons. J. Clim. 23, 5305-5310.

Derksen, C., Brown, R., 2012. Spring snow cover extent reductions in the 2008–2012 period exceeding climate model predictions. Geophys. Res. Lett. 39, L19504.

Dietz, A.J., Kuenzer, C., Gessner, U., Dech, S., 2012. Remote sensing of snow – a review of available methods. Int. J. Remote Sens. 33, 4094-4134.

Dozier, J., Green, R., Nolin, A., Painter, T., 2009. Interpretation of snow properties from imaging spectrometry. Remote Sens. Environ. 113, S25-S37.

Flanner, M.G., Shell, K.M., Barlage, M., Perovich, D.K., Tschudi, M.A., 2011. Radiative forcing and albedo feedback from the northern hemisphere cryosphere between 1979 and 2008. Nat. Geosci. 4, 151–155. http://dx.doi.org/10.1038/ngeo1062

Frei, A., Tedesco, M., Lee, S., Foster, J., Hall, D.K., Kelly, R., Robinson, D.A., 2012. A review of global satellite-derived snow products. Adv. Space Res. 50, 1007-1029.

Hall, D.K., Riggs, G.A., 2007. Accuracy assessment of the MODIS snow products. Hydrol. Process. 21, 1534–1547.

Hall, D., Riggs, G.A., Salomonson, V.V., DiGirolamo, N.E., Bayr, K.J., 2002. MODIS snow-cover products. Remote Sens. Environ. 83, 181-194.

Helfrich, S.R., McNamara, D., Ramsay, B.H., Baldwin, T., Kasheta, T., 2007. Enhancements to, and forthcoming developments in the interactive multisensory snow and ice mapping system (IMS). Hydrol. Process. 21, 1576-1586.

Hori, M., Sugiura, K., Kobayashi, K., Aoki, T., Tanikawa, T., Kuchiki, K., Niwano, M., Enomoto, H., 2017. A 38-year (1978–2015) Northern Hemisphere daily snow cover extent product derived using consistent objective criteria from satellite-borne optical sensors. Remote Sens. Environ. 191, 402–418.

Hudson, S.R., Warren, S.G., Brandt, R.E., Grenfell, T.C., Six, D., 2006. Spectral bidirectional reflectance of Antarctic snow: Measurements and parameterization. J. Geophys. Res. 111, D18106.

IPCC, 2013. Climate Change 2013: The Physical Science Basis. Contribution of Working Group I to the Fifth Assessment Report of the Intergovernmental Panel on Climate Change, [Stocker, T.F., Qin, D., Plattner, G.-K., Tignor, M., Allen, S.K., Boschung, J., Nauels, A., Xia, Y., Bex, V., Midgley, P.M., (Eds.)], Cambridge University Press, Cambridge, United Kingdom and New York, NY, USA, 1535 pp.

Klein, A.G., Hall, D.K., Riggs, G.A., 1998. Improving snow-cover mapping in forests through the use of a canopy reflectance model. Hydrol. Process. 12, 1723–1744.

Metsämäki, S., Anttila, S., Huttunen, M., Vepsäläinen, J., 2005. A feasible method for fractional snow cover mapping in boreal zone based on a reflectance model. Remote Sens. Environ. 95, 77-95.

Metsämäki, S., Mattila, O.-P., Pulliainen, J., Niemi, K., Luojus, K. Böttcher, K., 2012. An optical reflectance model-based method for fractional snow cover mapping applicable to continental scale. Remote Sens. Environ. 123, 508-521.

Metsämäki, S., Pulliainen, J., Salminen, M., Luojus, K., Wiesmann, A., Solberg, R., Böttcher, K., Hiltunen, M., Ripper, E., 2015. Introduction to GlobSnow Snow Extent products with considerations for accuracy assessment. Remote Sens. Environ. 156, 96-108.

Nicodemus, F.E., Richmond, J.C., Hsia, J.J., Ginsberg, I.W., Limperis, T., 1977. Geometrical considerations and nomenclature for reflectance. NBS Monograph 160. US Department of Commerce, National Bureau of Standards. 52 p.

Nolin, A.W., 2010. Recent advances in remote sensing of seasonal snow. J. Glaciol. 56, 1141-1150.

Painter, T.H., Dozier, J., 2004. Measurements of the hemispherical-directional reflectance of snow at fine spectral and angular resolution. J. Geophys. Res. 109, D18115.

Painter, T.H., Dozier, J., Roberts, D.A., Davis, R.E., Green, R.O., 2003. Retrieval of subpixel snow-covered area and grain size from imaging spectrometer data. Remote Sens. Environ. 85, 64-77.

Painter, T. H., Rittger, K., McKenzie, C., Slaughter, P., Davis, R.E., Dozier, J., 2009. Retrieval of subpixel snow covered area, grain size, and albedo from MODIS. Remote Sens. Environ. 113, 868–879.

Pan, Y. D., Birdsey, R.A., Fang, J., Houghton, R., Kauppi, P.E., Kurz, W.A., Phillips, O.L., Shvidenko, A., Lewis, S.L., Canadell, J.G., Ciais, P., Jackson, R.B., Pacala, S.W., McGuire, A.D., Piao, S., Rautiainen, A., Sitch, S., Hayes, D., 2011. A large and persistent carbon sink in the world's forests. Science 333, 988-993.

Pellikka, P., 1998. Development of correction chain for multispectral airborne video camera data for natural resource assessment. Fennia 176:1. Geographical Society of Finland, Helsinki, pp. 1-110.

Pellikka, P., Rees, G.W., 2009. Remote Sensing of Glaciers: Techniques for Topographic, Spatial and Thematic Mapping of Glaciers. CRC/Taylor & Francis Group. 340 pp.

Peltoniemi, J.I., Kaasalainen, S., Näränen, J., Rautiainen, M., Stenberg, P., Smolander, H., Smolander, S., Voipio, P., 2005. BRDF measurement of understorey vegetation in pine forests: dwarf shrubs, lichen, and moss. Remote Sens. Environ. 94, 343-354.

Ramsay, B.H., 1998. The interactive multisensory snow and ice mapping system. Hydrol. Process. 12, 1537-1546.

Rees, W.G., 2006. Remote sensing of snow and ice, CRC/Taylor & Francis Group. 285 pp.

Rittger, K., Painter, T.H., Dozier, J., 2013. Assessment of methods for mapping snow cover from MODIS. Adv. Water Resour. 51, 367-380.

Salomonson, V. V., Appel, I., 2004. Estimating fractional snow cover from MODIS using the normalized difference snow index. Remote Sens. Environ. 89, 351– 360.

Salomonson, V. V., Appel, I., 2006. Development of the Aqua MODIS NDSI fractional snow cover algorithm and validation results. IEEE Trans. Geosci. Remote Sens. 44, 1747–1756.

Schaepman-Strub, G., Schaepman, M.E., Painter, T.H., Dangel, S., Martonchik, J.V., 2006. Reflectance quantities in optical remote sensing – definitions and case studies. Remote Sens. Environ. 103, 27-42.

Steffen, W., Richardson, K., Rockström, J., Cornell, S.E., Fetzer, I., Bennett, E.M., Biggs, R., Carpenter, S.R., de Vries, W., de Wit, C.A., Folke, C., Gerten, D., Heinke, J., Mace, G.M., Persson, L.M., Ramanathan, V., Reyers, B., Sörlin, S., 2015. Planetary boundaries: Guiding human development on a changing planet. Science 347, 1259855-1- 1259855-10.

Stroeve, J., Box, J.E., Gao, F., Liang, S., Nolin, A., Schaaf, C., 2005. Accuracy assessment of the MODIS 16-day albedo product for snow : comparisons with Greenland in situ measurements. Remote Sens. Environ. 94, 46-60.

Taylor, J.R., 1982. An introduction to error analysis. The study of uncertainties in physical measurements. First Edition, University Science Books, London, UK.

Vaughan, D.G., Comiso, J.C., Allison, I., Carrasco, J., Kaser, G., Kwok, R., Mote, P., Murray, T., Paul, F., Ren, J., Rignot, E., Solomina, O., Steffen, K., Zhang, T., 2013. Observations: Cryosphere, in: Stocker, T.F., Qin, D., Plattner, G.-K., Tignor, M., Allen, S.K., Boschung, J., Nauels, A., Xia, Y., Bex, V., Midgley, P.M. (Eds.), Climate Change 2013: The physical science basis. Contribution of working group I to the fifth assessment report of the

intergovernmental panel on climate change. Cambridge University Press, Cambridge, United Kingdom and New York, NY, USA. pp. 317-382.

Vikhamar, D., Sohlberg, R., 2002. Subpixel mapping of snow cover in forests by optical remote sensing. Remote Sens. Environ. 84, 69-82.

Vikhamar, D., Solberg, R., 2003. Snow-cover mapping in forests by constrained linear spectral unmixing of MODIS data. Remote Sens. Environ. 88, 309-323.

Warren, S.G., 1982. Optical properties of snow. Rev. Geophys. Space Phys. 20, 67-89.

Wiscombe, J.W., Warren, S.G., 1980. A model for the spectral albedo of snow. I: Pure snow. J. Atmos. Sci. 37, 2712-2733.

I

Remote Sensing of Environment 113 (2009) 907–918

Contents lists available at ScienceDirect

Remote Sensing of Environment

journal homepage: www.elsevier.com/locate/rse

# The behaviour of snow and snow-free surface reflectance in boreal forests: Implications to the performance of snow covered area monitoring

Miia Salminen [a], Jouni Pulliainen [b], Sari Metsämäki [a,*], Anna Kontu [b], Hanne Suokanerva [b]

[a] Finnish Environment Institute, Geoinformatics and Land Use Division, P.O.Box 140, FI-00251 Helsinki, Finland
[b] Finnish Meteorological Institute, Arctic Research, Tähteläntie 62, 99600 Sodankylä, Finland

ARTICLE INFO

*Article history:*
Received 28 May 2008
Received in revised form 15 December 2008
Accepted 16 December 2008

*Keywords:*
Snow cover
Surface reflectance
Field spectroscopy
Boreal forest

ABSTRACT

Optical methods for snow mapping typically exploit wavelengths in the visible and near-infrared range, where reflectances from snow and snow-free ground may significantly vary, especially during the melting season. In this study, the variability of ground reflectance in the boreal forest zone was investigated in order to assess the feasibility of satellite sensors to the mapping of snow covered area (SCA). This aims at the improvement of the existing snow mapping algorithms, such as the reflectance model-based snow monitoring method *SCAmod* of the Finnish Environment Institute (SYKE). We acquired and identified some statistical features for reflectance spectra of seasonally snow covered and snow-free terrain by using a field spectroradiometer (ASD Field Spec Pro JR). Extensive measurement campaigns were carried out in 2007–2008 in northern Finland, resulting to hundreds of spectral samples between 350 and 2500 nm. The main emphasis was put on the determination of the melting snow reflectance under different weather conditions and stages of snow metamorphosis as well as over different terrain types. The gained reflectance spectra provide useful information for optical snow mapping studies in general. In this investigation, the primary function of the spectrometer data was the accuracy assessment and optimal band selection when applying the *SCAmod*-method to different space-borne instruments (MODIS, MERIS and AVHRR). The correspondence of small scale field observations with scene reflectance was also addressed. This was performed by comparing field spectrometer data with mast-based observations.

Based on the inversibility of the *SCAmod* reflectance model, we addressed the standard deviation (standard error) of SCA estimation contributed by wet snow and snow-free ground reflectance fluctuations. An average error in the determination of the fractional Snow Covered Area (SCA) of about 5–7 %-units was obtained (range from 0% = snow-free ground to 100% = full snow cover), the maximum error of 10–12 %-units occurring at full snow cover conditions (for the moment when first open patches are emerging). These investigations show that the variability in the reflectances of snow and snow-free ground is a significant error source in snow mapping. However, providing the SCA with descriptive error statistics is very beneficial for further use as the error statistics are needed for data assimilation approaches, e.g. in using SCA-values as input to hydrological models.



## 1. Introduction

The Northern Hemisphere seasonal snow cover influences highly the interactive Earth's surface and atmosphere system. For this reason, snow cover is a sensitive climate change indicator both regionally and on global scale. Typically, at northern latitudes most of the annual discharge originates from snowfall. Consequently, snow pack is also an important temporary fresh water storage. Terrestrial snow cover is a rapidly varying constituent of the hydrological cycle in particular during the spring and autumn transition months (Barry et al., 2007; Vavrus, 2007; Walsh, 2005). Spatial variability and long-term trends in snow cover distribution and related climate patterns have been analyzed based on observation data (Kitaev et al., 2002, 2005) and climate change prediction models (Jylhä et al., 2004; Mellander et al., 2007). The models project changes in the spatial and temporal distribution of snow in the boreal forest zone. Although the predictions generally indicate significant decrease in snow cover throughout the winter and the acceleration of the hydrologic cycle, the amount of snow increases in the coldest areas, such as the Canadian Arctic and Siberia (Räisänen, 2008). These changes can have widespread impacts on ecosystems and human activities, e.g. flooding, water resources management, agriculture, transportation, hydropower production, and recreational activities (Barry et al., 2007; Jaagus, 1997; Walsh, 2005). Accurate information on snow spatial and temporal distribution is essential for climate research, numerical

* Corresponding author.
*E-mail address:* sari.metsamaki@ymparisto.fi (S. Metsämäki).

0034-4257/$ – see front matter © 2008 Elsevier Inc. All rights reserved.
doi:10.1016/j.rse.2008.12.008

weather prediction and hydrological applications. Lundberg and Halldin (2001) review and assess ground-based snow measurement techniques for boreal areas and state the importance of both point and remote sensing observations.

Traditional in-situ weather station and snow-gauging networks are in practice handicapped by their spatial and temporal sparseness. Space-borne Earth Observation (EO) techniques provide a spatially and temporally effective means to obtain information on the snow cover extent, including the fraction of snow covered area (SCA) within a single pixel or a single calculation unit such as a hydrological drainage basin. Optical snow mapping methods are often based on the fact that snow has high reflectance in visible and near infrared (NIR) wavelengths compared to most other land surfaces (Warren, 1982; Wiscombe & Warren, 1980). This difference is used in operational snow cover monitoring systems, such as the National Oceanic and Atmospheric Administration (NOAA) snow map production for the Northern Hemisphere, fractional snow cover mapping for the Baltic Sea area with *SCAmod* (Metsämäki et al., 2005) and the retrieval of the global Moderate Resolution Imaging Spectroradiometer (MODIS) snow-cover products (Hall et al., 2002). The MODIS algorithm employs visible green and shortwave-infrared reflectances to calculate the Normalized Difference Snow Index (NDSI), which is used to provide either binary snow information (snow/no snow) or fractional SCA based on regression analysis between NDSI and Landsat 30-m observations used as "ground truth" (Salomonson & Appel, 2004). Additionally, linear spectral unmixing techniques have been applied for sub-pixel snow mapping by assuming that a pixel is composed of several spectral classes. (Nolin & Dozier, 1993; Painter et al., 1998, 2003; Rosenthal, 1996; Vikhamar & Solberg, 2003a,b). Spectral unmixing is specifically suitable for data with a considerable number of spectral bands, such as Airborne Visible/Infrared Imaging Spectrometer (AVIRIS), but less usable in remote sensing of snow with current space-borne instruments with limited number of bands (MODIS, AVHRR, MERIS). Using spectral unmixing approach, the aerial coverage of each class can be estimated. Unmixing often utilizes spectral libraries for comparison to estimate the mixture spectral endmembers i.e. pure spectral classes of each pixel. For that purpose, the spectra obtained from this investigation can be exploited and are relevant with instruments such as AVIRIS, although the study does not directly concern spectral unmixing.

There are characteristic sources of error for different satellite data retrieval methods caused by the spatial and temporal variation in the observed reflectance. In order to quantify the effects of this variation on the SCA estimation, measurements under controlled conditions are fundamental. The variation in the observed reflectance can be compiled to statistics by collecting reference spectra with field spectroscopy measurements performed at ground level. Field spectroscopy advances remote sensing (imaging spectroscopy) through feasibility studies, image analysis and vicarious calibration of satellite products (Schaepman et al., 2006). For example, the retrieval of optically equivalent snow grain size is at present only possible by utilizing high spectral resolution spectroscopy data (Painter & Dozier, 2004; Painter et al., 1998). Previous investigations concerning the behaviour of surface reflectance also include the employment of simulated spectra based on theoretical models (Nolin & Dozier, 2000; Wiscombe & Warren, 1980). Problems in theoretical investigations include that they often consider snow grains as spherical scatterers. This adduces the difficulty of determining the effective grain radius for real non-spherical snow crystals, or otherwise, how to describe non-spherical shapes for more advanced models (Kokhanovsky et al., 2005; Painter & Dozier, 2004; Xie et al., 2006).

In this work, we study the variability of surface reflectance in the boreal forest area in order to enable the improvement of existing optical EO-based snow mapping algorithms, such as the reflectance model-based *SCAmod* method (Metsämäki et al., 2005) developed and operated at the Finnish Environment Institute (SYKE). *SCAmod* is particularly designed for boreal forests, excluding mountainous areas (Anttila et al., 2005). It provides the fraction of Snow Covered Area (SCA) during the melting season, presented as average percentages (0–100%) for calculation unit areas. These can be drainage basins or grid cells equivalent to the satellite pixel size. The operational snow mapping at SYKE is currently based on 500-meter resolution Terra/MODIS-imagery. The *SCAmod* algorithm is based on a single band reflectance model, where the observed satellite reflectance for a selected wavelength channel is expressed as a function of SCA. The typical reflectance values, again for the selected wavelength band, of three major reflective contributors (wet snow, snow-free ground, and dense forest canopy) serve as input parameters. *SCAmod* is, however, applicable to a variety of optical sensors; switching between sensors only requires tuning the values of the constant parameters of the algorithm. These are (a) reflectance of wet snow cover, (b) reflectance of snow-free ground and (c) reflectance of forest canopy (crowns and trunks). In addition to those, dry snow reflectance must be concerned as it affects at-satellite reflectance-derived apparent forest canopy transmissivity, which is *a priori* information required by *SCAmod* and is based on the same reflectance model as the actual SCA estimate. The snow information provided by SYKE is primarily used for hydropower management and hydrological modelling (Metsämäki et al., 2004). The principle of the *SCAmod* method is described in Section 2.4.

We consider here the accuracy of the above-described *SCAmod* method using ground spectrometer-derived average reflectances as input to *SCAmod* at applied satellite-sensor-specific wavelengths. As *SCAmod* is based on a reflectance model and applies typical average reflectances, contributions (a)–(c) above, as input parameters, a critical error source must be related to the presumed absolute level and variation in these reflectance values. Since *SCAmod* uses single band reflectances, we concentrated on selected wavelength bands in our analyses. However, the data set introduced here is also relevant in general, e.g. for approaches that use a wide range of spectrum, such as that by Painter et al. (2003). An essential issue here is to investigate the variability of snow and snow-free surface reflectances, particularly under different state of snow metamorphosis, within several land-cover categories and under various weather and illumination conditions. The current paper concentrates on the effects of wet snow and snow-free ground reflectance variability to the *SCAmod* algorithm performance as we assume their effect to be more significant compared to more invariant dry snow and forest canopy reflectance.

In order to investigate the scene reflectance contributions indicated above, we collected an extensive field spectrum data set using a portable spectroradiometer (ASD Field Spec Pro JR) in 2007 and 2008 in Finnish Lapland. The obtained spectral data was divided into selected reflectance classes for which mean and standard deviation were calculated. Another similar spectrometer was permanently installed in a 30-m mast providing data for a pine forest and open terrain (partially shadowed by pine trees). The comparison of field and mast spectrometer observations enabled the investigation how well the scene reflectance observed by a space-borne system can be modelled using point-wise observed field spectrometer data.

To perform the actual accuracy assessment of *SCAmod*, we calculate the contributions of both wet snow and snow-free ground reflectance fluctuations to the standard deviation (standard error) of an SCA estimate. The goal of analyses is to investigate the temporal and spatial variability in the average reflectances and to find out their effect to performance of SCA estimation. The gained estimates for the variance of snow covered and snow-free terrain reflectance directly provide information for the future *SCAmod* algorithm modification as well as for error analyses. The objective also includes the study of the dependence of wet snow reflectance on depth of the snowpack. Furthermore, optimal band alternatives are indicated for current and future satellite instruments by determining the wavelength areas where the variability is only minor or has only a slight effect on the performance of a snow covered area algorithm. In this study, we focus

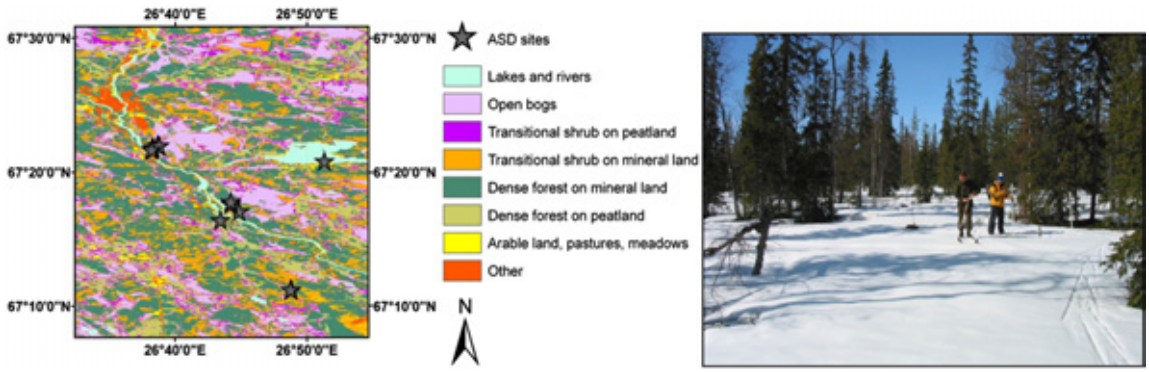


**Fig. 1.** (Left) The reflectance sites are located in Sodankylä and Inari districts in Finnish Lapland, an additional site was located in an open fjeld region north of the map region. (Right) Typically, the landscape represents an open canopy conifer-dominated boreal forest.

on wavelength areas related to three satellite sensors commonly used in snow mapping: the MODIS aboard Terra, the Medium Resolution Imaging Spectrometer (MERIS) aboard Envisat and the Advanced Very High Resolution Radiometer (AVHRR) aboard NOAA satellite series.

## 2. Data set and methods

### 2.1. Study area

The target area for fieldwork is in the Sodankylä district in Finnish Lapland, located on latitude 67 N about 100 km north of the Arctic Circle (Fig. 1). This sub-arctic environment is characterized by seasonally snow covered boreal coniferous forests and large open bogs or sparsely forested mires. Typical for the terrain in Lapland are numerous tundra-like treeless fjelds, although the overall topography is relatively flat. The Sodankylä region is undulating moderately up to 500 m in altitude. The extent of forests (forests and scrubland) in Finland is 74% of the total land area compared to the 44% in Europe (FAO, 2003). In Finnish Lapland the areal extent of forest is 73%, but forests are sparse with an average stem volume of only 64 $m^3$/ha on forestland (METLA, 2007). Dominant tree species are Scots pine (76% of the forestland coverage) and Norway spruce, but small birches are also usual especially at fjeld-regions.

The most active period regarding snow hydrology is spring when the seasonal snow melts, often causing severe flooding particularly in the North. Snow characteristics of Finnish Lapland are more homogeneous compared to Southern Finland, where the repeated freezing and thawing usually result into a highly metamorphosed snowpack. In Finnish Lapland snow cover period tends to last more than 6 months in open areas and the average annual snow water equivalent is as high as 140–200 mm (Kuusisto, 1984). The structure of snowpack depends mainly on solar irradiation, air temperature, wind speed and rainfall that determine the type of metamorphosis process (Colbeck et al., 1990; Oksanen, 1999; Sturm et al., 1995). During spring melt metamorphosis, snowpack is typically structured with layers that may contain ice lenses or refrozen particles. In the Sodankylä region taiga type snow is predominant, but there is also tundra type snow, particularly on top of wind-induced fjelds. Fig. 1 depicts the location of the reflectance sites and indicates the high spatial heterogeneity of the landscape of the region.

### 2.2. Data acquisition

The overall strategy of the field measurements is to collect spatially and temporally extensive data sets that are needed for analysing the performance and error characteristics of SCA mapping. In addition, by combining spatially extensive point-wise (very small footprint) measurements with mast-based (185 $m^2$ footprint) experiments at a single location, we can then link the ground-based ASD measurements also to scene reflectances actually observed by space-borne remote sensing systems. Hundreds of reflectance spectra were sampled at the Sodankylä area in Finnish Lapland with a portable spectrometer (Analytical Spectral Devices (ASD) Field Spec Pro JR, spectral range 350–2500 nm). The purpose of the ASD measurements was to determine the reflectance variability of snow and snow-free ground. In order to identify and locate the most typical land cover categories, CORINE2000 Land Cover (CLC2000) map was used (Härmä et al., 2004). We found that open peat bog, transitional shrub on mineral or peat land and coniferous forest on mineral or peat land are the most typical land cover categories in the area (Fig. 1). Among those, several representative reflectance measurement sites were selected.

In addition to using the portable spectrometer, a similar spectrometer was installed on a top of a 30-m mast to constantly monitor reflectance of a target area including a Scots pine forest with a mean tree height of 7 m (stem volume 70 $m^3$/ha) and an adjacent forest opening. Same observation settings as with the portable spectrometer were used, except that the instrument was tilted 11° off the nadir. The main mast-borne data of this study was acquired for a single date, 27 March 2008. Additional data representing snow-free free conditions were used in order to find out the reference value for vegetation reflectance (multiple observations of the forested target area from August 2006). The mast-based spectrometer system is described in (Sukuvaara et al., 2007).

Simultaneously with mast-based spectrometer observations on March 2008, digital photographs were acquired for the target area enabling the determination of the fractions of forest canopy, tree shadows and directly illuminated snow surface (an automatic camera system is installed to mast-top together with the azimuthally rotating spectrometer front-end). In case of winter-time measurements this is possible as the visible contrast between different target composites is high. Analogously to ground-based observations, the mast-based reflected radiance observations were calibrated to reflectance values applying white reference panel measurements with an automatic mast-top calibration system.

Field campaigns in 2007 and 2008 consist of reflectance and concurrent snow measurements in 36 sites (each including 3–5 subsampling sites) from the time period of March to May, both in 2007 and 2008. Additional monitoring was carried out using the mast-based spectrometer system. Snow pits were excavated at each reflectance site and average snow depth, snow pack temperature (at −5 cm and middle of snowpack), ground surface temperature and air temperature were measured. Based on the temperature measurements and the so-called snowball test suggested by Colbeck et al.

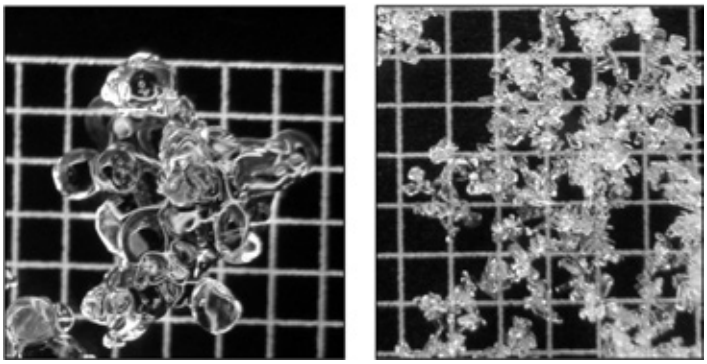

**Fig. 2.** (Left) Example of typical wet snow grains with 1 mm grid at the background. (Right) Example of typical dry snow grains with 1 mm grid at the background. The grain sizes range from 1.0 to 1.5 mm (mean of maximum diameter) for wet snow, 1.0 mm being the dominant grain size. Dry snow grain sizes range from 0.3 mm to 0.8 mm, the dominant size being 0.5 mm.

(1990), the surface snow layer was defined either dry or wet. Various reflectance cases from snow-free ground to snow depths up to 84 cm were recorded. The optically equivalent snow grain size was visually estimated by comparing a snow sample to a snow crystal screen with 1, 2 and 3-mm-grids, see Fig. 2. If the grain sample's average maximum diameter size was larger than 1 mm, the average value was estimated with a precision of 0.5 mm. With grains smaller than 1 mm, a precision of 0.25 was used. In cases with a mixture of different grain sizes, the range of sizes was recorded, but the typical or average value was used for the whole layer. From each range of sizes, outliers were excluded from the results by visual inspection. The obtained snow grain average maximum diameter sizes ranged between 0.2–2 mm for dry snow and 0.5–3.5 mm for wet snow, respectively. This method was found practical; although more advanced methods can be found from the literature (e.g. Aoki et al., 2000; Matzl & Schneebeli, 2006; Painter et al., 2007). The prevailing solar illumination conditions were visually determined to be either direct i.e. clear (0/8 to 2/8 cloud cover), diffuse i.e. cloudy (6/8 to 8/8 cloud cover) or varying conditions (3/8 to 5/8 cloud cover). Finally, digital photographs were taken from each snow sample and the surrounding environment for possible reanalysis, see Fig. 2. Table 1 summarizes snow, weather and environmental conditions during the measurements.

At the reflectance measurement sites, ground spectrometer-based spectra of wet snow, dry snow and snow-free ground were measured under various weather and sun illumination conditions and at different stages of snow metamorphosis. Generally we followed similar measurement pattern at each site with respect to measurement geometry, sampling strategy and calibration. The instrument foreoptic unit (measurement head) was set to look at nadir (0°) direction with 25° field of view (FOV). The angular anisotropy of the target reflectance was not specifically observed in this investigation. As the measurement head was mounted on a tripod at the height of around 45 cm, it was looking at a surface illumination area of 20 cm diameter. Approximately 90% of the ground-based observations were obtained with 50°–75° sun zenith angle range. Table 2 summarizes the measurement setup for spectrometer observations. Also the key characteristics of mast-borne ASD-observations are listed in Table 2. It should be noted that in northern latitudes during the winter and at the beginning of the snow melt season, solar zenith angles at solar noon are large (>50°).

It is necessary to observe the radiance (W m-2 sr-1 nm-1) reflected from the target and Lambertian standard reference to obtain the reflectance. Calibrated white reference optical panel with known reflectance spectrum was used as a reference (also in the mast-based system). During the calibration, the panel was placed horizontally above the snow surface close to the field of view of the spectrometer in a way that it is consistently under illumination. The calibration was carried out after each measurement series or whenever the illumination or weather conditions changed. Solar irradiation was also measured for each data series with cosine receptor for reanalysis.

The obtained ASD reflectance quantities approximate generally two different measurable reflectance quantities defined by Schaepman-Strub et al. (2006), see Fig. 3. As the used spectrometer has a 25° FOV and the data have been collected under clear (direct) and cloudy (diffuse) solar illumination conditions, the obtained ground spectra approximate the biconical reflectance factor and the hemispherical–conical reflectance factor. Here these quantities are referred to as ASD reflectances in a way that the biconical quantity relates to conditions where irradiance composes mostly of direct component (direct) and the hemispherical–conical quantity relates to cloudy conditions

**Table 1**
Weather and snow conditions for dry and wet snow reflectance acquisitions.

| Parameter | Dry snow spectra | | Wet snow spectra | | Dry snow spectra in shadow | | Wet snow spectra in shadow | |
|---|---|---|---|---|---|---|---|---|
| | Min | Max | Min | Max | Min | Max | Min | Max |
| Air temperature range (°C) | −10.0 | +3.7 | −2.4 | +10.3 | −10.0 | −0.7 | −2.4 | +5.5 |
| Snow surface temperature range (°C) | −10.5 | −0.8 | −2.3 | +1.5 | −10.5 | −1.0 | −2.3 | +0.5 |
| Snow depth range (cm) | 54 | 84 | 0.5 | 73 | 55 | 84 | 45 | 70 |
| Snow grain size range (mm) (mean of max. diameter) | 0.2 | 2 | 0.5 | 3.5 | 0.2 | 1.5 | 0.5 | 3.5 |
| No. of diffuse/direct reflectance sites[a] | 3/5 | | 15/11 | | −/3 | | −/6 | |

Field work period lasted from March to May during 2007 and 2008 consisting of 36 reflectance sites measured in 14 separate days.

[a] 2 of the total of 36 in-situ sites were rejected due to varying illumination conditions; some sites include both direct and diffuse illumination cases.

**Table 2**
Characteristics of ASD instrumentation and measurement set-up.

| Parameter | Ground ASD value | Mast ASD value |
|---|---|---|
| Spectrum | 350–2500 nm | 350–2500 nm |
| Sampling interval | 1.4 nm for 350–1000 nm, 2 nm for 1000–2500 nm | 1.4 nm for 350–1000 nm, 2 nm for 1000–2500 nm |
| Calibration | Spectralon® white panel with known reflectance | Spectralon® white panel with known reflectance |
| Field of view (FOV) | 25° bare fibre | 25° bare fibre |
| View angle direction | 0° i.e. nadir | 11° (8° in Aug. 2006) |
| Average footprint diameter/size | 20 cm | 185 $m^2$ |
| FOV mean distance to target | 45 cm | 33 m |

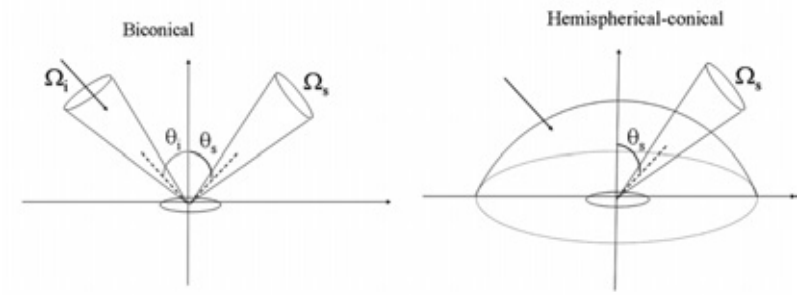


**Fig. 3.** (Left) Biconical reflectance factor here referred to as the direct ASD reflectance obtained in clear sky conditions and (Right) the hemispherical–conical reflectance factor here referred to as diffuse ASD reflectance obtained in cloudy conditions. $\theta_i$ denotes the sun zenith angle and $\theta_s$ the observation angle. Definitions and images are according to (Schaepman-Strub et al., 2006).

where irradiance has mainly diffuse components (diffuse). This is an approximation because in natural conditions the irradiance is not completely hemispherical even in uniformly cloudy weather. In the direct case the Sun disc is the conical source of illumination (almost directional). To be exact, the reflectance under clear skies approximates the biconical case better at the longer wavelengths. At shorter wavelengths, where the diffuse irradiance component is stronger and nontrivial, the reflectance then includes contributions representing both biconical and hemispherical–conical cases. The observed reflectance factor quantities can have values above 1 as the reflected radiation to a certain direction can exceed that of the Lambertian surface. The diffuse ASD reflectance is a quantity that approximates the hemispherical–directional reflectance factor (HDRF), whereas the direct ASD reflectance approximates the bidirectional reflectance factor (BRF) even though the instantaneous FOV of the instrument is 25° (in practice we assume that the reflectance is uniform across that FOV). Satellite instruments are often referred to observe BRF that can be used to estimate the actual surface reflectance (i.e. directional to hemispherical reflectance), typically using the crude assumption that the Earth's surface would be Lambertian.

Analogously to Schaepman-Strub et al. (2006), we can define the equation of BRF and HDRF as:

$$\mathrm{BRF} = \pi \cdot f_s(\theta_i, \varphi_i, \theta_s, \varphi_s; \lambda) = \pi \frac{L(\theta_i, \varphi_i, \theta_s, \varphi_s; \lambda)}{E_i(\lambda)} \quad (1)$$

where the incoming (projected to horizontal level) irradiance $E_i(\lambda) = E_0(\theta_i, \varphi_i; \lambda) \cos\theta_i$, $E_0$ is the incoming irradiance, $L$ is the reflected radiance and $f$ is the BRDF (bidirectional reflectance distribution function). $\theta_i$ and $\varphi_i$ denote sun zenith angle and sun azimuth angle, respectively; $\theta_s$ and $\varphi_s$ denote view zenith angle and view azimuth angle, respectively.

In case of HDRF irradiance is predominantly a hemispherically isotropic quantity and thus

$$\mathrm{HDRF} = \mathrm{BRF} \cdot d + (1-d) \int_0^{2\pi} \int_0^{\frac{\pi}{2}} f_s(\theta_i, \varphi_i, \theta_s, \varphi_s; \lambda) \cos\theta_i \sin\theta_i d\theta_i d\varphi_i \quad (2)$$

where $d$ is the fraction of direct radiant flux.

The absolute accuracy of the reflectance data presented here depends upon the calibration carried out using the white reference panel. In practice, the anisotropic bidirectional reflectance factor of spectralon panel affects the absolute calibration accuracy, especially for the measurement of BRF under clear sky conditions for high zenith angles. We estimated the maximum possible error arising from this in our case by applying data on spectralon BRF presented by Sandmeier et al. (1998). The analysis indicated that at the wavelength band of 459–479 nm, the values reported for reflectance under direct solar illumination conditions, for the very high solar zenith angles of 75°, can be overestimated at the highest of about 6% (assuming that no diffuse irradiance component is present, $d=1$ in Eq. (2)). In case of ideally diffuse conditions $d=0$ in Eq. (2). Then the resulting overestimation at the band of 459–479 nm can be at the highest of about 4%, respectively.

### 2.3. Evaluation of snow reflectance and scene reflectance

Eventually, 36 different ground targets were measured the selection being based on snow properties (snow depth, snow wetness, snow grain size, snow metamorphosis stage and impurity (mainly forest litter) content), target type, illumination conditions, forest shading and land cover type. The selected ground targets' standard deviation and mean are composed of from several dozens up to around 1500 individual spectra at 350–2500 nm. Additionally, reflectances related to selected satellite sensor bands were extracted for *SCAmod* accuracy analysis and method development. These data were classified to represent the following general cases (both for direct and diffuse illumination):

- wet snow (average of all sub-cases)
- dry snow (average of all sub-cases)
- snow-free ground (average for different soil types directly after the snow melt: open bogs, other peat lands, mineral soil sites)
- wet snow in forest shadow (only for direct illumination conditions)
- dry snow in forest shadow (only for direct illumination conditions)
- wet snow, snow depth >20 cm
- wet snow, snow depth <20 cm.

The mast-based spectrometer observations representing both the open and forested area were compared against ground-based snow reflectance measurements. The applied ground-based reflectance data include observations from directly illuminated and shadowed snow surfaces (shadowed by tree trunks and crowns). In practice, a linear mixing model was used to describe the tower-based observations as a function of ground-based ASD-reflectances in cases of the open target area Eq. (3a) and the forested area Eq. (3b):

$$\begin{cases} R_{\lambda,\mathrm{obs}} = F_{\mathrm{direct}}\rho_{\lambda,\mathrm{snow}} + (1 - F_{\mathrm{direct}})\rho_{\lambda,\mathrm{shadow}} & (3a) \\ R_{\lambda,\mathrm{obs}} = F_{\mathrm{direct}}\rho_{\lambda,\mathrm{snow}} + (1 - F_{\mathrm{direct}} - F_{\mathrm{trees}})\rho_{\lambda,\mathrm{shadow}} + F_{\mathrm{trees}}\rho_{\lambda,\mathrm{trees}} & (3b) \end{cases}$$

where $R_{\lambda,\mathrm{obs}}$ is the scene reflectance simulated by ground-based observations, $F_{\mathrm{direct}}$ is the areal fraction of directly illuminated area, $\rho_{\lambda,\mathrm{snow}}$ is the reflectance of directly illuminated snow and $\rho_{\lambda,\mathrm{shadow}}$ is the reflectance of snow in shadow (calibrated to downwelling irradiance at non-shadowed conditions). $F_{\mathrm{trees}}$ is the fraction of tree crowns and trunks in the mast-borne reflectance

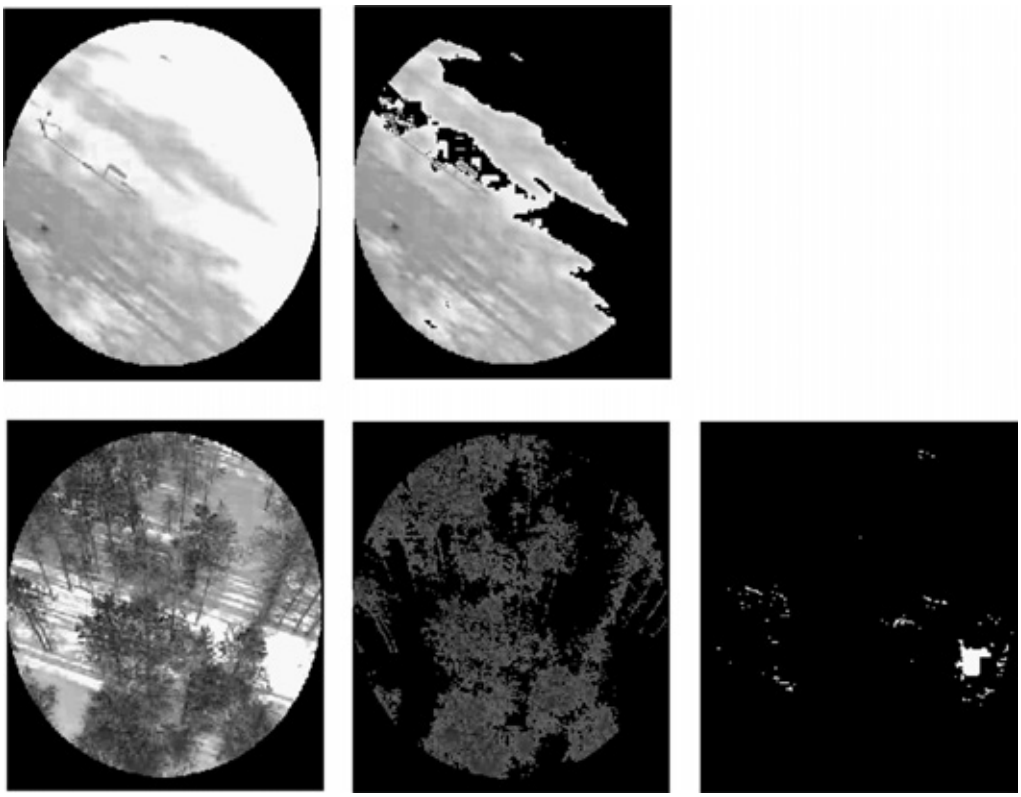

**Fig. 4.** (Above) Digital image and image classification for the mast-borne open area ASD measurement and (Below) for the ASD measurement of the forested area for 28 March 2008. The open area is partially shadowed by trees, the classification (above right) suggest an areal fraction of 60% for the shadowed area. The pixels from the forested area are classified to tree crowns and trunks (44%), and directly illuminated areas (1%), below middle and right respectively (thus the fraction of shadowed area is estimated to be 55%).

observation of the forested area. $\rho_{\lambda,\mathrm{trees}}$ was approximated here from the summer-time measurements of the forested area (when ground is covered by green vegetation, such as heather and lingonberry). One should note that this consideration is not ideal, for example due to the fact that multiple scattering from the snow surface strongly differs from that of green vegetation. Factors $F_{\mathrm{direct}}$ and $F_{\mathrm{trees}}$ are estimated through the analysis of concurrent high-resolution digital photographs of the area (ellipse) observed by the mast-based spectrometer, see Fig. 4.

### 2.4. SCAmod method accuracy assessment

*SCAmod* is based on a reflectance model, where the (space-borne) observed reflectance $R$ is expressed as a function of SCA. The average

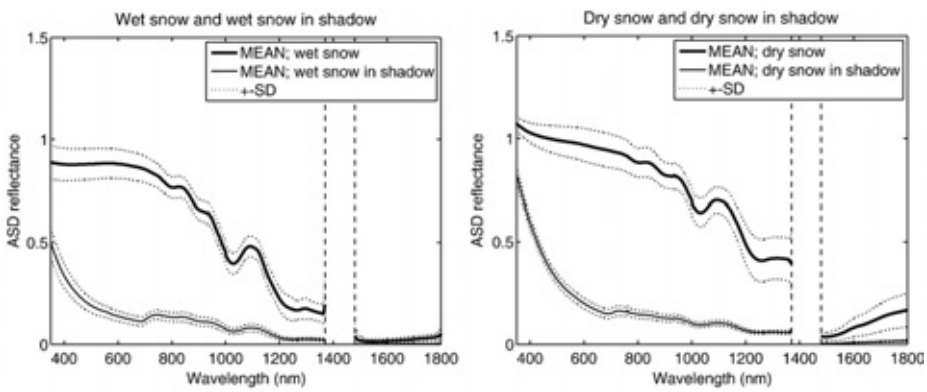


**Fig. 5.** (Left) Mean reflectance ± standard deviation for wet snow and (Right) mean ± standard deviation for dry snow in cases where snow is either under natural direct or diffuse illumination or fully shaded by forest trees (only including direct illumination). The wavelength area around 1400 nm is affected by a bad SNR.

apparent forest canopy transmissivity $t_\lambda$ and reflectances from wet snow $\rho_{\lambda,\text{snow}}$, snow-free ground $\rho_{\lambda,\text{ground}}$, and dense forest canopy $\rho_{\lambda,\text{forest}}$ at wavelength λ, serve as model parameters (Metsämäki et al., 2005):

$$R_{\lambda,\text{obs}} = R_{\lambda,\text{obs}}(\text{SCA}) = \left(1 - t_\lambda^2\right)\rho_{\lambda,\text{forest}} + t_\lambda^2\left[\text{SCA}\rho_{\lambda,\text{snow}} + (1 - \text{SCA})\rho_{\lambda,\text{ground}}\right] \quad (4)$$

The value for effective transmissivity $t_\lambda^2$ is characteristic for each target unit area. It describes how much of the upwelling radiance is originated underneath the forest canopy. Transmissivity is determined from Eq. (4) with at-satellite reflectance observation made at full dry snow cover conditions (SCA = 1). This approach is based on the fact that under full cover dry snow conditions the required reflectance contrast between forest canopy and snow covered ground in forest openings is notable (so the estimate for transmissivity can be derived from satellite data). The applied transmissivity value also includes the effect of tree shadows. Once the transmissivity is determined, the SCA estimate for forested terrain during the spring melt period is obtained by inverting Eq. (4), as follows:

$$\text{SCA} = \frac{\frac{1}{t_\lambda^2}R_{\lambda,\text{obs}} + \left(1 - \frac{1}{t_\lambda^2}\right)\rho_{\lambda,\text{forest}} - \rho_{\lambda,\text{ground}}}{\rho_{\lambda,\text{wetsnow}} - \rho_{\lambda,\text{ground}}} \quad (5)$$

Algorithm (5) is applied for SCA mapping from space-borne data using reflectances from a single channel, typically e.g. MODIS band 3 (459–479 nm) or MERIS band 2 (436–449 nm). Additionally, NDSI or Normalized Difference Vegetation Index (NDVI) is applied in operational snow mapping to detect the disturbing effect of emerging green vegetation at the end of snow melt period. In the statistical accuracy analysis the law of error propagation can be applied. This approach provides the standard deviation of the SCA as a sum of partial derivatives (separately with respect to each model parameter) multiplied by these parameters' variances (Metsämäki et al., 2005). Therefore, the information on the variability of the model parameters is essential. These variances can be derived from experimental at-field reflectance measurements, from spectral libraries or from the space-borne earth observation data. In this work, at-ground reflectance measurements with ASD were used in order to determine variances for two reflectance contributors: wet snow and snow-free ground. The term for forest canopy reflectance was not considered in the sensitivity analyses here (one should note that the magnitude of forest canopy reflectance is only few percentages in blue wavelength often applied in snow algorithms).

The contribution of wet snow reflectance fluctuations to the standard deviation (standard error) of an SCA estimate is:

$$\text{std}(SCA)_{|\rho_{\lambda,\text{wetsnow}}} = \frac{\partial(\text{SCA})}{\partial\rho_{\lambda,\text{wetsnow}}}\text{std}\left(\rho_{\lambda,\text{wetsnow}}\right) = \frac{-\left[\frac{1}{t_\lambda^2}R_{\lambda,\text{obs}} + \left(1 - \frac{1}{t_\lambda^2}\right)\rho_{\lambda,\text{forest}} - \rho_{\lambda,\text{ground}}\right]}{\left(\rho_{\lambda,\text{wetsnow}} - \rho_{\lambda,\text{ground}}\right)^2}\text{std}\left(\rho_{\lambda,\text{wetsnow}}\right) \quad (6)$$

The contribution of ground surface reflectance fluctuations to the standard deviation (standard error) of an SCA estimate is:

$$\text{std}(\text{SCA})_{|\rho_{\lambda,\text{ground}}} = \frac{\partial(\text{SCA})}{\partial\rho_{\lambda,\text{ground}}}\text{std}\left(\rho_{\lambda,\text{ground}}\right) = \frac{\frac{1}{t_\lambda^2}R_{\lambda,\text{obs}} + \left(1 - \frac{1}{t_\lambda^2}\right)\rho_{\lambda,\text{forest}} - \rho_{\lambda,\text{snow}}}{\left(\rho_{\lambda,\text{wetsnow}} - \rho_{\lambda,\text{ground}}\right)^2}\text{std}\left(\rho_{\lambda,\text{ground}}\right) \quad (7)$$

Finally, the total error is gained as a sum of these terms:

$$\text{std}_{\text{tot}} = \sqrt{\left(\text{std}(\text{SCA})_{|\rho_{\lambda,\text{ground}}}\right)^2 + \left(\text{std}(\text{SCA})_{|\rho_{\lambda,\text{ground}}}\right)^2} \quad (8)$$

We calculated the total error for different SCA values and for three different wavelength bands related to operating space-borne optical sensors (MODIS, MERIS and AVHRR).

## 3. Results and discussion

Figs. 5 and 6 (Left) present the obtained standard deviation and mean reflectance spectra (biconical and hemispherical–conical reflectance factors) for wet snow, dry snow and snow-free ground, respectively. Note that the reflectance considered here refers to an *apparent* reflectance, i.e. a physical quantity observed by an Earth Observation sensor. For example, the apparent reflectance in shade stands for measured radiance (in shade) divided by the full irradiance (no shade). The corresponding quantitative information for selected wavelength bands relevant to MODIS-based snow monitoring is given in Table 3. The focused bands are essential for snow applications as MODIS band 3 (459–479 nm) is used e.g. in SYKE's operational snow map production based on *SCAmod*, while bands 4 (545–565 nm) and 6 (1628–1652 nm) are used for the Normalized Difference Snow Index (NDSI) to obtain global snow map products (Hall et al., 2002). Table 3 shows the obtained ASD reflectance values separately for direct and diffuse illumination conditions and for the combination of these two. Reflectance statistics for relevant MERIS and AVHRR wavelength

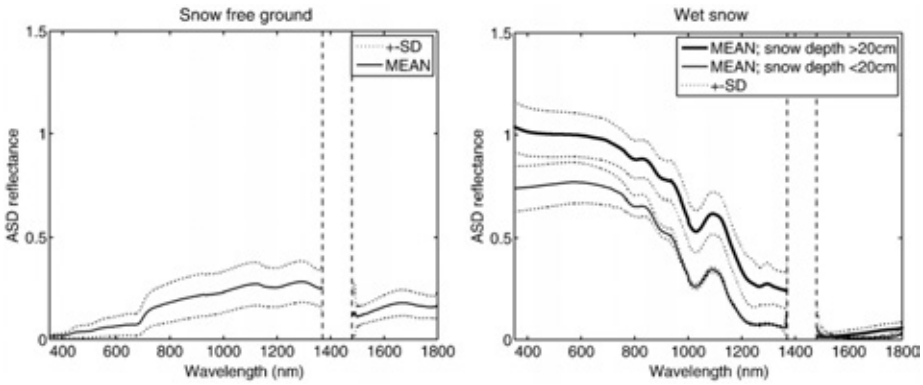


**Fig. 6.** (Left) Mean reflectance ± standard deviation for snow-free ground and (Right) mean reflectance ± standard deviation for wet snow in cases where snow depth is either above or below 20 cm. Results include both direct and diffuse illumination. The wavelength area around 1400 nm is affected by a bad SNR.

**Table 3**
Ground spectrometer derived reflectance for wet snow, dry snow and snow-free ground: mean and standard deviation under direct, diffuse and combined sunlight illumination conditions.

| Direct illumination | No. of obs. | ASD 459–479 nm | | ASD 545–565 nm | | ASD 1628–1652 nm | |
|---|---|---|---|---|---|---|---|
| | | Mean | SD | Mean | SD | Mean | SD |
| Wet snow | 450 | 0.95 | 0.09 | 0.94 | 0.10 | 0.03 | 0.01 |
| Dry snow | 240 | 1.00 | 0.08 | 0.98 | 0.10 | 0.09 | 0.06 |
| Snow-free ground | 120 | 0.03 | 0.02 | 0.04 | 0.02 | 0.14 | 0.05 |
| Wet snow, snow depth >20 cm | 450 | 0.95 | 0.09 | 0.94 | 0.10 | 0.03 | 0.01 |
| Wet snow, snow depth <20 cm | – | – | – | – | – | – | – |
| Wet snow, in shadow | 180 | 0.22 | 0.04 | 0.16 | 0.03 | 0.00 | – |
| Dry snow, in shadow | 90 | 0.38 | 0.03 | 0.24 | 0.03 | 0.01 | 0.00 |
| Diffuse illumination | No. of obs. | Mean | SD | Mean | SD | Mean | SD |
| Wet snow* | 840 | 0.89 | 0.08 | 0.90 | 0.07 | 0.02 | 0.02 |
| Dry snow | 190 | 1.00 | 0.02 | 0.98 | 0.03 | 0.11 | 0.04 |
| Snow-free ground | 210 | 0.04 | 0.03 | 0.07 | 0.05 | 0.19 | 0.06 |
| Wet snow, snow depth >20 cm | 750 | 1.04 | 0.12 | 1.04 | 0.10 | 0.03 | 0.03 |
| Wet snow, snow depth <20 cm | 90 | 0.75 | 0.10 | 0.77 | 0.10 | 0.01 | 0.01 |
| Direct and diffuse illumination | No. of obs. | Mean | SD | Mean | SD | Mean | SD |
| Wet snow* | 1290 | 0.88 | 0.08 | 0.88 | 0.07 | 0.02 | 0.01 |
| Dry snow | 430 | 1.00 | 0.06 | 0.98 | 0.08 | 0.10 | 0.05 |
| Snow-free ground | 330 | 0.04 | 0.03 | 0.06 | 0.04 | 0.17 | 0.06 |
| Wet snow, snow depth >20 cm | 1270 | 1.00 | 0.11 | 1.00 | 0.11 | 0.03 | 0.02 |
| Wet snow, snow depth <20 cm | 90 | 0.75 | 0.10 | 0.77 | 0.10 | 0.01 | 0.01 |

The used wavelengths correspond to MODIS bands 3 (459–479 nm), 4 (545–565 nm) and 6 (1628–1652 nm).
*Average values for classes: wet snow depth >20 cm and wet snow depth <20 cm (root mean squared value in case of standard deviation).

bands are given in Table 4, respectively. The grain size range in the results of Fig. 5, and those of Tables 3 and 4 was 0.5–3.5 mm (mean of maximum diameter) for wet snow and 0.2–2 mm for dry snow. Snow depth distribution was 0.5–73 cm for wet snow and 54–84 cm for dry snow. As wet snow case includes several sub-cases, such as very shallow snowpack, we calculated weighted standard deviation and mean in order to obtain representative average wet snow reflectance (the weighted values are presented in Tables 3 and 4). In order to obtain the snow-free ground reflectance spectrum presented in Fig. 6 (Left), ASD observations from typical boreal forest understorey ground targets were averaged, such as mixture of low shrubs and grasses, heather, lichen, moss, lingonberry and forest litter (from measurements carried out directly after the snow melt).

The results indicate that in general, for visible wavelengths, the overall reflectance of dry snow is only slightly higher than that of wet snow, but the difference is significant in NIR and SWIR wavelengths especially for thick snow (with no contribution from the underlying soil). This coincides well with the results by Odermatt et al. (2005). Likewise, measurements by Li and Zhou (2004) indicate that with low sun and nadir view geometry, visible reflectance (HDRF) of both large and fine grained snow is close to 1, but at NIR wavelengths reflectance of larger grains is clearly lower. We also compared the spectra collected either under direct or under diffuse illumination and found that for selected wavelengths used in this study, the difference is small: the highest differences in the mean values were found for wet snow indicating a shift of 6%-units at the MODIS band of 459–479 nm (a relative difference of 6.5%), refer to Table 3 (direct and diffuse illumination). With different combinations of large/fine-grained and wet/dry snow, there was no observable difference. Thus, we calculated the overall standard deviation and mean for wet and dry snow from both direct and diffuse cases in order to obtain a more comprehensive data set to represent the melting season conditions presumed by *SCAmod*. These values are also given in Table 3.

Tables 3 and 4 also indicate that the standard deviations of observed reflectances for diffuse and direct illumination conditions do not differ significantly in general. This is an important notice, as it suggests that the variance in observations is due to the variability of in target characteristics, not due to the varying sun zenith angle (the variance observed under diffuse conditions cannot result from the changes in the sun zenith angle).

In Fig. 6 (Right), standard deviation and mean of shallow and thick wet snow are compared. This is an important aspect concerning the SCA estimation as towards the end of the melting season shallow snow conditions are usually predominant and the percentage of patchiness increases. The results show that under snow depths less than 20 cm the reflectance values decrease significantly. Also snow optical depth (and thus transmissivity through snowpack), which is related to snow density, depth, grain size and wavelength in concern, decreases with decreasing snow depth. The results in Fig. 6 clearly show that snow depth has a strong effect on the observed snow reflectance, in fact even much more significant than that of snow grain size. This was observed from the measurements by comparing data with different grain sizes and wetnesses for all snow depths. Snow depth was the only factor explaining the behaviour. Note that in Figs. 5 and 6, the data at wavelengths around 1400 nm was removed due to an insufficient signal to noise ratio (SNR).

Fig. 7 shows how the standard deviation of reflectance behaves for wet snow and snow-free ground in wavelengths below 1000 nm. Since an SCA-estimation method should be as much invariant to fluctuations of reflectances as possible, these data are very useful in choosing the optimal wavelengths to be applied. The coefficient of variation (SD/mean ratio) also given in Fig. 7 provides us valuable information for this judgement. For example, in the case of *SCAmod*, those satellite-sensor bands for which we obtained the smallest coefficients of variation both for wet snow and snow-free ground, are the most applicable and will minimize the error in the SCA estimation (note that this investigation does not discuss the spectral effects of atmospheric disturbances nor the performance of atmospheric corrections). Again, as *SCAmod* uses single band reflectances, we

**Table 4**
Ground spectrometer derived reflectance for wet snow, dry snow and snow-free ground: mean and standard deviation under direct, diffuse and combined sunlight illumination conditions.

| Direct illumination | No. of obs. | ASD-derived MERIS 436–449 nm | | ASD-derived AVHRR 580–680 nm | |
|---|---|---|---|---|---|
| | | Mean | SD | Mean | SD |
| Wet snow | 450 | 0.96 | 0.09 | 0.93 | 0.10 |
| Dry snow | 240 | 1.01 | 0.08 | 0.96 | 0.10 |
| Snow-free ground | 120 | 0.03 | 0.01 | 0.05 | 0.02 |
| Wet snow, snow depth >20 cm | 450 | 0.96 | 0.09 | 0.93 | 0.10 |
| Wet snow, snow depth <20 cm | – | – | – | – | – |
| Wet snow, in shadow | 180 | 0.26 | 0.05 | 0.13 | 0.02 |
| Dry snow, in shadow | 90 | 0.45 | 0.03 | 0.18 | 0.02 |
| Diffuse illumination | No. of obs. | Mean | SD | Mean | SD |
| Wet snow* | 840 | 0.89 | 0.08 | 0.89 | 0.07 |
| Dry snow | 190 | 1.01 | 0.02 | 0.96 | 0.04 |
| Snow-free ground | 210 | 0.04 | 0.03 | 0.08 | 0.06 |
| Wet snow, snow depth >20 cm | 750 | 1.04 | 0.12 | 1.03 | 0.09 |
| Wet snow, snow depth <20 cm | 90 | 0.75 | 0.10 | 0.76 | 0.09 |
| Direct and diffuse illumination | No. of obs. | Mean | SD | Mean | SD |
| Wet snow[a] | 1290 | 0.88 | 0.08 | 0.87 | 0.07 |
| Dry snow | 430 | 1.01 | 0.06 | 0.96 | 0.08 |
| Snow-free ground | 330 | 0.03 | 0.02 | 0.07 | 0.05 |
| Wet snow, snow depth >20 cm | 1270 | 1.01 | 0.11 | 0.99 | 1.10 |
| Wet snow, snow depth <20 cm | 90 | 0.75 | 0.10 | 0.76 | 0.09 |

The used wavelengths correspond to MERIS band 2 (436–449 nm) and AVHRR band 1 (580–680 nm).
[a] Average values for classes: wet snow depth >20 cm and wet snow depth <20 cm (root mean squared value in case of standard deviation).

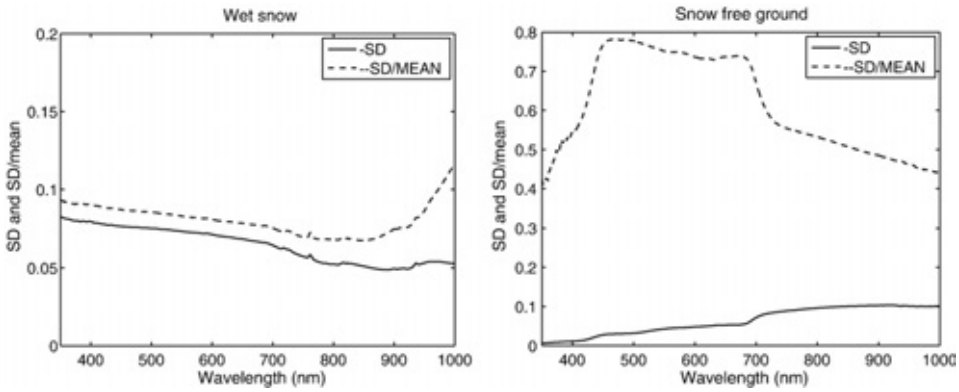


**Fig. 7.** (Left) Standard deviation and the coefficient of variation of reflectance (standard deviation/mean) for wet snow and (Right) snow-free ground.

focused on the selected wavelength areas in contrast to Painter et al. (2003), who focus on wide spectrum to consider the reflectance variation. According to the results in Fig. 7, wavelengths between 450 nm and 700 nm exhibit a high variability for the reflectivity of snow-free ground reducing their feasibility to wet snow detection. In contrast to that, the coefficient of variation for wet snow reflectance decreases with increasing wavelength. However, the practical usability of NIR bands during spring-melt is deteriorated by the effect of green vegetation hampering the difference in signal between snow and snow-free ground. The blue wavelengths correspond to MODIS band 3 (459–479 nm) and MERIS band 2 (436–449 nm). The usability of NIR bands is deteriorated by the effect of green vegetation hampering the difference in signal between snow and snow-free ground.

Figs. 8 and 9 show the behaviour of the statistical error contribution to SCA estimation performance due to the spatial and temporal variability of wet snow and snow-free ground reflectance. The results are obtained for *SCAmod* applying Eqs. (6)–(8) for the collected ASD reflectance data set. Again, wavelengths related to MODIS, MERIS and AVHRR bands are in focus. In Fig. 8, the standard error for SCA estimate as a function of SCA is presented due to wet snow reflectance variability only (Left) and due to snow-free ground reflectance variability only (Right). The behaviour of standard error in both cases is very logical: when wet snow reflectance is accounted for, the error increases together with increasing SCA, and when snow-free area is accounted for, the error is highest when the ground has no snow, decreasing with increasing SCA. The results of Fig. 8 are calculated by inserting Eq. (4) to either Eq. (6) or (7). Thus, the effect of forests is negligible in the error behaviour depicted. That is, these error contributors are not affected by the forest canopy characteristics. Results depicted in Fig. 8 are combined in Fig. 9 by applying Eq. (8). Thus, Fig. 9 illustrates the total standard error (Left) and total relative standard error (Right) for different fractions of snow coverage. The results show that although the reflectances of wet snow and snow-free ground do have significant variation, their influence to the actual SCA-estimate is tolerable, the maximum total error being 12%-units, depending on the value of SCA. The relative errors also show a satisfying accuracy; less than 20% for most of the SCA-cases (the increase of the relative error towards low SCA-values is insignificant as the absolute SCA-level is very small). It is also worth noting that the gained standard errors, when only wet snow and snow-free ground fluctuations are concerned, are independent from the apparent forest transmissivity.

However, forest cover is a major disturbing factor in snow monitoring with satellite sensors, since forests block the visibility from the snow surface to satellite sensor and since shadows of the trees decrease the reflectance observed above the forest canopy. This is difficult to accurately consider for varying sun and view zenith angles in models such as Eq. (4). Additionally, forest canopy (crowns and trunks) reflects a part of incoming radiation, though a very small percentage in blue to green wavelengths, such as MODIS bands 3 (459–479 nm) and 4 (545–565 nm), and MERIS band 2 (436–449 nm). Nevertheless, as *SCAmod* is based on Eq. (4), the apparent (two-way) forest canopy transmissivity considers and reduces the blocking effect

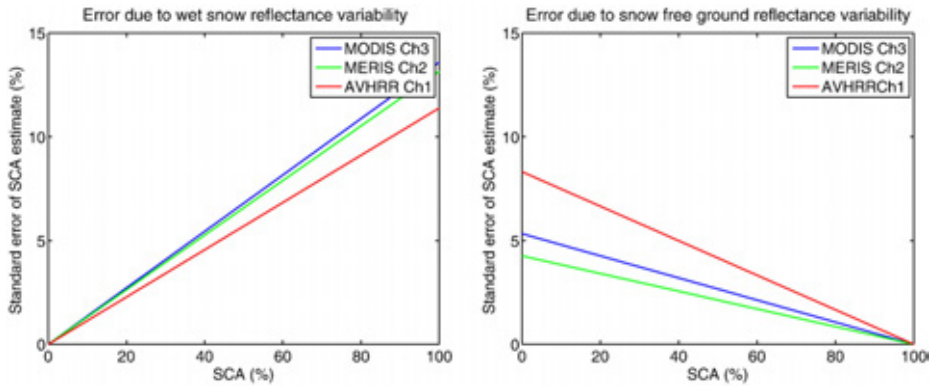


**Fig. 8.** (Left) The standard error of SCA estimation due to wet snow reflectance variability and (Right) snow-free ground reflectance variability. The error is estimated using wavelengths corresponding to MODIS band 3 (459–479 nm), MERIS band 2 (436–449 nm) and AVHRR band 1 (579–681 nm).

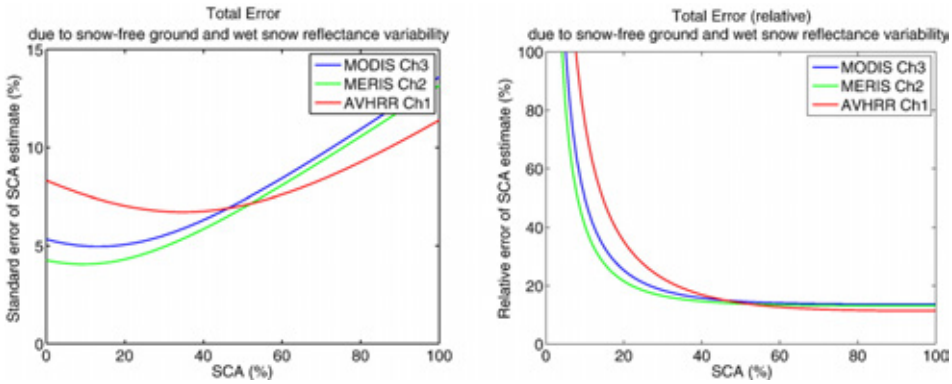


**Fig. 9.** (Left) The standard error (%-units) of SCA estimation due to both wet snow and snow-free ground reflectance variability. The error is estimated using wavelengths corresponding to MODIS band 3 (459–479 nm), MERIS band 2 (436–449 nm) and AVHRR band 1 (579–681 nm). (Right) The relative error (total error divided by SCA) due to both wet snow and snow-free ground reflectance variability.

of forest canopy as well as tree shadowing effects. In this study, the absolute effect of forest cover on scene reflectance was demonstrated with mast-based ASD-observations. In practise, mast-based spectrometer measurements were simulated with linear spectral mixing of ground-based ASD reflectances. This enabled the investigation of scene reflectances observed above the tree cover.

The scene reflectance was modelled using Eq. (3a) for the forest opening also measured with the mast-based spectrometer. The same was repeated for the forested area by applying Eq. (3b). The image analysis of data shown in Fig. 4 indicated that pine tree shadows covered a fraction of 60% of the spectrometer footprint during the mast-based measurement of the open area. In case of the forested area, the areal fractions of different target constitutes were: 43.5% for the tree shadows, 55.3% for the crowns/trunks and 1.3% for the directly illuminated snow cover. This information accompanied with dry snow reflectance and tree shadow reflectance data (examples for certain wavelengths given in Table 3 were used as input to (3a and 3b). For the forested area (3b) the crown reflectance was approximated by the mast-based summer-time measurements of the forested target area (assuming that ground reflectance is close to forest canopy reflectance).

The resulting reflectance spectrum simulation is presented in Fig. 10. Fig. 10 also depicts the actual observation with the mast-based spectrometer indicating a higher level of reflectance for the visible wavelengths, but spectrally an analogous response. Figs. 4 and 10 demonstrate the strong effect of tree cover even for forest openings, which has to be considered by snow monitoring algorithms if they are applied to forested regions, such as northern Finland. In case of *SCAmod* these effects are primarily considered by introducing the apparent forest canopy transmissivity. The other evident alternative is the use of spectral unmixing techniques in SCA estimation to consider the effects of tree shadows, blocking by tree canopy and the influence of crown/trunk reflectance, thus inversion of Eqs. (3a and 3b). However, this requires detailed structural forest canopy *a priori* information for estimating different target type coverage fractions, i.e. such information as that demonstrated in Fig. 4.

The possible reasons for the reflectivity difference between the predicted and observed scene reflectance factor in Fig. 10 include the small difference in the imaging geometry. The mast-based spectrometer observation of the forest opening was performed for a forward scattering direction with an azimuth angle difference of 125° between the directions of the Sun and spectrometer measurement head, and additionally, the spectrometer was tilted 11° off the nadir. In case of the forested target area, the scattering geometry was slightly towards the backward direction (azimuth angle difference of 70°). In case of observations with portable spectrometer the measurement direction

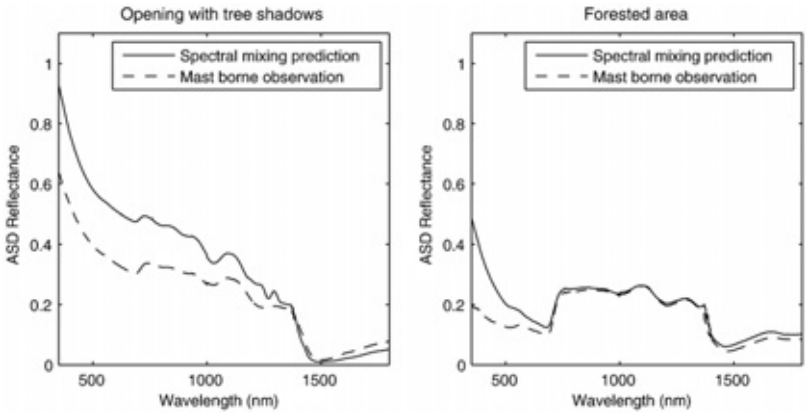


**Fig. 10.** (Left) Observed and predicted reflectance factor of a dry snow covered open area shadowed by pine trees and (Right) of a forested area. Measurements are carried out by the mast-borne ASD spectrometer on 28 March 2008. The corresponding prediction according to (3) is based on spectra measured by the ground-based portable ASD-system. The fraction of shadowed area is determined from Fig. 4. The dry snow and shadowed snow spectra correspond to mean observations (see Tables 3, 4 and Fig. 5).

was towards the nadir. The difference in the Sun elevation angle was marginal (slightly varying in the field spectrometer data set, refer to Table 2). Another possible reason for the difference in reflectance level may arise from the target geometry. Point-wise field spectrometer measurements represent small areas with a diameter of 20 cm, see Table 2. Mast-borne measurements are collected from a larger region (ellipse with main axes of 16.0 and 14.7 m), which include some surface undulations. As a consequence, Fig. 10 suggests that the absolute level of scene reflectance at visible wavelengths cannot be directly simulated with spectral mixing of field spectrometer-derived reflectance values.

## 4. Summary and conclusions

In this work, the variability of ground reflectance was investigated in order to assess the feasibility of satellite sensors to the mapping of snow covered area in the boreal forest zone. The results obtained here suggest certain requirements for space borne instruments applied to snow cover mapping. First of all, snow algorithm works best for visible wavelengths, as in this region, snow reflectance is most invariant to snow physical properties (e.g. grain size). From ASD-measurements, we found that using wavelengths at 400–480 nm or 700–800 nm, the lowest standard deviation of wet snow spectra was gained. However, in 700–800 nm region, the effect of green vegetation hampers the distinguishing of snow; therefore we concluded that when a single channel algorithm (such as *SCAmod*) is applied wavelengths 400–480 nm also with a very low standard deviation of reflectance variation, are most suitable for snow cover mapping. Due to the effect of atmospheric gases and aerosols into the reflectances in this region, it would be beneficial to use an atmospheric correction procedure in order to obtain surface reflectances instead of top-of-the-atmosphere reflectances. Neglecting the atmospheric effect will result to somewhat erroneous snow information; the magnitude of error is primarily dependent on the water vapour and aerosol content of the atmosphere during the image acquisitions.

We investigated the performance of the *SCAmod* method by applying ASD-derived reflectances for two of the *SCAmod* model parameters: wet snow and snow-free ground. Special focus was on the wavelengths related to MODIS, MERIS and AVHRR bands often utilized in snow detection. A standard error of about 5–7%-units was on average obtained, the maximum error of 10–12%-units occurring at full snow cover conditions. The results for MERIS and MODIS were notably better than those for AVHRR when SCA showed values below 40% suggesting that these instruments can be better used in snow mapping at the end of the melting season (which is the most essential period concerning hydrological end-use applications).

The investigation also demonstrates the feasibility of surface reflectance observations to predict scene reflectance characteristics actually observed by space-borne instruments. Combining the actual satellite observations with the ground-based data given in this paper is a topic of ongoing research and publication. The data presented here is also scheduled to be used in similar kind of analysis for NDSI as what is done here for *SCAmod*. The future work will further utilize the reflectance measurements of forest canopy, using spectrometer placed on the mast above the tree height. The collected data will be used in the further accuracy analysis of *SCAmod* and in the algorithm optimization. In order to derive the statistical accuracy of the apparent transmisivity, additional dry snow (illuminated and shadowed) reflectance measurements, together with forest canopy measurements, are required.

## Acknowledgements

This work has been supported by the SNOW-CLIM (Snow Mapping of Boreal and Sub-Arctic Zones: Earth Observation Data-Based Multi-Source Information Systems and Application to Climatic Studies) project funded by the Academy of Finland. The work has been also supported by Interreg IIIA Nordkalotten-program project NorSEN (Nordkalotten Satellite Evaluation co-operation Network), http://norsen.fmi.fi/.

## References

Anttila, S., Metsämäki, S., Pulliainen, J., & Luojus, K. (2005). From EO data to snow covered area end products using automated processing system. *Proceedings of the IEEE 2005 International Geoscience and Remote Sensing Symposium (IGARSS'05), Harmony Between Man and Nature, 25–29 July 2005, Seoul Korea, 1947–1950*.

Aoki, T., Aoki, T., Fukabori, M., Hachikubo, A., Tachibana, Y., & Nishio, F. (2000). Effects of snow physical parameters on spectral albedo and bidirectional reflectance of snow surface. *Journal of Geophysical Research, 105*(D8), 10,219−10,236.

Barry, R. G., Armstrong, R., Callaghan, T., Cherry, J., Gearheard, S., Nolin, A., et al. (2007). Snow. *Global Outlook for Ice and Snow* (pp. 39−62). : UNEP Available at http://www.unep.org/geo/geo_ice/PDF/full_report_LowRes.pdf

Colbeck, S., Akitaya, E., Armstrong, R., Gubler, H., Lafeuille, J., Lied, K., et al. (1990). *The international classification for seasonal snow on the groundWorking Group on Snow Classification*. (pp. 23) Available at www.crrel.usace.army.mil/techpub/CRREL_-Reports/reports/Seasonal_Snow.pdf

FAO (2003). Forest area statistics. Available at http://www.fao.org/forestry/site/32185/en/fin (Accessed 6 February 2008).

Hall, D., Riggs, G. A., Salomonson, V. V., DiGirolamo, N. E., & Bayr, K. J. (2002). MODIS snow-cover products. *Remote Sensing of Environment, 83*, 181−194.

Härmä, P., Teiniranta, R., Törmä, M., Repo, R., Järvenpää, E., & Kallio, M. (2004). Production of CORINE2000 land cover data using calibrated LANDSAT 7 ETM satellite image mosaics and digital maps in Finland. *Proceedings of the IEEE 2004 International Geoscience and Remote Sensing Symposium (IGARSS'04), Science for Society: Exploring and Managing a Changing Planet, 20–24 September 2004, Anchorage Alaska USA* (pp. 2703−2706).

Jaagus, J. (1997). The impact of climate change on the snow cover pattern in Estonia. *Climatic Change, 36*, 65−77.

Jylhä, K., Tuomenvirta, H., & Ruosteenoja, K. (2004). Climate change projections for Finland during the 21st century. *Boreal Environment Research, 9*, 127−152.

Kitaev, L., Førland, E., Razuvaev, V., Tveito, O. E., & Krueger, O. (2005). Distribution of snow cover over Northern Eurasia. *Nordic Hydrology, 36*, 311−319.

Kitaev, L., Kislov, A., Krenke, A., Razuvaev, V., Martuganov, R., & Konstantinov, I. (2002). The snow cover characteristics of northern Eurasia and their relationship to climatic parameters. *Boreal Environment Research, 7*, 437−445.

Kokhanovsky, A. A., Aoki, T., Hachikubo, A., Hori, M., & Zege, E. P. (2005). Reflective properties of natural snow: Approximate asymptotic theory versus *in situ* measurements. *IEEE Transactions on Geoscience and Remote Sensing, 43*, 1529−1535.

Kuusisto, E. (1984). Snow accumulation and snowmelt in Finland. *Publications of the Water Research Institute, vol. 55*. (pp. 149)Helsinki: National Board of Waters.

Li, S., & Zhou, X. (2004). Modelling and measuring the spectral bidirectional reflectance factor of snow-covered sea ice: an intercomparison study. *Hydrological processes, 18*, 3559−3581.

Lundberg, A., & Halldin, S. (2001). Snow measurement techniques for land-surface-atmosphere exchange studies in boreal landscapes. *Theoretical and Applied Climatology, 70*, 215−230.

Matzl, M., & Schneebeli, M. (2006). Measuring specific surface area of snow by near-infrared photography. *Journal of Glaciology, 52*(179), 558−564.

Mellander, P. -E., Löfvenius, M. O., & Laudon, H. (2007). Climate change impact on snow and soil temperature in boreal Scots pine stands. *Climatic Change, 85*, 179−193.

METLA (2007). *Finnish Statistical Yearbook of Forestry* (pp.149) : Finnish Forest Research Institute.

Metsämäki, S., Anttila, S. T., Huttunen, J. M., & Vepsäläinen, J. A. (2005). A feasible method for fractional snow cover mapping in boreal zone based on a reflectance model. *Remote Sensing of Environment, 95*, 77−95.

Metsämäki, S., Huttunen, M., & Anttila, S. (2004). The operative remote sensing of snow covered area in a service of hydrological modeling in Finland. *Proceedings of the 23rd Symposium of the European Association of Remote Sensing Laboratories (EARSeL), Remote Sensing in Transition, 2–5 June 2004, Rotterdam Belgium* (pp. 219−225).

Nolin, A. W., & Dozier, J. (1993). Estimating snow grain-size using AVIRIS data. *Remote sensing of Environment, 44*(2–3), 231−238.

Nolin, A. W., & Dozier, J. (2000). A hyperspectral method for remotely sensing the grain size of snow. *Remote Sensing of Environment, 74*, 207−216.

Odermatt, D., Schläpfer, D., Lehning, M., Schwikowski, M., Kneubühler, M., & Itten, K. I. (2005). Seasonal study of directional reflectance properties of snow. *European Association of Remote Sensing Laboratories EARSeL eProceedings 4, 2/2005* (pp. 203−214). Available at http://las.physik.uni-oldenburg.de/eProceedings/vol204_202/204_202_odermatt201.pdf

Oksanen, T. (1999). Suomen lumipeitteen alueellinen vaihtelu (p. 65): Master's thesis. University of Helsinki, Department of Physical Sciences. Available at http://ethesis.helsinki.fi (In Finnish).

Painter, T. H., & Dozier, J. (2004). Measurements of the hemispherical-directional reflectance of snow at fine spectral and angular resolution. *Journal of Geophysical Research, 109*, D18115.

Painter, T. H., Dozier, J., Roberts, D. A., Davis, R. E., & Green, R. O. (2003). Retrieval of subpixel snow-covered area and grain size from imaging spectrometer data. *Remote Sensing of Environment, 85*, 64−77.

Painter, T. H., Molotch, N. P., Cassidy, M., Flanner, M., & Steffen, K. (2007). Contact spectroscopy for the determination of stratigraphy of snow grain size. *Journal of Glaciology, 53*(180), 121−127.

Painter, T. H., Roberts, D. A., Green, R. O., & Dozier, J. (1998). The effect of grain size on spectral mixture analysis of snow-covered area from AVIRIS data. *Remote Sensing of Environment*, *65*, 320−332.

Rosenthal, W. (1996). Estimating alpine snow cover with unsupervised spectral unmixing. *Proceedings of the IEEE 1996 International Geoscience and Remote Sensing Symposium (IGARSS 1996), 27–31 May 1996, Lincoln Nebraska USA* (pp. 2252−2254).

Räisänen, J. (2008). Warmer climate: less or more snow? *Climate Dynamics*, *30*, 307−319.

Salomonson, V. V., & Appel, I. (2004). Estimating fractional snow cover from MODIS using the normalized difference snow index. *Remote Sensing of Environment*, *89*, 351−360.

Sandmeier, S., Müller, C., Hosgood, B., & Andreoli, G. (1998). Sensitivity analysis and quality assessment of laboratory BRDF data. *Remote Sensing of Environment*, *64*(2), 176−191.

Schaepman, M. E., Green, R. O., Ungar, S. G., Curtiss, B., Boardman, J., Plaza, A. J., et al. (2006). The future of imaging spectroscopy—Prospective technologies and applications. *Proceedings of the IEEE 2006 International Geoscience and Remote Sensing Symposium (IGARSS'06) and 27th Canadian Symposium on Remote Sensing, July 31–August 4, 2006, Denver Colorado USA, 2005–2009*.

Schaepman-Strub, G., Schaepman, M. E., Painter, T. H., Dangel, S., & Martonchik, J. V. (2006). Reflectance quantities in optical remote sensing—Definitions and case studies. *Remote Sensing of Environment*, *103*, 27−42.

Sturm, M., Holmgren, J., & Liston, G. E. (1995). A seasonal snow cover classification system for local to global applications. *Journal of Climate*, *8*, 1261−1283.

Sukuvaara, T., Pulliainen, J., Kyrö, E., Suokanerva, H., Heikkinen, P., & Suomalainen, J. (2007). Reflectance spectroradiometer measurement system in 30 meter mast for validating satellite images. *Proceedings of the IEEE 2007 International Geoscience and Remote Sensing Symposium (IGARSS), Sensing And Understanding Our Planet, 23–27 July 2007, Barcelona Spain* (pp. 1524−1528).

Walsh, J. E. (2005). Cryosphere and hydrology. *Arctic Climate Impact Assessment* (pp. 183−242) : Cambridge University Press Available at http://www.acia.uaf.edu

Warren, S. G. (1982). Optical properties of snow. *Reviews of Geophysics and Space Physics*, *20*, 67−89.

Vavrus, S. (2007). The role of terrestrial snow cover in the climate system. *Climate Dynamics*, *29*, 73−88.

Vikhamar, D., & Solberg, R. (2003). Snow-cover mapping in forests by constrained linear spectral unmixing of MODIS data. *Remote Sensing of Environment*, *88*, 309−323.

Vikhamar, D., & Solberg, R. (2003). Subpixel mapping of snow cover in forests by optical remote sensing. *Remote Sensing of Environment*, *84*, 69−82.

Wiscombe, W. J., & Warren, S. G. (1980). A model for the spectral albedo of snow. I: pure snow. *Journal of the Atmospheric Sciences*, *37*, 2712−2733.

Xie, Y., Yang, P., Gao, B. -C., Kattawar, G. W., & Mishchenko, M. I. (2006). Effect of ice crystal shape and effective size on snow bidirectional reflectance. *Journal of Quantitative Spectroscopy & Radiative Transfer*, *100*, 457−469.

II

Remote Sensing of Environment 138 (2013) 51–64

Contents lists available at SciVerse ScienceDirect

Remote Sensing of Environment

journal homepage: www.elsevier.com/locate/rse

# MODIS-derived snow-free ground reflectance statistics of selected Eurasian non-forested land cover types for the application of estimating fractional snow cover

Miia Salminen [a,b,*], Jouni Pulliainen [b], Sari Metsämäki [a], Kristin Böttcher [a], Kirsikka Heinilä [a]

[a] Finnish Environment Institute, Data and Information Centre, Geoinformatics, P.O. Box 140, FI-00251 Helsinki, Finland
[b] Finnish Meteorological Institute, Arctic Research, Tähteläntie 62, 99600 Sodankylä, Finland

ARTICLE INFO

*Article history:*
Received 4 February 2013
Received in revised form 12 June 2013
Accepted 6 July 2013
Available online xxxx

*Keywords:*
Snow-free ground
Reflectance
Seasonal snow
Land cover
MODIS
Fractional snow cover

ABSTRACT

This work aims at the improvement of the reflectance model-based methodology for mapping of fractional snow cover (FSC) in seasonally snow covered areas in the Northern Hemisphere. The investigations are focused to the determination and analyses of snow-free ground reflectance ($\rho_{ground}$). The objective is to derive information on typical average snow-free ground reflectance for predominant non-forested land cover classes in Eurasia and to investigate the implications of their variations to the FSC estimation accuracy. The snow-free ground reflectances are derived from MODIS time series, using single band reflectances and their related indices. Our approach for the determination of $\rho_{ground}$ is based on the assumption that the behavior of ground reflectance in conditions occurring directly after the snow melt adequately represents the snow-free ground reflectance during snow ablation i.e. melting snow cover including snow-free patches. Additionally, the effects of the $\rho_{ground}$ variability to snow mapping accuracy for different land cover types are analyzed focusing to the *SCAmod* algorithm. The current operational implementations of *SCAmod* use a fixed value for snow-free ground reflectance at the visible wavelengths around 555 nm (corresponding to Terra/MODIS band 4). The deviation between the true snow-free ground value and the fixed value causes error in FSC estimation and, thus, it is necessary to investigate the magnitude and variations of the true $\rho_{ground}$ for different land covers. Even so, our investigation for the target area of Europe, shows that the currently used fixed value of $\rho_{ground}$ (10.0%-units) in *SCAmod* seems to work adequately for land cover classes investigated here. For example, the obtained $\rho_{ground}$ mean and standard deviation 10.0 ± 1.3%-units for the agricultural areas and steppe at 555 nm seem to widely coincide with the fixed value. According to *SCAmod*, the error in FSC estimation caused by the deviation between the fixed and the land cover class-specific value of $\rho_{ground}$ for agricultural areas and steppe yields a systematic error close to zero and a random error ranging from 2.5 to 1.5%-units with the corresponding FSC range of 0–50%. However, in the case of wetlands (7.4 ± 0.8%-units), the systematic error caused to FSC estimation using the fixed value compared to using the estimated class-specific value is as large as from 5 to 2.5%-units with the FSC range of 0–50%. For FSC retrievals larger than 50% the error caused by the variability in $\rho_{ground}$ is considerably smaller for all of the studied land cover classes.

Our results show that the performance of *SCAmod* improves if land cover-specific $\rho_{ground}$ values are applied at least for wetlands. We also suggest that the global application of *SCAmod* would benefit from the generation of a $\rho_{ground}$ map for all land cover types by using the methods presented in this paper. This post-winter reflectance climatology map can be constructed by calculating and using the class-specific $\rho_{ground}$ statistics together with suitable land cover information.



## 1. Introduction

The seasonal snow cover of boreal forest and sub-arctic zones highly influences the Earth's surface–atmosphere interaction. In particular, the surface albedo of snow covered regions differs notably from that of the snow-free terrain; see e.g. Barlage, Zeng, Wei, and Mitchell (2005), Betts and Ball (1997), Moody, King, Schaaf, and Hall (2007) and Wiscombe and Warren (1980). During the spring snow ablation, vast areas in Eurasia and North America belong to a transitional melting snow zone, where the fraction of snow covered area (FSC) ranges between 0 and 100%, see e.g. Choi, Robinson, and Kang (2010). In major parts of Eurasia and North America the annual discharge originates from melting snow and large volumes of fresh water are temporarily stored in snow pack (Barnett, Adam, & Lettenmaier, 2005). Improved estimates on FSC or Snow Extent (SE) in general, and thereby on the behavior of

* Corresponding author at: Finnish Environment Institute, Data and Information Centre, Geoinformatics, P.O. Box 140, FI-00251 Helsinki, Finland. Tel.: +358 400148747 (mobile); fax: +358 95490 2690.
*E-mail address:* miia.salminen@ymparisto.fi (M. Salminen).

0034-4257/$ – see front matter © 2013 Elsevier Inc. All rights reserved.
http://dx.doi.org/10.1016/j.rse.2013.07.007

**Table 1**
Specifications for the MODIS bands and band indices that are exploited in snow mapping and snow-free ground detection under the melting period.

| | MODIS time series analysis specifications | | |
|---|---|---|---|
| MODIS bands | Central wavelength (nm) | Wavelength range (nm) | Application area in snow algorithms |
| MODIS 1 | 645 | 620–670 | Vegetation index (NDVI) |
| MODIS 2 | 858.5 | 841–875 | Vegetation indices (NDVI, NDWI), cloud detection |
| MODIS 3 | 469 | 459–479 | Snow mapping, FSC |
| MODIS 4 | 555 | 545–565 | Snow mapping (FSC, NDSI) |
| MODIS 5 | 1240 | 1230–1250 | Water index (NDWI) |
| MODIS 6 | 1640 | 1628–1652 | Snow mapping (NDSI) |
| | | | |
| MODIS-indices | Formulation | | Application area in snow algorithms |
| NDSI | (Band 4 − Band 6)/(Band 4 + Band 6) | | Snow mapping |
| NDVI | (Band 2 − Band 1)/(Band 2 + Band 1) | | Vegetation phenology, start of growing season |
| NDWI | (Band 2 − Band 5)/(Band 2 + Band 5) | | Vegetation phenology, start of growing season |

albedo, provide essential information for Climate research, Numerical Weather Prediction (NWP) and hydrological forecasting (Hall & Qu, 2006; Stewart, Cayan, & Dettinger, 2005). The temporal and spatial variability in the satellite-based observations of visible and near-infrared (VIS/NIR) surface reflectance is prone to cause error to Earth Observation (EO)-based SE estimation. The main objective of this work is to investigate the snow-free ground reflectance (referred to as $\rho_{ground}$ from now on) behavior for several predominant European land cover types and to derive reliable snow-free ground reference reflectances for seasonally snow covered areas. Reference reflectance signifies a generally applicable constant (mean and standard deviation) value for the snow-free ground reflectance of a specific land cover class, and thus, can be exploited in EO-based algorithms as a pre-set parameter. Regions with ephemeral snow cover are not in the scope of this investigation.

The main goal of this work is to develop a methodology to retrieve snow-free ground reflectances (directly after snow season with senescent vegetation) for the improvement of FSC retrieval algorithms, such as the *SCAmod* snow mapping algorithm. This particular method is applied in producing the hemispheric FSC information within the European Space Agency (ESA) DUE-GlobSnow initiative (Luojus et al., 2010; Metsämäki et al., 2012). In practice, time series of NASA Earth Observing System (EOS) Moderate Resolution Imaging Spectroradiometer (MODIS) onboard the Terra satellite are employed for the analyses. The other goal is to provide general information on the behavior of ground reflectance concerning the conditions apparent directly after the snow melt i.e. to provide end-member values for the $\rho_{ground}$. This is relevant e.g. for the spectral unmixing techniques employed in snow cover mapping, as they require information on the spectral end-member reflectances (Nolin & Dozier, 2000; Painter, Dozier, Roberts, Davis, & Dozier, 2003, Painter et al., 2009; Vikhamar & Solberg, 2003). For example, (linear) unmixing models estimate the abundance of spectral feature classes in each pixel and can utilize multispectral data. The observed reflectance is considered to be a mixture of pure-element reflectances, yet the limited number of end-members leads to only rough estimation results including (residual) error. Nonetheless, it is beneficial to extract high quality spectral end-members with known variation, which is also considered in this paper.

In particular MODIS band 4 (555 nm) is investigated here as this wavelength region is applied in *SCAmod* based FSC mapping, e.g. in GlobSnow (Luojus et al., 2010; Metsämäki et al., 2012). Further on, different channel indices relevant to the remote sensing of snow are considered. They include Normalized Difference Snow Index (NDSI) that employs MODIS bands 4 and 6 (1640 nm) and is widely used in global applications (Hall, Riggs, Salomonson, DiGirolamo, & Bayr, 2002; Rittger, Painter, & Dozier, 2013; Salomonson & Appel, 2004). Additionally, MODIS bands 2 (858.5 nm) and 1 (645 nm) are used to calculate the Normalized Difference Vegetation Index (NDVI) that is useful in investigating the spectral response of a forest with seasonal snow, as snow tends to decrease the NDVI. A complementary index to NDVI is the Normalized Difference Water Index (NDWI) that has been used for the retrieval of phenology in seasonal snow covered areas (Delbart, Kergoat, Le Toan, Lhermitte, & Picard, 2005). NDWI is calculated using MODIS bands 5 (1240 nm) and 2 (Gao, 1996). With respect to snow mapping, changes in NDVI and NDWI correspond to the time of snowmelt, and can be utilized in detecting snow clearance e.g. from MODIS time series (Delbart et al., 2005; Gonsamo, Chen, Price, Kurz, & Wu, 2012; Jönsson et al., 2010; Karlsen et al., 2008; Stow et al., 2004). The MODIS band related snow application areas are specified in Table 1.

The *SCAmod* method was originally developed for regional applications in the boreal forest zone and non-mountainous terrain by the Finnish Environment Institute (SYKE). There is a need to investigate the reliability of the resulting snow cover maps, as the application area has extended to cover the Northern Hemisphere thus including also different land cover categories from those the algorithm was developed for. The *SCAmod* is based on a semi-empirical reflectance modeling approach that applies radiative transfer theory in the consideration of forest canopy effects. It uses reference reflectances for wet snow $\rho_{snow}$, forest canopy $\rho_{forest}$ and snow-free ground $\rho_{ground}$ as model parameters; see Metsämäki, Anttila, Huttunen, and Vepsäläinen (2005). Additionally, the two-way forest canopy transmissivity ($t^2$) is applied as a spatially varying parameter. Transmissivity is related to forest density and can be estimated using multiple reflectance observations from a fully snow covered terrain (Metsämäki et al., 2005, 2012; Nolin, 2004). Our hypothesis is that $\rho_{ground}$ characteristics may vary considerably depending on the local conditions i.e. climate, soil, vegetation, land use and terrain/topography. This is also shown in the work by Peltoniemi et al. (2005), Stow et al. (2004) and Yu, Price, Ellis, and Kastens (2004). Metsämäki et al. (2005) and Salminen, Pulliainen, Metsämäki, Kontu, and Suokanerva (2009) showed that the FSC given by *SCAmod* is clearly dependent on the applied $\rho_{ground}$-value. Thus, although the *SCAmod* is a well performing algorithm (Metsämäki et al., 2012) for detecting the patchy, discontinuous snow cover in the vast snowmelt zone of the Northern boreal forest belt, it is important to:

a) Investigate the spatial variations of snow-free ground reflectance and
b) Facilitate the SE product and FSC value reliability estimation.

Accordingly, we investigate here the spatial and temporal variability of $\rho_{ground}$ that is a significant error source while applying the *SCAmod* on a large scale (Metsämäki et al., 2005; Salminen et al., 2009). Fortunately, due to the *SCAmod* formulation, simulating the FSC accuracies according to $\rho_{ground}$ fluctuations is straightforward and can be conducted by inserting error estimation formulas to the *SCAmod*, see Section 3.2.2 below. Firstly, however, a methodology for obtaining sufficient statistics to describe the $\rho_{ground}$ spatial and temporal behavior in general, and further for the FSC error estimation, must be developed. The methodology development is the central idea and result of this work, besides the actual FSC sensitivity analysis. Although our final goal is in developing a continental-scale approach, testing and demonstration are carried out by using a smaller number of land cover categories and a single study

region covering Central, Eastern and Northern Europe. The study region approach is feasible for efficiently obtaining an extensive cloud-free MODIS time series for the $\rho_{ground}$ statistics calculation and variability description. Additionally, the applied study region is large enough to provide satellite observations with varying imaging and illumination geometries corresponding to the characteristics of observations used in operational FSC retrieval algorithms.

Once the methodology is established, it can be expanded to include several study regions over the Northern Hemisphere and to encompass the land cover categories not investigated here. When we can determine the $\rho_{ground}$ behavior for all of the land cover classes, we can then generate a $\rho_{ground}$ map over the Northern Hemisphere using the land cover data. However, establishing the actual global $\rho_{ground}$ reference map is a relatively laborious task and outside the scope of this investigation. Consequently, the exploitation of the results of this work is expected to facilitate the improved performance of the *SCAmod* algorithm in the global scale. As well, the results can be used for investigating the performance of other snow cover mapping techniques, e.g. those using spectral unmixing methods. Further, the magnitude of the error associated with the variability of snow-free terrain reflectivity can be exhibited by the obtained data set and applied to the performance analysis of the *SCAmod* snow mapping approach, which is also discussed here.

## 2. Materials

### 2.1. Study region and land cover information

The applied study region covering Central, Eastern and Northern Europe is mainly located in the temperate climate zone, yet reaching to boreal forests and alpine (and even arctic) tundra in the northern regions. Seasonal snow cover is a characteristic phenomenon throughout this region, except for some southern- and westernmost low-altitude regions. Land cover (and topography) in Europe shows great variation within relatively small areas, so a large variety of terrain and land cover categories are included in the analysis. Both globally and regionally feasible land cover information is needed in the methodology development. We selected the European Space Agency (ESA) GlobCover products (resolution of 0.0025° × 0.0025°) as they cover the whole Northern Hemisphere and are applicable as supplementary information for global snow algorithm development and mapping purposes. The GlobCover products are based on ENVISAT's Medium Resolution Imaging Spectrometer (MERIS) Level 1B data acquired in a Full Resolution mode with a spatial resolution of 300 m (Bicheron, Huc, Henry, & Bontemps, 2008). We selected 3 predominant land cover classes in a single study region to represent the typical non-forested or very sparsely forested terrain types in Central, Eastern and Northern Europe (referred to as the European study region from now on), see Fig. 1. These land cover classes are:

I) Agricultural areas/steppe (class 20),
II) Sparse vegetation including tundra (class 150), and
III) Wetlands (class 180).

The three classes are eminently characteristic to the (mostly non-mountainous) regions of seasonal snow cover in the whole Northern Hemisphere. The classes correspond to the GlobCover (GC) classes depicted in Table 2 according to both Regional and Global GC legends (Bicheron et al., 2008). Agricultural areas (class 20) are widely represented also in other parts of Eurasia beside the study region. Sparse vegetation including tundra (class 150) needed to include subdivisions, as the generally very sparsely vegetated and regionally widely distributed land cover type comprises of spectrally distinct areas, which can be separated also by latitude and elevation. In practice, regions representing alpine tundra in Norway and arctic/sub-arctic tundra in northern Fennoscandia, Kola Peninsula and Kanin Peninsula are investigated both separately and together with the other regions of class 150. Wetlands (class 180) are composed of both open and forested wetlands and retain vast bogs/mires in addition to regularly flooded regions.

Although the previously described GC classes 20, 150 and 180 are the focus of this investigation, the developed method was additionally exploited for the following classes, see Table 2:

i) Rainfed croplands (class 14), that comprise e.g. of rainfed herbaceous crops or shrub or tree crops,
ii) Mosaic vegetation or cropland (class 30), that is a mixed class, where mosaic vegetation consists of a mixture of grassland, shrubland and forest up to 50–70% and the proportion of cropland ranges from 20% to 50%,
iii) Mosaic forest or shrubland (50–70%) or grassland (class 110) is also a mixed class with relatively sparsely forested areas, and
iv) Closed (>40%) grassland (class 141), which is a sub-class of 140, comprising of closed to open (>15%) herbaceous vegetation.

In addition to the land cover information, an estimate of the forest canopy transmissivity is important as we accept only non-forested or very sparsely forested terrain types for the snow-free land surface reference reflectance analysis. This also partly compensates for the errors possible in the GlobCover data. Therefore, in addition to the GlobCover information on the proportion of forest in each pixel, we used the 555 nm MODIS band 4-based transmissivity data, described in Metsämäki et al. (2012), to i) select to suitable (predominantly) non-forested pixels to be analyzed and ii) to assess the statistical accuracy of the FSC estimates by using *SCAmod* and the gained snow-free ground reflectance statistics.

### 2.2. MODIS time series

To obtain experimental data, i.e. reference reflectances to study the statistical behavior of the *SCAmod* algorithm reflectance contributors for the selected land cover classes, we used a Terra Moderate Resolution Imaging Spectroradiometer (MODIS) with 500 m and 250 m spatial resolution. Terra/MODIS has a good spatial and temporal coverage of the study region and MODIS data are widely used in global and local snow applications, see Table 1. We employed an extensive time series of MODIS Top-of-Atmosphere (TOA) reflectances for the 2011 snow-melt season, covering the time interval from full snow cover through low snow fractions till the appearance of green vegetation. The coverage of the European study region is shown in Fig. 1. Original MOD02HKM and MOD02QKM Level 1b Calibrated radiance products (500 m) are obtained from LAADS Level 1 and Atmosphere Archive and Distribution System by NASA (Xiong et al., 2005, 2006). The radiance products were converted to TOA reflectances using ENVIMON software by Technical Research Centre of Finland (VTT) at the Finnish Environment Institute (SYKE). The pixel-wise time series of snow-free land surface reference reflectance value i.e. $\rho_{ground}$ for the selected land cover categories are extracted from these georectified and cloud-masked MODIS data sets.

Before the actual MODIS time series extraction, large clusters of GlobCover pixels falling into the same land cover category were automatically searched. To ensure sufficiently large and homogeneous areas for the analysis, only central pixels (size of ~500 m) of homogeneous clusters with a minimum size of about 1.5 km × 1.5 km were accepted for the MODIS time series extraction. As an outcome, several thousands of clusters were extracted for each investigated land cover class.

Reflectance time series were generated for a large number of spatially distributed MODIS observations from various orbits with a varying viewing angle in order to compensate for the effects of the imaging geometry. High number of observations also ensures that the obtained data set includes a large variety of (non-cloudy) atmospheric conditions. The sensor viewing angle was limited to exclude the largest instrument view angles (>50°). We also excluded too high (>75°) sun zenith angles from the time series dataset.

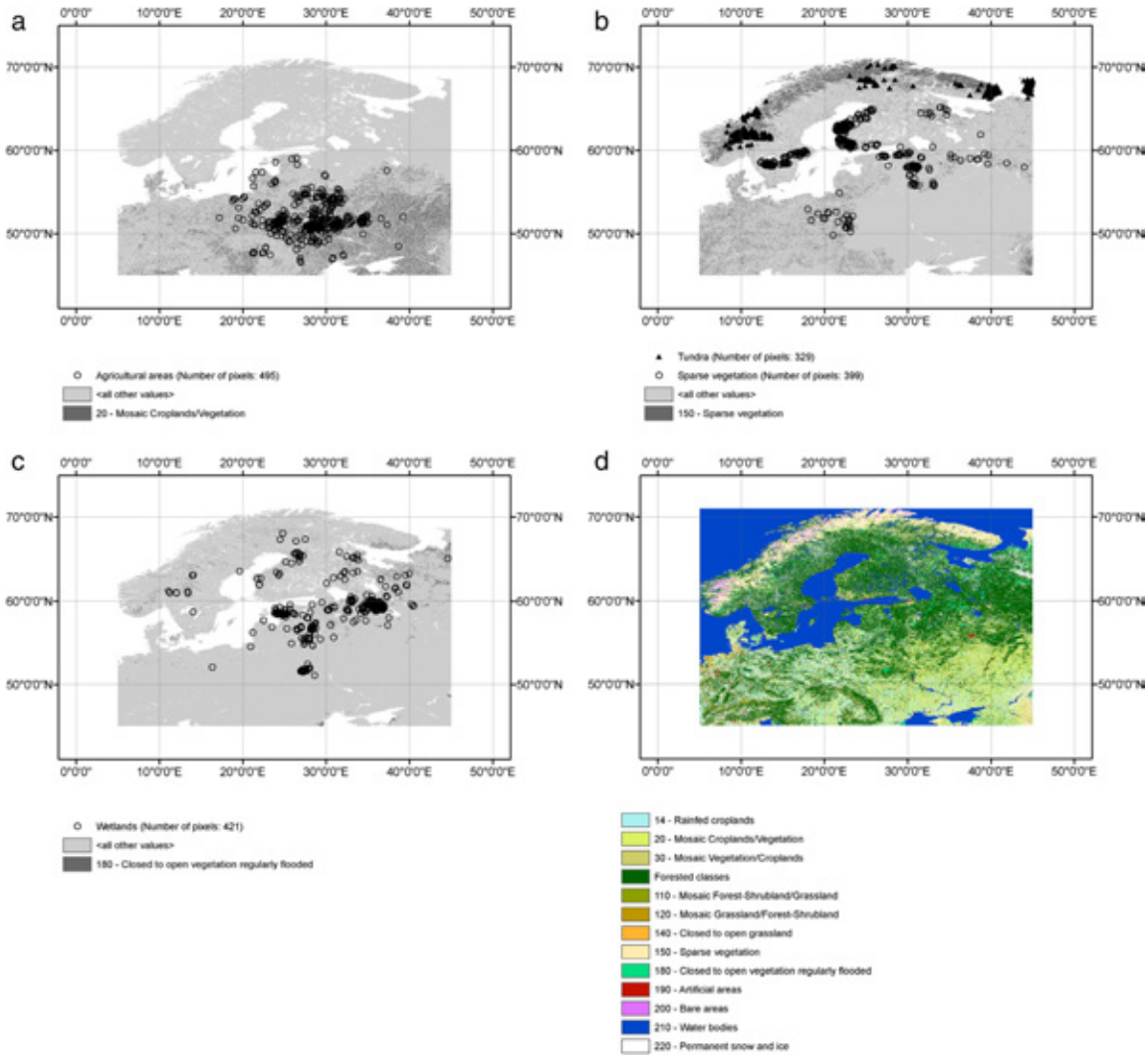


**Fig. 1.** The European study region and the distributions of the 3 predominant land cover classes a) agricultural areas/steppe, b) sparse vegetation including tundra, c) wetlands, and d) all relevant land cover classes in the study region derived from GlobCover product by ESA. The symbols in (a)–(c) represent the individual pixels applied in the time series analysis.

Snow-free ground reflectance for forested terrain is earlier derived from MODIS TOA reflectances and ASD ground-based field spectral measurements (Metsämäki et al., 2012; Niemi et al., 2012; Salminen et al., 2009). Based on the earlier work, it appears acceptable to use the current constant value for $\rho_{ground}$ (10%-units) to represent forest floor and several non-forested land cover types in the boreal forest region. In this work, we use the 10%-units constant not only in error estimation, but also to represent all densely and some sparsely forested areas for calculating the actual snow-free ground reflectance map.

## 3. Method development

The overall goal here is the investigation and extraction of post-winter snow-free ground reflectance statistics for continental scale snow mapping purposes. Effectively, this is achieved by developing a methodology to derive land cover class-wise snow-free ground reference reflectances ($\rho_{ground}$), that can be used in generating a $\rho_{ground}$ map. The methodology is developed by using time series of pixel-wise satellite observations from a large study area (Fig. 1) and for such land cover classes where forest canopy has a minor role. Once established, the method can be applied to other study regions and land cover classes in the Northern Hemisphere to get a global coverage (concerning the regions of seasonal snow cover). The key question in the time series analysis is to find the valid reflectance observation representing the snow-free conditions right after the last traces of snow have disappeared. This value is then assumed to represent snow-free ground reflectance during the actual ablation season, prior to the appearance of the green vegetation. This assumption is based on the earlier investigations e.g. (Stow et al., 2004), reporting that green vegetation – shown as increasing reflectances and particularly NDVI – appears only after the final snow clearance. The obtained feasible $\rho_{ground}$-values from all the selected pixels and their class-wise variability information can be exploited in generating a $\rho_{ground}$ map and, further, in the accuracy assessment of FSC estimation for each land cover class.

**Table 2**
The surface area of all the forested and non-forested and sparsely forested land cover classes in the European study region.

| GC Class | Class title | Surface area (%)[a] | Class description based on Bicheron et al. (2008) |
|---|---|---|---|
| 20 | Agricultural areas/steppe | 13.51 | Mosaic cropland (50–70%) or other vegetation (20–50%) |
| 150 | Sparse vegetation including tundra | 13.72 | Sparse (>15%) vegetation (woody vegetation, shrubs, grassland) |
| 150A | Tundra | | -Northern latitudes (including Alpine and arctic/sub-arctic tundra) |
| 150B | Sparse vegetation | | -Southern latitudes |
| 180 | Wetlands | 2.59 | Closed to open (>15%) grassland or woody vegetation on a regularly flooded or waterlogged soil, also with fresh, brackish or saline water |
| 14 | Rainfed croplands | 12.22 | Rainfed croplands |
| 30 | Mixed class with sparsely forested areas | 3.84 | Mosaic vegetation (50–70%)/cropland (20–50%) |
| 110 | Mixed class with sparsely forested areas | 2.92 | Mosaic forest or shrubland (50–70%)/grassland (20–50%) |
| 141 | Grassland | 0.93 | Closed (>40%) grassland (Sub-class of 140, which is closed to open (>15%) herbaceous vegetation) |
| 13, 15, 16, 21, 32, 120, 140, 151, 152, 185, 190, 200, 201, 202, 203, 220 | Other open/non-forested area classes in the study region | 3.89 | Non-forested and sparsely forested areas (including urban areas, bare areas and permanent snow and ice) |
| 50, 60,70, 90, 91, 92, 100, 101, 130, 131, 134 | Forested classes in the study region | 46.38 | Consisting of various broadleaved and needleleaved forests and (closed) shrublands |

[a] % of the total surface area of all classes excluding water bodies.

### 3.1. Snow-free reflectance determination using MODIS time series

#### 3.1.1. MODIS time series extraction

We applied GC land cover data to extract the land cover class-specific reflectance time series for different MODIS wavelength bands. For each GC class, MODIS time series from each selected pixel were generated, resulting to thousands of time series. However, proper time series were only retrieved for a much smaller number of pixels as shown in Fig. 1. This is because firstly, only those time series featuring also seasonal snow conditions were accepted to further studies. Secondly, the first approximation of snow clearance day was made by applying *SCAmod* (with a fixed value of $\rho_{ground} = 10\%$) in order to find the first occasion when FSC = 0%. After that, several criteria around that time must be met in order to obtain a valid observation representing the snow clearance day.

We focus on analyzing the MODIS bands essential for snow applications (see Table 1). The MODIS wavelength band 4 (555 nm), is utilized in the FSC estimation with *SCAmod*. MODIS band 4 and MODIS band 6 (1640 nm) are used in the NDSI calculation. NDVI is calculated using MODIS band 1 (645 nm) and 2 (858.5 nm), which benefits snow mapping in forested areas. NDWI calculated using MODIS band 2 and MODIS band 5 (1240 nm) has potential in phenological applications.

#### 3.1.2. Criteria for the selection of the valid moment after snow clearance

The extraction of the $\rho_{ground}$-value representing the reflectance directly after the snow melt is based on the analysis of the temporal changes in the observed reflectances and related channel indices. Various investigations show that the reflectance in visible bands drops to a local (or even to annual global) minimum with the snow clearance when soil is typically wet directly after snow melt (Duke & Guérif, 1998; Twomey, Bohren, & Mergenthaler, 1986). This is also the case for forests, if they are at least partially optically transparent. Additionally, different snow mapping algorithms for satellite data, discussed above, are based on this particular reflectance contrast apparent between the snow covered and melt-off conditions. Thus, we applied a decision rule method for detecting the value of $\rho_{ground}$ from the extracted MODIS time series. The outline of this method can be summarized as follows:

(a) Check that the MODIS time series for the pixel under investigation includes observations with (nearly) full snow cover conditions (e.g. FSC > 70% as criterion) and FSC = 0%, and that the time difference between these observations is smaller than a threshold value (e.g. in practice, based on the time series analysis we discovered that using a gap of 10 days is feasible).

(b) If condition (a) holds for the pixel, analyze the minimum values of different MODIS channels within a prefixed time window around/after the moment of snow clearance (FSC = 0% for the first time in the estimated FSC time series); the selection of the optimal length of the window is discussed in Section 4 below.

(c) Assign the day for $\rho_{ground}$ acquisition based on the most feasible MODIS channel reflectance or channel index, (the most feasible indicator for this moment determined from the analysis of the obtained data set, e.g. MODIS 555 nm, see Section 4 below).

(d) Extract $\rho_{ground}$-values for days identified in step (c) for different pixels and determine statistics for all pixels of the certain GC class within the study area.

The time series analysis algorithm defined in steps (a)–(d) above was implemented as an automatic procedure that was applied to data sets representing different land cover classes, see also Section 2.2. As an outcome, proper time series with extracted $\rho_{ground}$ values were obtained for 9 land cover classes with the number of $\rho_{ground}$ values ranging from 52 to 728 depending on class.

### 3.2. The exploitation of $\rho_{ground}$

#### 3.2.1. Statistical analysis of $\rho_{ground}$ for several land cover classes

The obtained $\rho_{ground}$ values for the selected pixels of each investigated GlobCover (GC)-class are utilized in statistical analysis. The purpose is to calculate the mean and standard deviation for the class-wise reflectances of the essential MODIS wavelength bands. This information is then used to represent the statistical behavior of the reflectance for the different land cover classes. The statistical reliabilities of the obtained class-wise $\rho_{ground}$ mean and standard deviation values for each MODIS band are assessed by calculating their confidence limits.

We use the forward modeling approach of *SCAmod* to describe the correspondence between reflectance constituents and the observed reflectance (Metsämäki et al., 2005). Thus, the model for the TOA reflectance, denoted here by $R_{mod}$ at the wavelength λ is

$$R_{\lambda,mod}(FSC) = \left(1-t_\lambda^2\right)\rho_{\lambda,forest} + t_\lambda^2\left[FSC\rho_{\lambda,snow} + (1-FSC)\left\langle\rho_{\lambda,ground}\right\rangle\right] \quad (1)$$

where $\langle\rho_{\lambda,ground}\rangle$ is the average value of the snow-free ground reflectance for a certain land cover category representing open areas or forest floor. The two-way forest canopy transmissivity is $t^2$, FSC is the fraction of snow covered area within the pixel, $\rho_{\lambda,snow}$ is the snow reflectance and $\rho_{\lambda,forest}$ is the reflectance of an opaque forest canopy, respectively.

When FSC = 0% and $t^2 \approx 1$, Eq. (1) directly yields the estimate for $\rho_{ground}$. If forest canopy is present, i.e. $t^2 < 1$, $\rho_{\lambda\_ground}$ is obtained by inverting Eq. (1), using the a priori value of (pixel-wise) forest canopy transmissivity and a constant parameter value for forest canopy reflectance of an opaque vegetation layer (constant 0.08 (or 8%-units) applied here based on Metsämäki et al. (2012). Hence, the forest canopy transmissivity corrected ($t^2$-corrected) estimate for the ground reflectance below the forest canopy (λ ignored from now on for simplicity) is given by:

$$\widehat{\rho}_{ground} = \frac{R_{obs} - \left(1 - t^2\right)\rho_{forest}}{t^2} \tag{2}$$

In Eq. (2), the $R_{obs}$ is the actual observation instead of the modeled TOA reflectance $R_{mod}$. Thus, $\rho_{ground}$ can be determined from the reflectance observations that were identified to represent snow clearance, as described above. When $\rho_{ground}$ is solved from Eq. (2) for a large number of pixels, an estimate for the standard deviation of $\rho_{ground}$ is obtained, in addition to the mean value of the investigated land cover class.

Also note that the fractional snow cover (FSC) can be solved from Eq. (1), given that the three values of reflectance constituents and transmissivity are known, which is the basis of the *SCAmod*.

*3.2.2. The impact of the $\rho_{ground}$ variability on snow mapping according to the SCAmod algorithm*

The effect of the obtained class-wise $\rho_{ground}$ mean values in FSC estimation is assessed by comparing the current (constant value of $\rho_{ground}$ used for all land cover categories) snow mapping results with the results obtained by using the class-wise $\rho_{ground}$ mean and standard deviation. The results will indicate if it is necessary to take into account the effect of various land cover types while using *SCAmod*.

According to *SCAmod* the FSC estimate for pixel representing a certain GC land cover class is obtained by inverting Eq. (1)

$$\widehat{FSC} = \frac{\frac{1}{t^2}R_{obs} + \left(1 - \frac{1}{t^2}\right)\rho_{forest} - \left\langle \rho_{ground} \right\rangle}{\rho_{snow} - \left\langle \rho_{ground} \right\rangle} \tag{3}$$

where $R_{obs}$ is the TOA-observed reflectance and $\langle\rho_{ground}\rangle$ is the class-wise mean reflectance.

Instead of having the mean class-wise snow-free reflectance value $\langle\rho_{ground}\rangle$ in Eq. (3), the biased estimate of FSC can be obtained by applying a constant value $\rho_{ground} = 10.0\%$. This value (for the MODIS band 4 TOA reflectance) is typically applied by the *SCAmod* to describe snow-free ground reflectance (Metsämäki et al., 2012). By setting $\langle\rho_{ground}\rangle = 10.0\%$ in Eq. (3), and thereafter, by inserting Eq. (1) to Eq. (3), we get the formula for the bias error of FSC estimation:

$$BIAS = \frac{FSC\rho_{snow} + (1 - FSC)\left\langle \rho_{ground} \right\rangle - 10.0}{\rho_{snow} - 10.0}. \tag{4}$$

As well the upper and lower bounds of FSC estimated can be obtained from the standard deviations of land cover class-wise estimates of $\rho_{ground}$:

$$BOUNDS_{upper/lower} = \frac{FSC\rho_{snow} + (1 - FSC)\left(\left\langle \rho_{ground} \right\rangle \pm std\left\langle \rho_{ground} \right\rangle\right) - 10.0}{\rho_{snow} - 10.0}. \tag{5}$$

Eqs. (4) and (5) characterize the systematic (bias) and random error levels of FSC estimation for different land cover categories when a constant value of $\rho_{ground} = 10.0\%$ is applied in *SCAmod* (for MODIS band 4). The same equations can be used to characterize the overall error level for a larger area (or even globally) by considering the areal fractions of different land covers and by summing their corresponding snow-free ground reflectance variances accordingly.

*3.2.3. Sensitivity of $\rho_{ground}$ estimation to forest transmissivity*

The forest canopy transmissivity corrected value of $\rho_{ground}$ can be obtained by using Eq. (2). If this correction is not performed, the value of $\rho_{ground}$ is directly obtained from solving Eq. (1) with FSC = 0. Hence the absolute error ignoring the effect of forest canopy transmissivity is given by:

$$\Delta\rho_{ground} = R_{obs} - \rho_{ground} = R_{obs} - \frac{R_{obs} - \left(1 - t^2\right)\rho_{forest}}{t^2}. \tag{6}$$

On the other hand, the transmissivity correction provided in Eq. (2) is sensitive to error in the applied transmissivity information. The statistical error level of transmissivity corrected $\rho_{ground}$ value can be obtained by the derivative of Eq. (2). As the inaccuracy of $\rho_{forest}$ is also considered we get according to the law of error propagation:

$$\left|\Delta\rho_{ground}\right| = \sqrt{\left(\frac{R_{obs} - \rho_{forest}}{\left(t^2\right)^2}\Delta\left(t^2\right)\right)^2 + \left(\frac{t^2 - 1}{t^2}\Delta\rho_{forest}\right)^2 + \left(\frac{1}{t^2}S_{obs}\right)^2} \tag{7}$$

where $\Delta(t^2)$ is the statistical error (standard deviation) of two-way transmissivity for the channel under investigation, $\Delta\rho_{forest}$ is that for the forest canopy reflectance and $S_{obs}$ is the standard deviation of observational noise, respectively. However, when $\Delta(t^2)$ and $\Delta\rho_{forest}$ are estimated from the space-borne observations the influence of observational noise is included into $\Delta(t^2)$ and $\Delta\rho_{forest}$. Thus, the third term of Eq. (7) can be ignored in that case.

## 4. Results and discussion

The behavior of $\rho_{ground}$ and NDVI since the day of snow melt-off is depicted in Fig. 2. Here, the depicted moment of snow melt is the estimate obtained by applying *SCAmod* with $\rho_{ground} = 10.0\%$. The results are shown for three land cover classes corresponding to pixels indicated in Fig. 1. When examining NDVI for the 20-day time window since this first snowmelt, it is evident that the growing season starts, and thus, NDVI starts to increase after 10–15 days, depending on the land cover class. So, it is justified to limit the analysis of $\rho_{ground}$ for a period of 15 days after the first snowmelt in order to avoid greening contaminating the representativeness of the demanded snow-free reflectance values. Additionally, the temporal behavior of MODIS band 4 reflectance, also shown in Fig. 2, suggests that the 15-day time window after the snowmelt is reasonable for the identification of the snow-free ground reflectance value representing the conditions apparent immediately after the snow disappearance. Since MODIS observations are not available for all days due to cloud cover, there has to be a window for searching the best estimate of $\rho_{ground}$. As discussed in Section 3.1, the problem is then to search the minimum value of a suitable reflectance channel within the 15-day window, and to assign the $\rho_{ground}$ values of other channels from the concurrent observations of the same day.

Fig. 3 depicts the behavior of different MODIS band TOA reflectance observations for selected typical cases demonstrating the feasibility of reflectances at different bands for the searching of the best estimate for the timing of melt-off conditions. As demonstrated in Fig. 3, MODIS band 4 reflectance is providing the clearest indication of snow melt timing, and thus it was chosen for $\rho_{ground}$ value

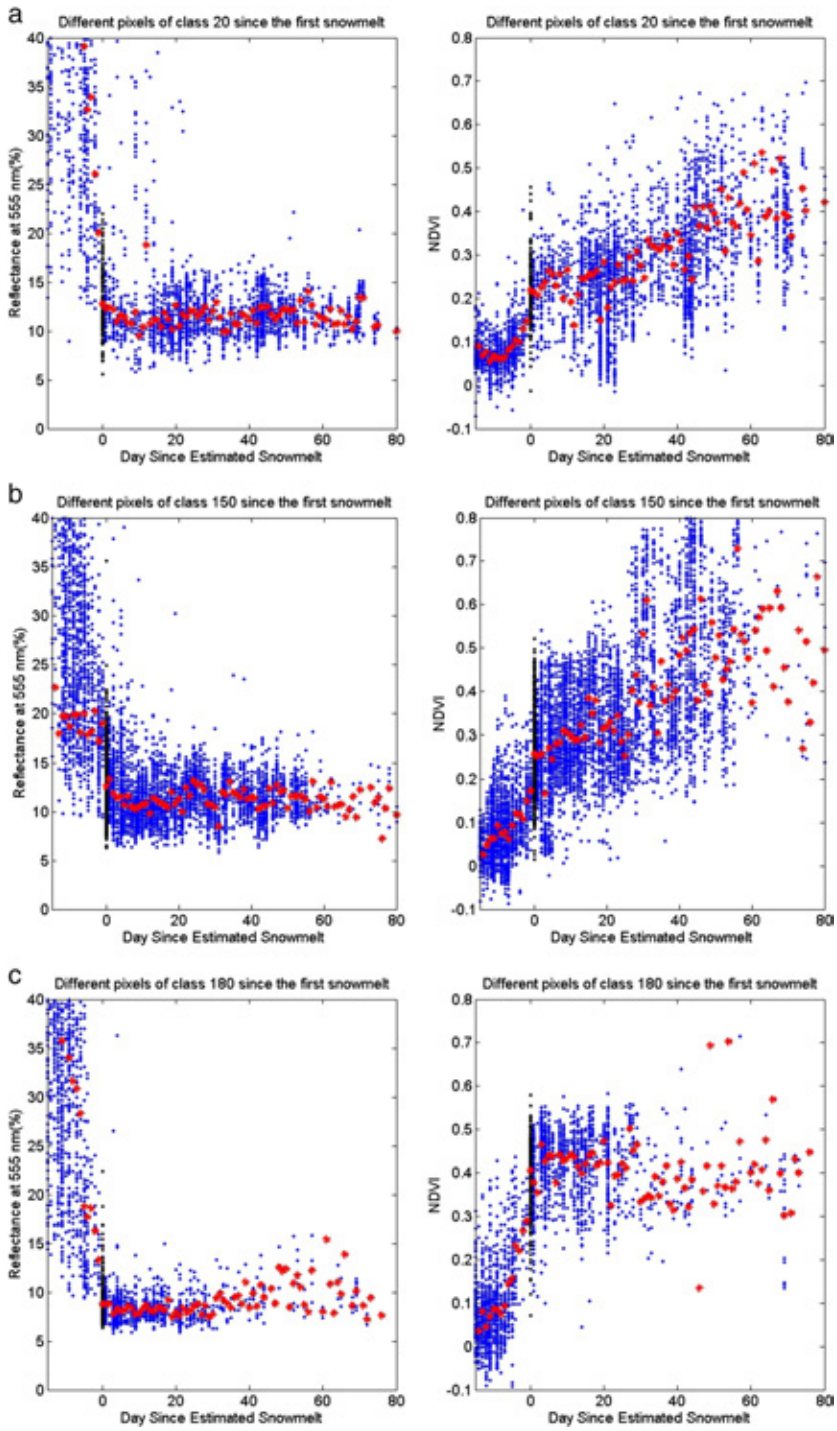


**Fig. 2.** Results depicting the behavior of snow-free reflectance (left) for MODIS band 4 (545–565 nm) and (right) NDVI with respect to the estimated first snowmelt occurrence for all observation points (not only those selected for statistical analysis) for (a) agricultural areas/steppe (b) sparse vegetation including tundra and (c) wetlands in the European study region. The average values (red asterisk) for all pixels and values (blue dots) for all individual observations are depicted.

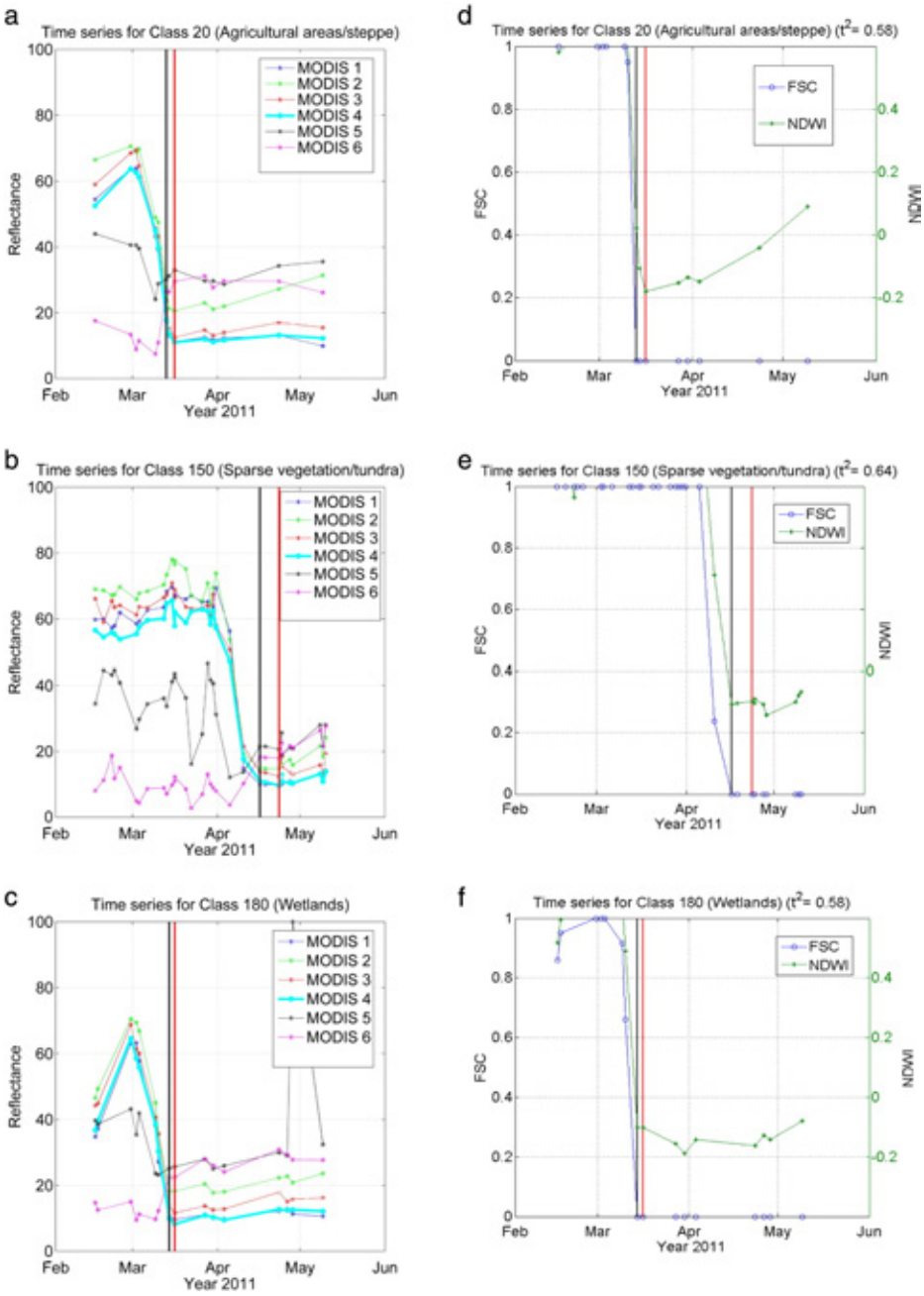


**Fig. 3.** Examples of typical pixel-wise MODIS time series. Reflectance is shown in a–c. FSC and NDWI time series are depicted in d–f. Examples for Agricultural areas/steppe are shown in a and d; Sparse vegetation (tundra) in b and e and Wetlands in c and f, respectively. The utilized MODIS bands are specified in Table 1. Black vertical line depicts the moment of estimated snow melt according to *SCAmod* algorithm (first observation with FSC = 0%). Red vertical line indicates the moment of the extracted snow-free ground reflectance estimates (minimum value of MODIS band 4 reflectance within the window of 15 days; note that MODIS band 4 is highlighted).

extraction. In addition to reflectance time series, Fig. 3 shows NDWI and FSC time series of predominant non-forested or sparsely forested land cover types. The behavior of the NDWI (local minimum directly after snowmelt, Delbart et al., 2005) confirms the feasibility of MODIS band 4 for the extraction of the $\rho_{ground}$ values. NDWI helps to identify the period, when ground is possibly still wet after snowmelt and the index should not, therefore, increase during the identified time window of 15 days.

**Table 3a**
Snow-free ground reflectance analysis results for GlobCover classes: agricultural areas/steppe (20), tundra/sparse vegetation (150) and wetlands (180). Mean, standard deviation (SD) and number of observations for the exploited MODIS wavelength bands and band indices. Mean and SD are accompanied by their confidence intervals. The snow-free ground reflectance statistics extraction was conducted using the time window of 15 days after snow clearance and pixel two-way forest canopy transmissivity $t^2 > 0.5$ as criterium.

| | $t^2 > 0.5$ and time window maximum of 15 days after snow clearance | | | | | | | | | |
|---|---|---|---|---|---|---|---|---|---|---|
| | Class 20 (N obs 495) | | Class 180 (N obs 421) | | Class 150 (N obs 728) | | Class 150 tundra (N obs 329) | | Class 150 sparse (N obs 399) | |
| Criteria | Mean (±95% conf.)[a] | SD[b] (95% bounds) | Mean (±95% conf.)[a] | SD[b] (95% bounds) | Mean (±95% conf.)[a] | SD[b] (95% bounds) | Mean (±95% conf.)[a] | SD[b] (95% bounds) | Mean (±95% conf.)[a] | SD[b] (95% bounds) |
| MODIS 4 | 10.01 (0.12) | 1.34 (1.26, 1.43) | 7.38 (0.07) | 0.75 (0.70, 0.80) | 10.02 (0.16) | 2.16 (2.05, 2.28) | 10.09 (0.30) | 2.73 (2.54, 2.96) | 9.96 (0.15) | 1.53 (1.43, 1.64) |
| MODIS 4 $t^2$-corr. | 11.04 (0.18) | 2.02 (1.90, 2.15) | 7.09 (0.11) | 1.14 (1.07, 1.22) | 10.89 (0.22) | 3.00 (2.85,3.16) | 10.84 (0.40) | 3.69 (3.43, 4.00) | 10.92 (0.22) | 2.27 (2.12, 2.44) |
| MODIS 3 | 12.95 (0.12) | 1.36 (1.28, 1.45) | 10.63 (0.09) | 0.97 (0.91, 1.04) | 13.18 (0.17) | 2.38 (2.26, 2.51) | 13.45 (0.32) | 2.96 (2.75, 3.21) | 12.96 (0.17) | 1.74 (1.63, 1.87) |
| NDSI | −0.37 (0.01) | 0.09 (0.09, 0.10) | −0.22 (0.01) | 0.11 (0.11, 0.12) | −0.34 (0.01) | 0.11 (0.10,0.12) | −0.34 (0.01) | 0.10 (0.09, 0.11) | −0.34 (0.01) | 0.12 (0.11, 0.13) |
| NDVI | 0.27 (0.01) | 0.07 (0.06, 0.079) | 0.44 (0.01) | 0.07 (0.06, 0.07) | 0.32 (0.01) | 0.10 (0.10, 0.11) | 0.37 (0.01) | 0.07 (0.07, 0.08) | 0.27 (0.01) | 0.09 (0.08, 0.10) |
| NDWI | −0.11 (0.01) | 0.10 (0.09, 0.10) | 0.21 (0.01) | 0.15 (0.14, 0.16) | −0.04 (0.01) | 0.11 (0.10, 0.12) | 0.00 (0.01) | 0.09 (0.08, 0.10) | −0.08 (0.01) | 0.10 (0.09, 0.11) |

[a] 95% ± confidence interval.
[b] SD = standard deviation; lower and upper bounds for the 95% confidence interval.

**Table 3b**
Snow-free ground reflectance analysis results for GlobCover classes: rainfed croplands (14), mosaic vegetation/cropland (30), mosaic forest or shrubland/grassland (110) and grassland (141). Mean, standard deviation (SD) and number of observations for the exploited MODIS wavelength bands and band indices. Mean and SD are accompanied by their confidence intervals. The snow-free ground reflectance statistics extraction was conducted using the time window of 15 days after snow clearance and pixel two-way forest canopy transmissivity $t^2 > 0.5$ as criterium.

| | $t^2 > 0.5$ and time window maximum of 15 days after snow clearance | | | | | | | |
|---|---|---|---|---|---|---|---|---|
| | Class 14 (N obs 398) | | Class 30 (N obs 127) | | Class 110 (N obs 52) | | Class 141 (N obs 110) | |
| Criteria | Mean (±95% conf.)[a] | SD[b] (95% bounds) | Mean (±95% conf.)[a] | SD[b] (95% bounds) | Mean (±95% conf.)[a] | SD[b] (95% bounds) | Mean (±95% conf.)[a] | SD[b] (95% bounds) |
| MODIS 4 | 10.68 (0.11) | 1.07 (1.00, 1.15) | 8.94 (0.44) | 2.49 (2.21, 2.84) | 10.41 (0.44) | 1.58 (1.33, 1.96) | 11.13 (0.43) | 2.28 (2.01, 2.63) |
| MODIS 4 $t^2$-corr. | 12.16 (0.17) | 1.74 (1.62, 1.87) | 9.46 (0.73) | 4.18 (3.72, 4.77) | 11.76 (0.70) | 2.50 (2.09, 3.10) | 12.71 (0.69) | 3.64 (3.22, 4.20) |
| MODIS 3 | 13.71 (0.15) | 1.54 (1.44, 1.66) | 12.29 (0.38) | 2.166 (1.93, 2.47) | 13.84 (0.72) | 2.60 (2.17, 3.22) | 13.90 (0.55) | 2.89 (2.55, 3.33) |
| NDSI | −0.29 (0.01) | 0.07 (0.06, 0.07) | −0.19 (0.05) | 0.27 (0.24, 0.31) | −0.35 (0.03) | 0.11 (0.09, 0.14) | −0.30 (0.03) | 0.13 (0.12, 0.16) |
| NDVI | 0.26 (0.01) | 0.06 (0.05, 0.06) | 0.17 (0.02) | 0.13 (0.12, 0.15) | 0.35 (0.03) | 0.09 (0.08, 0.11) | 0.32 (0.01) | 0.07 (0.06, 0.08) |
| NDWI | −0.05 (0.01) | 0.06 (0.06, 0.07) | −0.08 (0.03) | 0.16 (0.14, 0.18) | −0.01 (0.04) | 0.13 (0.11, 0.16) | 0.02 (0.02) | 0.11 (0.10, 0.13) |

[a] 95% ± confidence interval.
[b] SD = standard deviation; lower and upper bounds for the 95% confidence interval.

The main findings of this investigation are depicted in Tables 3a and 3b. It summarizes the statistical values of the obtained estimates on snow-free ground reflectance for different GC land cover classes of the study area. That is, mean and standard deviation values with their statistical confidence limits. Additionally, results for different indices are given. The presented $\rho_{ground}$ values are determined directly from MODIS TOA reflectances using the methodology outlined in Section 3.1.2. For the MODIS band 4 (555 nm), $t^2$-corrected $\rho_{ground}$ estimates according to Eq. (2) are also shown. The results are presented for seven GC land cover classes. However, class 150 representing tundra and other sparse vegetation areas are separated into two sub-classes: tundra and southern/low altitude sparsely vegetated areas. The presented standard deviation values also include the contribution of varying viewing geometry and sun illumination angles. However, the search procedure for $\rho_{ground}$ values outlined in Section 3.1.2 provides the estimates according to viewing geometry and atmospheric conditions that provide the minimum levels of reflectance in the search window of 15 days after the estimated snow melt. This criterion was selected in order to provide a set of $\rho_{ground}$ values as consistent as possible. Figs. 1 and 2 indicate that due to the high amount of pixels distributed around the European study area, the obtained statistics provide values indicating well the overall behavior of TOA-observed reflectance. The observed variability for the conditions directly after the snow melt is resulting from (a) the actual spatial variability of snow-free ground surface reflectance, (b) variability in imaging/illumination geometry and (c) variability in atmospheric conditions.

The results of Tables 3a and 3b are determined excluding pixels representing dense forests. For the areas with a low value of the two-way forest canopy transmissivity ($t^2$), i.e. dense forests, $t^2$-correction for the $\rho_{ground}$ values yields intolerable standard deviations and mean values, so the forest canopy transmissivity correction is not feasible for such regions. We tested several $t^2$-limits, and found that only observations from pixels with $t^2 > 0.5$ are feasible for the analysis. Thus, only these areas are considered in the results shown in Tables 3a and 3b. Fig. 4 depicts the error caused by forest canopy transmissivity in $\rho_{ground}$ estimates by showing the error as a function of $t^2$. Fig. 4 also demonstrates the absolute error of $\rho_{ground}$ estimation excluding forest canopy transmissivity correction. High estimation errors are obtained when $t^2 < 0.5$, both in cases including or excluding the transmissivity correction.

The results in Tables 3a and 3b indicate that even though the analysis focuses to areas (pixels) with a sparse or non-existing forest cover ($t^2 > 0.5$), there are systematic differences ranging from −1.6%-units to +0.29%-units between the $t^2$-corrected and not-corrected $\rho_{ground}$ estimates. As suggested by Fig. 4a, the negative difference in the determined $\rho_{ground}$ value is obtained for the case of wetlands (GC class 180) that exhibits an overall low level of $\rho_{ground}$. All other classes show higher mean values of the estimated $\rho_{ground}$ in case the forest canopy correction is performed. Since the $t^2$-data is only available representing the MODIS band 4, it is not possible to determine the correction for other wavelengths or channel indices. However, for band 4, the values in Tables 3a and 3b excluding or including canopy transmissivity correction indicate the upper and lower margins of the obtained GC class-wise determined mean values of $\rho_{ground}$. The standard deviations of $\rho_{ground}$ estimates appear to be smaller when $t^2$-correction is excluded, which also agrees with the predictions of Fig. 4.

Examples of the distributions of $\rho_{ground}$ estimates at MODIS band 4 are shown in Fig. 5 corresponding to Table 3a. The results for GC classes 20 and 180 demonstrate that typical snow-free ground reflectance histograms are close to a Gaussian distribution. The exception is class 150 that incorporates tundra and other sparsely vegetated areas. The split of class 150 into these two contributions is also shown in Fig. 5 indicating that tundra regions at north latitudes (or at high altitudes in the south) include surfaces with substantially higher reflectances than the class in general. The applied data set includes backscatter viewing geometries for tundra regions of the class 150 incorporating high sensor zenith angles, which may cause the high values e.g. for lichen-dominated regions (Peltoniemi et al., 2005). Due to this behavior, Tables 3a and 3b present statistics for the sub-divisions of class 150, in addition to the statistics of the whole GC class. In contrast to tundra regions, the reflectance histogram for other sparsely vegetated surfaces approaches the Gaussian distribution.

The obtained $\rho_{ground}$ statistics presented in Tables 3a and 3b can be used to investigate the performance of *SCAmod* by applying Eqs. (4) and (5). Eqs. (4) and (5) define the error levels of FSC estimation emerging from the use of the prefixed value of snow-free ground reflectance in *SCAmod*-algorithm. That is, the systematic and random errors of FSC estimation are given concerning the case when the prefixed value of 10.0%-units is used instead of land cover class-wise derived mean reflectances. The error assessment is carried out by inserting mean and standard deviation values of MODIS band 4 reflectances from Tables 3a and 3b to Eqs. (4) and (5). The results are shown in Fig. 6 for GC classes 20, 150 and 180. Solid lines depict systematic errors

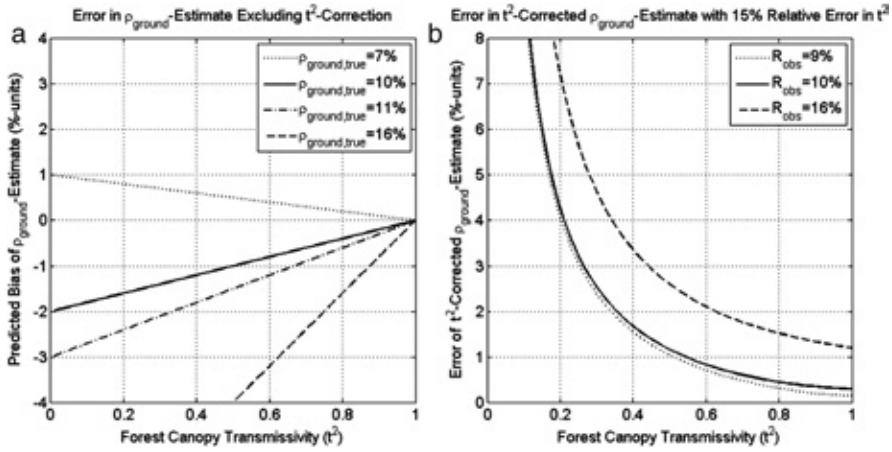


**Fig. 4.** (a) The predicted absolute error of $\rho_{ground}$-estimation according to Eq. (6) when the forest canopy transmissivity ($t^2$) correction is ignored and (b) the statistical error of $\rho_{ground}$ estimation when $t^2$-correction is included. The results are shown for different levels of true $\rho_{ground}$ values (a), and for different levels of space-borne observed reflectance, $R_{obs}$ (b). For transmissivity $t^2 < 0.5$, the effect of forest on the satellite observed reflectance is dominant and the absolute error is large, if $t^2$-correction is ignored. Also the statistical error of $t^2$-corrected estimate is high, if $t^2 < 0.5$. In 6 (b), the statistical error is calculated assuming a relative error of 15% in $t^2$ and a RMS-error level of 1.0%-units in $\rho_{forest}$.

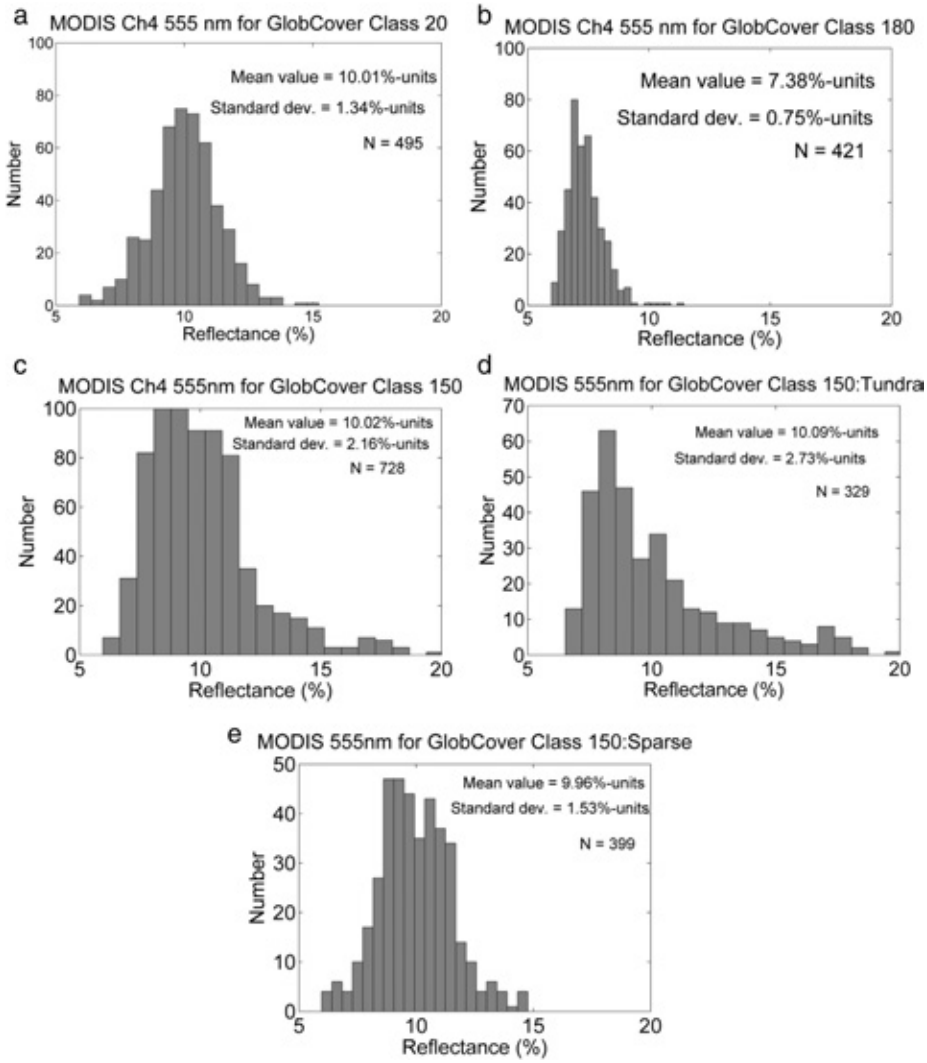


**Fig. 5.** Histograms for the MODIS band 4 (545–565 nm) reflectances for (a) agricultural areas/steppe, (b) wetlands and (c) sparse vegetation including tundra in the study area. Sub-division of class 150 to actual tundra and other sparsely vegetated (southern) regions is shown in (d) and (e), respectively.

(bias) according to Eq. (4), and the corresponding error bounds as a function of FSC are obtained by using Eq. (5). The results of Fig. 6 indicate that the systematic error of FSC estimation is close to zero for the two classes representing dry land areas; i.e. for classes 20 and 150 including steppe, agricultural areas, sparsely vegetated areas and tundra regions. However, in case of wetlands (class 180), the systematic error is significant causing the underestimation of FSC. The statistical error bounds are particularly high for class 150 due to the fact that this class combines tundra regions with southern sparsely vegetated areas which causes a high variability in $\rho_{ground}$ values, refer to Tables 3a and 3b and Fig. 5. As a conclusion, Fig. 6 and Tables 3a and 3b suggest that *SCAmod* provides reasonable accuracies of FSC for the study region even if a constant prefixed value of $\rho_{ground} = 10.0\%$-units is employed.

Fig. 7 depicts the estimated overall inaccuracy of FSC estimation due to the spatial variability of snow-free ground reflectance ($\rho_{ground}$). The results show the general performance of *SCAmod* for the applied European study region considering the open and sparsely forested land cover classes defined in Table 2. Analogous to Fig. 6, the FSC retrieval error is evaluated employing the constant $\rho_{ground} = 10.0\%$ for the MODIS band 4 (545–565 nm) in *SCAmod*. The analysis in Fig. 7 is based on the consideration of the areal coverage of different land cover classes and their representative snow-free ground reflectance histograms. The mean and standard deviation for $\rho_{ground}$ are calculated by a Monte Carlo simulation from the gained class-wise values (from Tables 3a and 3b), weighted by their areal proportions for the whole region (from Table 2). However, actual forest classes are excluded from the analysis. As a result, the weighted average of $\rho_{ground}$ is found to be 10.0%-units with a standard deviation of 1.8%-units, if forest canopy transmissivity effects are not compensated. If $t^2$-correction according to Eq. (2) is performed, the values are 11.0%-units and 2.7%-units, respectively. As the transmissivity correction approach yields higher

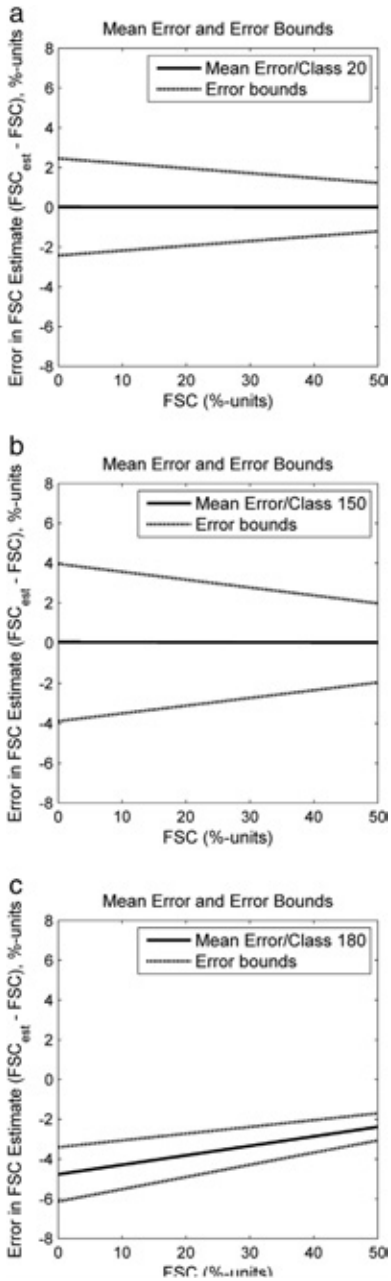


**Fig. 6.** The error (Mean and ± Standard Deviation) in the FSC estimation as a function FSC, when FSC < 50% for (a) agricultural areas/steppe, (b) sparse vegetation including tundra and (c) wetlands in the European study region. Mean error (solid lines) and error bounds (dashed lines) are obtained by using Eqs. (4) and (5), respectively. The shown error (including systematic (bias) and random error) is emerging when *SCAmod* is applied by using the fixed constant snow-free ground reflectance (10.0%) to describe all different land cover categories.

standard deviations of $\rho_{ground}$ estimates than the exclusion of $t^2$-correction, the error bounds of the two cases are slightly different. An important finding is also that the systematic error induced into the FSC estimation is close to zero whether the $t^2$-correction is applied or not.

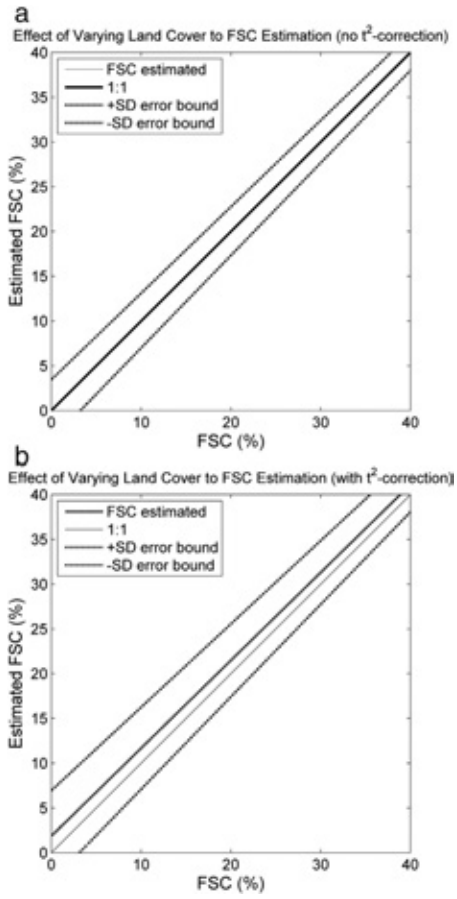


**Fig. 7.** The overall FSC retrieval error for the European study region as areal fractions of different land types within the region are considered. Error levels according to Eqs. (4) and (5) are shown for *SCAmod* when a pre-fixed constant snow-free ground reflectance (10,0%) is applied for MODIS band 4. Systematic and statistical error contributions are evaluated (a) excluding or (b) including forest canopy transmissivity correction in the determination of ground reflectance statistics.

As in Fig. 6, the results of Fig. 7 imply that *SCAmod* can be applied in the study region with a relatively good overall performance using a constant value $\rho_{ground} = 10.0\%$.

The snow-free ground reflectance values listed in Tables 3a and 3b can be used to derive maps on the spatial distribution of TOA-observed reflectance ($\rho_{ground}$) or reflectance indices (NDSI, NDVI and NDWI). As an example, the obtained MODIS band 4 reflectance and NDSI maps, covering the investigated European study region, are shown in Fig. 8. As indicated in Table 2, the analyzed GC classes in Tables 3a and 3b cover almost all open and sparsely forested areas of the region. For the sparsely forested and open land cover types, we already used the transmissivity condition as one of the reflectance selection criteria, so those values are applicable in $\rho_{ground}$ map generation. Thus, presented maps give a concise view of the TOA-observed surface reflectance and NDSI directly after the snow melt for non- and sparsely forested areas. As discussed above, this information (as well as the standard deviation of $\rho_{ground}$, also available from Tables 3a and 3b) is essential for the accuracy assessment of *SCAmod*-based FSC retrieval. Similarly, information on NDSI (and NDVI) of snow-free ground, also given in Tables 3a and 3b, can be applied to analyze the performance of algorithms that apply these indices.

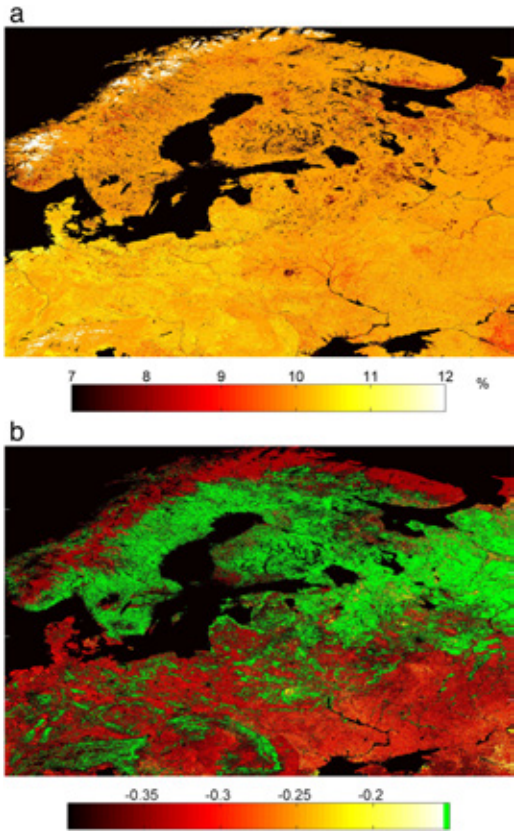


**Fig. 8.** Retrieved map of (a) TOA reflectance of snow-free ground at the MODIS band 4 (545–565 nm) covering the European study region and (b) NDSI, respectively. The study area is also shown in Fig. 1 indicating the locations of investigated pixels (three of the total of seven investigated GC land cover classes are shown in Fig. 1). Ice caps are shown by white color in (a); their reflectance is much higher than the image threshold value of 12%. In (b); forests are masked off by green color and ice caps/water by black color, respectively.

According to Table 2, forested areas cover about 46% of the land areas in the investigated European study region. As the forest canopy transmissivity is low for these areas, the retrieval of ground reflectance is not feasible, refer to Fig. 4. Hence we assign a constant reflectance of 10.0% for these areas when producing the map of Fig. 8. As discussed above, this value is feasible for the MODIS band 4 reflectance, based on earlier investigations for boreal forest zone (Salminen et al., 2009; Metsämäki et al., 2012). As the forests in the study region are mainly boreal forests or conifer-dominated forests in mountain/high altitude regions, we assign this value to represent all forests in Fig. 8a. Since NDSI was not analyzed for the forested areas, these regions are masked off by green color in Fig. 8b. Thus, Fig. 8b also shows the locations of forest pixels. Of all the investigated open and sparsely forested areas, the investigated classes cover a fraction of 93%. For the unanalyzed portion of 7% (4% of the total land area), we assigned $\rho_{ground}$ and NDSI from the closest resembling analyzed GC class (separately for each unanalyzed class). Thus, the map in Fig. 8 gives an estimate of $\rho_{ground}$ for all land areas of the European study site, and an estimate of NDSI is shown for all land areas, but forests. The exception is bare ground or glaciers/ice caps on mountains that are depicted by white color in Fig. 8a and by black color in Fig. 8b.

## 5. Summary and conclusions

The behavior of snow-free ground reflectance $\rho_{ground}$ directly after the snow melt was investigated by applying a time series of Terra MODIS TOA reflectance observations. In practice, the minimum $\rho_{ground}$ value at the 555 nm channel, occurring after the estimated time of snow melt, was searched within a time window of 15 days. This was carried out separately for all pixels of a certain class, in order to obtain a consistent data set that excludes possible observations with partial snow cover and in order to reduce the effects of viewing geometry variations. The same moment was selected to also represent snow-free ground conditions for other MODIS channels. The analysis was carried out for various land cover categories within Europe by applying ESA GlobCover data as reference. Thus, the results enabled the determination of the spatial behavior of TOA-observed snow-free ground reflectance and reflectance indices, such as NDSI and NDVI. The analyzed land cover classes represent 93% of the non-forested land in the investigated European study region.

The obtained $\rho_{ground}$ statistics facilitate the investigation of error level, resulting from the non-representative consideration of snow-free ground reflectance, in the mapping of the Fraction of Snow Covered Area (FSC). In particular, the performance of the *SCAmod* method was investigated here. The results show that in general, the *SCAmod* method that is based on the employment of the 555 nm band is applicable for the FSC mapping in Europe, even if $\rho_{ground}$ is treated by a present manner using a constant value for all land cover categories. According to the results, the exception is wetlands where $\rho_{ground}$ at 555 nm considerably differs from the presently employed constant $\rho_{ground}$ of 10%. However, additional land cover categories should be investigated in the future work aiming to global applicability. Further on, information on the snow-free ground NDSI is relevant for the FSC mapping approaches that are based on the use of this index.

Even though the variability of the mean value of $\rho_{ground}$ was found to be relatively small for different land cover classes of the study area (except for wetlands), the variance from pixel to pixel was found to be considerable. This also affects to the retrieval of FSC, as shown in Figs. 6 and 7 in the case of the *SCAmod* method. Further research will combine the analysis of different error contributions (e.g. those due to forest canopy transmissivity and variability of snow reflectance) to FSC estimation, in order to assess the general performance of retrieval algorithms both spatially and temporally.

## Acknowledgments

This work has been supported by the European Space Agency (ESA) DUE GlobSnow project. The GlobSnow product set, documentation and validation data are available at http://globsnow.info. ESA GlobCover project has provided the land use data for the research. The work has been also supported by the CLIMWATER (Climate Change and Water Cycle: Effect to Water Resources and their utilization in Finland) FICCA program project, funded by the Academy of Finland, and CLEEN (Cluster for Energy and Environment) MMEA (Measurement, Monitoring and Environmental Assessment) research program, funded by TEKES, respectively. The work has been conducted under the ACCC (Atmospheric Composition and Climate Change: From Molecular Processes to Global Observations and Models) doctoral program. Mikko Kervinen from SYKE is acknowledged for the help in data processing.

## References

Barlage, M., Zeng, X., Wei, H., & Mitchell, K. (2005). A global 0.05 maximum albedo dataset of snow covered land based on MODIS observations. *Geophysical Research Letters, 32*, L17405.

Barnett, T. P., Adam, J. C., & Lettenmaier, D. P. (2005). Potential impacts of a warming climate on water availability in snow dominated regions. *Nature, 438*, 303–309.

Betts, A. K., & Ball, J. H. (1997). Albedo over the boreal forest. *Journal of Geophysical Research, 102*, 901–909.

Bicheron, P., Huc, M., Henry, C., & Bontemps, S. (2008). *GLOBCOVER_PDM_I2.2. GLOBCOVER Product Description Manual, Issue 2, Rev. 2, 4/12/2008.*

Choi, G., Robinson, D. A., & Kang, S. (2010). Changing Northern Hemisphere snow seasons. *Journal of Climate*, *23*, 5305–5310.

Delbart, N., Kergoat, L., Le Toan, T., Lhermitte, J., & Picard, G. (2005). Determination of phenological dates in boreal regions using normalized difference water index. *Remote Sensing of Environment*, *97*, 26–38.

Duke, C., & Guérif, M. (1998). Crop reflectance estimate errors from the SAIL model due to spatial and temporal variability of canopy and soil characteristics. *Remote Sensing of Environment*, *66*, 286–297.

Gao, B. C. (1996). NDWI — A normalized difference water index for remote sensing of vegetation liquid water from space. *Remote Sensing of Environment*, *58*, 257–266.

Gonsamo, A., Chen, J. M., Price, D. T., Kurz, W. A., & Wu, C. (2012). Land surface phenology from optical satellite measurement and CO2 eddy covariance technique. *Journal of Geophysical Research*, *117*, G03032.

Hall, A., & Qu, X. (2006). Using the current seasonal cycle to constrain snow albedo feedback in future climate change. *Geophysical Research Letters*, *33*, L03502.

Hall, D. K., Riggs, G. A., Salomonson, V. V., DiGirolamo, N. E., & Bayr, K. J. (2002). MODIS snow-cover products. *Remote Sensing of Environment*, *83*, 181–194.

Jönsson, A.M., Eklundh, L., Hellström, M., Bärring, L., & Jönsson, P. (2010). Annual changes in MODIS vegetation indices of Swedish coniferous forests in relation to snow dynamics and tree phenology. *Remote Sensing of Environment*, *114*, 2719–2730.

Karlsen, S. R., Tolvanen, A., Kubin, E., Poikolainen, J., Hogda, K. A., Johansen, B., et al. (2008). MODIS NDVI-based mapping of the length of the growing season in northern Fennoscandia. *International Journal of Applied Earth Observation and Geoinformation*, *10*, 253–266.

Luojus, K., Pulliainen, J., Rott, H., Nagler, T., Solberg, R., Wiesmann, A., et al. (2010). ESA DUE GlobSnow — Global snow data-base for climate research. *Proceedings of the ESA Living Planet Symposium, June 28-July 2, 2010, Bergen, Norway, SP-686.*

Metsämäki, S., Anttila, S., Huttunen, M., & Vepsäläinen, J. (2005). A feasible method for fractional snow cover mapping in boreal zone based on a reflectance model. *Remote Sensing of Environment*, *95*, 77–95.

Metsämäki, S., Mattila, O. -P., Pulliainen, J., Niemi, K., Luojus, K., & Böttcher, K. (2012). An optical reflectance model-based method for fractional snow cover mapping applicable to continental scale. *Remote Sensing of Environment*, *123*, 508–521.

Moody, E. G., King, M.D., Schaaf, C. B., & Hall, D. K. (2007). Northern Hemisphere five year average (2000–2004) spectral albedos of surfaces in the presence of snow: Statistics computed from Terra MODIS land products. *Remote Sensing of Environment*, *111*, 337–345.

Niemi, K., Metsämäki, S., Pulliainen, J., Suokanerva, H., Böttcher, K., Leppäranta, M., et al. (2012). The behaviour of mast-borne spectra in a snow-covered boreal forest. *Remote Sensing of Environment*, *124*, 551–563.

Nolin, A. (2004). Towards retrieval of forest cover density over snow from the Multiangle Imaging SpectroRadiometer (MISR). *Hydrological Processes*, *18*, 3623–3636.

Nolin, A. W., & Dozier, J. (2000). A hyperspectral method for remotely sensing the grain size of snow. *Remote Sensing of Environment*, *74*, 207–216.

Painter, T. H., Dozier, J., Roberts, D. A., Davis, R. E., & Dozier, J. (2003). Retrieval of subpixel snow-covered area and grain size from imaging spectrometer data. *Remote Sensing of Environment*, *85*, 64–77.

Painter, T. H., Rittger, K., McKenzie, C., Slaughter, P., Davis, R. E., & Dozier, J. (2009). Retrieval of subpixel snow covered area, grain size, and albedo from MODIS. *Remote Sensing of Environment*, *113*, 868–879.

Peltoniemi, J., Kaasalainen, S., Näränen, J., Rautiainen, M., Stenberg, P., Smolander, H., et al. (2005). BRDF measurement of understory vegetation in pine forests: Dwarf shrubs, lichen and moss. *Remote Sensing of Environment*, *94*, 343–354.

Rittger, K., Painter, T. H., & Dozier, J. (2013). Assessment of methods for mapping snow cover from MODIS. *Advances in Water Resources*, *51*, 367–380.

Salminen, M., Pulliainen, J., Metsämäki, S., Kontu, A., & Suokanerva, H. (2009). The behaviour of snow and snow-free surface reflectance in boreal forests: Implications to the performance of snow covered area monitoring. *Remote Sensing of Environment*, *113*, 907–918.

Salomonson, V. V., & Appel, I. (2004). Estimating fractional snow cover from MODIS using the normalized difference snow index. *Remote Sensing of Environment*, *89*, 351–360.

Stewart, I. T., Cayan, D. R., & Dettinger, M.D. (2005). Changes toward earlier streamflow timing across western North America. *Journal of Climate*, *18*, 1136–1155.

Stow, D. A., Hope, A., McGuire, D., Verbyla, D., Gamon, J., Huemmrich, F., et al. (2004). Remote sensing of vegetation and land-cover change in Arctic tundra ecosystems. *Remote Sensing of Environment*, *89*, 281–308.

Twomey, S. A., Bohren, C. F., & Mergenthaler, J. L. (1986). Reflectance and albedo differences between wet and dry surfaces. *Applied Optics*, *25*, 431–437.

Vikhamar, D., & Solberg, R. (2003). Snow-cover mapping in forests by constrained linear spectral unmixing of MODIS data. *Remote Sensing of Environment*, *88*, 309–323.

Wiscombe, W. J., & Warren, S. G. (1980). A model for the spectral albedo of snow I: Pure snow. *Journal of the Atmospheric Sciences*, *37*, 2712–2733.

Xiong, X., Isaacman, A. T., & Barnes, W. (2006). MODIS level-1B products. In J. J. Qu, W. Gao, M. Kafatos, R. E. Murphy, & V. V. Salomonson (Eds.), *Earth science satellite remote sensing, science and instruments, vol. 1.* (pp. 33–49)New York: Springer-Verlag.

Xiong, J., Toller, G., Chiang, V., Sun, J., Esposito, J., & Barnes, W. (December 14). *MODIS Level 1B Algorithm Theoretical Basis Document, Version 3.* : MODIS Characterization Support Team.

Yu, F., Price, K. P., Ellis, J., & Kastens, D. (2004). Satellite observations of the seasonal vegetation growth in Central Asia: 1982–1990. *Photogrammetric Engineering and Remote Sensing*, *70*, 461–469.

III

International Journal of Applied Earth Observation and Geoinformation 27 (2014) 31–41

Contents lists available at ScienceDirect

International Journal of Applied Earth Observation and Geoinformation

journal homepage: www.elsevier.com/locate/jag

# The effect of boreal forest canopy to reflectance of snow covered terrain based on airborne imaging spectrometer observations

Kirsikka Heinilä[a,c], Miia Salminen[a,b,*], Jouni Pulliainen[b], Juval Cohen[b], Sari Metsämäki[a], Petri Pellikka[c]

[a] Finnish Environment Institute, P.O. Box 140, 00251 Helsinki, Finland
[b] Finnish Meteorological Institute, Arctic Research, Tähteläntie 62, 99600 Sodankylä, Finland
[c] Department of Geosciences and Geography, University of Helsinki, P.O. Box 64, FI-00014 Helsinki, Finland

ARTICLE INFO

*Article history:*
Received 20 December 2012
Accepted 18 June 2013

*Keywords:*
Spectral reflectance
NDSI
NDVI
Boreal forest
Snow
AisaDUAL

ABSTRACT

Optical remote sensing methods for mapping of the seasonal snow cover are often obstructed by the masking effect of forest canopy. Therefore, optical algorithms tend to underestimate the amount of snow cover in forested regions. In this paper, we investigate the influence of boreal forest stand characteristics on the observed scene reflectance under full dry snow cover conditions by applying an advantageous experimental setup combining airborne hyperspectral imaging and LIDAR data sets from a test region in Sodankylä, northern Finland. This is particularly useful to the understanding of the composition of the mixed satellite scene reflectance behavior and it is relation to the natural ground targets' spectral signatures.

At first, we demonstrate the effects of varying forest stand characteristics, including Canopy Cover (CC), Tree Height (TH) and the product of the these parameters referred to as CCxTH, on the reflectance measured by airborne imaging spectrometer AisaDUAL. Then, we analyze the effects of the presence of snow on forest canopy on the observed AisaDUAL data. The analysis of the effects of canopy was enabled by the high resolution LIDAR measurements which provide reference information on forest canopy characteristics. According to the results the change in Canopy Cover, as well as in CCxTH, is related to the observed change in reflectance, as well as to changes in such spectral indices as Normalized Difference Snow Index (NDSI) and Normalized Difference Vegetation Index (NDVI). Additionally, NDSI was found to vary extensively particularly in dense forests (CC > 85%), where the relative variation was over 100%. This should be considered when applying NDSI-based snow mapping methods in the case of forested areas. One notable finding was that the relation between the forest characteristics and reflectance was nearly exponential, while with reflectance indices it was linear. Besides, the results show that NDSI was a more effective parameter in detecting snow on canopy (values deviated 0.3 on average) than NDVI (values deviated 0.3 on average) in all Canopy Cover classes. The difference in NDSI between these two cases, snow-covered and snow-free canopy, increased when the canopy coverage increased.



## 1. Introduction

The development of improved and accurate methods to describe satellite-based observations as a function of regionally varying scene (target) characteristics, i.e. *forward modeling*, requires extensive and reliable experimental datasets. The feasibility of geo/biophysical variable estimates retrieved from satellite-data is most of all dependent on how reliable is this *forward modeling*. Thus, e.g. in developing and improving methods for seasonal snow cover monitoring in boreal forests, high spatial and spectral resolution information on the investigated scene properties and their temporal behavior are required. Above all, it is crucial to combine the employment of in situ data of the scene characteristics, coinciding near-range remote sensing reference observations (e.g. airborne, mast- or ground-based) and satellite observations. Using optical snow mapping instruments, such as the MODIS (Moderate Resolution Imaging Spectroradiometer) aboard Terra, specifically the forest disturbs the snow covered area detection as the trees prevent the visibility of snow-covered ground. In open areas with full snow cover the error in detecting snow from a satellite is usually very tolerable, typically less than 1%, but in forested areas the error has been found to be much larger, even 76% in Metsämäki et al. (2012).

Retrieval of fraction of snow covered area (FSC) using optical data is based on the high reflectance of snow in visible (VIS) and near-infrared (NIR) wavelengths compared to other natural

* Corresponding author. Tel.: +358 400 148 747; fax: +358 9 5490 2690.
*E-mail address:* miia.salminen@environment.fi (M. Salminen).

0303-2434/$ – see front matter © 2013 Published by Elsevier B.V.
http://dx.doi.org/10.1016/j.jag.2013.06.004

targets (Wiscombe and Warren, 1980). Spectral unmixing methods for FSC mapping are presented e.g. by Painter et al. (2003) and Vikhamar and Solberg (2003a,b). Moreover, the algorithm of NASA/Goddard Space Flight Center estimates the FSC from Normalized Difference Snow Index (NDSI) using linear regression (Hall and Riggs, 2007; Riggs et al., 2006; Salomonson and Appel, 2004, 2006). A typical defect with these methods is their weaker performance over forested areas. The semi-empirical reflectance model-based method *SCAmod* for FSC mapping in boreal forest and tundra belt using optical data was proposed by Metsämäki et al. (2005). *SCAmod* originates from radiative transfer theory and describes the scene-level reflectance as a mixture of three major constituents – opaque forest canopy, snow and snow-free ground, which are interconnected through forest canopy transmissivity and snow fraction. The method has proven to be feasible for global scale snow cover mapping and is particularly designed to give a good performance also for forested areas (Metsämäki et al., 2012). However, in *SCAmod*, the spatial and temporal variation in the utilized reflectance causes potential error in the satellite FSC retrieval when different constituents of modeled reflectance have standard constant values in the parametrization of *SCAmod* (Metsämäki et al., 2012; Niemi et al., 2012; Salminen et al., 2009). In order to quantify the magnitude of this error, high resolution measurements in controlled condition are required. The usability of satellite data can be improved (e.g. by better forward modeling) by applying more accurate snow-free ground, forest canopy and wet snow reflectances as model parameters (Metsämäki et al., 2012; Niemi et al., 2012; Salminen et al., 2009).

High resolution airborne optical measurements of snow-covered forests accompanied with LIDAR (Light Detection and Ranging) data-derived detailed forest canopy characteristics enable an advanced analysis of forest cover effects on space-borne observations, which is the key novelty of this investigation. The use of extensive data sets from Sodankylä test region, northern Finland, enables the development of optical snow mapping method, and their further validation and regional parameterization. Additionally, the mast-based spectral observations are particularly useful for determining the temporal behavior of forest scene reflectance (Niemi et al., 2012; Salminen et al., 2009). The effects of tree characteristics on the observed reflectance have been investigated earlier, while there is less information available on the spectral differences between various coniferous forest stands in snow-covered conditions (e.g. Betts and Ball, 1997; Ni and Woodcock, 2000; Rautiainen et al., 2004). The combined utilization of the airborne AisaDUAL (Airborne Imaging Spectrometer for Applications) hyperspectral data and LIDAR data with full dry snow cover enables the detailed examination of the effects of the forest stand properties, such as Canopy Cover (CC) and Tree Height (TH), to the observed scene reflectance. Moreover, the exploitation of the high spatial resolution airborne and ground based reflectances acquired under homogeneous dry snow cover conditions is beneficial for the modeling of the scene reflectance of forested terrain. Additionally, the airborne AISA and LIDAR data were utilized in the investigation of the effects of snow on canopy on scene reflectance in different types of forest. This is a further contribution to earlier work that indicates the significant influence of snow on canopy to boreal forest albedo (Kuusinen et al., 2012; Manninen and Stenberg, 2009; Niemi et al., 2012).

The scope of this research is the modeling of the effect of tree canopy on snow mapping in boreal forests. In the next step of the research the results will be used in the developing spectral un-mixing methods and reflectance model-based snow monitoring. Furthermore, the obtained full spectrum dataset facilitates the adaptation and development of snow mapping methods for current and future optical satellite sensors with different optical channels. To summarize, we apply scene-level observations from aerial campaigns to provide information on the behavior of optical spectral signatures relevant to the parameterization of forward models including canopy and ground components.

**Table 1**
The measurement conditions on 18 March 2010 when the canopy was snow-free and on 21 March 2010 when the canopy was snow-covered. The proportions are from the area monitored by mast-borne spectrometer analyzed from digital image.

| | 18 March 2010 at 10:05 UTC | 21 March 2010 at 10:05 UTC |
|---|---|---|
| Solar azimuth (°) | 175.5 | 175.7 |
| Solar elevation (°) | 21.7 | 22.9 |
| Snow depth (cm) | 77 | 83 |
| Grain size (mm) | 0.54 | 0.38 |
| Proportion of snow-free canopy (%) | 62.4 | 39.5 |
| Proportion of directly illuminated snow at ground and on canopy (%) | 3.8 | 11.9 |
| Proportion of shadowed snow at ground and on canopy (%) | 34.0 | 48.6 |
| Snow surface temperature (°C) | −6 | −7 |
| Air temperature (°C) | −4 | −5 |

## 2. Material and methods

### 2.1. Study area

Sparse coniferous forest dominates the study area in the surroundings of the Arctic Research Center of the Finnish Meteorological Institute (FMI-ARC) in Sodankylä located in southern Lapland of Finland at 26.6°E 67.4°N, about 100 km north of the Arctic Circle and 180 m above the sea level. This sub-arctic environment has long, cold continental winters, and it is characterized by seasonally snow covered forests and open wetlands. In general, snow layer in Lapland is rather homogenous until the spring melt-freeze metamorphosis starts. The Scots Pine (*Pinus sylvestris*) dominated forests are characteristic for the area as overall 92% of forests in southern Lapland are dominated by Scots Pines (fraction of pines > 75%) (METLA, 2010).

### 2.2. Airborne spectrometer data and processing

The airborne hyperspectral data was acquired utilizing AisaDUAL, which combines two sensors. It provides very high spatial and spectral resolution data covering with VNIR sensor the spectral range of 400–970 nm and with SWIR sensor the range of 970–2500 nm. The campaign was carried out in Sodankylä during full dry snow cover and ideal weather conditions, i.e. several minus degrees and cloudless sky, on 18 March and on 21 March 2010 (Table 1). On 18 March, the trees were snow-free and snow cover on ground was several days old, while on 21 March, the trees were snow-covered and the snow on trees and ground was newly fallen (Fig. 1). The hyperspectral data was acquired from helicopter at the altitude of 800 m producing a spatial resolution of 0.8 m. The spectral resolution for the VNIR bands was 5 nm and for SWIR bands 6 nm totaling to 359 spectral bands. The image swath was 240 m and flight lines were several kilometers long. All measurements were carried out in direct illumination (i.e., clear sky: 0/8 to 2/8 cloud cover). In both campaigns, Oxford Technical Solutions RT4000 GPS/INS was used, which enables high accuracy measurements with low drift rates. The instrument foreoptics unit was set to look at nadir (0°) direction and the field of view (FOV) was 17°. The data was radiometrically and geometrically corrected by using CaliGeo tool by SPECIM in the ENVI software. The AISA data was first filtered with mean filter using $12 \times 12$ window corresponding to pixel size of 10 m and then reprojected to the same grid with

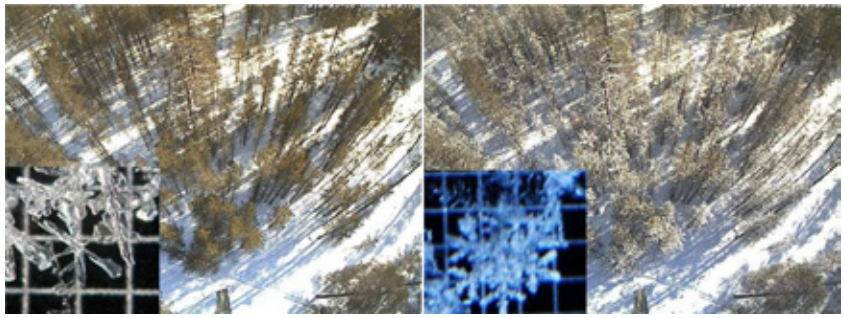

**Fig. 1.** The forest canopy and grain size on 18 March 2010 on the left and on 21 March 2010 on the right. Snow grain samples are on the 1-mm grid.

LIDAR data. Besides obtaining the correspondence with the LIDAR data, using the average value for 10 m grid reduces the error caused by irregular noise. The calibration of the absolute reflectance level of the AISA observations was performed by applying well calibrated ASD-spectrometer data from a 30-m high mast. The mast-borne system (calibrated by a white Spectralon panel) made reflectance measurements of a forest footprint concurrently with AISA image acquisitions. To get same level of reflectance for the mast-borne and AISA-observations of the forest footprint, calibration coefficients (for different VIS, NIR and SWIR wavelength ranges) were determined for the AISA data, see Section 2.4.

The AISA data was investigated using the bands and spectral indices relevant to MODIS snow mapping (Klein et al., 1998) (Table 2). The bands were extracted from the AISA spectra by using the band specific FWHM criterion (full width at half maximum) corresponding to MODIS bands (Table 2). AISA derived green (555 nm) and near infrared (858.5 nm) bands, and NDSI and NDVI indices, were compared with the LIDAR based Canopy Cover (CC) and Tree Height (TH) maps. In addition, the AISA data was compared with the product of CC and TH, referred to as CCxTH. In order to find out the correspondence with the total forest canopy volume, CCxTH values were compared with the 25 m resolution volume of growing stock (VOL) data, which was calculated from Landsat images by the Finnish Forest Research Institute (METLA) (Tomppo et al., 2008). The comparison of these data sets is shown in Fig. 2 indicating a slightly non-linear relation between VOL and CCxTH values. The obtained second-degree fit is

$$\mathrm{VOL}_{\mathrm{modelled}} = -2.5e-05 \times \mathrm{CCxTH}^2 + 0.081 \times \mathrm{CCxTH} + 17 \quad (1)$$

Additionally, the comparison of the volume estimates (VOL) with the LIDAR data-derived Tree Height (TH) and Canopy Cover (CC) indicated that the product of these factors (CCxTH) has a higher correlation to total volume than when comparing these variables solely. Since the data on growing stock volume is not spatially as accurate as the LIDAR data-based reference information, it is reasonable to apply in the analyses here the CCxTH data instead of volume estimates retrieved from satellite data.

**Table 2**
Resampled reflectance bands and indices from AISA spectra.

| MODIS bands | Central wavelength (nm) | Bandwidth (nm) |
|---|---|---|
| Band 1 | 645 | 620–670 |
| Band 2 | 858.5 | 841–875 |
| Band 4 | 555 | 545–565 |
| Band 6 | 1640 | 1628–1652 |

| MODIS-based indices | Formulation |
|---|---|
| NDSI | (Band 4 – Band 6)/(Band 4 + Band 6) |
| NDVI | (Band 2 – Band 1)/(Band 2 + Band 1) |

The number of observations ($N$) (i.e. the amount of 10 m grid cells) was 50 200 except in the investigation of the TH. When the effect of TH was analyzed, only observations where CC was 30–70% and TH >1 m ($N$ = 19 100) were included in order to reduce the correlation between TH and CC (Fig. 3.). When studying the relation between the CC and indices, a linear model was fitted. An exponential model was used in describing the relation between the CC and AISA reflectances. For all the cases, the root mean squared error (RMSE) was calculated as follows:

$$\mathrm{RMSE} = \sqrt{\frac{1}{N}\sum (V_{\mathrm{estim}} - V_{\mathrm{AISA}})^2} \quad (2)$$

where $N$ is the number of observations, $V_{\mathrm{estim}}$ is the value predicted by the fitted model (linear or exponential) and $V_{\mathrm{AISA}}$ is the reflectance or index derived from AISA data. Additionally, the interdependency between the NDSI and NDVI was investigated in the study area by analyzing the behavior of observations in NDSI–NDVI space. These indices are used in operational snow mapping, e.g. in NASA's binary snow algorithm a pixel is labeled as snow-covered if it has NDSI and NDVI values within a certain range taking into account the forest cover of the pixel (Klein et al., 1998). The effect of snow on trees on scene reflectance was analyzed by using NDSI

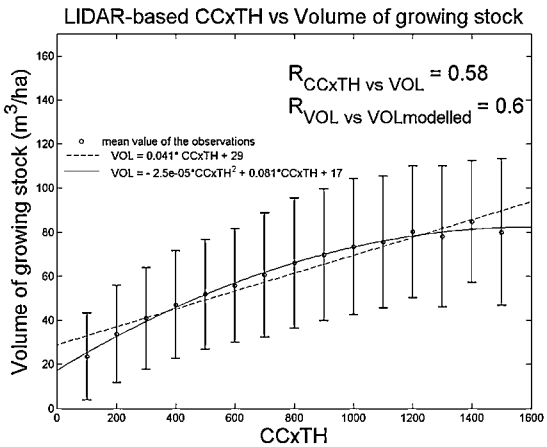


**Figure 2.** The mean values and the standard deviation of the volume of the growing stock (VOL) in different CCxTH classes (CCxTH-values are divided into 15 classes). The regression lines between CCxTH and the VOL data are also shown. Pearson's correlation coefficient $R$ is calculated between the CCxTH and the VOL data as well as between the modeled VOL values and VOL estimates determined from the coarser resolution satellite data.

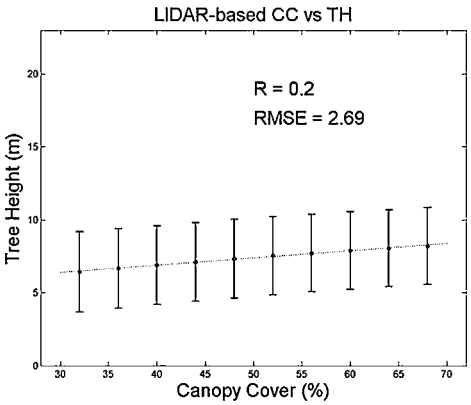


**Fig. 3.** The mean Tree Height (TH) and standard deviation were calculated for Canopy Cover (CC) classes. A linear regression line between TH and CC is also shown. *R* refers to Pearson's correlation coefficient and RMSE to Eq. (2).

and NDVI indices. They were employed as these indices are less sensitive to (small) differences in illumination geometry than band reflectances. AISA imaging spectrometer was set to look at nadir, which minimizes the effect of solar azimuth. The effect of solar elevation could be expected to be low due to the fact that it varied maximum 1 degree between the measurements from two days. Additionally, the relative difference $d_r$ between the indices from two different days was calculated as follows:

$$d_r = \frac{V_{sf} - V_{sc}}{(V_{sf} + V_{sc})/2} \times 100\% \quad (3)$$

where $V_{sf}$ is the AISA data-derived index value (NDSI or NDVI) for forest with snow-free canopy and $V_{sc}$ is the index value for forest with snow-covered canopy. In the visualization of the mean and standard deviation for reflectance or index, the forest characteristics are presented in equal interval classes.

### 2.3. LIDAR reference data processing

The reference data covering the airborne spectrometer flight lines includes airborne high-resolution LIDAR measurements of forest canopy and terrain topography (Fig. 4). Based on LIDAR measurements at snow-free conditions, a vegetation height map and a Canopy Cover map were derived for grid cells of 10 m. First, LIDAR point-cloud data was acquired for Sodankylä area from the National Land Survey of Finland. After, the point-clouds, with the point density of at least 0.5 points/m$^2$ (distance between each point approximately 1.4 m), were transformed to a vegetation height raster image with a resolution of 2 m. The vegetation height was retrieved by creating a digital surface model (DSM) from the LIDAR point cloud data, and subtracting the ground elevation from the DSM. The 10 m resolution Canopy Cover (CC) and Tree Height (TH) maps were both derived from the 2 m resolution vegetation height map. In the CC map, the value in percentage for each grid cell was retrieved by calculating the ratio between tree pixels (vegetation height over 1.5 m) and the total number of 2 m pixels inside a 10 m grid cell. In the TH map, each pixel value in meters was either the mean value of the low vegetation pixels, or the mean value of the tree pixels if at least one tree pixel was inside the 10 m grid cell. The LIDAR measurements were acquired under leafless conditions, and therefore the CC map was suitable for AISA-based analysis from snow-covered forests. In the observed area, there were only sparsely distributed individual deciduous trees of birch (*Betula* ssp.) present.

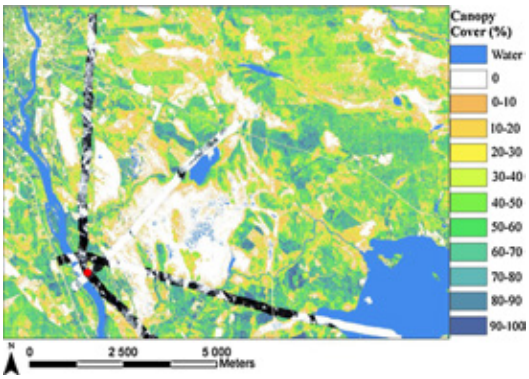


**Fig. 4.** Utilized AisaDUAL data from 18 March 2010 consists of four flight lines, same four flight lines was measured on 21 March 2010. In the background is forest Canopy Cover (CC) map derived from the LIDAR data. Red spot represents the location of mast-based spectrometer.

### 2.4. Mast-borne spectrometer data

In addition to AISA observations, mast-borne spectrometer data was applied in the study, also for calibrating the AISA data. The ASD Field Spec Pro JR spectrometer, maintained by the FMI-ARC, measures radiance from a 30-m-high mast. Spectral range of the instrument is 350–2500 nm with a spectral resolution about three nm for the band 350–1000 nm and of 10–12 nm for the band 1000–2500 nm. The detector is at the end of an adjustable 6-m-long pole and is tilted 11° from nadir (Sukuvaara et al., 2007). The sensor azimuth is 110° and the FOV is 25°. The incoming radiation was determined by measuring the radiance from a white Spectralon panel at a particular wavelength $L_{IR}(\lambda)$ and by calibrating the measured radiance as follows:

$$L_{IR}(\lambda) = \frac{1}{R_{CAL(\lambda)}} \times \frac{L_{CAL}(\lambda)}{L_{REF}(\lambda)} \times L_{Ref}(\lambda) \quad (4)$$

where $R_{CAL}$ is the instrument background noise, $L_{REF}$ is the radiance of the white Spectralon panel from the mast measured simultaneously with the new white Spectralon panel ($L_{CAL}$) in the laboratory, and $L_{Ref}$ is the radiance of the white Spectralon panel of the mast at the time of the measurement.

The mast-borne spectrometer provides radiance data from two sites: (1) a forest and (2) a forest opening with tree shadows. For both of these 185 m$^2$ sized areas an average instantaneous reflectance spectrum and simultaneously acquired digital images are obtained on a daily basis (Niemi et al., 2012; Salminen et al., 2009). The in situ (nadir) Canopy Cover in the observed forest stand is 40%, though the canopy covered 48% of the spectrometer view due to the tilted imaging angle. The mast-borne reflectance data from snow covered forest (Fig. 5) from the field campaign dates, 18 March 2010 and 21 March 2010 was utilized. The reflectance data was used for illustrating the effect of solar position on scene reflectance with snow-free canopy and with snow-covered canopy.

## 3. Results and discussion

### 3.1. The effect of tree characteristics on scene reflectance and indices

Fig. 6 presents the mean reflectance or index values and standard deviation for each Canopy Cover (CC) equal interval class of 10%-units (±5% from the mean CC value). We found that CC

**Fig. 5.** The specific forest area of mast-borne ASD spectrometer measurements.

is nearly linearly related to both NDSI and NDVI, see Fig. 6c and d. Also, the exponential relation between CC and the reflectance at wavelengths 555 nm and 858.5 nm is considerable (Fig. 6). The reflectances decreased, when the CC increased, due to the low reflectance of forest canopy compared to snow in the visible wavelengths (Fig. 6a and b). However, in this case the decrease of reflectance with increasing CC appears to obey an exponential function $a \times \exp(b \times \mathrm{CC})$, which is fitted to the Fig. 6a and b. This appears to be in an agreement with modeling results, see e.g. Metsämäki et al. (2005, 2012), Niemi et al. (2012), Salminen et al. (2009), Schlerf and Atzberger (2006). As CC has such a strong correlation with the scene reflectance, it is beneficial to include valid forest canopy transparency information (i.e. the proportion of the radiation that penetrates through the tree canopy layer) as input to satellite data retrieval algorithms. This is the case with the *SCAmod* that employs the forest canopy two-way transmissivity information. Ni and Woodcock (2000) investigated the effect of Canopy Cover on forest albedo and found that also the forest albedo varied dramatically as a function of Canopy Cover when the ground was snow covered. They also noticed that when CC > 70% the presence of snow had only a minor effect on the observed albedo. This coincides well with our results in Fig. 6, where the reflectances did not vary considerably within the three highest CC classes (75–100% CC).

Additionally, we found, that the standard deviation of the reflectances decreases with increasing CC, while NDVI and NDSI behaved oppositely gaining low variability in sparse forests (i.e. variation increases when CC gets higher). In dense forests (CC > 85%), the relative variation of NDSI was over 100% while in sparse forests (CC < 45%) it was less than 30%. This agrees with the findings by Niemi et al. (2012), where NDSI and NDVI were less sensitive to variations in illumination geometry (including the

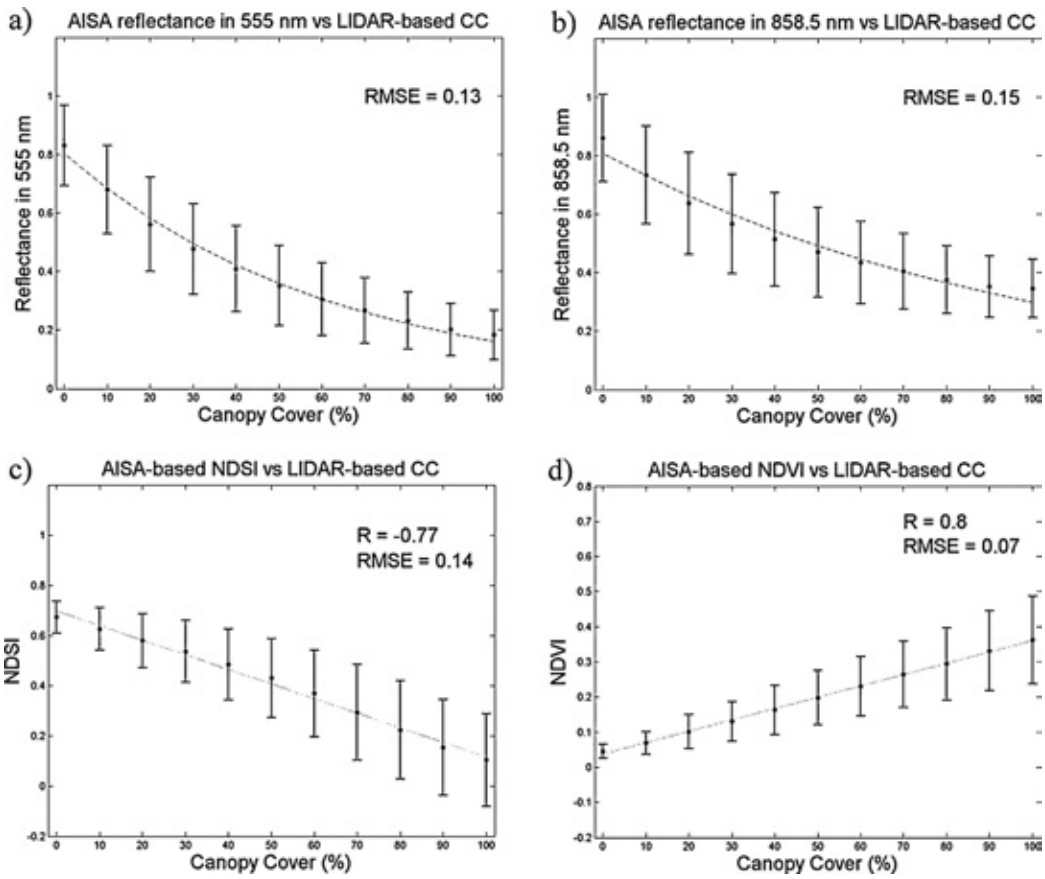


**Fig. 6.** (a) Green band reflectance (555 nm), (b) NIR band reflectance (858.5 nm), (c) NDSI and (d) NDVI, and the standard deviation, for forests with varying Canopy Cover (CC). CC-values are divided into 11 classes. Mean values and standard deviations are depicted for each class. The exponential regression lines data ($a \times \exp(b \times \mathrm{CC})$) between CC and reflectances and linear regression lines between CC data and indices are also shown. *R* is Pearson's correlation coefficient between the indices and TH and RMSE is calculated using Eq. (2).

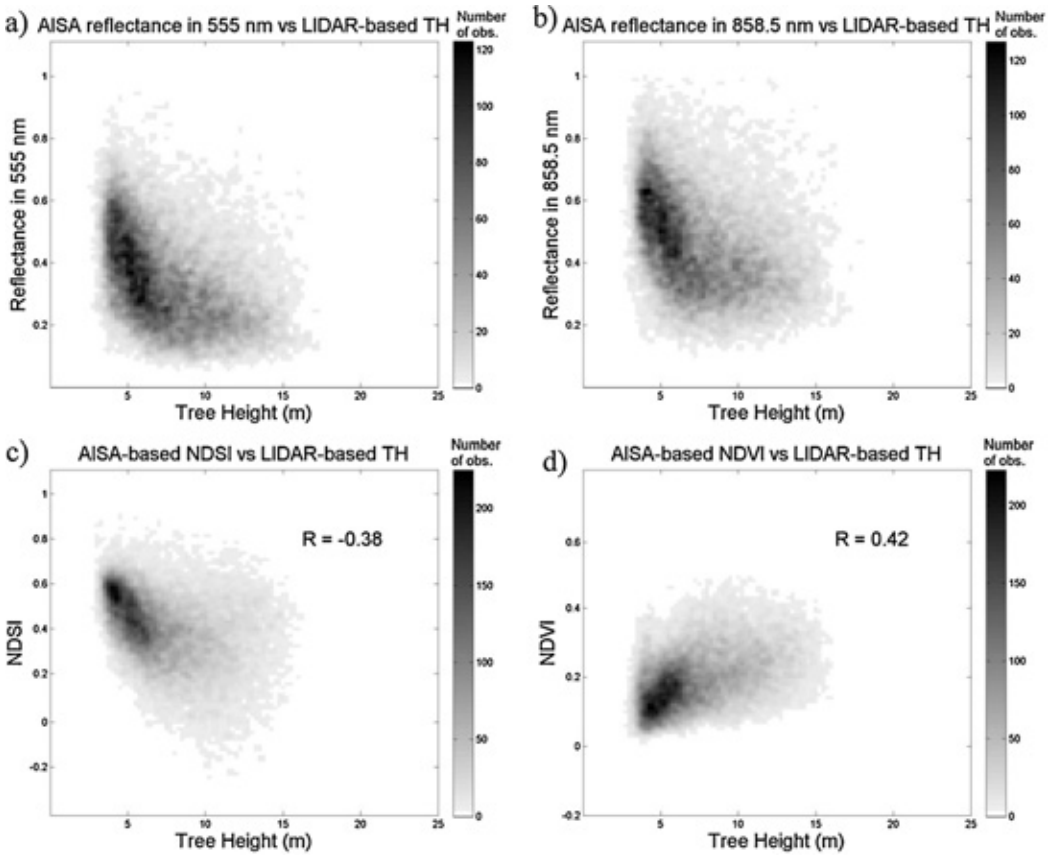


**Fig. 7.** The relation between Tree Height (TH) and (a) green band reflectance (555 nm), (b) NIR band reflectance (858.5 nm), (c) NDSI and (d) NDVI. *R* is Pearson's correlation coefficient between the indices and TH.

amount of shadows) in open areas. Moreover, illumination geometry induced large variation in the obtained reflectances. Results by Niemi et al. (2012) showed that it is beneficial to apply these indices for snow mapping in sparsely vegetated or open areas, based on the analysis of time-series of mast-based observations at single site (Sodankylä mast). This agrees well with the results obtained here using spatially distributed airborne observations. On the other hand, in forests the indices varied strongly, similar to our findings in dense forests. Cao and Liu (2006) have correspondingly found that the variation in NDSI (caused by e.g. solar zenith angle and instrument view angle) increased with decreasing snow covered area.

The Pearson's correlation coefficient (*R*) between the TH and AISA data-derived reflectances or indices was not as strong as that in the case of CC (Fig. 7). When TH was around 5 m, the reflectance varied in the range of 80%. This might be explained by the variation in CC, though the lowest (<30%) and the highest (>70%) values of CC were excluded from the analysis. According to results, TH seems to correlate negatively with the reflectance values. Consistently with the CC, Fig. 7 illustrates that the response of reflectance to the increase of TH is merely nonlinear than linear. The reflectance is predominantly less than 0.2 in the band of 555 nm when the trees are higher than 15 m (Fig. 7a). The study of Heiskanen (2006) showed that the accuracy of the Tree Height estimates in the tundra-taiga transitions reduced around 10% when multispectral nadir data was used together with the multi-angle data, when compared with the utilization of multispectral nadir data only. Similar improvements were found in the case of tree cover. When indices were plotted in the Canopy Cover and Tree Height space an interesting effect is observed for dense forests (Fig. 8): NDSI decreases for the highest and densest forests whereas NDVI increases with the increasing TH for all CC levels.

The behavior of reflectance and channel indices as a function of CCxTH is investigated in Fig. 9. As shown by Fig. 2, the product CCxTH has a slightly non-linear relation with the volume of growing stock. As the level of ground biomass is related to the volume of the growing stock (e.g. Boudewyn et al., 2007), CCxTH is also related to the level of biomass. Fig. 9 indicates that the reflectances observed at the 555 nm and 858.5 nm bands decrease non-linearly as a function of CCxTH. The sensitivity of NDSI and NDVI to the increase in CCxTH is also considerable with a negative nearly linear response in the case of NDSI and a positive response in the case of NDVI. Muukkonen and Heiskanen (2005) found that particularly green band reflectance was sensitive to tree biomass and, correspondingly to our CCxTH results, the shape of the correlation between the green band and biomass was more nonlinear than linear (Fig. 9a). NDVI has a low value in all cases with a low level of CCxTH. The increase of NDVI with increasing CCxTH is clear, but

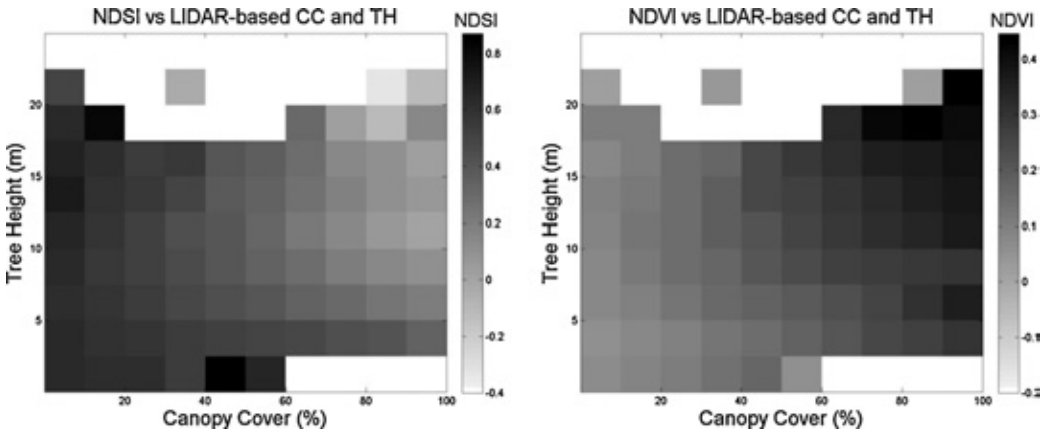


**Fig. 8.** NDSI versus Canopy Cover and Tree Height on the left and NDVI versus Canopy Cover and Tree Height on the right.

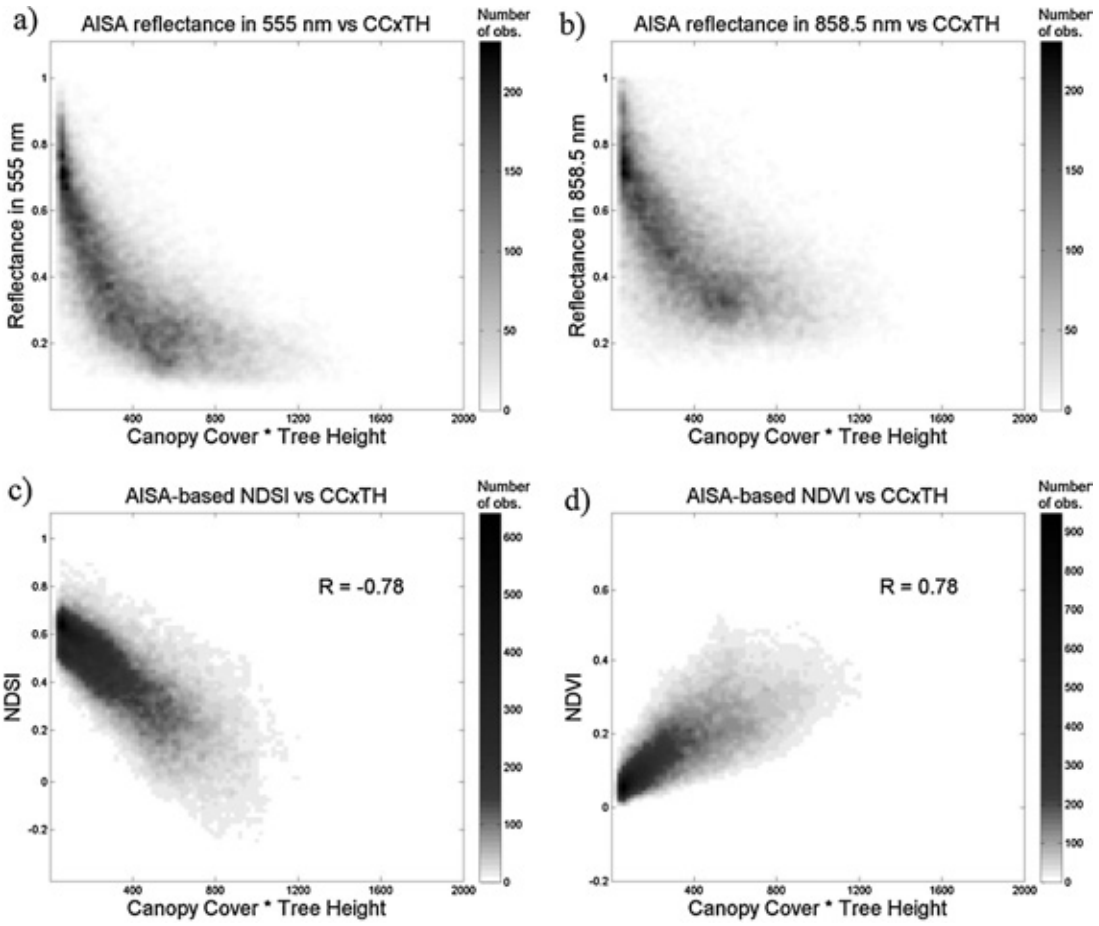


**Fig. 9.** The relation between the CCxTH and (a) green band reflectance (555 nm), (b) NIR band reflectance (858.5 nm), (c) NDSI and (d) NDVI. *R* is Pearson's correlation coefficient between the indices and TH.

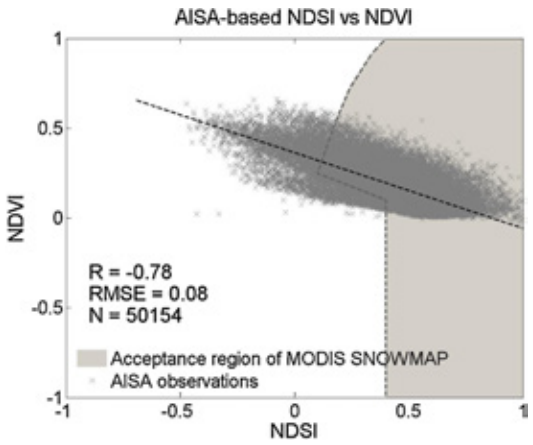


**Fig. 10.** The correlation between the NDSI and NDVI based on AISA observations with fully snow-covered open and forested areas (CC = 0–100%). *R* is Pearson's correlation coefficient between NDSI and NDVI and RMSE is calculated with Eq. (2).

also the variation significantly increases (Fig. 9d). Rautiainen et al. (2004) found that reflectances increase with increasing crown volume, but in our case with CCxTH the correlation was negative. This is because the ground is covered by snow, and therefore, has high VIS and NIR reflectance dominating the signal at scene-level.

In addition, e.g. Fig. 9 illustrates that NDSI tends to get also negative values when CCxTH increases. The lowest observed NDSI was as low as −0.47 for forest area with CC of 76%, CCxTH of 980 and NDVI of 0.63. This coincides well with the results by Niemi et al. (2012) obtained by using mast-borne spectrometer data where the NDSI was found to obtained negative values in the forest with CC of 40%. Similarly, Klein et al. (1998) modeled negative NDSI values in snow-covered forest stands, but the limit of NDSI to classify pixel as snow-covered in NASA's snow mapping method is set to minimum of 0.1 (Hall et al., 1998; Klein et al., 1998; Riggs et al., 2006). This is to avoid false snow interpretations in the case of snow-free conditions, as similar values for snow-free forests were obtained. In NASA's algorithm the threshold value for NDSI to detect snow cover depends on the NDVI value. In Fig. 10 is showed this region of MODIS binary snow algorithm which is set to detect snow cover.

Additionally, Fig. 10 demonstrates the behavior of NDSI against NDVI based on AISA observations on 18 March 2012 in fully snow-covered areas (snow-free canopy, snow depth about 80 cm, see Table 1). NDSI and NDVI were found to be nearly linearly correlated. However, the spread in the observations is high, even though the measurement conditions were rather stabile during the data acquisition that was carried out within 1 h. Thus, the variation is probably induced by forest characteristics. Most of the negative NDSI values were found in the forests where NDVI was >0.3. Xin et al. (2012) has described that the NDSI value determined using MODIS satellite images is prone to the changes in View Zenith Angle (VZA). They found that when VZA increases, NDSI decreases. In the case of AISA data, the effect of the variation of the VZA is negligible with the FOV only 17° and allows us to investigate the relation between NDSI and NDVI without the disturbance of VZA. The NDSI-NDVI relation will be further investigated with AISA data acquired in snow-free conditions right after snow melt to discover the proper limits of NDSI to capture snow in boreal forests.

### 3.2. *The effect of snow on canopy on spectral behavior of reflectance and indices*

The applied AISA data set and the mast-based ASD spectrometer observation data set enabled the investigation the difference between the scenes with snow-free and snow-covered forest canopy. The presence of snow on canopy is a regular phenomenon in high latitudes and has been found to effect strongly on forest reflectance and albedo, see results e.g. by Manninen and Stenberg (2009) and Niemi et al. (2012).

In particular, the mast-based observations are used here to demonstrate the effect of illumination geometry on scene reflectance in both cases (Fig. 11). The results for snow-free and snow-covered canopies are analogously showing an increased level of reflectance for the case of backscatter. However, the effect of solar azimuth angle (with respect to instrument view angle) is stronger in the case of snow covered canopy for the infrared region (Fig. 11, right). Correspondingly, Kuusinen et al. (2012) found large variation in pine forest albedo, when the canopy was fully snow-covered. They deduced that changes in illumination conditions as well as the amount and properties of snow caused the variation. According the results from mast-borne spectra, the differences in the calibration or illumination geometry may cause variation to the reflectances from these two measurement days and only indices were employed in further investigations on canopy effect. The overall low values

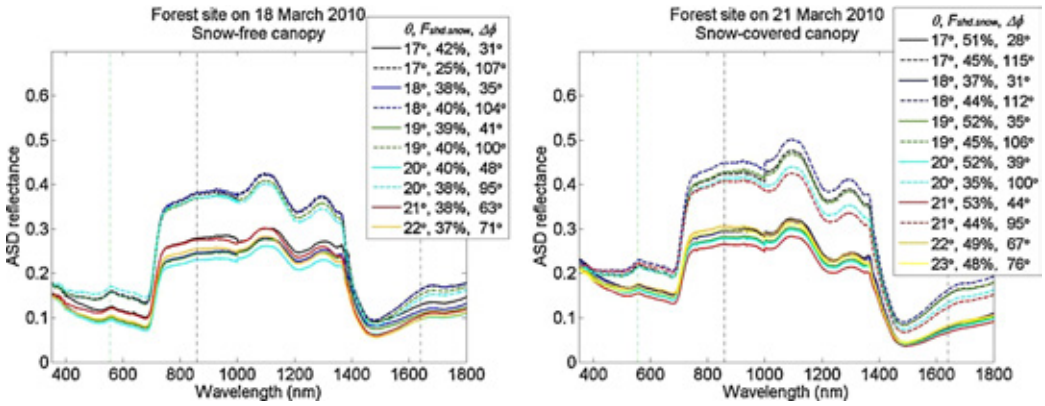


**Fig. 11.** The effect of solar elevation $\theta$, fraction of shadowed snow $F_{\mathrm{shd.snow}}$ and the relative azimuth $\Delta\varphi$ on scene reflectance of forest area in dry snow conditions. The sun is in the direction of instrument view when $\Delta\varphi = 0$ (case of forward scatter). Dashed curves and solid curves represent backscattered and forward scattered spectra, respectively. Left: Snow-free canopy. Right: Snow-covered canopy.

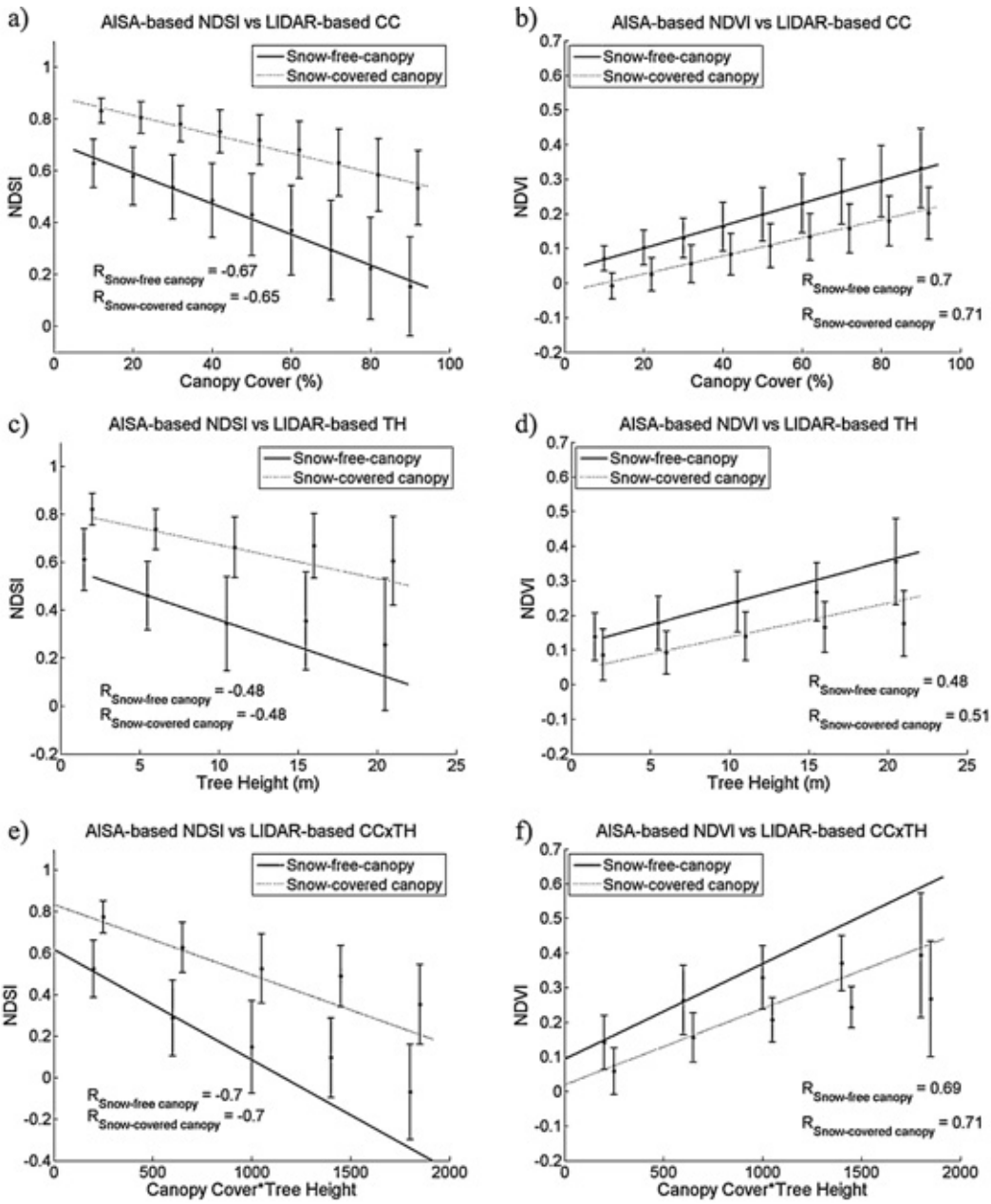


**Fig. 12.** The mean and standard deviation of observed spectral indices on 18 March 2010 when canopy was snow-free and on 21 March 2010 when canopy was snow covered. (a) NDSI vs. CC, (b) NDVI vs. CC, (c) NDSI vs. TH, (d) NDVI vs. TH, (e) NDSI vs. CCxTH and (f) NDVI vs. CCxTH. Majority of the observations represents lower values of CCxTH. R refers to Pearson's correlation coefficient and RMSE to Eq. (2).

especially in the visible wavelengths of the mast-borne spectra (Fig. 11, left) might be caused by the relatively high trees in the forest stand (TH around 12 m), as the mean reflectance e.g. in 555 nm is 0.27 with std of 0.12 when TH is 12 m (see also Fig. 7a).

Fig. 12 depicts the AISA data-derived response of NDSI and NDVI to increase in CC, TH and CCxTH. For all Canopy Covers, snow-covered canopy introduces higher NDSI compared to snow-free canopy. The behavior of NDVI is the opposite. The strong effect of snow-covered canopy on forest albedo has been found in various investigations, see e.g. Manninen and Stenberg (2009) and Kuusinen et al. (2012). According to our results, the difference in indices between forest with snow-free and snow-covered canopy

**Table 3**
The NDSI and NDVI for forest scene with snow-free canopy $V_{sf}$ and snow-covered canopy $V_{sc}$ and their relative difference $d_r$ for different forest categories.

| | Canopy Cover 10–30% | | | Canopy Cover 30–50% | | | Canopy Cover 50–70% | | | Canopy Cover 70–90% | | |
|---|---|---|---|---|---|---|---|---|---|---|---|---|
| | $V_{sf}$ | $V_{sc}$ | $d_r$ | $V_{sf}$ | $V_{sc}$ | $d_r$ | $V_{sf}$ | $V_{sc}$ | $d_r$ | $V_{sf}$ | $V_{sc}$ | $d_r$ |
| NDSI | 0.58 | 0.80 | −32% | 0.48 | 0.75 | −43% | 0.37 | 0.68 | −60% | 0.23 | 0.59 | −88% |
| NDVI | 0.10 | 0.02 | 123% | 0.16 | 0.08 | 65% | 0.23 | 0.13 | 54% | 0.29 | 0.18 | 49% |

increases when the CC or CCxTH increases. In addition, the variation in NDSI increases when CC increase, which can be seen from the behavior of standard deviation (Fig. 12). However, the snow-covered canopy reduces this variation. Table 3 presents a summary of the indices as well as relative difference (Eq. (3)) between the two cases. The difference between the snow covered and snow-free canopy is more than 30% in all CC classes in the case of both indices. The relative difference in NDVI increases when CC decreases. The relative difference of NDSI behaves oppositely i.e. increases when CC increases. This sensitivity of NDSI to the presence of snow on canopy in dense forests is explained by the higher change in total snow covered area (consisting of both snow on the ground and on the canopy). However, the lower impact of snow-covered canopy on NDSI especially in sparsely forested areas, where the proportion of snow-covered area is high (the visibility to snow layer is more extensive than in denser forests), might be partly explained by the smaller grain size of new snow. The increasing grain size as well as snow aging has been found to raise the NDSI value (Negi et al., 2010; Niemi et al., 2012). Niemi et al. (2012) found the strong impact of snow-covered canopy on NDSI and NDVI from mast-borne spectra. The CC of the area illuminated by mast-borne spectrometer is 40%. In that case the relative difference was 156% for NDSI and 46% for NDVI. The higher impact on NDSI is explained by the differences in instrument viewing angle; AISA has a nadir view while the mast-borne spectrometer viewing angle is 11°. Xin et al. (2012) has found that in snow-covered forests NDSI decreased when VZA increased. They also discovered that with small VZA the effect was lower in sparse forest stands compared to dense forests. Overall, Fig. 12 depicts that NDSI values between snow-free and snow-covered canopy overlap less (deviated 0.31 on average) than in the case of NDVI (values deviated 0.10 on average) suggesting to utilize NDSI to detect the snow on canopy.

## 4. Conclusions

The behavior of remotely sensed spectral reflectance in selected bands, as well as the NDSI and NDVI, was found to be strongly affected by the spatial variations of forest canopy characteristics. An important finding was that the relation between the forest canopy properties and the observed reflectances shows a nonlinear curve, whereas with the investigated indices this relation is nearly linear. Canopy Cover (CC) as well as the product of CC and Tree Height (TH) CCxTH (corresponding with the volume of growing stock as well as with biomass), correlated rather well with the NDSI and NDVI (Pearson's correlation coefficient was 0.8). The obtained results demonstrate the feasibility of NDSI and NDVI for snow monitoring algorithms to detect snow cover underneath the forest canopy, but only for relatively sparse forests or in non-forested areas. In dense forest, the indices are less sensitive in detecting snow covered terrain, which is indicated by the increase of the variance of indices when CC increases, see Fig. 6b and c. Especially with high NDVI (>0.3), NDSI was found to show also negative values (even −0.5, with NDVI = 0.6). This large variation in the NDSI values depending on forest characteristics should be considered in NDSI-based snow mapping methods in case of forested areas.

When NDSI and NDVI of forests with full under-canopy snow cover were investigated with snow on canopy and with snow-free canopy, the results show NDVI values were almost similar (deviated 0.10 on average) for the scene with snow-covered canopy and snow-free canopy, whereas the NDSI values deviated more clearly (0.31 on average) between these two cases. The relative difference of NDSI between the two conditions increased with increasing CC.

These results could be used in the validation of the transmissivity data by analyzing their dependency on forest characteristics. This is important in order to reduce the obscuring effect of forest canopy over snow cover and to improve the accuracy of snow mapping algorithms. Moreover, the AisaDUAL data enables the improvement of the forward modeling using full spectral range, which is valuable as the terrain physical properties affect various spectral regions. Furthermore, the obtained full spectrum dataset facilitates the adaptation and development of snow mapping methods for current and future optical satellite sensors with different optical channels.

## Acknowledgements

This work has been funded by the Airborne Imaging Spectroscopy Application and Research on Earth Sciences (AISARES) graduate school of the University of Helsinki. The work has been also supported by SPECIM (Spectral Imaging Ltd.) and CLIMWATER (Climate Change and Water Cycle: Effect to Water Resources and their Utilization in Finland) FICCA program project, funded by the Academy of Finland. Acquired AISA data was also supported by Bestcomp 97. Kft. and Meteo France. The work was also supported by the foundation Väisälän rahasto.

## References

Betts, A.K., Ball, J.H., 1997. Albedo over the boreal forest. Journal of Geophysical Research: Atmospheres 102, 28901–28909.
Boudewyn, P.A., Song, X., Magnussen, S., Gillis, M.D., 2007. Model-based, Volume-to-Biomass Conversion for Forested and Vegetated Land in. Natural Resources Canada, Canada, Victoria, BC.
Cao, Y.-g., Liu, C., 2006. Normalized difference snow index simulation for snow-cover mapping in forest by geosail model. Chinese Geographical Science 16, 171–175.
Hall, D.K., Foster, J.L., Verbyla, D.L., Klein, A.G., Benson, C.S., 1998. Assessment of snow-cover mapping accuracy in a variety of vegetation-cover densities in Central Alaska. Remote Sensing of Environment 66, 129–137.
Hall, D.K., Riggs, G.A., 2007. Accuracy assessment of the MODIS snow products. Hydrological Processes 21, 1534–1547.
Heiskanen, J., 2006. Tree cover and height estimation in the Fennoscandian tundra-taiga transition zone using multiangular MISR data. Remote Sensing of Environment 103, 97–114.
Klein, A.G., Hall, D.K., Riggs, G.A., 1998. Improving snow cover mapping in forests through the use of a canopy reflectance model. Hydrological Processes 12, 1723–1744.
Kuusinen, N., Kolari, P., Levula, J., Porcar-Castell, A., Stenberg, P., Berninger, F., 2012. Seasonal variation in boreal pine forest albedo and effects of canopy snow on forest reflectance. Agricultural and Forest Meteorology 164, 53–60.
Manninen, T., Stenberg, P., 2009. Simulation of the effect of snow covered forest floor on the total forest albedo. Agricultural and Forest Meteorology 149, 303–319.
METLA, 2010. Finnish Statistical Yearbook of Forestry. Finnish Forest Research Institute, Vammala, Finland.
Metsämäki, S., Mattila, O.-P., Pulliainen, J., Niemi, K., Luojus, K., Böttcher, K., 2012. An optical reflectance model-based method for fractional snow cover mapping applicable to continental scale. Remote Sensing of Environment 123, 508–521.
Metsämäki, S.J., Anttila, S.T., Markus, H.J., Vepsäläinen, J.M., 2005. A feasible method for fractional snow cover mapping in boreal zone based on a reflectance model. Remote Sensing of Environment 95, 77–95.
Muukkonen, P., Heiskanen, J., 2005. Estimating biomass for boreal forests using ASTER satellite data combined with standwise forest inventory data. Remote Sensing of Environment 99, 434–447.

Negi, H.S., Singh, S.K., Kulkarni, A.V., Semwal, B.S., 2010. Field-based spectral reflectance measurements of seasonal snow cover in the Indian Himalaya. International Journal of Remote Sensing 31, 2393–2417.
Ni, W., Woodcock, C.E., 2000. Effect of canopy structure and the presence of snow on the albedo of boreal conifer forests. Journal of Geophysical Research-Atmospheres 105, 11879–11888.
Niemi, K., Metsämäki, S., Pulliainen, J., Suokanerva, H., Böttcher, K., Leppäranta, M., Pellikka, P., 2012. The behaviour of mast-borne spectra in a snow-covered boreal forest. Remote Sensing of Environment 124, 551–563.
Painter, T.H., Dozier, J., Roberts, D.A., Davis, R.E., Green, R.O., 2003. Retrieval of subpixel snow-covered area and grain size from imaging spectrometer data. Remote Sensing of Environment 85, 64–77.
Rautiainen, M., Stenberg, P., Nilson, T., Kuusk, A., 2004. The effect of crown shape on the reflectance of coniferous stands. Remote Sensing of Environment 89, 41–52.
Riggs, G.A., Hall, D.K., Salomonson, V.V., 2006. MODIS Snow Product User Guide to Collection 5. http://modis-snow-ice.gsfc.nasa.gov/uploads/sug_c5.pdf
Salminen, M., Pulliainen, J., Metsämäki, S., Kontu, A., Suokanerva, H., 2009. The behaviour of snow and snow-free surface reflectance in boreal forests: implications to the performance of snow covered area monitoring. Remote Sensing of Environment 113, 907–918.
Salomonson, V.V., Appel, I., 2004. Estimating fractional snow cover from MODIS using the normalized difference snow index. Remote Sensing of Environment 89, 351–360.
Salomonson, V.V., Appel, I., 2006. Development of the Aqua MODIS NDSI fractional snow cover algorithm and validation results. IEEE Transactions on Geoscience and Remote Sensing 44, 1747–1756.
Schlerf, M., Atzberger, C., 2006. Inversion of a forest reflectance model to estimate structural canopy variables from hyperspectral remote sensing data. Remote Sensing of Environment 100, 281–294.
Sukuvaara, T., Kyrö, E., Suokanerva, H., Heikkinen, P., Suomalainen, J., 2007. Reflectance spectroradiometer measurement system in 30 meter mast for validating satellite images. In: Proceedings of the IEEE 2007 International Geoscience and Remote Sensing Symposium (IGARSS), Barcelona Spain, pp. 2885–2889.
Tomppo, E., Haakana, M., Katila, M., Peräsaari, J., 2008. Multi-source National Forest Inventory – Methods and Applications. Springer, New York.
Vikhamar, D., Solberg, R., 2003a. Snow-cover mapping in forests by constrained linear spectral unmixing of MODIS data. Remote Sensing of Environment 88, 309–323.
Vikhamar, D., Solberg, R., 2003b. Subpixel mapping of snow cover in forests by optical remote sensing. Remote Sensing of Environment 84, 69–82.
Wiscombe, W.J., Warren, S.G., 1980. A model for the spectral albedo of snow. I: pure snow. Journal of the Atmospheric Sciences 37, 2712–2733.
Xin, Q.C., Woodcock, C.E., Liu, J.C., Tan, B., Melloh, R.A., Davis, R.E., 2012. View angle effects on MODIS snow mapping in forests. Remote Sensing of Environment 118, 50–59.

IV

Remote Sensing of Environment 155 (2014) 303–311

Contents lists available at ScienceDirect

Remote Sensing of Environment

journal homepage: www.elsevier.com/locate/rse

# Semi-empirical modeling of the scene reflectance of snow-covered boreal forest: Validation with airborne spectrometer and LIDAR observations

Jouni Pulliainen [a], Miia Salminen [a,b,*], Kirsikka Heinilä [b,c], Juval Cohen [a], Henna-Reetta Hannula [a]

[a] Finnish Meteorological Institute, P.O. Box 503, FI-00101 Helsinki, Finland
[b] Finnish Environment Institute, P.O. Box 140, FI-00251 Helsinki, Finland
[c] Department of Geosciences and Geography, University of Helsinki, P.O. Box 64, FI-00014 Helsinki, Finland

ARTICLE INFO

*Article history:*
Received 25 April 2014
Received in revised form 1 September 2014
Accepted 4 September 2014
Available online 20 September 2014

*Keywords:*
Snow reflectance
Remote sensing of snow
Boreal forests
Space-borne observed scene reflectance
Seasonal snow

ABSTRACT

This work aims at the development and validation of a zeroth order radiative transfer (RT) approach to describe the visible band (555 nm) reflectance of conifer-dominated boreal forest for the needs of remote sensing of snow. This is accomplished by applying airborne and mast-borne spectrometer data sets together with high-resolution information on forest canopy characteristics. In case of aerial spectrometer observations, tree characteristics determined from airborne LIDAR observations are applied to quantify the effect of forest canopy on scene reflectance. The results indicate that a simple RT model is feasible to describe extinction and reflectance properties of both homogeneous and heterogeneous forest scenes (corresponding to varying scales of satellite data footprints and varying structures of forest canopies). The obtained results also justify the application of apparent forest canopy transmissivity to describe the influence of forest to reflectance, as is done e.g. in the *SCAmod* method for the continental scale monitoring of fractional snow cover (FSC) from optical satellite data. Additionally, the feasibility of the zeroth order RT approach is compared with the use of linear mixing model of scene reflectance. Results suggest that the non-linear RT approach describes the scene reflectance of a snow-covered boreal forest more realistically than the linear mixing model (in case when shadows on tree crowns and surface are not modeled separately, which is a relevant suggestion when considering the use of models for large scale snow mapping applications).



## 1. Introduction

The appearance of seasonal snow cover and its melting dominate the annual hydrological and climatic patterns in vast regions of boreal forests and tundra in the Northern Hemisphere. Spatial and temporal changes in global snow cover are strongly connected to changes in Earth surface albedo and permafrost, and they, in turn, can have large effects on global carbon cycling, radiation balance and climate conditions (Barnett, Adam, & Lettenmaier, 2005; Betts & Ball, 1997; Brown & Mote, 2009). The Northern Hemisphere snow cover extent has decreased since the mid-1900, in particular in spring, due to climate change (Brown & Mote, 2009; Choi, Robinson, & Kang, 2010; Robinson, Dewey, & Heim, 1993; Vaughan et al., 2013). Long-term time series of satellite data estimates on seasonal snow cover extent (and its albedo) are needed for constructing climate data records (CDR) essential for climate research whereas near-real-time observations are needed for hydrological forecasting and water resource management; see e.g. Hall and Riggs (2007) and Vaughan et al. (2013). Currently, the available optical satellite data records for the Northern Hemisphere snow monitoring reach back for several decades; nearly 50 years (Robinson et al., 1993; Vaughan et al., 2013). Various algorithms for different sensors are summarized and evaluated by Dietz, Kuenzer, Gessner, and Dech (2012), Frei et al. (2012) and Nolin (2010). The usefulness of satellite data based results is strongly dependent on the quality of the interpretation (Hall & Riggs, 2007; Rittger, Painter, & Dozier, 2013). Imprecise remote sensing retrievals used as input may cause uncertainties to climate change predictions and hydrological modeling results (Rittger et al., 2013; Robinson et al., 1993; Vaughan et al., 2013). Despite the several feasible approaches to snow mapping there are defects that decrease their performance, e.g. the presence of cloud cover (Dietz, Wohner, & Kuenzer, 2012; Hall & Riggs, 2007). Lower accuracy in snow mapping is also typical in the transitional snowmelt areas and especially in the case of forested regions (Dietz, Kuenzer, et al., 2012; Hall & Riggs, 2007; Rittger et al., 2013). The effect of forest cover to the satellite observations applied to snow monitoring is the topic of this study.

The binary (two classes: snow-covered or snow-free) methods, such as the National Oceanic and Atmospheric Administration (NOAA)

* Corresponding author at: Finnish Meteorological Institute, P.O. Box 503, FI-00101 Helsinki, Finland. Tel.: +358 50 4485476.
*E-mail address:* miia.salminen@fmi.fi (M. Salminen).

http://dx.doi.org/10.1016/j.rse.2014.09.004

multisensor snow mapping method or the National Space Administration (NASA) Global Moderate Resolution Imaging Spectroradiometer (MODIS) snow map production, are mostly effective in large scale snow detection yielding products with good spatial and temporal resolution (Hall, Riggs, Salomonson, DiGirolamo, & Bayr, 2002; Helfrich, McNamara, Ramsay, Baldwin, & Kasheta, 2007; Ramsay, 1998). However, there are extensive areas in the northern latitudes with seasonal snow (annual accumulation and ablation of snow), where relatively large satellite data pixels are not fully snow covered or snow-free. Moreover, the satellite footprint often contains both forested and non-forested proportions in regions with seasonal snow causing wide-ranging problems in snow mapping when optical methods are used (Hall & Riggs, 2007; Hall, Foster, Salomonson, Klein, & Chien, 2001, Hall, Foster, Verbyla, Klein, & Benson, 1998; Klein & Barnett, 2003; Klein, Hall, & Riggs, 1998; Nolin, 2004; Parajka & Blöschl, 2006). Metsämäki et al. (2012) showed that MODIS baseline algorithm for FSC mapping (Salomonson & Appel, 2004, 2006) tends to strongly underestimate snow cover, in particular under dense canopy. The trees prevent visibility to snow covered or snow-free forest floor, whereas the crown layer and the related shadows contribute to the satellite observations. Apart from that, the proportion of (snow covered or snow-free) forest floor visible to the satellite sensor varies according to the sensor view zenith angle (Liu et al., 2008; Nolin, 2004). The inevitably erroneous binary mapping results for the boreal forest zone impair the further exploitation of the snow mapping retrievals; this includes the obtained often artificially narrow continental scale snowline instead of the actual wider transitional patchy snow zone.

Further approaches have been developed to obtain the fraction of snow covered area i.e. the fractional snow cover (FSC) within a pixel (Painter, Dozier, Roberts, Davis, & Green, 2003, Painter et al., 2009; Salomonson & Appel, 2004, 2006; Vikhamar & Sohlberg, 2002, Vikhamar & Solberg, 2003). Nonetheless, majority of the developed linear unmixing methods assume that the tree crowns are opaque (Painter et al., 2003, 2009; Vikhamar & Sohlberg, 2002, Vikhamar & Solberg, 2003). Several studies indicate that the other FSC retrieval algorithms also have problems in discerning snow beneath forest canopies (Metsämäki, Vepsäläinen, Pulliainen, & Sucksdorff, 2002; Nolin, 2010; Rittger et al., 2013; Salomonson & Appel, 2004). To compensate the adverse influence of the forest canopy to snow algorithm performance, these effects have to be reliably modeled. Often, snow mapping algorithms are founded on an inverse solution of a forward model that describes the satellite observation. The success of the method over forested regions is dependent on how well the model represents the forest canopy effect. So far, there are three methods for the forward modeling of forest effects in optical remote sensing of snow (Table 1). In the case of boreal forests, trees are apparently not opaque (see e.g. Painter et al., 2003, 2009 and Schlerf & Atzberger, 2006). Therefore, algorithms that treat forest canopy as a partially transparent layer have been developed and also implemented for operational use. An example of such approach is the *SCAmod* method for the mapping of FSC (Metsämäki, Anttila, Huttunen, & Vepsäläinen, 2005). *SCAmod* has been applied to a hemispheric scale in ESA DUE-GlobSnow (Luojus et al., 2010; Metsämäki et al., 2012). In *SCAmod*, forested areas are considered as a single forest canopy layer (permeable to light), characterized by a canopy transmissivity and reflectance according to the zeroth order radiative transfer theory. The apparent forest transmissivity in *SCAmod* is related to the fraction of forest floor visible from above and the penetration of light through the canopy. Basically, more advanced methods can be constructed by combining radiative transfer for considering trees and physical optics to account for openings between the trees (Li, Strahler, & Woodcock, 1995; Liu et al., 2008; Rosema, Verhoef, Noorbergen, & Borgesius, 1992; Schlerf & Atzberger, 2006). This kind of models can be called as hybrid models.

Table 1 summarizes the three basic modeling approaches for forest canopy effects to scene reflectance; geometrical optics (GO) with opaque trees, radiative transfer (RT) and hybrid modeling. Additionally, some typical empirical snow retrieval algorithms are listed in Table 1. These empirical algorithms are often based on the employment of NDSI (with thresholding) (Hall et al., 2002; Salomonson & Appel, 2004, 2006). Apart from using NDSI, NDVI (derived during summer) can be useful in snow algorithms to estimate vegetation density when the goal is the reduction of disturbances due to forests (Nolin, 2004). Alternatively, static maps of land cover or forest properties could be considered as input to snow algorithms but they suffer from infrequent updating. Hall et al. (1998), Klein et al. (1998) and Nolin (2004) suggested the estimation of forest properties by using satellite observations on fully snow covered forests. These can be considered preliminary to the *SCAmod* that has operationally applied this approach. The *SCAmod*

**Table 1**
Methods for the forward modeling of forest effects in optical remote sensing of snow and related snow parameter retrieval algorithms. Selected examples of empirical snow mapping methods applied to forested regions are also included.

| Author | Forward (forest) model | Related (snow) inversion approach | Comments |
|---|---|---|---|
| | GO (geometrical optics) | | GO considers tree canopy opaque |
| Li & Strahler (1985)[a] | (Linear) spectral mixing | – | Forest stand model |
| Painter et al. (2003, 2009) | -II- | (Linear) spectral unmixing | MEMSCAG, MODSCAG (RT)[b] for FSC |
| Dozier, Green, Nolin, & Painter (2009) | -II- | (Linear) spectral unmixing | FSC, Albedo |
| Vikhamar and Sohlberg (2002), Vikhamar and Solberg (2003) | -II- | (Linear) spectral unmixing | *SnowFor* for snow-covered forest, *SnowFrac* for FSC |
| Salminen et al. (2009) | -II- | – | No shadowed/sunlit canopy components considered |
| | GO + RT (hybrid) | | Hybrid considers tree canopy non-opaque, otherwise as GO |
| Schlerf and Atzberger (2006) | INFORM | – | More sophisticated/complex to FLIM |
| Rosema et al. (1992) | FLIM | – | Simplified model similar to INFORM |
| Niemi et al. (2012) | – | – | Simplified model similar to FLIM and INFORM |
| Li et al. (1995) | GORT | – | Spectral mixing forward model[c] |
| Liu et al. (2008) | GORT | – | Viewable (forest) Gap Fraction (VGF) estimated[d] |
| | RT radiative transfer | | RT considers tree canopy non-opaque (turbid medium) |
| Metsämäki et al. (2005, 2012) | Zeroth order RT | Analytical inverse solution | *SCAmod* for FSC |
| Klein et al. (1998) | GeoSAIL | – | Thresholds for MODIS binary algorithm |
| Salomonson and Appel (2004, 2006) | – | Empirical | Linear regression algorithm (using NDSI) for FSC[e] |
| Hall et al. (2002) | – | -II- | Snow binary classification using NDSI and NDVI[f] |

[a] Later spectral mixing models are based on Li and Strahler (1985) that consider shadows and directly illuminated background.
[b] Reflectance of the opaque tree canopy can be calculated for MODSCAG using the RT model (Liu et al., 2008; Painter et al., 2009).
[c] For partially non-opaque forest canopy.
[d] Airborne LIDAR data-aided model parameterization.
[e] MODIS fractional method.
[f] MODIS binary method based on Klein et al. (1998).

algorithm is an example of an approach that attempts to compensate for the effects of forest cover based on the use of the zeroth order RT approach for the forward modeling of the influence of forest canopy (Metsämäki et al., 2005, 2012). In practice, this is carried out with the aid of forest canopy transmissivity estimated from the optical satellite data that represents full snow cover conditions. More complicated hybrid forward modeling approaches have been also investigated in case of boreal forests, e.g. by applying mast-borne spectrometer observations where shadowing effects and gaps between trees have been considered (Niemi et al., 2012). This Niemi et al. (2012) model can be considered as a simplification of the approach used by Schlerf and Atzberger (2006). However, hybrid approaches are complicated and thereby difficult to apply to the satellite data inversion. Thus, the topic of this paper is concerned whether a simple zeroth order RT approach – that considers forests of a satellite pixel as a single layer of turbid medium – is valid for boreal forests and whether this approach applies to different scales. This is also a central issue concerning the basis of the *SCAmod* algorithm.

Earlier investigations of forest canopy effects in boreal forest zone have indicated that the assumption of opaque canopy does not hold, as discussed above. This is also apparent from the earlier work with data from the Sodankylä site (the experimental region of this investigation), as the hybrid approach in Niemi et al. (2012) indicated better agreement with observations than the (simplified) GO approach (Salminen, Pulliainen, Metsämäki, Kontu, & Suokanerva, 2009). Thus, the hybrid approaches are arguably physically most accurate for boreal forests. However, physical approaches are difficult for inversion purposes due to the model complexity. Therefore, a simpler RT approach is thoroughly investigated and validated here. This is accomplished by quantifying the effect of forest canopy on scene reflectance using tree characteristics determined from airborne LIDAR observations of high spatial accuracy. These data are compared with the predictions by the zeroth order RT modeling. The investigations are carried out at the condition of full thick snow cover on ground and with snow free canopy, which enables the separation of the effect of trees from that of soil/understory vegetation. The RT model performance is further compared with simplified linear GO approach (analogous to Li & Strahler, 1985), in order to find out whether the RT approach with a single forest canopy layer (in a footprint) explains the observations better than the simplified GO approach. The investigated and compared forward modeling approaches are such that they are feasible for the continental scale satellite data inversion, i.e. to be used for snow cover monitoring if detailed information on tree distribution are not available for a pixel scale (instead only bulk characteristics such as mean tree height, stem volume, canopy cover or apparent forest canopy transmissivity were available).

The investigation is carried out in Sodankylä region, northern Finland, which is a typical example of a classical boreal forest site. The airborne imaging and mast-borne forest plot monitoring spectrometer data sets provide unique material to investigate (a) the spatial behavior of scene reflectance at boreal forests and (b) the temporal variability of forest scene reflectance due to varying illumination geometries. The results shown here focus on the wavelength channel of 555 nm as this region is essential for the remote sensing of snow, and since earlier investigations for the Sodankylä site (Heinilä et al., 2014) demonstrated the results for other wavelength regions. The investigation is also restricted to the case of near-nadir observations due to the applied experimental data sets.

## 2. Materials

### 2.1. Test area, land cover and forest information

The test area in Sodankylä, northern Finland, represents a typical conifer-dominated northern boreal forest. The dominant species in the Sodankylä region are Scots pine and Norway spruce. Pine-dominated forests comprise 92% of the total forest area of the southern part of Finnish Lapland (METLA, 2010). Birches including dwarf birches are typical at wetlands. Fig. 1 shows the scenery of typical pine forests of the area. The detailed forest canopy characteristics corresponding to the airborne reflectance data acquisition are summarized in Table 2. In addition to the region of airborne surveys, the multi-temporal mast-borne spectrometer experiments were carried out for a single forest plot coinciding one of the flight lines. This particular plot represents pine forest on mineral soil with a canopy cover $C = 40\%$. Fig. 2 shows the land cover map of the study area with flight lines of airborne spectrometer observations (see also Fig. 4 in Heinilä et al. (2014)).

The forests of the Sodankylä test area are also inventoried using Airborne Laser Scanning (ALS), i.e. LIDAR observations. Tree characteristics determined from these data were applied as main reference data on forest properties of the site. The ALS data, with a point density of at least one point per 2 $m^2$, were provided by the National Land Survey (NLS) of Finland. These observations were used to create canopy cover percentage ($C$) and tree height ($H$) maps for a spatial ground resolution of 10 m. The first step in processing the LIDAR data was to create vegetation height ($H$) grids with a pixel size of 1 m for the $C$ retrieval and 2 m for the $H$ retrieval. The vegetation height grids were generated first by subtracting the ground level height (Digital Terrain Model) from the top of the vegetation height (Digital Surface Model) and then, by converting the resulted point cloud to grids of 1 m and 2 m pixel size. The second step was to generate the $C$ map from the 1 m $H$ grid and the $H$ map from the 2 m $H$ grid. The $C$ was generated first by classifying 1 m by 1 m-sized pixels to either tree or no tree based on the height (the limit being 1.5 m) derived to ALS observation of that pixel. Then, the ratio between tree pixels and all pixels inside a grid cell of $10 \times 10$ m was calculated. The $H$ map was generated by 1) removing low vegetation and water; 2) applying a circle shaped dilation (maximum) filter with a radius of 2 pixels (equivalent to 4 m on the ground) and; 3) calculating the mean height inside a grid cell of $10 \times 10$ m. The quality control for the retrieved maps was performed (at the spatial resolution of 20 m) by evaluating the retrieved maps against corresponding National Forest Inventory (NFI) digital maps (Tomppo, Haakana, Katila, & Peräsaari, 2008). For example, the correlation coefficient between NFI- and ALS-based $C$ was found to be $r = 0.72$, RMSE $= 11.8\%$-units and BIAS $= 0.89\%$-units.

### 2.2. AISA airborne imaging spectrometer data

The employed airborne spectrometer data set was acquired on March 18, 2010 at cloud-free conditions; see Heinilä et al. (2014) for details. Trees were snow free during the airborne campaign, and the snow pack was dry (temperature −6 °C on average) and the air temperature was −4 °C at 10 UTC. Further, as described in Heinilä et al. (2014), the AISA imaging spectrometer data were radiometrically and

**Fig. 1.** Scots pine-dominated northern boreal forests at the Sodankylä site.

**Table 2**
Tree canopy characteristics of the Sodankylä test area at spatial scales of 10 m and 100 m (mineral soil and peat lands).

| Forest characteristic | Mean | Median | Min/Max | Standard deviation |
|---|---|---|---|---|
| *Canopy cover, C (%)* | | | | |
| 10 m | 24.4 | 22.5 | 0/100 | 20.3 |
| 100 m | 24.7 | 24.9 | 0/59 | 15.1 |
| *Stem volume, V ($m^3$/ha)* | | | | |
| 10 m | 33.7 | 28.0 | 0/179 | 31.1 |
| 100 m | 33.4 | 31.7 | 0/113 | 24.1 |
| *Tree height, H (m)* | | | | |
| 10 m | 7.5 | 7.3 | 0/24.2 | 5.1 |
| 100 m | 7.1 | 7.2 | 0/17.8 | 4.3 |

geometrically corrected and mean-filtered to pixel size of 10 m. This investigation is performed using this 10 m gridded data together with ALS-based forest parameter data processed to the same grid. Fig. 3 depicts an example of the gridded airborne AISA spectrometer data at the channel of 545–565 nm used for analyses here (corresponding to MODIS band 4).

Since the field of View (FOV) of AISA observations is 17°, the analyses here are limited to near-nadir angles of observation (from 0° to 8.5° off nadir). As indicated in Fig. 2, the flight lines have varying orientations. Additionally, they were measured during an interval of one hour. Thus, the Sun zenith angle is close to 70° for all observations and the azimuthal angle difference between the direction of illumination and measurements has a relatively high range from 45° to 135°. As a consequence, both backscattering and forward scattering geometries are included in the airborne spectrometer data set.

### 2.3. Mast-borne and field spectrometry

The applied data sets include mast-borne ASD spectrometer observations from the day of airborne data acquisition (March 18, 2010), accompanied with observations from 12 days during the spring–winter of 2013 (also representing full snow cover conditions). All observations represent the same forest plot with the same sensor azimuth and look angle characteristics (measurement angle 11° off nadir); see Niemi et al. (2012) and Salminen et al. (2009) for details. These data are used for the analysis of the variability of forest scene reflectance due to varying illumination and viewing conditions. Since several mast-borne measurements were conducted for each day of observation, the data set includes both forward and backscattering geometries (corresponding to airborne data set). The Sun zenith angle varies from 59.0° to 77.2°, and the Sun azimuth and sensor view angle difference is from 2.7° to 136.5°. All data represents dry snow conditions with thick snow pack (tree canopy snow free).

In addition to mast-borne observations, nadir view-angle field spectrometry measurement of natural snow packs using a similar spectrometer system was applied to incorporate information on average level of dry snow reflectance (Salminen et al., 2009).

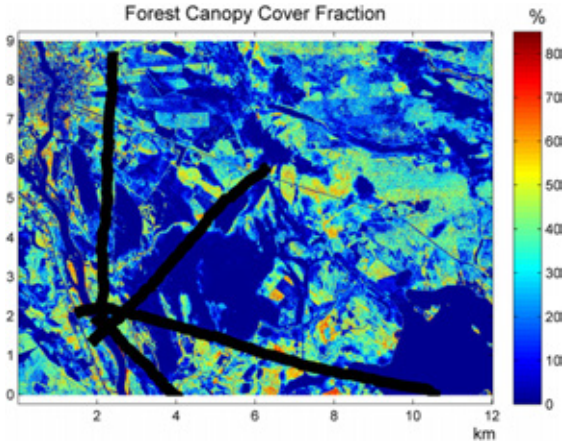


**Fig. 2.** AISA data from 18 March 2010 comprise four flight lines (depicted in black color). The underlying forest canopy cover (*C*) fraction is derived using LIDAR data.

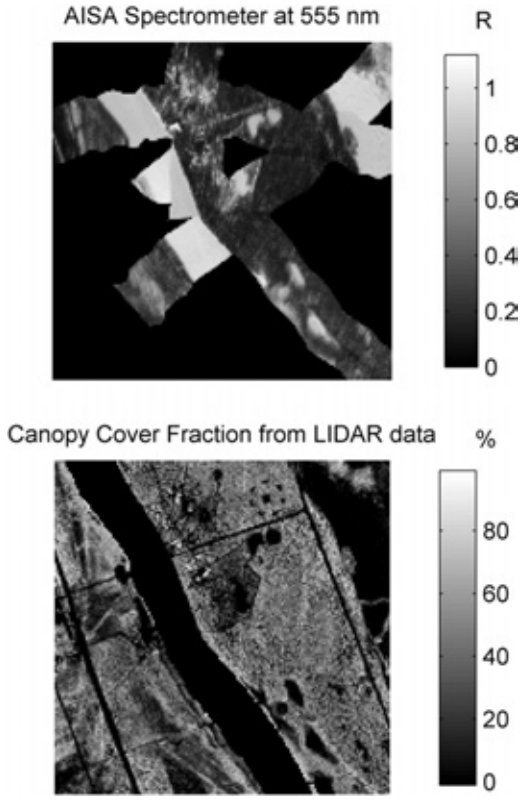


**Fig. 3.** A close-up of 18 March 2010 AISA data (above) and the corresponding canopy cover fraction obtained by using LIDAR data.

## 3. Methods

The scene reflectance of a (partially) snow-covered boreal forest at the wavelength λ can be modeled by an approach incorporating the reflectance contributions of snow-covered ground $\rho_{\lambda,snow}$ and snow-free ground $\rho_{\lambda,ground}$, and by considering the forest canopy as a partially transparent reflecting layer. When the model is based on the zeroth order solution of the radiative transfer equation (RT), the parameters that define the effects of the tree layer are the reflectance of an opaque forest canopy $\rho_{\lambda,forest}$ and the two-way forest canopy transmissivity $t^2$ (Metsämäki et al., 2005, 2012; Pulliainen, Heiska, Hyyppä, & Hallikainen, 1994; Salminen et al., 2009). Additionally, analogous approaches for the canopy transmissivity, or transmittance, with a different notation have been used e.g. by Schlerf and Atzberger (2006). Based on this approach, if the fraction of the terrain covered by snow

is denoted by *FSC* (ranging from 0 to 1), the model for the observed reflectance $R_{mod}$ at the wavelength λ is obtained by

$$R_{\lambda,mod}(FSC) = \left(1-t_\lambda^2\right)\rho_{\lambda,forest} + t_\lambda^2\left[FSC\,\rho_{\lambda,snow} + (1-FSC)\,\rho_{\lambda,ground}\right]. \quad (1)$$

If the scene has a full snow cover on ground $FSC = 1$, we get

$$R_{\lambda,mod} = \left(1-t_\lambda^2\right)\rho_{\lambda,forest} + t_\lambda^2\,\rho_{\lambda,snow}. \quad (2)$$

The two-way forest canopy transmissivity $t^2$ in Eqs. (1) and (2) is related to the extinction properties of the vegetation canopy, which is discussed next.

### 3.1. Modeling of boreal forest scene reflectance based on the zeroth order solution of the radiative transfer (RT) equation

The zeroth order solution to RT equation excludes multiple scattering. Thus, analogous to Pulliainen et al. (1994), an analytical formula can be written to consider the effect of forest canopy to the reflected radiance (now on, ignoring λ for simplicity):

$$\frac{L(\theta_s)}{E_0(\theta_i)}\pi = \int_0^H \left[\pi\gamma_s(\theta_i,\theta_s,h)\exp\left(\int_0^{H-h}\frac{-\kappa_e(\theta_i,\theta_s,h')}{\cos(\theta_i)}dh'\right)\exp\left(\int_0^{H-h}\frac{-\kappa_e(\theta_i,\theta_s,h')}{\cos(\theta_s)}dh'\right)\right]dh \quad (3)$$

where $L$ is the reflected radiance [W sr$^{-1}$ m$^{-2}$], $E_0$ is the incoming irradiance above the canopy [W m$^{-2}$], $\pi\gamma_s$ is the reflectance of an infinitesimal volume unit and $\kappa_e$ is the canopy extinction coefficient [1/m]. The concept of Eq. (3) illustrated in Fig. 4 shows the geometrical consideration of the approach: $H$ is the total height of the forest canopy, $h$ is the height within the canopy, $\theta_s$ is the angle of observation (scattering/reflection angle) and $\theta_i$ is the angle of incident radiation. According to Eq. (3) the total two-way transmissivity of the forest canopy along the directional path of light propagation is

$$t^2(\theta_i,\theta_s) = \exp\left(\int_0^H\frac{-\kappa_e(\theta_i,\theta_s,h)}{\cos(\theta_i)}dh\right)\exp\left(\int_0^H\frac{-\kappa_e(\theta_i,\theta_s,h)}{\cos(\theta_s)}dh\right). \quad (4)$$

If $\kappa_e$ and $\pi\gamma_s$ are assumed to be constants as function of illumination and reflection angles and the height $h$ within the forest canopy (Eq. 3) is simplified to

$$\frac{L(\theta_s)}{E_0(\theta_i)}\pi = \frac{\pi\gamma_s}{\kappa_e\left(\cos^{-1}(\theta_i)+\cos^{-1}(\theta_s)\right)}\left[1-t^2(\theta_i,\theta_s)\right] = \rho_{forest}\left[1-t^2(\theta_i,\theta_s)\right], \quad (5)$$

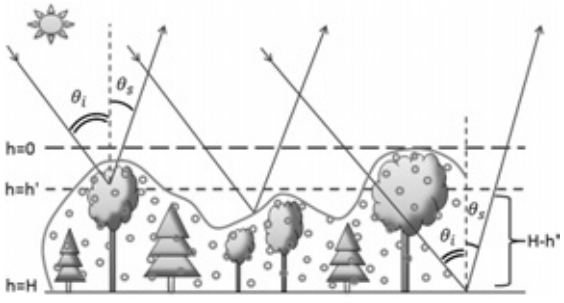


**Fig. 4.** Geometrical consideration of the bidirectional reflectance of a forest scene. $\theta_i$ is the incidence angle of incoming irradiance and $\theta_s$ is the angle of observation (and hence also the scattering angle under investigation in the forest canopy). The applied RT approach considers a forested scene (pixel) as a single turbid medium layer characterized by bulk volume scattering and extinction properties $\pi\gamma_s$ and $\kappa_e$; see Eq. (3).

thus, Eq. (5) provides the first term of Eq. (1), and the second term of Eq. (1) is simply the reflection from the snow-covered ground attenuated by the two-way forest canopy transmissivity. In the case of the two-way transmissivity $t^2$ the assumption of a constant extinction coefficient leads from Eq. (4) to:

$$t^2(\theta_i,\theta_s) = \exp\left(-\kappa_e H\left(\frac{1}{\cos(\theta_i)}+\frac{1}{\cos(\theta_s)}\right)\right). \quad (6)$$

To summarize, if scene reflectance is modeled for observation angles close to nadir $\theta_s \approx 0$, then $\cos^{-1}(\theta_i)+\cos^{-1}(\theta_s) \approx \cos^{-1}(\theta_i)+1$. Then by denoting $\cos^{-1}(\theta_i)+1 = 2g'(\theta_i)$, Eq. (2) can be rewritten as

$$R_{mod} = (1-\exp(-2\kappa_e g'(\theta_i)H))\rho_{forest} + \exp(-2\kappa_e g'(\theta_i)H)\rho_{snow}. \quad (7)$$

### 3.2. Parametrization and validation of the model using airborne spectrometer and LIDAR data

In Eq. (7), the semi-empirical scene reflectance model, derived from the zeroth order solution of RT equation, is parameterized as a function of tree height $H$ [m]. The model can be as well given as a function of canopy cover ($C$ in %-units) or forest stem volume ($V$ in m$^3$/ha) which is related to the product $V \sim C \times H$ (Heinilä et al., 2014). As discussed in Section 2.2 all canopy characteristics are derived from LIDAR observations. In the case of $V$, the product $C \times H$ is calibrated to volume estimate using a regression between the LIDAR data-derived product and NFI forest stem volume map (available with a coarser spatial resolution of 20 m).

Thus, we can write by denoting $\kappa_e = \kappa_{e,H}$, $\kappa_e = \kappa_{e,C}$ or $\kappa_e = \kappa_{e,V}$ when the formula is derived for tree height ($H$), canopy cover ($C$) or stem volume ($V$), respectively:

$$R_{mod,H} = \left(1-\exp\left(-2\kappa_{e,H}g'(\theta_i)H\right)\right)\rho_{forest} + \exp\left(-2\kappa_{e,H}g'(\theta_i)H\right)\rho_{snow} \quad (8a)$$

$$R_{mod,C} = \left(1-\exp\left(-2\kappa_{e,C}g'(\theta_i)C\right)\right)\rho_{forest} + \exp\left(-2\kappa_{e,C}g'(\theta_i)C\right)\rho_{snow} \quad 8b$$

$$R_{mod,V} = \left(1-\exp\left(-2\kappa_{e,V}g'(\theta_i)V\right)\right)\rho_{forest} + \exp\left(-2\kappa_{e,V}g'(\theta_i)V\right)\rho_{snow}. \quad 8c$$

Parameters $\kappa_e$, $\rho_{snow}$ and $\rho_{forest}$ in Eqs. (8a)–(8c) can be estimated for certain conditions by fitting the model into an observation data set representing certain specific measurement conditions. Here, the observational data consist of AISA measurements carried out at the Sodankylä site (see Section 2.3). Thus, the assumption is that the three parameters can be treated with their mean effective values over the image scene. The model fitting is performed by the least squares method by searching the global minimum for the cost function $J$ with respect to $\kappa_e$, $\rho_{snow}$ and $\rho_{forest}$:

$$J\left(\kappa_e,\rho_{forest},\rho_{snow}\right) = \sum_{i=1}^{N}\left(\left(R_{mod,i}(\kappa_e,\rho_{forest},\rho_{snow},\begin{Bmatrix}H_i\\C_i\\V_i\end{Bmatrix}\right) - R_{obs,i}\right)^2 \quad (9)$$

where sub-index $i$ refers to an observation case with specific forest characteristics $H_i$, $C_i$ and $V_i$. The fitting is carried out separately for $H$, $C$ and $V$. That is, models by Eqs. (8a), (8b) and (8c) are fitted separately to observational data by estimating three scalars for each case.

As an outcome of the fitting procedure, the modeled response of scene reflectance to the two forest canopy ($\kappa_e$, $\rho_{forest}$) and one surface characteristic ($\rho_{snow}$) is obtained. As shown by Eqs. (8a)–(8c) this response is exponential. In order to assess the validity of the model fit, it is compared with the statistical performances of a linear fit (two parameters in fitting) and of a second-degree polynomial fit (three parameters

in the fitting as in the case of Eq. (9)). In practice, the correlation coefficient between the model prediction of reflectance and observed reflectance is determined for different approaches.

Especially, the comparison of the applied radiative transfer approach with linear modeling is essential, as the linear approach can be considered as a simpler characterization of the physical problem. In that case we can consider that the reflectance is an areally weighted sum of reflectance contributions from an opaque forest canopy and from surface, i.e. from openings between the trees:

$$\begin{aligned} R_{mod} &= C\rho_{forest} + (1-C)\rho_{snow} \\ &= C\left(\rho_{forest}-\rho_{snow}\right) + \rho_{snow} \\ &= a_1 C + a_0. \end{aligned} \tag{10}$$

Note that Eq. (10) is actually a simplification of the geometric optics approach introduced by Li and Strahler (1985). Thus, the comparison of Eqs. (8a)–(8c) and Eq. (10) with the experimental Sodankylä data enables the analysis whether the radiative transfer approach (Eq. 8) or geometric optics (Eq. 10) applies better to describe the reflectance observations as a function of quantitative forest canopy characteristics.

### 3.3. Assessment of spatial and viewing/illumination geometry related characteristics of boreal forest scene reflectance

The applied airborne imaging spectrometer and LIDAR data set also enables the investigation the effect of spatial scale to the modeling of observations. Due to image swath and LIDAR data processing limitations the influence of scale is here investigated from 10 m to 100 m. That is, the model parameters are estimated separately for data processed to the grid sizes ranging from $10 \times 10$ m$^2$ to $100 \times 100$ m$^2$. This is relevant to the point of view of satellite data retrieval approaches. For example *SCAmod* applies reflectance modeling in the scale of the employed satellite data (Metsämäki et al., 2012).

As described in Section 3.2, the analysis of aerial spectrometer data facilitates the determination of the spatial variability of scene reflectance as a function of forest canopy characteristics. Another important issue is the temporal variability of forest canopy reflectance, which is, ignoring bio-physical issues, sensitive to imaging geometry (Sun and instrument view angles). Since the mast-borne spectrometer data from a forest plot (described in Section 2.4) represents variable bidirectional measurement configurations, these data can be used to derive information on the temporal variability of forest canopy effects to observed scene reflectance. The basis of this consideration is the error propagation analysis of scene reflectance. We can write for the total variance of observed reflectance as a sum of contributions due to canopy extinction, snow reflectance and reflectance of an opaque forest canopy:

$$\mathrm{var}(R) = \mathrm{var}(R)_{|\kappa_e} + \mathrm{var}(R)_{|\rho_{snow}} + \mathrm{var}(R)_{|\rho_{forest}}. \tag{11}$$

When the variance contribution resulting from the temporal variability of forest canopy extinction coefficient ($\mathrm{var}(R)_{|\kappa_e}$ in Eq. (11)) is approximated through the Taylor-series expansion of Eq. (8b) we can rewrite Eq. (11) as

$$\begin{aligned} \mathrm{var}(R) &\approx \left(\frac{\partial R}{\partial \kappa_e}\right)^2 \mathrm{var}(\kappa_e) + \left(\frac{\partial R}{\partial \rho_{snow}}\right)^2 \mathrm{var}(\rho_{snow}) + \left(\frac{\partial R}{\partial \rho_{forest}}\right)^2 \mathrm{var}\left(\rho_{forest}\right) \\ &= \left[2g'C\left(\rho_{forest}-\rho_{snow}\right)\exp(-2\kappa_e g'C)\right]^2 \mathrm{var}(\kappa_e) \\ &\quad + \left[\exp(-2\kappa_e g'C)\right]^2 \mathrm{var}(\rho_{snow}) \\ &\quad + \left[1-\exp(-2\kappa_e g'C)\right]^2 \mathrm{var}\left(\rho_{forest}\right). \end{aligned} \tag{12}$$

Thus, the estimate on $\mathrm{var}(\kappa_e)$, the variance of forest canopy extinction coefficient, can be obtained by

$$\mathrm{var}(\kappa_e) = \frac{\mathrm{var}(R) - \left[\exp(-2\kappa_e g'C)\right]^2 \mathrm{var}(\rho_{snow}) - \left[1-\exp(-2\kappa_e g'C)\right]^2 \mathrm{var}\left(\rho_{forest}\right)}{\left[2g'C\left(\rho_{forest}-\rho_{snow}\right)\exp(-2\kappa_e g'C)\right]^2} \tag{13}$$

where the $\mathrm{var}(R)$ is directly determined from the multi-temporal observations of forested terrain reflectance of the single forest plot; see Niemi et al. (2012) and Heinilä et al. (2014). Note that the term $\exp(-2\kappa_e g'C)$ can be derived from the AISA data analysis of this investigation, whereas the terms $\rho_{forest}$, $\mathrm{var}(\rho_{forest})$, $\rho_{snow}$ and $\mathrm{var}(\rho_{snow})$ can be derived from the results of earlier investigations (Niemi et al., 2012; Salminen et al., 2009).

When Eq. (13) is used to estimate the variance of the two-way forest canopy transmissivity, we can write:

$$\mathrm{var}\left(t^2\right) \approx \left[-2Cg' \exp(-2\kappa_e g'C)\right]^2 \mathrm{var}(\kappa_e). \tag{14}$$

## 4. Results and discussion

Fig. 5 depicts the fit of the Eq. (8b) to AISA observations from 18 of March 2011. The fitting according to Eq. (9) is performed to median reflectances observed for nine canopy cover ($C$) classes (for eight classes when open areas are ignored). The class-stratified data are applied for the fitting procedure, since the random fluctuations in the observations at the processing resolution of 10 m are high. This causes instability to the used non-linear optimization procedure (search result dependent on the starting value), which is avoided by the use of averaged/median values. When the fitting is performed for the class-wise median values the effect of occasional very high reflectance values are better removed

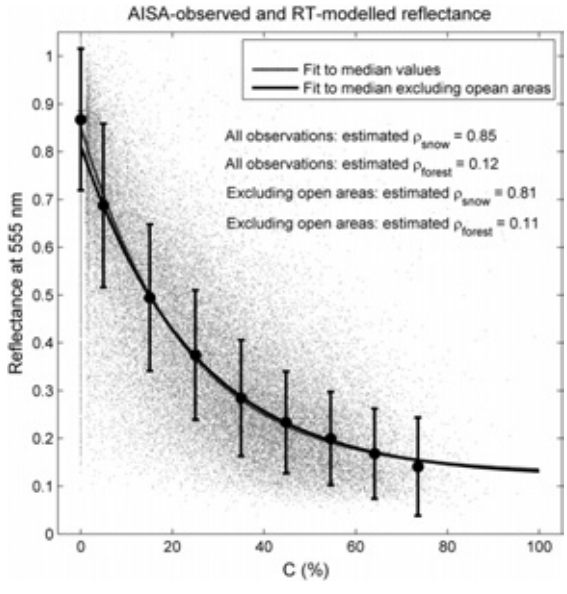


**Fig. 5.** Scene reflectance at 555 nm as a function of canopy cover ($C$). The scene reflectance model (Eq. 8b) is fitted to AISA observations of the Sodankylä site by optimizing the values of $\rho_{\lambda,forest}$, $\kappa_{e,forest}$ and $\rho_{\lambda,snow}$. Spatial resolution is 10 m. The fitting was done for $C$ class stratified median values. Bars indicate ±standard deviation from the $C$ class-wise mean values.

than when using mean values. Note that the actual individual data points are also shown in Fig. 5.

The effect of spatial scale to modeling is shown in Fig. 6. The dotted line shows the model prediction (Eq. 8b) when fitting parameters ($\rho_{forest}$, $\kappa_{e,forest}$ and $\rho_{snow}$) are estimated from data sets processed to a resolution of 10 m corresponding to Fig. 5. Solid line depicts the model prediction when the same parameters are estimated from data averaged to a resolution of 100 m with a two-dimensional box convolution function (10 × 10 window). The individual data points in 100 m resolution are presented by dots, and the standard deviations from class-wise averages are shown by solid bars, respectively. According to the results, model parameters slightly change as a function of spatial resolution, as the canopy cover ($C$) averaged to a scale of 100 m does not include values exceeding 59% (refer to Table 2) unlike in the scale of 10 m. However, the radiative transfer model according to Eq. (8b) well describes the behavior of reflectance. This implies that the suggested modeling approach is a valid methodology to describe the influence of forests for instruments with varying spatial resolution characteristics.

The comparison of radiative transfer (RT) approach Eq. (8b) with a linear mixing model (Eq. 10) indicates a higher validity for the RT than for the linear mixing model. The correlation coefficient between the reflectance predicted by Eq. (8b) is as high as $R^2 = 0.91$ for all data points processed to 100 m spatial resolution, whereas it is $R^2 = 0.87$ for the linear mixing formula; see Table 3 (the corresponding behavior of reflectance as a function of canopy cover is shown in Fig. 6). Table 3 presents the overall model fittings with respect to canopy cover ($C$), stem volume ($V$) and tree height ($H$), as well as the comparison of RT modeling performance with respect to linear mixing and polynomial fitting indicating the better performance of the RT approach, even though Eq. (10) applies two fitting parameters, whereas the radiative transfer model requires three parameters estimated by Eq. (9). Nevertheless, the results indicate that the behavior of reflectance is clearly non-linear and obeys well with Eq. (8b). If a second degree polynomial is fitted to data (three fitting parameters) we obtain about the same correlation coefficient ($R^2 = 0.918$) than with the exponential

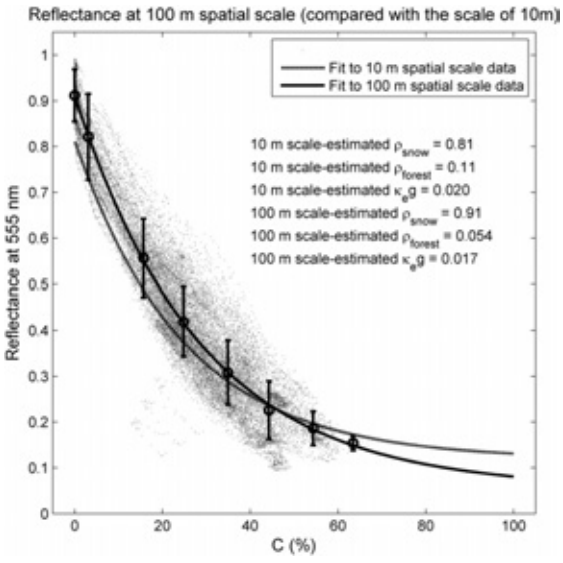


**Fig. 6.** Scene reflectance at 555 nm as a function of canopy cover for data averaged to spatial resolution of 100 m. The comparison for the model fitting at the scale of 10 m is also shown (dotted curve). Individual data points at the scale of 100 m are depicted by gray dots, whereas the error bars show the standard deviations from class stratified mean values. The case $C = 0\%$ is excluded in the fitting procedure (Eq. 9).

radiative transfer approach; see Table 3. However, the use of second degree polynomial lacks any physical significance, whereas both the RT approach and linear mixing model are based on physical assumptions.

The effect of pixel (footprint) homogeneity to observed scene reflectance is investigated in Fig. 7. In practice, the AISA data is processed (block averaged) to a spatial grid of 100 m. Thereafter, each grid cell is assigned to represent either a homogenous or a heterogeneous target with respect to forest canopy cover ($C$) by analyzing the canopy cover at four sub-grid cells of each footprint of 100 m × 100 m. A footprint is considered as heterogeneous, if any of the four (50 m × 50 m-sized) sub-grid cells shows a value $C_{sub} < 0.5\ C_{ave}$ or $C_{sub} > 2 \cdot C_{ave}$, where $C_{ave}$ stands for the canopy cover of the whole 100 m × 100 m pixel. Additionally, grid cell is considered as homogeneous, if all four sub-grid cells show a value $C_{sub} < 1\%$.

Both the data and model fittings by Eq. (9) in Fig. 7 indicate that the heterogeneity of forest cover within the pixel has an effect to the scene reflectance as a function of canopy cover fraction $C$. However, the results also show that the modeling approach of Eqs. (8a)–(8c) is appropriate even for forested targets heterogeneous at the scale of the applied instrument. This is also indicated by the two fit curves of Fig. 7. Additionally, Fig. 6 suggests that, if the mixture of homogeneous and heterogeneous pixels is corresponding to that of the Sodankylä site, the deviation of individual observations from the general fit curve is rather small.

As demonstrated by Fig. 7, the variability of forest canopy effects to scene reflectance is influenced by the structural heterogeneity of forest cover. On the other hand, results of earlier investigations, e.g. Niemi et al. (2012), suggest that variability of forest effects is related to the variability of bidirectional illumination conditions (which is the case with the applied AISA data). This is further shown in Fig. 8 that depicts the overall variability of forest scene reflectance due to varying illumination conditions (deep snow pack and snow-free pine canopy). The mast-borne spectrometer observations shown in Fig. 8 are obtained for 12 days during the year 2013 from 26 March to 12 April and for a single day in 2010 (18 March corresponding to airborne AISA data acquisition). Fig. 8 indicates the strong effect of bidirectional imaging conditions. For forward scattering cases the reflectance at 555 nm drops with increasing Sun zenith angle to values as low as about 0.07. For the backscatter, the behavior of reflectance is quite opposite; the reflectance shows high levels up to 0.17, and may even increase with the increasing Sun zenith angle. However, the standard deviation of reflectance corresponds well with the reflectance variability of mast-borne spectrometer observations carried out simultaneously with airborne AISA-imaging (Niemi et al., 2012).

Fig. 9 depicts the prediction of the variability of the two-way forest canopy transmissivity $t^2$ as a function of canopy cover ($C$) based on Eq. (14). The results of Fig. 9 are determined using the value $\mathrm{var}(\kappa_e) = 0.00083\%^{-1}$ for the variance of forest canopy extinction coefficient. This value is estimated by Eq. (13) using the following parameter values, mainly based on mast-borne spectrometer measurements carried out simultaneously with AISA imaging (green data points in Fig. 8):

- $\kappa_{e,forest} g'(\theta) = 0.017\%^{-1}$ (from Table 3)
- $C = 40\%$ (canopy cover fraction in the forest plot observed by the mast-borne spectrometer (Niemi et al., 2012))
- $\rho_{forest} = 0.089$ (Niemi et al., 2012)
- $\mathrm{var}(\rho_{forest}) = (0.01)^2$ (Niemi et al., 2012)
- $\rho_{snow} = 0.98$ (Salminen et al., 2009)
- $\mathrm{var}(\rho_{snow}) \approx 0$ (observations from a single day applied)
- $\mathrm{var}(R) = (0.03)^2$ (observed variance for the single day measurements according to Niemi et al. (2012)).

The results of Fig. 9 suggest that the relative standard deviation of the variability of forest canopy transmissivity is 13% (due to the variability of BRDF configuration). One should note that this variability is only a valid estimate for cases of near-nadir observations as the sensor look angle in mast-borne experiments is fixed to 11° off nadir. It should be

**Table 3**
Fitting parameters of the RT model for reflectance at 555 nm and comparison of its performance with that of the linear mixing model and second degree polynomial fitting curve. The spatial scale of modeling is 100 m.

| Forest parameter | RT model fitting parameters | | | $R^2$ (coefficient of determination) for different modeling approaches | | |
|---|---|---|---|---|---|---|
| | $\rho_{\lambda,forest}$, | $\kappa_{e,forest}g'(\theta)$[a] | $\rho_{\lambda,snow}$ | Radiative transfer (RT) | Linear mixing[b] | 2nd deg. polynomial[a] |
| Canopy cover, $C$ (%) | 0.054 | 0.017 (1/%) | 0.91 | 0.920[c] | 0.865 | 919 |
| Stem volume, $V$ ($m^3$/ha) | 0.112 | 0.015 (ha/$m^3$) | 0.86 | 0.878[d] | 0.758 | 0.864 |
| Tree height, $H$ (m) | 0.116 | 0.069 (1/m) | 0.96 | 0.841[e] | 0.750 | 0.843 |

[a] Note that $g'(\theta) \approx 1.96$.
[b] All individual data points in algorithm training and testing.
[c] Seven classes (excluding $C = 0\%$) in algorithm training, all individual points in testing.
[d] Eleven classes (excluding $V = 0$ $m^3$/ha) in algorithm training, all individual points in testing.
[e] Eight classes (excluding $H = 0$ m) in algorithm training, all individual points in testing.

noted that Fig. 9 considers the variability of forest scene reflectance for a single day, March 18, 2010, corresponding to airborne data acquisition (see green symbols in Fig. 8). In that case the range in azimuthal difference between the sensor and the Sun angles is from 31° to 107° (i.e. both forward and backscattering geometries are included as source of transmissivity variability in Fig. 9, but sensor look angle is constant).

## 5. Summary and conclusions

This investigation shows that the approach using the zeroth order solution of the radiative transfer (RT) equation to describe forest effects to scene reflectance is valid for typical boreal forests. The results also indicate that this applies both to homogeneous or heterogeneous forest scenes (satellite/remote sensing data footprints). However, the parameterization of the model changes according to heterogeneity of the sensor's footprint. The obtained results justify the appliance of apparent forest canopy transmissivity to describe the influence of forest to reflectance, as done in the *SCAmod* method for the continental scale FSC monitoring. The analyses carried out here are limited to the wavelength band of 545–565 nm as this range (MODIS band 4) is operationally feasible to snow monitoring purposes. Apart from that, Heinilä et al. (2014) presented results using several wavelengths for comparison.

The feasibility of the zeroth order RT approach is also compared with the use of linear mixing model of scene reflectance. This analysis shows that the non-linear RT approach describes the scene reflectance of a snow-covered boreal forest more realistically than the linear mixing model (in case when shadows on tree crowns and surface are not modeled separately, which is a relevant suggestion when considering the use of models for large scale snow mapping applications). The results also suggest that the consideration of forest canopy by estimating the apparent canopy transmissivity from the applied satellite data, as performed in *SCAmod* approach, is in practice a more feasible approach than the use of modeled value of forest canopy extinction coefficient. That is the case, since the modeled value of extinction coefficient is slightly dependent on scale, as indicated in Figs. 6 and 7. When the apparent canopy transmissivity is estimated from the employed satellite data, this effect is eliminated.

The obtained results also demonstrate the variability of scene reflectance due to varying illumination and bidirectional measurement geometries; see Fig. 8 for mast-borne observations. Also in the case of the applied airborne data set, the variability of reflectance around the curve of model prediction is in the same order, and apparently predominantly caused by these factors; see Figs. 6 and 7. However, the results show that the overall variability is quite small. This suggests that simple

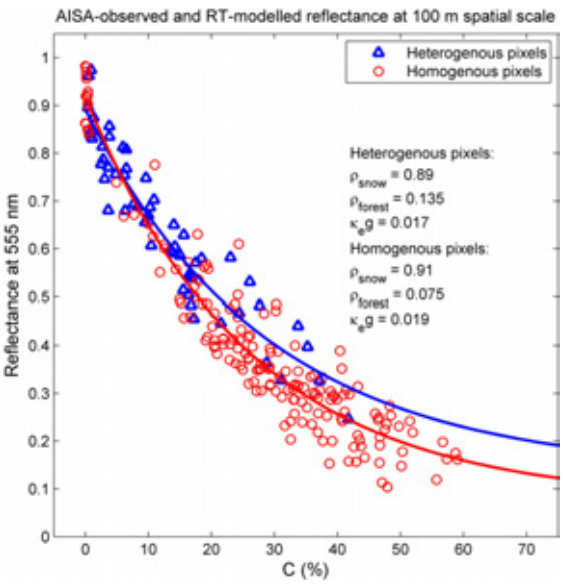


**Fig. 7.** Scene reflectance at 555 nm at the scale of 100 m separately for pixels homogenous or heterogeneous with respect to forest cover. Red and blue curves show the model fittings according to Eq. (9).

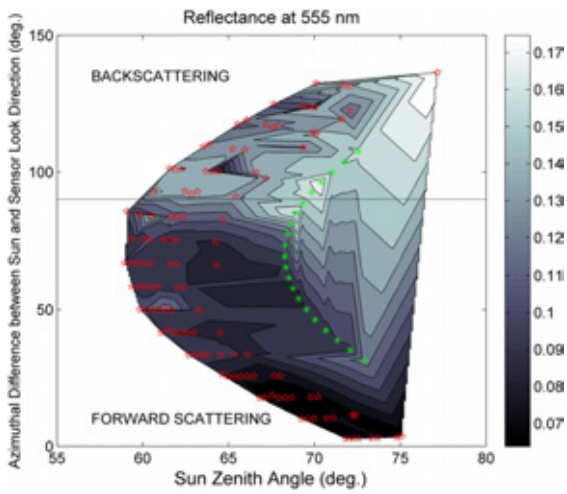


**Fig. 8.** Bidirectional reflectance of the forest plot of mast-borne spectrometer observations. Red and green symbols show the geometry of actual measurements representing full snow cover condition. The behavior of reflectance (contour plot) is interpolated from measurements at the locations of all the symbols (red pentagrams and green asterisks). Red pentagrams depict observations conducted for 12 days at different hours of day during the year 2013. Measurements from 18 March 2010 coinciding airborne data acquisition are shown by green asterisks.

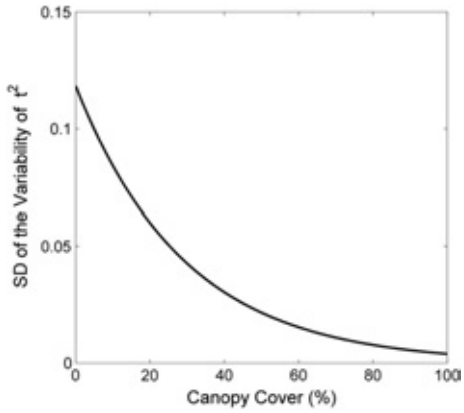


**Fig. 9.** Estimated variability of forest canopy transmissivity at 555 nm due to variability of illumination conditions for near-nadir observations.

RT approach is feasible to describe bulk extinction and reflectance (scattering) properties of forests on average.

## Acknowledgments

The work has been supported by the national CLEEN (Cluster for Energy and Environment) MMEA (Measurement, Monitoring and Environmental Assessment) research program, funded by TEKES, and CLIMWATER (Climate Change and Water Cycle: Effect to Water Resources and their utilization in Finland) FICCA program project, funded by the Academy of Finland (Grant number 140915). This work has been also supported by the Airborne Imaging Spectroscopy Application and Research on Earth Sciences (AISARES) graduate school of the University of Helsinki.

## References

Barnett, T. P., Adam, J. C., & Lettenmaier, D. P. (2005). Potential impacts of a warming climate on water availability in snow dominated regions. *Nature, 438*, 303–309.
Betts, A. K., & Ball, J. H. (1997). Albedo over the boreal forest. *Journal of Geophysical Research, 102*, 901–909.
Brown, R. D., & Mote, P. W. (2009). The response of northern hemisphere snow cover to a changing climate. *Journal of Climate, 22*, 2124–2145.
Choi, G., Robinson, D. A., & Kang, S. (2010). Changing northern hemisphere snow seasons. *Journal of Climate, 23*, 5305–5310.
Dietz, J. A., Kuenzer, C., Gessner, U., & Dech, S. (2012). Remote sensing of snow — A review of available methods. *International Journal of Remote Sensing, 33*, 4094–4134.
Dietz, J., Wohner, C., & Kuenzer, C. (2012). European snow cover characteristics between 2000 and 2011 derived from improved MODIS daily snow cover products. *Remote Sensing, 4*, 2434–2454.
Dozier, J., Green, R., Nolin, A., & Painter, T. (2009). Interpretation of snow properties from imaging spectrometry. *Remote Sensing of Environment, 113*, S25–S37.
Frei, A., Tedesco, M., Lee, S., Foster, J., Hall, D. K., Kelly, R., & Robinson, D. A. (2012). A review of global satellite-derived snow products. *Advances in Space Research, 50*, 1007–1029.
Hall, D. K., Foster, J. L., Salomonson, V. V., Klein, A. G., & Chien, J. Y. L. (2001). Development of a technique to assess snow-cover mapping errors from space. *IEEE Transactions on Geoscience and Remote Sensing, 39*, 432–438.
Hall, D. K., Foster, J. L., Verbyla, D. L., Klein, A. G., & Benson, C. S. (1998). Assessment of snow-cover mapping accuracy in a variety of vegetation-cover densities in central Alaska. *Remote Sensing of Environment, 66*, 129–137.
Hall, D. K., & Riggs, G. A. (2007). Accuracy assessment of the MODIS snow products. *Hydrological Processes, 21*, 1534–1547.
Hall, D. K., Riggs, G. A., Salomonson, V. V., DiGirolamo, N. E., & Bayr, K. J. (2002). MODIS snow-cover products. *Remote Sensing of Environment, 83*, 181–194.
Heinilä, K., Salminen, M., Pulliainen, J., Cohen, J., Metsämäki, S., & Pellikka, P. (2014). The effect of boreal forest canopy to reflectance of snow covered terrain based on airborne imaging spectrometer observations. *International Journal of Applied Earth Observation and Geoinformation, 27*, 31–41.
Helfrich, S. R., McNamara, D., Ramsay, B. H., Baldwin, T., & Kasheta, T. (2007). Enhancements to, and forthcoming developments in the interactive multisensory snow and ice mapping system (IMS). *Hydrological Processes, 21*, 1576–1586.
Klein, A. G., & Barnett, A.C. (2003). Validation of daily MODIS snow cover maps of the upper Rio Grande River Basin for the 2000–2001 snow year. *Remote Sensing of Environment, 86*, 162–176.
Klein, A. G., Hall, D. K., & Riggs, G. A. (1998). Improving snow cover mapping in forests through the use of a canopy reflectance model. *Hydrological Processes, 12*, 1723–1744.
Li, X., & Strahler, A. H. (1985). Geometric-optical modeling of a conifer forest canopy. *IEEE Transactions on Geoscience and Remote Sensing, 23*, 705–721.
Li, X., Strahler, A. H., & Woodcock, C. E. (1995). A hybrid geometric optical-radiative transfer approach for modeling albedo and directional reflectance of discontinuous canopies. *IEEE Transactions on Geoscience and Remote Sensing, 33*, 467–480.
Liu, J., Woodcock, C., Melloh, R., Davis, R., McKenzie, C., & Painter, T. (2008). Modeling the view angle dependence of gap fractions in forest canopies: Implications for mapping fractional snow cover using optical remote sensing. *Journal of Hydrometeorology, 9*, 1005–1019.
Luojus, K., Pulliainen, J., Rott, H., Nagler, T., Solberg, R., Wiesmann, A., Derksen, C., Metsämäki, S., Malnes, El, & Bojkov, B. (2010). ESA DUE GlobSnow — Global snow data-base for climate research. *Proceedings of the ESA Living Planet Symposium, June 28–July 2, 2010, Bergen, Norway, SP-686*.
METLA (2010). *Finnish statistical yearbook of forestry*. Vammala, Finland: Finnish Forest Research Institute, 62.
Metsämäki, S., Anttila, S., Huttunen, M., & Vepsäläinen, J. (2005). A feasible method for fractional snow cover mapping in boreal zone based on a reflectance model. *Remote Sensing of Environment, 95*, 77–95.
Metsämäki, S., Mattila, O. -P., Pulliainen, J., Niemi, K., Luojus, K., & Böttcher, K. (2012). An optical reflectance model-based method for fractional snow cover mapping applicable to continental scale. *Remote Sensing of Environment, 123*, 508–521.
Metsämäki, S., Vepsäläinen, J., Pulliainen, J., & Sucksdorff, Y. (2002). Improved linear interpolation method for the estimation of snow-covered area from optical data. *Remote Sensing of Environment, 82*, 64–78.
Niemi, K., Metsämäki, S., Pulliainen, J., Suokanerva, H., Böttcher, K., Leppäranta, M., & Pellikka, P. (2012). The behaviour of mast-borne spectra in a snow-covered boreal forest. *Remote Sensing of Environment, 124*, 551–563.
Nolin, A. W. (2004). Towards retrieval of forest cover density over snow from the multiangle imaging spectroradiometer (MISR). *Hydrological Processes, 18*, 3623–3636.
Nolin, A. W. (2010). Recent advances in remote sensing of seasonal snow. *Journal of Glaciology, 56*, 1141–1150.
Painter, T. H., Dozier, J., Roberts, D. A., Davis, R. E., & Green, R. O. (2003). Retrieval of subpixel snow-covered area and grain size from imaging spectrometer data. *Remote Sensing of Environment, 85*, 64–77.
Painter, T. H., Rittger, K., McKenzie, C., Slaughter, P., Davis, R. E., & Dozier, J. (2009). Retrieval of subpixel snow covered area, grain size, and albedo from MODIS. *Remote Sensing of Environment, 113*, 868–879.
Parajka, J., & Blöschl (2006). Validation of MODIS snow cover images over Austria. *Hydrology and Earth System Sciences, 10*, 679–689.
Pulliainen, J., Heiska, K., Hyyppä, J., & Hallikainen, M. (1994). Backscattering properties of boreal forests at the C- and X-bands. *IEEE Transactions on Geoscience and Remote Sensing, 32*, 1041–1050.
Ramsay, B. H. (1998). The interactive multisensory snow and ice mapping system. *Hydrological Processes, 12*, 1537–1546.
Rittger, K., Painter, T. H., & Dozier, J. (2013). Assessment of methods for mapping snow cover from MODIS. *Advances in Water Resources, 51*, 367–380.
Robinson, D. A., Dewey, K. F., & Heim, R. R., Jr. (1993). Global snow cover monitoring: An update. *Bulletin of the American Meteorological Society, 74*, 1689–1696.
Rosema, A., Verhoef, W., Noorbergen, H., & Borgesius, J. J. (1992). A new forest light interaction model in support of forest monitoring. *Remote Sensing of Environment, 42*, 23–41.
Salminen, M., Pulliainen, J., Metsämäki, S., Kontu, A., & Suokanerva, H. (2009). The behaviour of snow and snow-free surface reflectance in boreal forests: Implications to the performance of snow covered area monitoring. *Remote Sensing of Environment, 113*, 907–918.
Salomonson, V. V., & Appel, I. (2004). Estimating fractional snow cover from MODIS using the normalized difference snow index. *Remote Sensing of Environment, 89*, 351–360.
Salomonson, V. V., & Appel, I. (2006). Development of the Aqua MODIS NDSI fractional snow cover algorithm and validation results. *IEEE Transactions on Geoscience and Remote Sensing, 44*, 1747–1756.
Schlerf, M., & Atzberger, C. (2006). Inversion of a forest reflectance model to estimate structural canopy variables from hyperspectral remote sensing data. *Remote Sensing of Environment, 100*, 281–294.
Tomppo, E., Haakana, M., Katila, M., & Peräsaari, J. (2008). *Multi-source national forest inventory — Methods and applications. (Managing forest ecosystems)*. New York: Springer.
Vaughan, D.G., Comiso, J. C., Allison, I., Carrasco, J., Kaser, G., Kwok, R., Mote, P., Murray, T., Paul, F., Ren, J., Rignot, E., Solomina, O., Steffen, K., & Zhang, T. (2013). Observations: Cryosphere. In T. F. Stocker, D. Qin, G. -K. Plattner, M. Tignor, S. K. Allen, J. Boschung, A. Nauels, Y. Xia, V. Bex, & P.M. Midgley (Eds.), *Climate change 2013: The physical science basis. Contribution of working group I to the fifth assessment report of the intergovernmental panel on climate change* (pp. 317–382). Cambridge, United Kingdom and New York, NY, USA: Cambridge University Press.
Vikhamar, D., & Sohlberg, R. (2002). Subpixel mapping of snow cover in forests by optical remote sensing. *Remote Sensing of Environment, 84*, 69–82.
Vikhamar, D., & Solberg, R. (2003). Snow-cover mapping in forests by constrained linear spectral unmixing of MODIS data. *Remote Sensing of Environment, 88*, 309–323.

This article is submitted to Remote Sensing of Environment and is under revision.

# DETERMINATION OF UNCERTAINTY CHARACTERISTICS FOR THE OPTICAL SATELLITE DATA-BASED ESTIMATION OF FRACTIONAL SNOW COVER

Miia Salminen[(1)], Jouni Pulliainen[(1)], Sari Metsämäki[(2)], Jaakko Ikonen[(1)], Kirsikka Heinilä[(2)], Kari Luojus[(1)]

[(1)] *Finnish Meteorological Institute, P.O. Box 503, FI-00101 Helsinki, Finland*
[(2)] *Finnish Environment Institute, P.O.Box 140, FI-00251 Helsinki, Finland*

## Abstract

Remote sensing provides observations of snow cover based on images with increasingly high spatial, spectral and temporal resolution. Yet, a certain amount of intrinsic uncertainty and errors affect the usability of these snow products in climatological and hydrological applications. The main goal of this work is to develop a methodology to assess the total product error in optical, satellite data-based, Fractional Snow Cover (*FSC*) estimation. Here the FSC estimation is based on an algorithm allowing the consideration of the effect of different error sources; a semi-empirical reflectance model describing the relationship of the observed reflectance and FSC through several variables. First we define a statistical error component through the theory of error propagation, and then utilize a new experimental analysis approach and a unique regional data set covering Finland to calculate the remaining systematic error component. The results are used to derive a product error (*PE*) value, which is the sum of systematic and statistical error components. The experimental analysis approach is conducted through an analysis of the observed estimation errors (*i.e.* residuals) in the GlobSnow Snow Extent (SE) v2.1 products on FSC (determined from Envisat AATSR observations). In practice, independent snow course observations from Finland on *FSC* are compared to corresponding satellite FSC estimates to quantify the residuals. We assume that after the statistical error analysis, the remaining portion of error arises due to systematic factors. Thus, through the analysis of the observed residuals we obtain a realistic estimate on the total *PE*. Although such distributed *in situ* reference data are not available elsewhere, we demonstrate the error considerations for a larger region of European boreal forest, where the results are applicable. Our results show that the total *PE* in the GlobSnow SE v2.1 product is significantly higher than the originally delivered statistical error. This is due to deficiencies in the parameterization of the applied forward modelling approach, in particular in the consideration of the forest canopy effects. In this study these deficiencies are both analysed and further discussed from an algorithm accuracy point of view.

*Keywords*: Fractional Snow Cover; reflectance; seasonal snow; optical; remote sensing; snow mapping; accuracy

*Corresponding author*: miia.salminen@fmi.fi, Finnish Meteorological Institute, P.O. Box 503, FI-00101 Helsinki, Finland, mobile: +358 40 7068078

## 1. Introduction

Over the last decades considerable decline in the appearance of snow cover and related changes in hydrology and temperature have been measured at the high latitudes, especially in the Arctic (Robinson et al., 1993; Mote et al., 2005; Brown and Mote, 2009; Takala et al., 2009; Choi et al., 2010; Flanner et al., 2011; Derksen and Brown, 2012; IPCC, 2013; Hori et al., 2017). Although being merely a single component of the entire cryosphere, snow interacts strongly with most of the other constituents due to its high albedo and low thermal conductivity. For instance, snow has an insulating effect over permafrost and the seasonally frozen/thawed layer, and it also has an ability to sustain ice sheets and glaciers (see e.g. ACIA, 2004; Flanner et al., 2011; Vaughan et al., 2013). Besides, seasonal snow is an enormous fresh water resource. The boreal region, characterized by seasonal snow cover, is a vast zone of forest south of the tundra across Eurasia and North America, being the largest continuous land ecosystem in the world (ACIA, 2005). Seasonal snow cover is one of the most important features in boreal ecology. With its high reflectivity versus light absorbing evergreen forest canopy, snow affects the global radiative balance. Furthermore, boreal forests are both affected and contribute to the global climate system through their carbon uptake and storage capacity, which is also influenced by snow cover (Pan et al., 2011). Thus, monitoring and understanding snow processes is highly relevant to all of these interconnected themes (ACIA, 2004; Callaghan et al., 2011; Vaughan et al., 2013; Bokhorst et al., 2016). Our work mainly focuses on quantitative characterization of snow mapping performance in the boreal forest zone.

Estimation of Snow Extent (SE) through optical Earth Observation (EO) data is particularly advantageous during the end of the melting season. Passive microwave-based SE detection methods typically fail to detect patchy wet snow areas, whereas optical observations have been shown to provide far more reliable SE estimates (Dietz et al., 2012a; Frei et al., 2012). Since it is possible to obtain observations underneath clouds using microwave data (unlike using optical instruments), it is desirable to develop advanced methods for snow detection exploiting both these data types. Together the two complementary satellite remote sensing methods enable both frequent as well as high resolution spatial retrievals of snow cover necessary for global and regional scale hydrologic and climate models (Nolin, 2010; Dietz et al., 2012b). The combined use of optical and microwave data benefits from knowing the accuracy statistic of both the observation types. In addition to annual regional and global snow monitoring, acquiring long decadal scale time-series of snow observations has high relevance for climate research (e.g. for building consistent climate data records), provided that the accuracy of the different snow products is known and the products exhibit sufficient accuracy (Ramsay, 1998; Hall and Riggs, 2007; Helfrich et al., 2007; Nolin, 2010; Brown and Robinson, 2011; Dietz et al., 2012a; Frei et al., 2012; Rittger et al., 2013; Metsämäki et al., 2015; Hori et al., 2017). Errors in daily SE and/or albedo products can propagate to the succeeding composite products. As a result, the underlying uncertainties and errors contained in different snow products can be inherited by operational hydrological and meteorological models (Dozier et al., 2009; Rittger et al., 2013). Therefore, the provision of quantitative uncertainty estimates for each remote sensing product, such as SE or Fractional Snow Cover (FSC) is highly important. Often, information on uncertainties is in fact a requirement for data assimilation schemes, for both hydrological and

meteorological models. Previously e.g. Hall and Riggs (2007), Rittger et al. (2013) and Metsämäki et al. (2005; 2012; 2015) have discussed and quantified the uncertainty in measurements of fractional snow cover.

There are few extensively used global snow extent data sets, such as NOAA Climate Data Record (CDR) of Northern Hemisphere Snow Cover Extent (Robinson et al., 2012), NASA MODIS and VIIRS snow products (https://modis-snow-ice.gsfc.nasa.gov/) as well as ESA's GlobSnow fractional snow cover products (www.globsnow.info). MODIS/VIIRS and GlobSnow databases include validated daily FSC products, of which the GlobSnow database also provides pixel-wise uncertainty estimates (Metsämäki et al., 2015; Hall and Riggs, 2007). The FSC define the patchiness of snow cover by assigning a value of FSC ranging from 0 to 1 (or from 0 to 100%-units). For the current optical FSC-methods, the presence of forest cover in particular is typically problematic and usually causing an underestimation of the area covered by snow (Salomonson and Appel, 2004; 2006; Nolin, 2010; Metsämäki et. al., 2012; Rittger et al., 2013). Metsämäki et al. (2012) showed that their semi-empirical reflectance model-based *SCAmod* algorithm is feasible for continental-scale snow mapping and is relatively accurate also in forested regions. The success of the *SCAmod* algorithm in forested areas is related to the utilization of the *apparent forest transmissivity* (derived from space borne reflectance observations under full snow cover) that enables the consideration of the masking effect of forest canopy. Since the *SCAmod* is in practice the only widely used FSC method that is based on the forward modelling of (Top-of-Atmosphere (TOA) /scene) reflectance, here we examine its uncertainty characteristics. Currently the *SCAmod*-based GlobSnow products include a statistical error layer (Metsämäki et al., 2015), but they do not consider systematic errors, and thus, the provided error does not describe the observed residuals (*RMSE*) very well, *i.e.* the root mean squared average of individual residuals for a certain snow cover percentage interval. By combining the theoretically calculated statistical error ($E_{stat}$) and the data analysis based systematic error ($\Delta$) we can derive a FSC-product error (*PE*) value that should describe the data analysis based observed FSC-interval-wise *RMS* error.

As already stated, quantitative and qualitative information on the uncertainty of optical data-derived snow coverage maps is essential in the application of satellite data in third party data processing systems. In this paper the focus is on issues that determine the accuracy of FSC estimates for cloud-free screened pixels.

The accuracy of FSC information can be investigated by analysing the factors that affect the space-borne observed Top-of-Atmosphere (TOA) reflectance and thus, the FSC retrieval performance of *SCAmod*. These factors include the reflectance signatures of the various constituents of snow-covered and snow-free scenery. With *SCAmod*, these constituents comprise of the effects of forest (canopy closure and transmissivity), as well as the contribution of snow-free and wet snow covered ground variations. The statistical (random) error (which is unbiased by nature) of an FSC estimate is obtained here by applying an error propagation analysis to the inverted reflectance model (Metsämäki et al., 2005; 2012; 2015; Salminen et al., 2013). However, the total error in FSC estimation is composed of statistical error and systematic error, and the goal of this study is to define both of them. So, here we describe our method for

product error (*PE*) estimation using a novel analysis approach, where the novelty is based on using *in situ* analysis in addition to the prior theoretical statistical error component calculations. Defining systematic errors requires the determination of residuals (*i.e.* FSC estimation errors) from validation experiments. Systematic error is demonstrated here by analysing satellite-data (Envisat AATSR from 2003 until 2012) derived GlobSnow SE products and their related FSC retrieval uncertainty estimates (*i.e.* statistical errors) for each studied pixel together with the *in situ* analysis. The factors typically affecting the systematic error are e.g. the sun zenith angle, instrument viewing angle and topography. In addition, the levels and variations in atmospheric transmittance and reflectivity have an effect on TOA reflectance. These issues are only indirectly considered here, since part of the analyses are carried out using TOA reflectance observations (additionally, surface-level values of reflectance are shifted to TOA reflectances using constant atmospheric parameters when appropriate). Further, inadequate parameterization of the applied inversion algorithm causes systematic error. As the different systematic error components (as well as their proportions and magnitudes) are intangible, we start off with the statistical analysis and assume that the remaining component to the observed error (residuals) stems from the systematic factors.

To summarize, we analyse the behaviour of the FSC-product error using first the theory of error propagation for defining the statistical component and then utilize regional data from Finland for calculating the remaining systematic component (such distributed *in situ* reference data are not available elsewhere). Finally, the error considerations are demonstrated for a larger region of boreal forest.

## 2. Materials

### *Data for analysing the systematic error component*

Quantitative analyses are carried out for the region of Finland using the GlobSnow Snow Extent (SE) v2.1 products on Fractional Snow Cover (FSC), generated by using the *SCAmod* algorithm (Metsämäki et al., 2015). As a study area, Finland represents southern, central and northern boreal forests. In Finland, the total forest area of 22 million ha is mostly dominated by conifers (Scots pine, Norway spruce); even though broad-leaved trees (mainly Birch) can be locally dominant (ACIA, 2005). As the same coniferous species are typical for the boreal forest belt as a whole, data from the Finnish study area can be extrapolated to larger regions, basically, for all boreal forests in the Northern Hemisphere with similar landscapes of evergreen conifer dominance (except larch dominated regions in Siberia). Therefore, this investigation can also be considered relevant for the evergreen regions in Russia, Alaska, Canada and Scandinavia between latitudes of roughly 45º and 70º N, where the largest part of the world's boreal forests are located (ACIA, 2005). However, as both the parameterization used in the statistical error analysis and the *in situ* data applied in the analysis of residuals (estimation errors) are mostly conducted for moderately dense forests, the results are not likely to be representative for the densest forests existing e.g. in Northern Siberia.

The applied ground truth data consists of the Finnish Environment Institute's (SYKE) snow course observations that include spatially distributed information on FSC for the spring melt period. This unique data set enables the quantitative investigation of residuals in FSC retrieval in case of southern, central and northern boreal forests. The Finnish snow courses are typically 3-4 km long paths where observations are made at 50 m intervals.

The employed GlobSnow FSC product is based on Envisat AATSR data from the period of 2003 – 2011. The product pixel size is 0.01° × 0.01°, i.e. about 1 km × 1 km. We extracted (non-cloudy) FSC estimates from daily products corresponding to each snow course observation within a time window of three days (only those estimates where FSC product showed values 0% < FSC < 100% to represent the melting conditions). The mean FSC values of each snow course visit were applied as reference ground truth. The GlobSnow FSC estimate was extracted from the pixel hitting the central point of the snow course, and from eight surrounding pixels. This cluster of 3 × 3 pixels approximately corresponds to the areal extent of snow courses, and thus, FSC values averaged over the cluster are used for the analysis (in case of product provided statistical error of FSC estimate the average is the root mean squared value). In total the amount of cloud-free 3 × 3 pixel clusters obtained for the analyses was 173 representing the spring melt period (March, April and May during the years 2003 - 2011).

***Data for statistical error analysis***

In this investigation we also summarize in detail the consideration of the spatially and temporally varying statistical error in the GlobSnow FSC product. A brief description was given earlier in (Metsämäki et al., 2015). The static data sets required for determining the statistical error characteristics through error propagation analyses are given in Table 1. In addition to the data sets and values listed in Table 1, the GlobSnow v2.1 SE product applies MODIS data derived snow-free ground reflectance statistics as a source of statistical error considerations for those regions that are not covered by seasonal snow (Metsämäki et al., 2015). This investigation is, however, limited to regions of seasonal snow where Table 1 is relevant (regions of ephemeral snow are excluded).

**Table 1**. Parameters influencing the statistical error of *SCAmod* algorithm in GlobSnow SE product on FSC.

| **Relevant parameter** | **Value at 555 nm (TOA) and/or characterization** | **Source** |
|---|---|---|
| Two-way apparent forest canopy transmissivity ($t^2$) | Calculated from MODIS reflectance-derived transmissivity combined with land cover information | GlobCover data set (Bontemps et al. (2011); Metsämäki et al. (2015) |
| Variance of forest canopy transmissivity ($S_{t^2}^2$) | Analyzed through MODIS data | See section 3 here |
| Forest canopy reflectance ($\rho_{forest}$) | **0.08** Based on MODIS data analysis and laboratory measurements (spectroscopy) | Niemi et al. (2012); Metsämäki et al. (2012) |
| Variance of forest canopy reflectance ($S_{forest}^2$) | **$(0.01)^2$** Based on laboratory measurements (spectroscopy) | Niemi et al. (2012); Salminen et al. (2013) |
| Snow free ground reflectance ($\rho_{ground}$) | Values according to land cover class, based on MODIS data analysis | Salminen et al. (2013) |
| Variance of snow free ground reflectance ($S_{ground}^2$) | Values according to land cover class based on MODIS data analysis | Salminen et al. (2013) |
| Wet snow reflectance ($\rho_{snow}$) | **0.65** Based on field spectrometry and MODIS data analysis | Salminen et al. (2009); Metsämäki et al. (2012); Niemi et al. (2012) |
| Variance of wet snow reflectance ($S_{snow}^2$) | **$(0.10)^2$** Based on field spectrometry | Salminen et al. (2009); Niemi et al. (2012) |

## 3. Methods

### *Definition of error terms*

The product error (*PE*) in *FSC* estimation can be considered to include the components of (a) systematic error and (b) statistical error (*i.e.* random error). Here, statistical error is defined as a theoretical error estimated through an error propagation analysis (see e.g. Metsämäki et al., 2005; Salminen et al., 2009; Salminen et al., 2013; Metsämäki et al., 2015). Systematic errors emerge e.g. from the unknown biases in retrieval algorithm parameters (for example, the assumed mean value of wet snow reflectance, a parameter in the *SCAmod* algorithm, may be biased). Thus, the general formula for product error *PE* can be given as

$$PE(x,y,t) = \sqrt{(E_{stat}(x,y,t))^2 + (\Delta(\mathrm{FSC}))^2} \quad (1)$$

where $E_{stat}$ refers to statistical error, $\Delta$ to systematic error $x$ and $y$ refer to pixel coordinates and $t$ to the time of observation, respectively. FSC is the estimated (SE product provided) fractional snow cover. A key topic in this investigation is the analysis of systematic error as a function of FSC and the concurrent advanced consideration of the statistical error, in order to provide a realistic estimate on *PE*. The applied error terminology is defined in Table 2.

**Table 2.** Applied error terminology description.

| **Error terminology** | **Symbol** | **Description** | **Source** |
|---|---|---|---|
| Product error | *PE* | Effective sum of statistical and systematic errors | Statistical and Systematic error |
| Statistical error | $E_{stat}$ | Random error based on error propagation analysis | Theoretical |
| Systematic error | $\Delta$ | Error component not described by statistical error | *RMS* error based |
| Residual; | - | Estimation error; FSC* Estimate – *in situ FSC* (single case) | Directly observed; *in situ* analysis |
| *RMS* error | *RMSE* | Root mean squared sum of residuals (Effective mean, positive) | Directly observed; *in situ* analysis |
| BIAS | *BIAS* | Mean of observed residuals (Positive or negative) | Directly observed; *in situ* analysis |

*directly observed *in situ* value of *FSC* is denoted here by italics letters, whereas its estimate is FSC

The observed *FSC* estimation error *RMSE* calculated from residuals should correspond to *PE* (note that the real value of *FSC* is denoted here by italics letters, whereas its estimate is FSC). Residuals can be quantified through the analysis of available independent snow course-observed ground truth on *FSC*. In practice, by comparing snow course observations on *FSC* to satellite data-derived estimates, residuals of each FSC estimate can be determined.

For a certain interval of FSC estimates denoted by index j, we can approximately relate *RMSE* (determined from residuals) to systematic error $\Delta$ and statistical error $E_{stat}$ by:

$$RMSE\left(\mathrm{FSC}^{j}\right) \approx \sqrt{\frac{1}{N_j}\sum_{i=1}^{N_j}\left(E_{stat}(\mathrm{FSC}_i^j)\right)^2 + \left(\Delta(\mathrm{FSC}^j)\right)^2} \qquad (2)$$

where $\mathrm{FSC}_i^j$ refers to the $i$:th FSC estimate obtained for a certain discrete interval $j$, e.g. denoting values $0\% < \mathrm{FSC} \leq 20\%$, and $N_j$ is the number of estimates for the interval $j$ (note that in practice this discretisation is needed as the amount of available data points for the analysis of error characteristics is limited).

In order to estimate the systematic error for a FSC interval $j$, Eq. (2) directly leads to

$$\Delta(\mathrm{FSC}^j) = \sqrt{\frac{1}{N_j}\sum_{i=1}^{N_j}\left(RMSE(\mathrm{FSC}_i^j)\right)^2 - \frac{1}{N_j}\sum_{i=1}^{N_j}\left(E_{stat}(\mathrm{FSC}_i^j)\right)^2} \quad (3)$$

that provides the systematic *FSC* estimation error for the investigated interval of FSC estimates. One should notice that the observed interval-wise *RMSE* and *BIAS* are on the other hand:

$$RMSE(\mathrm{FSC}^j) = \sqrt{\frac{1}{N_j}\sum_{i=1}^{N_j}\left(\mathrm{FSC}_{i(estimated)}^j - FSC_{i(ground\ truth)}^j\right)^2} \quad (4)$$

$$BIAS(\mathrm{FSC}^j) = \frac{1}{N_j}\sum_{i=1}^{N_j}\left(\mathrm{FSC}_{i(estimated)}^j - FSC_{i(ground\ truth)}^j\right) \quad (5)$$

When Eq. (3) is applied to several intervals of FSC we obtain discrete estimates of systematic error Δ as a function of FSC. This enables the fitting of a regression curve to values of Δ, in order to extract a continuous representation of systematic error. When this information is applied to (1), the values of *PE* can be provided to any satellite data provided FSC value (given that the statistical error of each estimate is calculated), see Fig. 1.

***Determination of statistical FSC retrieval error in case of SCAmod algorithm***

The fundamental formula of the *SCAmod* algorithm in order to estimate the fraction of snow covered area (FSC) for an individual pixel is:

$$\mathrm{FSC} = \frac{\frac{1}{t^2}\rho_{obs} + \left(1 - \frac{1}{t^2}\right)\rho_{forest} - \rho_{ground}}{\rho_{snow} - \rho_{ground}} \quad (6)$$

where $\rho_{obs}$ is the TOA-observed reflectance (at a channel close to 555 nm). $t^2$, $\rho_{forest}$, $\rho_{ground}$ and $\rho_{snow}$ are pre-fixed model parameters describing the apparent (two-way) forest canopy transsmissivity, reflectance of an opaque forest canopy, reflectance of snow-free ground and reflectance of (wet) snow reflectance, respectively. The values applied in the GlobSnow SE product on FSC are given in Table 1 above.

Eq. (6) is based on the inversion of the forward model that describes the TOA-observed reflectance as a function of *FSC*:

$$\rho_{obs}(FSC) = (1 - t^2)\rho_{forest} + t^2\left[FSC\rho_{snow} + (1 - FSC)\rho_{ground}\right] \quad (7)$$

Following (Metsämäki et al., 2005), the *statistical accuracy* of *SCAmod*-derived FSC can be obtained from Eq. (6) using the law of error propagation (e.g. Taylor, 1982), which gives the variance $S_{FSC}^2 = (E_{stat})^2$ of FSC estimate as follows:

$$S_{\mathrm{FSC}}^2(\rho_{obs}(FSC), t^2) = \left(\frac{\partial(FSC)}{\partial\rho_{obs}(FSC)}\right)^2 S_{obs}^2 + \left(\frac{\partial(FSC)}{\partial t^2}\right)^2 S_{t^2}^2 + \left(\frac{\partial(FSC)}{\partial\rho_{snow}}\right)^2 S_{snow}^2 + \left(\frac{\partial(FSC)}{\partial\rho_{forest}}\right)^2 S_{forest}^2 + \left(\frac{\partial(FSC)}{\partial\rho_{ground}}\right)^2 S_{ground}^2 = E_{obs}^2 + E_{t^2}^2 + E_{snow}^2 + E_{forest}^2 + E_{ground}^2 \quad (8)$$

where $\rho_{obs}(FSC)$ can be obtained from Eq. (7). The variance of observation accuracy is denoted by $S_{obs}^2$, whereas $S_{t^2}^2$, $S_{snow}^2$, $S_{forest}^2$ and $S_{ground}^2$ are variances of apparent forest canopy transmissivity, snow reflectance, opaque forest canopy reflectance and snow-free ground reflectance.

Different terms contributing to Eq. (8) are described below, and applied parameter values are listed in Table 1. When Eq. (8) is applied to the determination of statistical error of satellite data retrievals, the formulas for different terms have to be presented as a function of FSC. That is, the product provided FSC is used as input in the error calculation.

Error contribution due to observation noise, $E_{obs}^2$

The observation noise $S_{\mathrm{obs}}^2$ includes the effect of the inaccuracy of instrument, as well as the effect of other fluctuating variables not considered by other terms of Eq. (8); e.g. the influence of the atmosphere to the TOA reflectance. However, the effect of this term is included in the other error contributions (Salminen et. al., 2013). Therefore, we assume $S_{\mathrm{obs}}^2 = 0$ in the determination of the statistical *FSC* retrieval error.

Error contribution due to the two-way forest canopy transmissivity variability, $E_{t^2}^2$

The contribution of the variance of the two-way forest canopy transmissivity ($t^2$) is obtained by:

$$E_{t^2}^2 = \left(\frac{\partial(FSC)}{\partial t^2}\right)^2 S_{t^2}^2 = \left(\frac{1}{(t^2)^2}\frac{\rho_{forest} - \rho_{obs}(FSC)}{\rho_{snow} - \rho_{ground}}\right)^2 S_{t^2}^2 = \left(\frac{1}{t^2}\frac{(\rho_{forest} - \rho_{ground}) + \mathrm{FSC}(\rho_{ground} - \rho_{snow})}{\rho_{snow} - \rho_{ground}}\right)^2 S_{t^2}^2 \quad (9)$$

The variance of transmissivity ($S_{t^2}^2$) can be estimated from the variance of MODIS reflectances used in the transmissivity calculations for target areas in Finland and the surroundings. Each pixel-wise transmissivity is determined from averaged multiple reflectance observations for that pixel (see Metsämäki et al., 2012). Hence the pixel-wise variance of transmissivity can be estimated by analysing the variability of transmissivities obtained for different reflectance

observations of a single pixel. By calculating variances of transmissivity for a large number of observations representing different transmissivity levels, a general formula approximating the variance as a function of $t^2$ is obtained

$$S_{t^2}^2 = [\,0.01\,(38.8616\,exp(-19.8517\,t^2) + 9.50151)t^2]^2 \quad (10)$$

Error contribution due to snow reflectance variability, $E_{snow}^2$
From Eq. (8) we obtain:

$$E_{snow}^2 = \left( -\frac{\frac{1}{t^2}\rho_{obs}(FSC) + \left(1-\frac{1}{t^2}\right)\rho_{forest} - \rho_{ground}}{\left(\rho_{snow} - \rho_{ground}\right)^2} \right)^2 S_{snow}^2$$
$$= \left( \frac{-\mathrm{FSC}}{\rho_{snow} - \rho_{ground}} \right)^2 S_{snow}^2 \quad (11)$$

Error contribution due to (opaque) forest canopy reflectance variability, $E_{forest}^2$
$E_{forest}^2$ contribution is equal to

$$E_{forest}^2 = \left( \frac{1-\frac{1}{t^2}}{\rho_{snow} - \rho_{ground}} \right)^2 S_{forest}^2 \quad (12)$$

Error contribution due to snow-free ground reflectance variability, $E_{ground}^2$
The contribution of snow-free ground reflectance to total variance is

$$E_{ground}^2 = \left( \frac{\partial F(FSC)}{\partial \rho_{ground}} \right)^2 S_{ground}^2 = \left( \frac{\frac{1}{t^2}\rho_{obs}(FSC) + \left(1-\frac{1}{t^2}\right)\rho_{forest} - \rho_{snow}}{\left(\rho_{snow} - \rho_{ground}\right)^2} \right)^2 S_{ground}^2$$
$$= \left( \frac{\mathrm{FSC} - 1}{\rho_{snow} - \rho_{ground}} \right)^2 S_{ground}^2 \quad (13)$$

where $S_{ground}^2$ is the variance of snow-free ground reflectance estimated for the grid cell under investigation (AATSR pixel in GlobSnow SE product). As each pixel is composed of 16 GlobCover sub-grid cells that exhibit different reflectance levels due to varying land cover, $S_{ground}^2$ is given by

$$S_{ground}^2 = \sum_{i=1}^{N_{classes}} \left(\frac{n_i}{16}\right)^2 \mathrm{var}\left(\rho_{ground,i}\right) \quad (14)$$

The used value for the variance of snow-free ground reflectance in Table 1 is most likely to be too small, since the snow-free ground investigation was conducted using satellite data only from one year, regardless of the high number of observations (including a large variety of non-cloudy atmospheric conditions and variety of orbits with varying viewing angles) and extensive spatial coverage for each studied land cover type in Central, Eastern and Northern Europe (Salminen et al., 2013). This may affect the relative proportions of error terms so that the contribution of $S^2_{ground}$ is slightly underestimated at the expense of other terms. However, this is not crucial, as the purpose of the paper is to present the theoretical background of the accuracy determination.

***Determination of product error for FSC estimates***

The outline of the procedure for determining the product error *PE* in *FSC* estimation according to Eq. (1) is presented in Fig. 1. This procedure is applied in this paper for the GlobSnow SE product on *FSC*. The method is applicable to any problem where an analytical inverse solution of a forward model is employed.

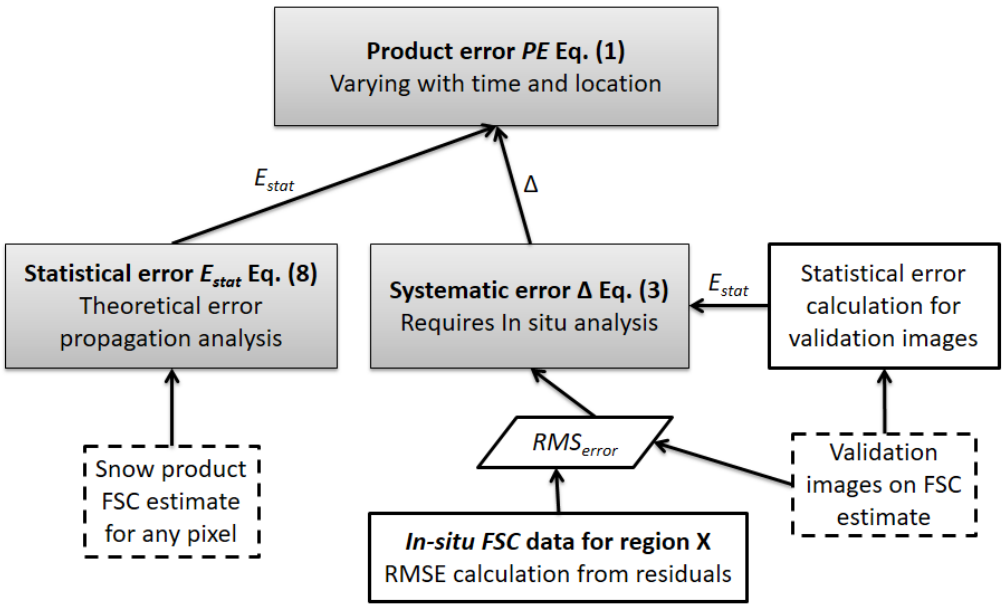


**Fig. 1**. Procedure for the determination of the total product error *PE*. The calculation of systematic error is performed by using *in situ* data set.

## 4. Results and discussion

The spatial behaviour of the optical Snow Extent total product error is demonstrated for boreal forest regions along with a definition of both the systematic and statistical components. The results compose first of the statistical component calculated by using the theory of error propagation. An extensive dataset from Finland enabled then the calculation of the remaining systematic component. The behaviour of statistical error component in GlobSnow SE product is illustrated in Fig. 2 using model calculations, Eqs. (8) – (14). As discussed above GlobSnow SE products apply *SCAmod* algorithm according to Eq. (6) to estimate the level of *FSC*. Different statistical error component contributors of *FSC* retrieval, and their sum, are calculated by Eqs. (8) – (14) for two typical levels of forest canopy transmissivity corresponding to dense ($t^2$=0.2) and sparse ($t^2$=0.6) boreal forests. Fig. 2 clearly shows the high impact of forest density on the behaviour and the relative proportions of the different statistical error component contributors. Parameter values given in Table 1 are employed, except that for the spatially varying parameters typical constant values are used for simulation, *i.e.* $S^2_{ground} = (0.18)^2$ and $\rho_{ground} = 0.10$. Further, Eq. (10) is applied to determine the variance of forest canopy transmissivity $S^2_{t^2}$. The results indicate that when the true level of *FSC* is close to 100%, the highest uncertainty of FSC estimates emerges from the variability of wet snow reflectance. For low levels of *FSC* the influence of ground reflectance variability is dominant in the case of sparse forests. As for dense forests, the variance of forest canopy reflectance $S^2_{forest}$ is assumed to be $0.01^2$ based on Table 1, and the accuracy of FSC estimates is predicted to be dominated by $S^2_{forest}$ at low levels of FSC.

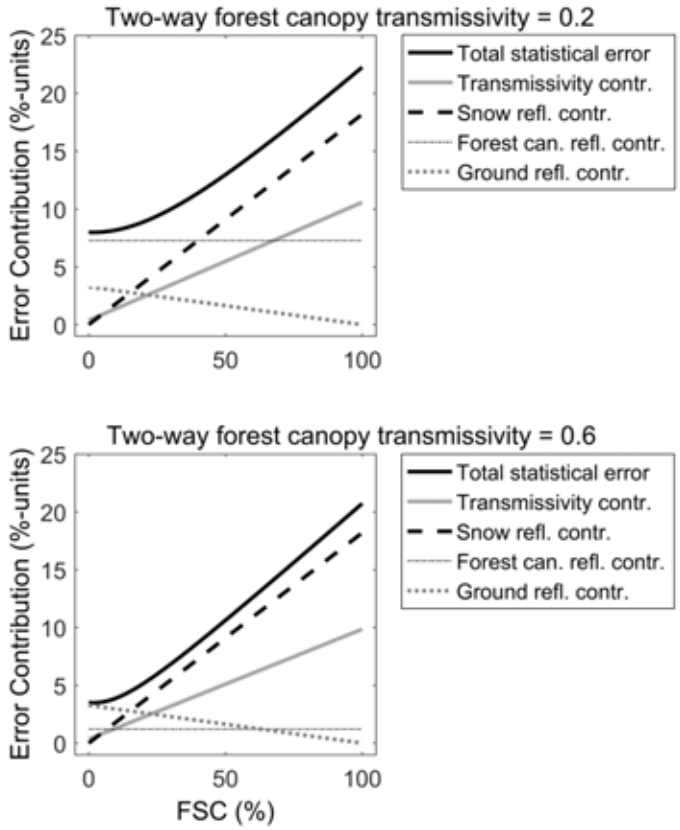


**Fig. 2**. Modelled FSC retrieval statistical error component and its contributors (y-axis: error standard deviation in FSC percentage units) as a function of *FSC* for two typical levels of forest canopy transmissivity corresponding to dense (upper panel) and sparse (lower panel) boreal forests. The statistical error component and its contributors are determined by Eqs. (8) – (14).

Fig. 3 demonstrates a spatial map of the statistical FSC estimation error in GlobSnow SE product and the corresponding FSC estimation map for a 14-day composite from April 02 to April 15, 2010. The composites are produced by taking the image of 15 April, 2010 as a baseline, and replacing cloudy pixels with the previous image, if the previous day is cloud-free. This procedure is repeated for 14 days to get a good coverage. The region of Fig. 3 is selected to represent boreal forest dominated areas where the analyses of this study are valid. The statistical error levels in Fig. 3 are determined by Eqs. (8) – (14). Thus, the map corresponds to the quantitative analysis of Fig. 2. In addition to the behaviour of statistical error, the FSC map according to Eq. (6) is also shown for comparison in Fig. 3.

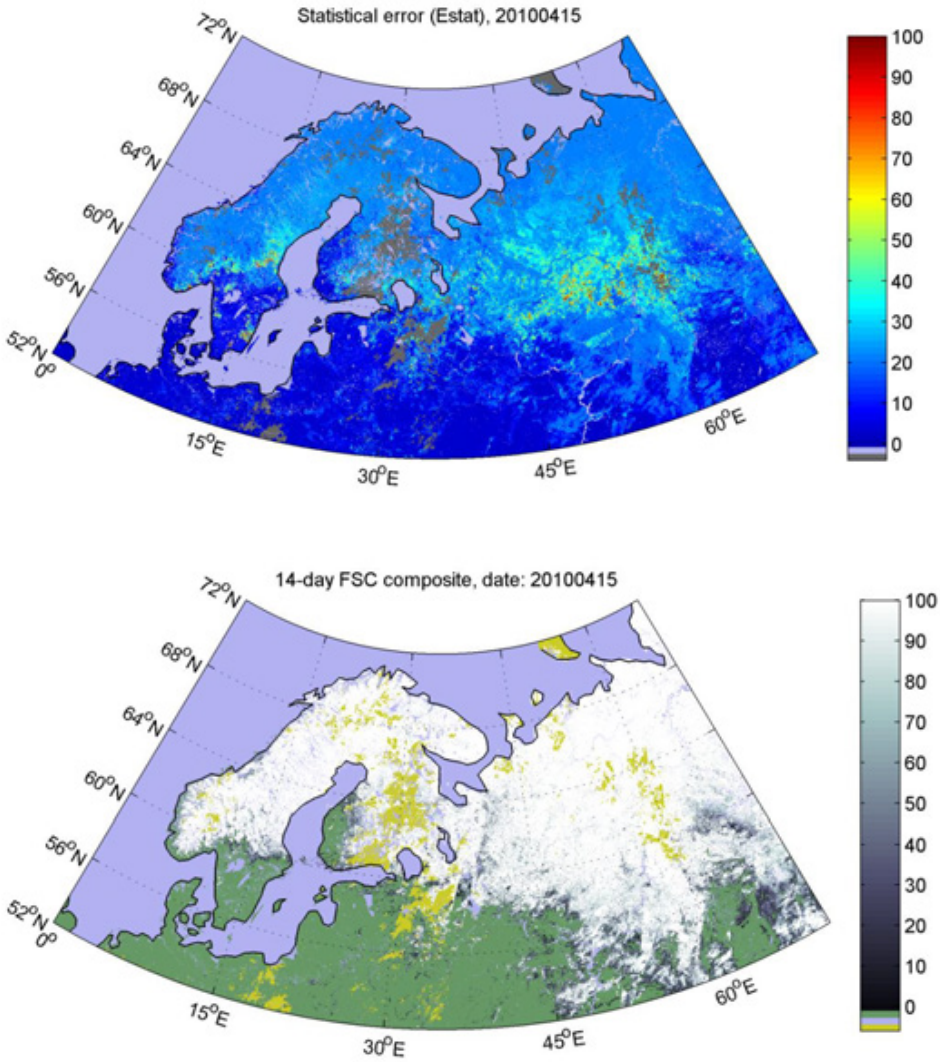


**Fig. 3**. Statistical error (FSC %-units) of GlobSnow FSC estimate for a composite of daily products between April 02 and April 15, 2010 (upper panel), and the corresponding FSC (%-units) estimation map (lower panel). Clouds are depicted in brown-grey color (upper panel), and yellow (lower panel), respectively.

FSC estimates by *SCAmod* are compared with *in situ* observations of FSC from Finnish snow courses in the left and central panels of Fig. 4a. The obtained residuals indicate that the systematic error of FSC estimates is typically higher than the statistical error depicted in the right panel of Fig. 4a. Note that statistical error in Fig 4 (8 years of reference data, 173 matching pairs of *in situ* and satellite data, where each data point is an average of nine pixels) corresponds to Figs. 2 (modelled situation using typical values) and 3 (composite of daily products where each pixel value represents single observation from one day). As described in Section 2, results of Fig. 4 are determined for clusters of 3 × 3 pixels covering the regions of reference snow

courses, so that each data point is an average of nine pixels. Therefore, the statistical error in the right-hand panel is the *RMS*-value of nine pixel-wise errors. Further, the behaviour of the systematic error component appears to be strongly dependent on the level of the FSC estimate. That is, bias changes from negative (underestimation) to positive (overestimation) as FSC increases from 0% to 100%. Forest canopy transmissivity data in the GlobSnow FSC product is evidently the cause of the observed bias. Namely, instead of directly using the satellite derived apparent transmissivity, which provided the highest accuracy (Metsämäki et al., 2005), a global generalization from transmissivities of selected training regions are used, which is based on the analysis of satellite data derived transmissivities of different GlobCover classes at these regions (Metsämäki et al., 2015). In practice Finnish boreal forests with a moderate canopy closure are treated with low values of apparent canopy transmissivity as some of the training areas for this particular GlobCover class also include denser Russian forests. As the residuals of FSC estimates depicted in Fig. 4 are obtained for snow courses located in Finland, the results show a predominantly positive bias resulting from the assigned low level of canopy transmissivity. This is illustrated in Fig. 4b, where the left and central panels show the residuals of FSC estimates as a function of GlobSnow forest canopy transmissivity indicating overestimation for the densest forests (lowest values of transmissivity). The right panel of Fig. 4b indicates that the GlobSnow product derived statistical accuracy by Eq. (8) is strongly dependent on forest cover, which was expected, as the forest cover affects the signal both by two-way attenuation process and by reflecting. Fig. 4 suggests that the systematic error can be estimated for those regions where independent reliable reference data are available. Fig. 4 also indicates that there is no significant impact by the timing of estimates, as data are collected for March to April during the period of nine years.

Based on the results shown in Fig. 4, we can apply Eqs. (1) - (3) according to the procedure of Fig. 1 to estimate the levels of systematic and total error. In practice, the determination of systematic error has to be performed from FSC-interval stratified data according to Eq. (3). Thereafter, Eq. (1) can be used to derive the total estimation error *PE*. Fig. 5 depicts the obtained total error components as determined by FSC estimates from Finnish snow courses. Thus, Fig. 5 shows (a) the statistical errors calculated for the FSC estimates from snow courses, (b) the interval-wise estimated systematic error levels according to Eq. (3) as well as (c) the observed interval-wise *RMSE*. Additionally, the behaviour of *BIAS* determined by Eq. (5) is shown. For the statistical error, both the interval-stratified values and individual estimates according to Eq. (8) are depicted. For the lowest levels of estimated FSC, the *BIAS* is negative (underestimation of FSC), but typically it shows positive values for the investigated GlobSnow FSC product.

The obtained values of systematic errors for different FSC estimate intervals (shown in Fig. 5) can be further applied to describe the overall behaviour of systematic error. As discussed in Section 3 this general behaviour can be approximated by a regression curve that gives $\Delta$ as a function of FSC, Fig. 6. The exponential regression function giving $\Delta$ is combined with the FSC product statistical error according to Eq. (1) to provide the map of total FSC product error in Fig. 7. The comparison of the map of Fig. 7 with that of the statistical error, shown in Fig. 3, demonstrates the increase of error level due to the consideration of systematic error.

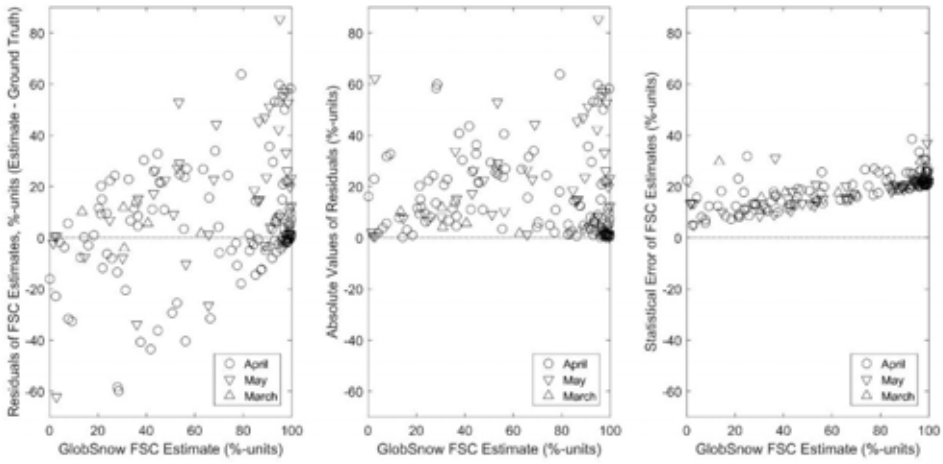


(a)

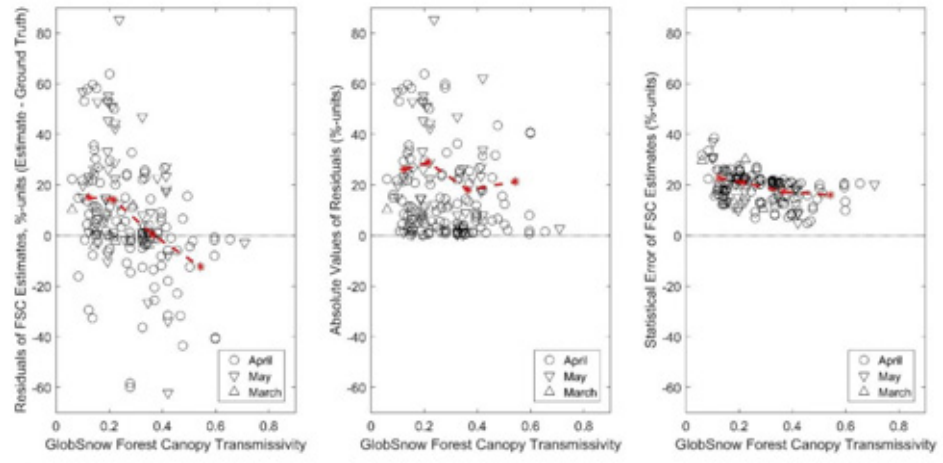


(b)

**Fig. 4**. Residuals and statistical accuracy for FSC at Finnish snow courses as a function of (a) estimated FSC and (b) forest canopy transmissivity. Red asterisks show transmissivity interval-stratified averages. For the central and right-hand panels the averages are root mean squared effective values instead of arithmetic means (left-hand panel).

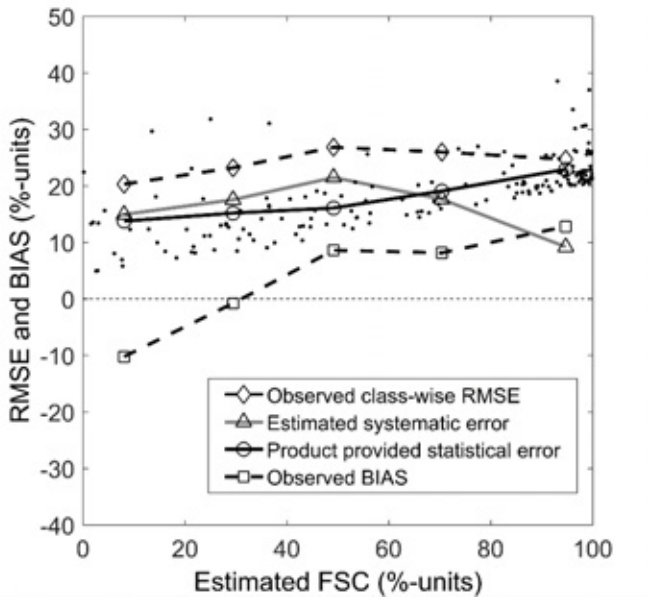


**Fig. 5**. Estimated components of total FSC product error and the observed *RMSE* for FSC estimates over the Finnish snow courses stratified into five FSC-intervals. Statistical error is also shown for individual observations (product grid cells).

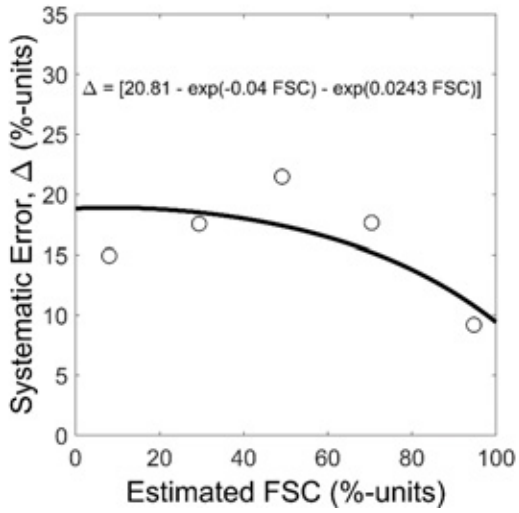


**Fig. 6**. Regression curve determined from the results of Fig. 5 to describe the systematic error Δ as a function of FSC.

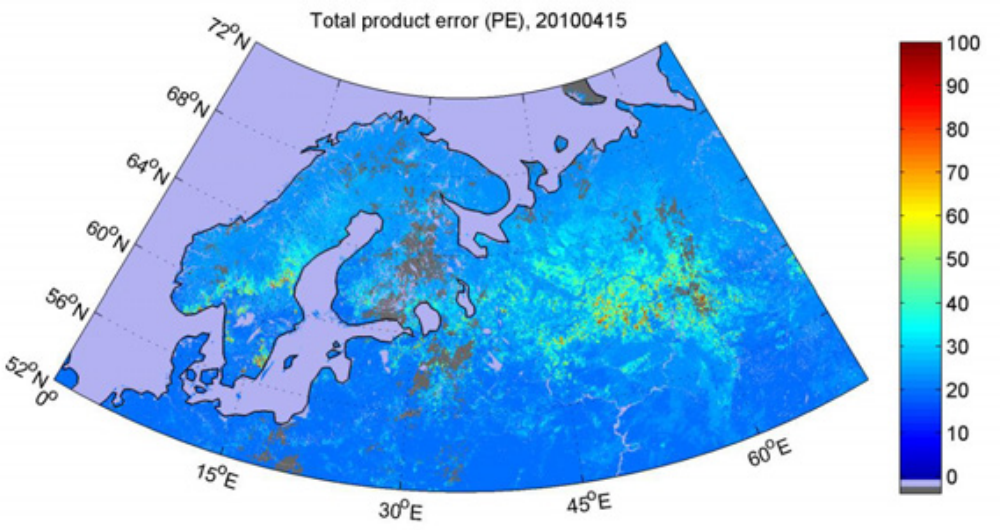


**Fig. 7.** Total FSC product error *PE* (FSC %-units) between April 02 and April 15, 2010. The corresponding maps of the statistical error and FSC product are presented in Fig. 3. Clouds are depicted in brown-grey color.

## 5. Summary and conclusions

We introduced an approach to assess the uncertainty characteristics of Fractional Snow Cover (FSC) estimates as provided by the *SCAmod* –FSC retrieval algorithm employed in the provision of the GlobSnow SE v2.1 products. The approach builds on the idea of describing the FSC uncertainty through error propagation, given that the statistical variation of the algorithm constituents are *a priori* defined. The novelty is the consideration of systematic error, which is carried out with the aid of independent *in situ* reference data. An approach to provide an estimate of the FSC product error by summing the systematic and statistical error components is suggested. The results show that for seasonal snow in boreal forests when the level of FSC is low, the total GlobSnow FSC product error is dominated by the systematic error component. At high levels of FSC the demonstrated product error remains close to the levels of error propagation analysis derived statistical error. It is shown that the systematic error in the GlobSnow SE product stems from inherent inaccuracies of the applied method to estimate apparent forest canopy transmissivity characteristics. This means that inaccuracies of the applied forward model result in systematic errors that can be quantified using the methodology introduced here. Further, since the values for the variances of e.g. snow-free ground reflectance in statistical error analysis are suspected to be partially underestimated, the difference between the total product error and the statistical error could be diminished by obtaining more comprehensive observations to recalculate the variances. Then, presumably, the compensating effect of the systematic error component to the statistical error level would also be diminished. Even though the quantitative analyses are performed for the region of Finland, the demonstration of FSC estimation error characteristics are showed for a larger region of

European boreal forests covering the regions spanning from Denmark and Scandinavian Peninsula to eastern side of the Ural Mountains in Russia.

The developed approach is also applicable to other satellite data-based products given that the estimation of the quantitative geophysical parameter of interest is derived by an inverse solution of a forward model and a representative set of independent reference data is available for the determination of *RMS* estimation error characteristics.

## Acknowledgements

This work is supported by the Academy of Finland CARBARC (285630) and Centre of Excellence in Atmospheric Science – From Molecular and Biological processes to the Global Climate (118780). The Snow Extent (SE) and Land Cover data were provided by the European Space Agency (ESA) Data User Element (DUE) GlobSnow-2 and GlobCover 2009 projects: www.globsnow.info and http://due.esrin.esa.int/page_globcover.php.

## References

ACIA, 2004. Impacts of a Warming Arctic: Arctic Climate Impact Assessment. ACIA Overview report. Cambridge University Press. 1020 pp. http://www.amap.no/documents/doc/impacts-of-a-warming-arctic-2004/786

ACIA, 2005. Chapter 14: Forests, Land Management, and Agriculture, in: Arctic Climate Impact Assessment. ACIA Overview report. Cambridge University Press, pp. 781-862. https://www.amap.no/documents/doc/arctic-arctic-climate-impact-assessment/796

Bokhorst, S., Pedersen, S.H., Brucker, L., Anisimov, O., Bjerke, J.W., Brown, R.D., Ehrich, D., Essery, R.L., Heilig, A., Ingvander, S., Johansson, C., Johansson, M., Jónsdóttir, I.S., Inga, N., Luojus, K., Macelloni, G., Mariash, H., McLennan, D., Rosqvist, G.N., Sato, A., Savela, H., Schneebeli, M., Sokolov, A., Sokratov, S.A., Terzago, S., Vikhamar-Schuler, D., Williamson, S., Qiu, Y., Callaghan, T.V., 2016. Changing Arctic snow cover: A review of recent developments and assessment of future needs for observations, modelling, and impacts. Ambio. 45, 516–537. http://dx.doi.org/10.1007/s13280-016-0770-0

Bontemps, S., Defourny, P., Van Bogaert, E., Arino, O., Kalogirou, V., Perez, J.R., 2011. GlobCover 2009: Product description and validation report. ESA GlobCover 2009 project. http://due.esrin.esa.int/files/GLOBCOVER2009_Validation_Report_2.2.pdf (accessed 23.03.2017)

Brown, R.D., Mote, P.W., 2009. The response of Northern Hemisphere snow cover to a changing climate. J. Clim. 22, 2124-2144. http://dx.doi.org/10.1175/2008JCLI2665.1

Brown, R.D., Robinson, D.A., 2011. Northern Hemisphere spring snow cover variability and change over 1922–2010 including an assessment of uncertainty. Cryosphere. 5, 219-229. http://dx.doi.org/10.5194/tc-5-219-2011

Choi, G., Robinson, D.A., Kang, S., 2010. Changing Northern Hemisphere snow seasons. J. Clim. 23, 5305-5310. http://dx.doi.org/10.1175/2010JCLI3644.1

Derksen, C., Brown, R., 2012. Spring snow cover extent reductions in the 2008–2012 period exceeding climate model predictions. Geophys. Res. Lett. 39, L19504. http://dx.doi.org/10.1029/2012GL053387

Dietz, A.J., Kuenzer, C., Gessner, U., Dech, S., 2012a. Remote sensing of snow – a review of available methods. Int. J. Remote Sens. 33, 4094-4134.

Dietz, J., Wohner, C., Kuenzer, C., 2012b. European snow cover characteristics between 2000 and 2011 derived from improved MODIS daily snow cover products. Remote Sens. 4, 2434-2454.

Dozier, J., Green, R., Nolin, A., Painter, T., 2009. Interpretation of snow properties from imaging spectrometry. Remote Sens. Environ. 113, S25-S37.

Flanner, M.G., Shell, K.M., Barlage, M., Perovich, D.K., Tschudi, M.A., 2011. Radiative forcing and albedo feedback from the northern hemisphere cryosphere between 1979 and 2008. Nat. Geosci. 4, 151–155. http://dx.doi.org/10.1038/ngeo1062

Frei, A., Tedesco, M., Lee, S., Foster, J., Hall, D.K., Kelly, R., Robinson, D.A., 2012. A review of global satellite-derived snow products. Adv. Space Res. 50, 1007-1029.

Hall, D.K., Riggs, G.A., 2007. Accuracy assessment of the MODIS snow products. Hydrol. Process. 21, 1534–1547.

Helfrich, S.R., McNamara, D., Ramsay, B.H., Baldwin, T., Kasheta, T., 2007. Enhancements to, and forthcoming developments in the interactive multisensory snow and ice mapping system (IMS). Hydrol. Process. 21, 1576-1586.

Hori, M., Sugiura, K., Kobayashi, K., Aoki, T., Tanikawa, T., Kuchiki, K., Niwano, M., Enomoto, H., 2017. A 38-year (1978–2015) Northern Hemisphere daily snow cover extent product derived using consistent objective criteria from satellite-borne optical sensors. Remote Sens. Environ. 191, 402–418. http://dx.doi.org/10.1016/j.rse.2017.01.023

IPCC, 2013. Climate Change 2013: The Physical Science Basis. Contribution of Working Group I to the Fifth Assessment Report of the Intergovernmental Panel on Climate Change, [Stocker, T.F., Qin, D., Plattner, G.-K., Tignor, M., Allen, S.K., Boschung, J., Nauels, A., Xia, Y., Bex, V., Midgley, P.M., (Eds.)], Cambridge University Press, Cambridge, United Kingdom and New York, NY, USA, 1535 pp.

Metsämäki, S., Anttila, S., Huttunen, M., Vepsäläinen, J., 2005. A feasible method for fractional snow cover mapping in boreal zone based on a reflectance model. Remote Sens. Environ. 95, 77-95.

Metsämäki, S., Mattila, O.-P., Pulliainen, J., Niemi, K., Luojus, K. Böttcher, K., 2012. An optical reflectance model-based method for fractional snow cover mapping applicable to continental scale. Remote Sens. Environ. 123, 508-521.

Metsämäki, S., Pulliainen, J., Salminen, M., Luojus, K., Wiesmann, A., Solberg, R., Böttcher, K., Hiltunen, M., Ripper, E., 2015. Introduction to GlobSnow Snow Extent products with considerations for accuracy assessment. Remote Sens. Environ. 156, 96-108.

Mote, P.W., Hamlet, A.F., Clark, M.P., Lettenmaier, D.P., 2005. Declining mountain snowpack in western North America. Bull. Am. Meteorol. Soc. 86, 39-49. http://dx.doi.org/10.1175/BAMS-86-1-39

Niemi, K., Metsämäki, S., Pulliainen, J., Suokanerva, H., Böttcher, K., Leppäranta, M., Pellikka, P., 2012. The behaviour of mast-borne spectra in a snow-covered boreal forest. Remote Sens. Environ. 124, 551-563.

Nolin, A. W., 2010. Recent advances in remote sensing of seasonal snow. J. Glaciol. 56, 1141-1150.

Pan, Y. D., Birdsey, R.A., Fang, J., Houghton, R., Kauppi, P.E., Kurz, W.A., Phillips, O.L., Shvidenko, A., Lewis, S.L., Canadell, J.G., Ciais, P., Jackson, R.B., Pacala, S.W., McGuire, A.D., Piao, S., Rautiainen, A., Sitch, S., Hayes, D., 2011. A large and persistent carbon sink in the world's forests. Science 333, 988-993.

Ramsay, B.H., 1998. The interactive multisensory snow and ice mapping system. Hydrol. Process. 12, 1537-1546.

Rittger, K., Painter, T.H., Dozier, J., 2013. Assessment of methods for mapping snow cover from MODIS. Adv. Water Resour. 51, 367-380.

Robinson, D.A., Dewey, K.F., Heim Jr., R.R., 1993. Global snow cover monitoring: an up-date. Bull. Am. Meteorol. Soc. 74, 1689–1696. http://dx.doi.org/10.1175/1520-0477(1993)074<1689:GSCMAU>2.0.CO;2

Robinson, D.A., Estilow, T.W., NOAA CDR Program, 2012. NOAA Climate Date Record (CDR) of Northern Hemisphere (NH) Snow Cover Extent (SCE). NOAA National Climatic Data Center. http://dx.doi.org/10.7289/V5N014G9

Salminen, M., Pulliainen, J., Metsämäki, S., Kontu, A., Suokanerva, H., 2009. The behaviour of snow and snow-free surface reflectance in boreal forests: Implications to the performance of snow covered area monitoring. Remote Sens. Environ. 113, 907-918.

Salminen, M., Pulliainen, J., Metsämäki, S., Böttcher, K. Heinilä, K., 2013. MODIS-derived snow-free ground reflectance statistics of selected Eurasian non-forested land cover types for the application of estimating fractional snow cover. Remote Sens. Environ. 138, 51-64.

Salomonson, V.V., Appel, I., 2004. Estimating fractional snow cover from MODIS using the normalized difference snow index. Remote Sens. Environ. 89, 351– 360.

Salomonson, V.V., Appel, I., 2006. Development of the Aqua MODIS NDSI fractional snow cover algorithm and validation results. IEEE Trans. Geosci. Remote Sens. 44, 1747–1756.

Takala, M., Pulliainen, J., Metsämäki, S., Koskinen, J., 2009. Detection of snow melt using spaceborne microwave radiometer data in Eurasia from 1979-2007. IEEE Trans. Geosci. Remote Sens. 47, 2996-3007.

Taylor, J. R., 1982. An introduction to error analysis. The study of uncertainties in physical measurements. First Edition, University Science Books, London, UK.

Vaughan, D.G., Comiso, J.C., Allison, I., Carrasco, J., Kaser, G., Kwok, R., Mote, P., Murray, T., Paul, F., Ren, J., Rignot, E., Solomina, O., Steffen, K., Zhang, T., 2013. Observations: Cryosphere, in: Stocker, T.F., Qin, D., Plattner, G.-K., Tignor, M., Allen, S.K., Boschung, J., Nauels, A., Xia, Y., Bex, V., Midgley, P.M. (Eds.), Climate Change 2013: The physical science basis. Contribution of working group I to the fifth assessment report of the intergovernmental panel on climate change. Cambridge University Press, Cambridge, United Kingdom and New York, NY, USA. pp. 317-382.

**FINNISH METEOROLOGICAL INSTITUTE**
Erik Palménin aukio 1
P.O. Box 503
FI-00101 HELSINKI
tel. +358 29 539 1000
**WWW.FMI.FI**

FINNISH METEOROLOGICAL INSTITUTE
CONTRIBUTIONS No. 139
ISBN 978-952-336-036-5 (paperback)
ISSN 0782-6117
Erweko
Helsinki 2017

ISBN 978-952-336-037-2 (pdf)
Helsinki 2017